COMPUTATIONAL INVESTIGATIONS

OF THERMAL HYDRAULICS

WITHIN FAST REACTOR FUEL PIN BUNDLE

By

GAJAPATHY R

(Enrollment No: ENGG 02 2008 04 003)

Indira Gandhi Centre for Atomic Research , Kalpakkam

Thesis submitted to the board of studies in Engineering Sciences

in partial fulfillment of the requirements

for the degree of

DOCTOR OF PHILOSOPHY

of

HOMI BHABHA NATIONAL INSTITUTE

August, 2014

COMPUTATIONAL INVESTIGATIONS

OF THERMAL HYDRAULICS

WITHIN FAST REACTOR FUEL PIN BUNDLE

By

GAJAPATHY R

(Enrollment No: ENGG 02 2008 04 003)

Indira Gandhi Centre for Atomic Research , Kalpakkam

Thesis submitted to the board of studies in Engineering Sciences

in partial fulfillment of the requirements

for the degree of

DOCTOR OF PHILOSOPHY

of

HOMI BHABHA NATIONAL INSTITUTE

August, 2014

Homi Bhabha National Institue

Recommendations of the Viva Voce Board

As members of the Viva Voce Board, we certify that we have read the dissertation prepared by **Mr. Gajapathy R.** entitled **"Computational Investigations of Thermal Hydraulics within Fast Reactor Fuel Pin Bundle"** and recommend that it may be accepted as fulfilling the dissertation requirement for the Degree of Doctor of Philosophy.

Member : **Dr. M. Saibaba** **Date :**

Guide / Convener : **Dr. K. Velusamy** **Date :**

Chairman : **Dr. B.P.C. Rao** **Date :**

Member : **Dr. V.S. Srinivasan** **Date :**

External Examiner :

Final approval and acceptance of this dissertation is contingent upon the candidate's submission of the final copies of the dissertation to HBNI.

I hereby certify that I have read this dissertation prepared under my direction and recommend that it may be accepted as fulfilling the dissertation requirement.

Date:

Place: Indira Gandhi Centre for Atomic Research (IGCAR) **Dr. K. Velusamy**
Kalpakkam **(Guide)**

STATEMENT BY AUTHOR

Kalpakkam **(Gajapathy R)**

August, 2014

DECLARATION

I, hereby declare that the investigation presented in the thesis has been carried out by me. The work is original and has not been submitted earlier as a whole or in part for a degree / diploma at this or any other Institution / University.

Kalpakkam **(Gajapathy R)**

August, 2014

This work is dedicated to

‘My beloved Wife and Son’

ACKNOWLEDGEMENTS

I take this opportunity to express my thanks to the people who have been very helpful to me during the time it took me to complete this thesis.

First and foremost I acknowledge my Guide **Dr. K. Velusamy,** *Head, Mechanics and Hydraulics Division, Reactor Design Group (RDG), IGCAR* for his persistent encouragement, constant motivation, everlasting patience and valuable technical inputs right from the attending the courses till the end of my thesis work. The joy and enthusiasm he has for his research was contagious and motivational for me, even during tough times in the Ph.D.

I record my sincere gratitude to my *Doctoral Committee (DC) Chairman* **Dr. B.P.C Rao,** *Head, NDED, IGCAR* for his guidance, constant support and invaluable technical inputs starting from course work up to thesis submission.

I am highly grateful to my *Doctoral Committee (DC) members* **(Dr. M. Sai Baba and Dr. V.S. Srinivasan),** for their valuable inputs, continuous monitoring of my progress and valuable supports throughout the course of my research.

I sincerely thank to **Dr. Baldev raj**, *Former Director, IGCAR* and **S.C. Chetal**, *Former Director, IGCAR*, who motivated me to register in HBNI, **Dr. P. Chellapandi,** *Director, RDG*, for assigning this important work to me and motivating to publish the work in International Journal, **Dr. P.R. Vasudeva Rao,** *Director, IGCAR*, **Dr. R.B. Grover,** Director, HBNI, Mumbai, **Dr. B.K. Dutta,** Dean, HBNI, Mumbai, **T. Jayakumar,** Dean, HBNI, IGCAR and **Dr. M. Sai Baba,** *Associate Director, RMG* for allowing me to continue my research work.

My special thanks are due to the officers of Thermal Hydraulics Section **S/Shri K. Natesan** ***SO/G*** **and R. Arulbaskar,** ***SO/D*** for sharing their knowledge and support during my thesis work. I also sincerely appreciate **Mr. N. Govindharasu, and Mr. Ravi,** ***Ph. D scholars*****,** for their kind help and sharing scientific and technical knowledge.

My special thanks are due to **Shri SAV. Sathyamurthy,** *Director, EIRSG* and **Shri R. Jahadeesan,** *SO/G* and **Shri. Jayalal**, *SO/F* for providing High Performance Scientific Computing Facility with separate nodes. I also acknowledge the support of **Mr. A. Sivakumar,** *DM/D, THS*, **Mr. B. Madhavan**, *SA/C, CDO, IGCAR* and **Mrs. M. Banumathi,** *Steno Gr-II* during the thesis work.

I thank all my family members for their constant support, especially my wife **(Mrs. G. Lakshmi)** and my son **(G. Srivathsan)** who have sacrificed my occasions. Last but not least, I thank the Almighty for the blessings to complete my thesis.

CONTENTS

SYNOPSIS

The CFD investigation of 217 pin bundle which is used in commercial FBRs is essential to be carried out for the thermal hydraulic design of the subassembly. The thermal hydraulics within the subassembly has been studied by (a) experiments using water as medium and in few cases using sodium as medium, (b) porous body models for pin bundle and (c) 3-Dimensional CFD studies with limited number of pins using 7, 19 and 37 pin bundle models. Experimental and porous body model studies do not provide adequate details of cross flow characteristics in the fuel pin bundle with helically wound spacer wire. On the other hand, 3-dimensional CFD studies are capable of providing intricate details about them. Number of CFD based numerical studies have been performed for bundles with smaller number of pins in the pin bundle. However, studies with larger fuel pin bundle such as 217 pins are not reported. Also, the Nusselt number correlation as a function of helical wire parameters has not been reported. The hotspot and hot channel factors are also required to be estimated for 217 pin bundle for comparing them with those estimated from safety analysis and finally arrive at the available safety margin. The possibility of extending the results of pin bundles with smaller number of pins to pin bundles with larger number of pins also need to be explored. These form motivation for the current research.

For the thermal hydraulic analysis of the helical wire wrap pin bundle, three dimensional conservation equations of mass, momentum and energy are solved using finite volume based CFD codes for a wide range of parameters. The computational time and memory required for a 217 pin bundle with 5 helical pitches is estimated to be very large. Hence, efforts were directed towards adopting a parallel CFD solver and a structured mesh generation tool for pin bundle analysis. In the present model standard k-ε High Reynolds turbulence model is employed. The computational model is validated against published experimental results reported for friction factor and Nusselt number. In order to develop deeper understanding of the effect of helical wire wrap induced transverse flow, to optimize the mesh density and to select the turbulence model, it is sufficient to study pin bundles with small number of pins.

Hence, in the first part of the research, CFD investigation of helical wire wrap 7 pin bundle is carried out in commercially available CFD codes. For a mean axial velocity of 8.0 m/s, the average value of cross stream velocity in the bundle is found to be ~ 0.7 m/s with a maximum value of ~ 2.2 m/s. This secondary flow velocity is maximum in the vicinity of the wire. It is found that the ratio of axial velocity to the transverse velocity is nearly equal to the tangent of the rolling up angle of the helical wire. This swirl flow occurring at the peripheral sub-channels is found to be periodic and is a function of wire position. It also increases the level of turbulence (which ensures a good mixing of the coolant). Hence, the frictional resistance to flow increases which increases the pressure drop through the bundle. It is found that the friction factor increases with decrease in helical pitch. This transverse flow due to the helical wire is found to be enhancing the heat transfer coefficient of coolant compared to straight wire pin bundle. Due to the wire wrap, the difference in bulk sodium temperature between the central and peripheral sub-channels is reduced when compared to straight spacer wire. The hot spot around the pins also gets reduced due to this. The predicted results are found to be in close agreement with that of the experimental results reported in open literature. The mixing characteristics of the flow among the peripheral and central zones are also compared for 7, 19 and 37 fuel pin bundles. It is found that the friction factor marginally increases with number of pins for fixed Reynolds number. It is seen that the Nusselt number also increases with number of pins in the bundle which is predominant in the turbulent regime compared to laminar regime. These are due to increased level of turbulence due to the transverse flow induced by the helical wire.

In the second part of the research, flow and temperature distributions of sodium in a helical wire wrap 217 pin fuel bundle with single and multiple pitches have been predicted using a customized CFD code. The friction factor is compared with the experimental results for 217 pin bundle and the correlations available in open literature. It is seen that the friction factor values in the turbulent regime obtained by CFD analysis matches with that of the experimental values within 2 %. The friction factor values in the laminar regime obtained by CFD analysis are higher (15 %) than that of the experimental values. Hence, the present model is best suited for turbulent flow through the pin bundle and can also be used for laminar regime with marginal over prediction. The Nusselt number at the exit of the bundle decreases with decrease in Reynolds number The Nusselt number obtained for 217 pin bundle using sodium as coolant is compared with experimental correlations for turbulent flow. The predicted Nusselt number in the turbulent regime is higher than the experimental correlation by 20 % and matches with the correlation in the laminar regime. The higher values of Nusselt number may be due to (a) shorter length of the pin bundle (200 mm), (b) due to the helical wire induced heat transfer from the pins which are not considered in the experimental correlation.

The ligament gap between the peripheral row of pins and hexagonal sheath is varied as a parameter. Reduction of this gap is found to reduce the flow bypass in the peripheral sub channels and increase in friction factor and Nusselt number marginally. Hence, the nominal ligament gap for the 217 pin bundle is retained.

The effect of helical wire wrap parameters on the flow and temperature distributions has also been investigated. It is seen that the transverse velocity is more with shorter helical pitches. Consequently, the value of friction factor is larger for shorter helical pitch for all values of Reynolds number. As expected, the Nusselt number is more for shorter helical pitch. Also, it is found that the transverse velocity is directly proportional to the wire diameter. Due to this, both the friction factor and Nusselt number increase with increase in wire diameter. Based on detailed parametric studies, correlations have been derived for estimation of Nusselt number in a 217 pin fuel bundle for a wide range of parameters of practical interest in fast reactor core design. As the friction factor and Nusselt number increase with decrease in helical pitch and increase in wire diameter, a helical pitch of 200 mm and wire diameter of 1.65 mm are found to be optimum, economical and also easy to manufacture.

Due to the enhancement of heat transfer coefficient by the transverse flow, the clad temperature is lower for shorter helical pitch. The clad temperature around the pin exhibits intense variation with alternate crests and troughs. These crests and troughs are strongly influenced by (i) the radial gap between the pin under consideration and the neighboring pin and (ii) cross flow velocity induced by the spacer wire. While a smaller radial gap increases the clad temperature, large cross stream velocity reduces the clad temperature. In the peripheral pins, clad temperature also decreases with decrease in helical pitch as the transverse flow is higher in the peripheral sub-channels. With larger wire diameters, the normalized clad temperature is lower due to enhanced heat transfer induced by higher cross flow.

The sodium temperature is higher in the central sub-channels and the same is lower in the peripheral sub-channels. It is seen that the sodium temperature difference between the central sub-channels in the eight rows of pin bundle and the peripheral sub-channels at the same hexagonal face is lower for shorter helical pitch which is attributed to the enhanced mixing due to higher cross flow for shorter helical pitch.

The hot spot factor and hot channel factor were estimated from the CFD studies. Their dependence on the number of pins, wire dimensions and helical pitch are also studied. Their variation along the flow direction (or along the length of the bundle) has also been investigated. The maximum sodium temperature occurs at the location beneath the wire wrap as well as in the minimum gap between the wire wrap and the neighboring fuel pin. It is seen that the hot spot factor increases with number of rows of pins. For example, it increases from 1.87 for a 19 pin bundle to 2.6 for a 217 pin bundle. The hot spot factor increases along the length due to reduction in Nusselt number along the length of the bundle. It is seen that the hot channel factor decreases with number of rows of pins. On the other hand, it decreases as axial length of the fuel bundle increases. It is found that the hotspot and hot channel factors are lower than that used in conventional safety analysis. This confirms the conservatism in the core design.

A simple relationship has been developed to predict the mean sodium velocities and temperatures of central and peripheral sub channels from the results of CFD study. From this relationship, it is possible to extend the results of pin bundle with small number of pins to pin bundle with large number of pins. The validity of this relationship has been verified by comparing the predictions against detailed CFD study.

LIST OF FIGURES

LIST OF TABLES

CHAPTER - 1

INTRODUCTION

1.0 FOREWORD

Fast reactor is one of the promising energy options for India. Hence, India pursues Research and Development activities in the domain of fast reactor technology. In this direction, a 40 MW thermal power Fast Breeder Test Reactor (FBTR) is being operational at Kalpakkam, India (Srinivasan et al. 2006). Following FBTR, a 500 MWe Prototype Fast Breeder Reactor (PFBR) is under the final stages of construction (Chetal et al. 2006). The flow sheet of a typical pool type fast reactor is depicted in Fig. 1.1 (a). A typical fast breeder reactor consists of three heat transport circuit viz., two sodium circuits to transfer the nuclear heat generated in the core to the steam-water system and convectional power plant circuit.

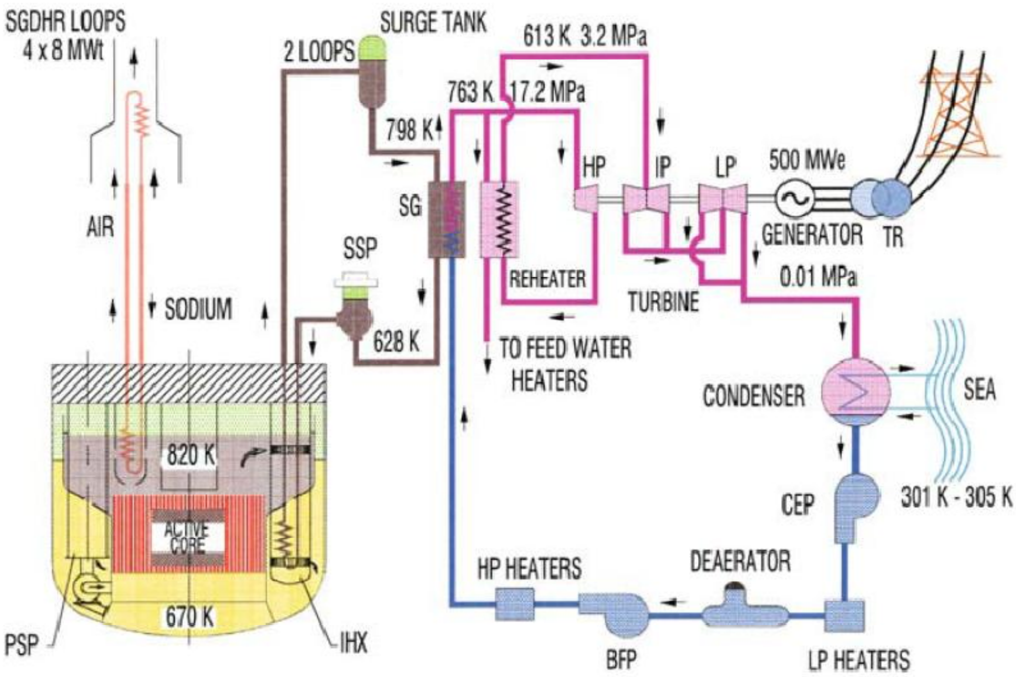

Fig. 1.1 (a) Flow sheet of typical pool type fast reactor

The close-up view of the primary circuit is depicted in Fig. 1.1 (b). Cold sodium at 670 K enters the bottom of the core subassemblies, cools the fuel pins in the core subassemblies while passing through them and finally transfers the heat to secondary sodium in Intermediate Heat Exchanger.

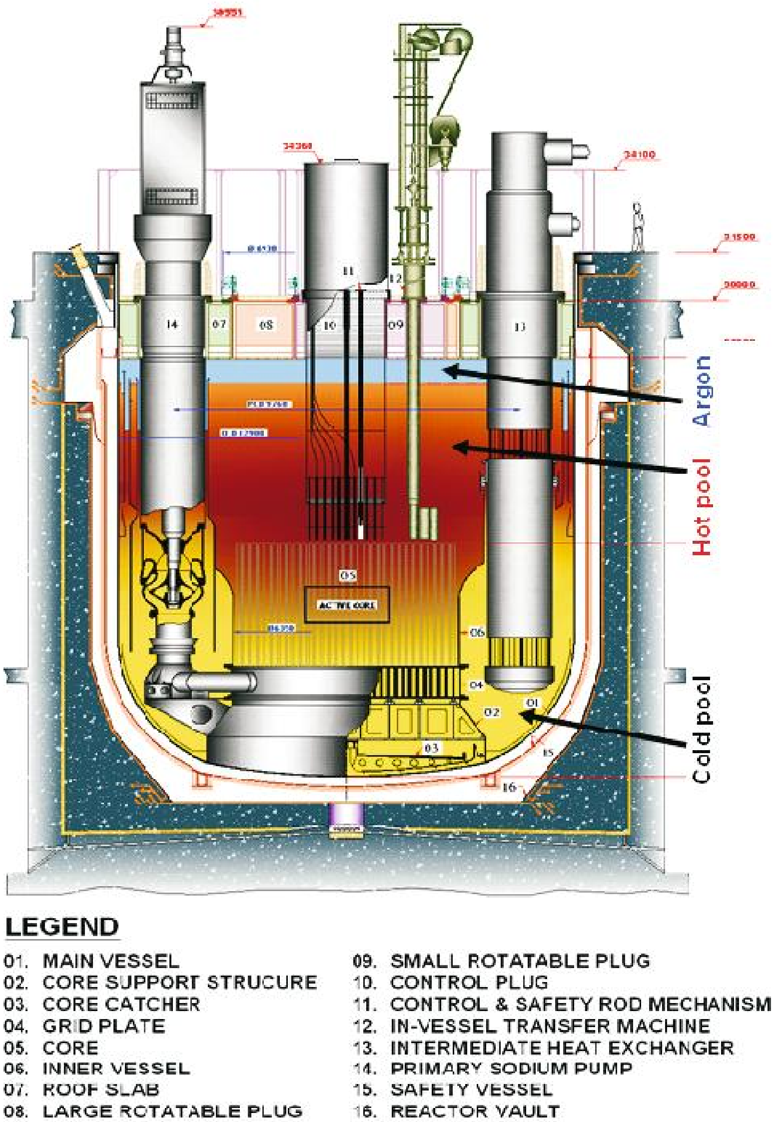

Fig. 1.1 (b) Vertical section of Primary circuit of typical Fast Reactor

1.1 THERMAL HYDRAULICS OF FUEL PIN BUNDLE

The fast reactors are characterized by high power density and compact core. To extract large heat flux without pressurizing the coolant, liquid sodium is used as coolant due to its high boiling point and large heat transfer coefficient. A typical medium size sodium cooled fast reactor fuel subassembly consists of 217 fuel pins kept as bundle inside a hexagonal sheath (Fig. 1.2 (a)). The fuel pins are wound with helical wire-wrap spacer to provide lateral support for the fuel pins and to provide space for sodium coolant to flow through the bundle. The fuel pins are arranged in a triangular pitch and the space between the adjacent fuel pins forms coolant sub-channels (Fig. 1.2 (b)). Due to helical wire-wrap spacer, the coolant not only flows in axial direction but also in a transverse direction. This transverse flow provides better mixing of coolant among the sub-channels. Due to this, the heat transfer coefficient of the coolant increases. Also, the hot spot around the pins gets reduced. But, the frictional resistance to flow also increases which increases the pressure drop through the bundle. Thus, thermal hydraulics of fuel pin bundle exhibit interesting and complex thermal hydraulic features such as (i) secondary flows, (ii) periodic flow exchange among the neighboring sub-channels, (iii) development of swirl flow in the peripheral sub-channels with magnitude varying as function of wire position, (iv) non homogeneous temperature variation among the sub-channels, (v) large circumferential variation in clad temperature and formation of hotspot etc. Experimental determination of these fine-scale features even in an ideal small pin bundle is highly challenging. On the other hand, CFD simulation of thermal hydraulics in pin bundle offers all these features in adequate detail.

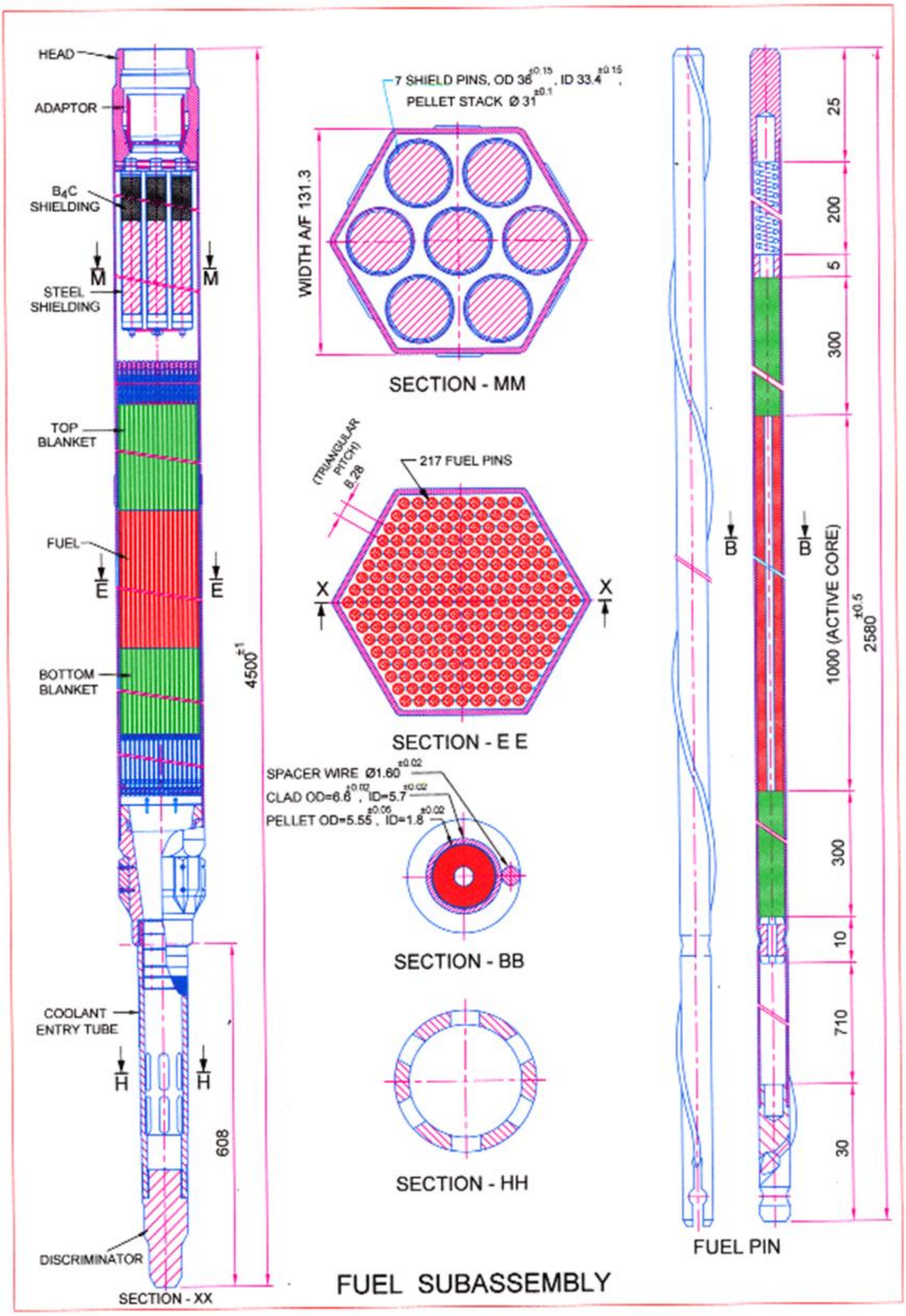

Fig. 1.2 (a) Fuel subassembly of a medium size fast breeder reactor

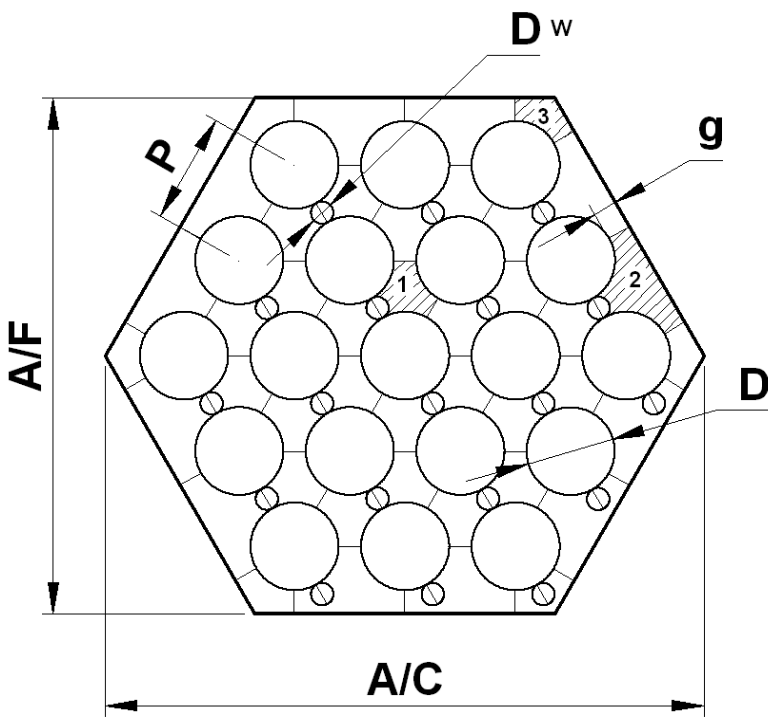

D – Pin diameter

D_w- Wire diameter

g - Ligament gap between the last row of pins and the hexagonal sheath.

P – Triangular pitch distance

A/F – Width across flats

A/C – Width across corners

1 – Central sub-channels

2 – Peripheral sub-channels

3 – Corner sub channels

Fig. 1.2 (b) Terminology and different types of sub-channels in a subassembly

Investigation of the physics of this complex flow and temperature distributions in a heat generating fuel pin bundle with helical wire from basic principles is very important for the design of the core. Towards this, three dimensional conservation equations of mass, momentum and energy are solved by using finite volume based commercial Computational Fluid Dynamics (CFD) codes for a wide range of parameters employing appropriate turbulence models. As a first step, multi-dimensional modeling of 7-pin bundle with one pitch helical spacer wire has been carried out using the CFD code STAR-CD, (2001). Using the CFD code CFDEXPERT, (2008), the flow and temperature distributions of sodium in 217 pin fuel bundle with helically wound spacer wire have been predicted. The results of the above thermal hydraulic analysis are investigated in the present thesis work. The effect of helical spacer wire on turbulent flow of sodium through the fuel pin bundle, the secondary flow created by the wire and the consequent mixing of sodium coolant have been studied. In order to assess the effectiveness of helical spacer wire and the associated penalty in terms of pressure drop, straight wire-wrap fuel pin bundle is also analyzed. Correlations for Nusselt number for 217 pin bundle with different helical pitch of the wire and wire diameters have been proposed. From clad and sodium temperature distribution, the hot spot factor and the hot channel factors are evaluated and compared with that used in safety analysis. The mixing characteristics of the flow and temperature among the peripheral and central zones and their dependence on number of fuel pins in the bundle are critically evaluated for a 217 pin bundle.

1.2 MOTIVATION FOR THE PRESENT STUDY

Traditionally, thermal hydraulics within the subassembly has been studied by (a) experiments using water as medium and in few cases using sodium as medium, (b) porous body models for pin bundle and (c) 3-Dimensional CFD studies with limited number of pins using 7, 19 and 37 pin bundle models. Experimental and porous body model studies do not provide adequate details of cross flow characteristics in the fuel pin bundle with helically wound spacer wire. On the other hand, 3-dimensional CFD studies are capable of providing intricate details about them. Number of CFD based numerical studies have been performed for bundles with smaller number of pins. However, studies with large fuel pin bundle such as 217 pins are not reported in open literature. Also, the Nusselt number correlation as a function of helical wire parameters has not been reported. In order to develop deeper understanding on the effect of helical wire wrap induced transverse flow, to optimize the mesh density, to select the turbulence model and finally to validate the CFD model, it is adequate to study pin bundles with small number of pins. But, studies on 217 pin bundle which is used in commercial FBRs is essential for the thermal hydraulic design of the subassembly including the development of correlations for friction factor and Nusselt number. The hotspot and hot channel factors are also required to be estimated for 217 pin bundle for validating the values used in one dimensional safety analysis and finally arrive at the available safety margin. The possibility of extending the results of pin bundles with smaller number of pins to pin bundles with larger number of pins also need to be explored. These form the motivation for the current research.

1.3 OBJECTIVES AND SCOPE OF THE THESIS WORK

The scope of this thesis work is basically computational in nature, wherein, the three dimensional conservation equations of mass, momentum and energy are solved using finite volume based commercial computational fluid dynamics codes for a wide range of parameters employing appropriate turbulence models. Encouraged by the requirement of detailed understanding of thermal hydraulic features, the following objectives have been identified.

- **a)** To investigate the physics of the complex flow and temperature distributions in a heat generating fuel pin bundle with helical wire from basic principles which is very relevant in core thermal design.
- **b)** To develop fundamental understanding in the thermal hydraulics of fuel pin bundle, computational simulation of bundle with small number of pins (7, 19 and 37) with one or two helical pitches.
- **c)** To quantify the magnitude of secondary flow generated by helical spacer wire and its influence on coolant mixing and its dependence on number of fuel pins in the bundle.
- **d)** To assess the effectiveness of helical spacer wire and the associated penalty in terms of pressure drop by comparing the results with that of straight wire-wrap fuel pin bundle.
- **e)** To study the thermal hydraulics of 217 pin fuel bundle using a parallel CFD solver.
- **f)** To understand the effect of helical wire wrap parameters (viz., helical pitch and wire diameter) on the thermal hydraulics of sodium in 217 pin fuel bundle.
- **g)** To develop correlations for Nusselt number as a function of helical wire parameters based on detailed parametric study.
- **h)** To estimate the adequacy of the ligament gap between the peripheral row of the pin bundle and hexagonal sheath and commend the size of the hexagonal sheath.
- **i)** To suggest the optimum helical wire -wrap pitch length and wire diameter.
- **j)** To determine the hot spot factors from the clad and sodium temperature distributions in 217 pin fuel bundle and compare them with traditional values used in safety analysis and arrive at the available safety margin.
- **k)** To extend the results of 7, 19 and 37 pin bundle to 217 pin bundle and compare them with the actual results of 217 pin bundle.

1.4 ORGANIZATION OF THE THESIS

The thesis is divided into five major parts. The first part introduces the research topic along with motivation and objectives of the present study in Chapter-1. The second part comprises of detailed literature review in chapter-2 while the mathematical model and solution method are presented in Chapter-3. The third part comprises of basic studies on bundles with small number of pins, viz., (i) study of 7 pin bundle in Chapter-4 and (ii) the comparative study of 19, 37 and 91 pin bundles in Chapter-5. The fourth part comprises of (i) detailed parametric study of 217 pin bundle employing a parallel CFD code in Chapter-6, (ii) the effect of helical wire parameters in Chapter-7 including development of correlations for Nusselt number in the pin bundle and (iii) the clad and sodium temperature distributions in Chapter-8. The final part of the thesis comprises of (i) the study of hot spot factors in the bundle, its comparison with that used in safety analysis in Chapter-9, (ii) the study of extendibility of 7, 19 and 37 pin bundles results to 217 pin bundle in Chapter-10, and (iii) conclusions of the thesis in Chapter-11.

CHAPTER - 2

LITERATURE REVIEW

2.0 INTRODUCTION

The thermal hydraulics of coolant flow through fast reactor fuel pin bundle is being studied for the past 50 years. As India also pursuing the fast reactors in its second stage of nuclear program, the study of fast reactor fuel pin bundle thermal hydraulics is very important in the Indian context. Many commercial fast reactors use helical wire wrap as the spacers in the fuel pin bundle (Walter and Reynolds, 1981). The helical wire is easy to manufacture and less expensive compared to other types of spacers. Further, mechanical vibrations and hence possibility of reactivity oscillations are minimized by using wire wraps. The wire-wrap design also enables better thermal mixing of coolant due to transverse flow induced in the pin bundle which enhances heat transfer at the expense of the friction factor of the pin bundle. Numerous water experiments have been carried out for the pin bundle as early as 1980. Limited sodium experiments have been carried out with fewer pins. Vast number of numerical studies has been carried out earlier using the sub-channel approach. Recently, the investigation of thermal hydraulics is being carried out using Computational Fluid Dynamics codes. A comprehensive literature review on the thermal hydraulics of helical wire wrapped pin bundle has been carried out and is presented in this chapter.

2.1 WATER EXPERIMENTS

An experimental study of pin bundle with various helical wire parameters using water as the working fluid was carried out by Rehme (1973 and 1987). The helical pitch of the wire spacer was varied from 100 to 600 mm. The ratio of the triangular pitch of the pins to the diameter of the pins was varied from 1.125 to 1.417. The number of pins was varied from 7 to 19 with a pin diameter of 12 mm. The friction factor for various combinations of the wire diameter and helical pitch has been plotted against the Reynolds number. Novendstern (1972) presented a pressure drop model developed by him using experimental data and ideas of Rehme (1973 and 1987) and others. This model determines the flow distribution between the fuel pins theoretically, and multiplies the pressure drop for a smooth pipe, using equivalent diameter techniques, by an empirical correction factor. This empirical factor depends on fuel pin dimensions and flow rate. Chen and Todreas (1986b) correlated wire wrap pressure losses utilizing the much larger database existing in the literature based on experimental studies up to 1984. Very useful friction factor correlations for laminar, transition and turbulent flow regimes and calculation of hydraulic diameter with wire-wrapped pin bundle has been presented by Chen et al. (2014). The transition regime correlations have been modified by Chen et al. (2013). Hydraulic experiments on a helical wire wrapped 91 pin bundle of 2/1 scale model of Fast Flux Test Facility fuel Subassembly are presented by Lorenz et al. (1974) and Lorenz and Ginsberg (1977). Pressure drop offered by the 217 pin fuel subassembly has been reported by Roychowdhury et al. (1998).

2.2 FLOW DEVELOPMENT IN THE BUNDLE

Due to large heat transfer coefficient and friction factor in the entrance region, a detailed survey of literature on flow and temperature developments in channels and tubes can be found in Shah and London (1978), Feldman et al. (1982) and Velusamy et al. (2010), Manglik (1988, 1996). All these studies dealing with straight channels indicate that both the friction factor and heat transfer coefficient decrease monotonically along the flow direction in the developing region to stabilize to a constant value in the fully developed region. Acharya et al. (1993) studied the flow through coiled tubes and found that the Nusselt number in the entrance region falls well below the fully developed value. But, in the developed region, the heat transfer coefficient and friction factor are constant. The complex interaction between growth of boundary layer along the duct wall and the development of secondary flows due to coiled geometry of tubes, leads to this non-monotonic variation (Govindarasu et al. 2014).

2.3 SODIUM EXPERIMENTS

It is known that the viscosity of sodium at 673 K is nearly equal to the viscosity of water at 363 K. This feature of sodium is very helpful in the hydraulic studies of the flow in fuel pin bundle using water as medium. But, the heat transfer coefficient is a strong function of Prandtl number and experimental determination demands the use of sodium itself as the simulant. It is known that sodium experiments are difficult to conduct, due to the violent exothermic reaction of sodium with air. Also, sodium experiments need to be performed at elevated temperatures, as its solidification temperature is close to 371 K. To compound these difficulties, sodium is opaque offering little scope for flow visualization. The hydraulic diameter of the sub-channels being of the order of a few mm, small scale experimental mock-ups having identical geometric similarity is very difficult to manufacture. In addition to this, measurement of fine details of flow and temperature within small sub-channels calls for non-intrusive type instruments with their associated limitations for use in high temperature environment, adequate number of measurement locations, reliable calibration, etc. Hence, the temperature simulation using experiments in sodium is highly prohibitive. In spite of the difficulty associated with sodium experiments, a few experimental studies have been carried out in the past with a small number of fuel pins in bundle so that the quantity of sodium handled is kept minimum. Sodium experiments with large number of pins are highly restricted as the quantity of sodium to be handled will be high. An experimental study of thermal hydraulics of sodium in an electrically heated 7 pin bundle has been carried out by Collingham et al (1970). It was observed that the coolant flow and mixing around a wire wrap was sufficient to prevent a severe hotspot beneath a wire wrap. It was also observed that the helical wire wrap causes a forced diversion of the coolant between inner and outer sub-channels. Due to this sweeping mechanism, the bulk coolant temperature difference between the sub-channels reduces by 50 % compared to the value in the case of without wire. In heat transfer experiments, the heat is supplied to the coolant in two ways. Heat is supplied to the wall either by constant temperature or by constant heat flux. The fully developed Nusselt number is identical in both method of heat supply for turbulent flow conditions. But, for laminar flow through pipe, the fully developed Nusselt numbers are different. It is 4.36 for pipe flow with constant heat flux boundary condition and 3.66 with constant temperature boundary condition (Cengel, 2007). Rensen (1981) carried out sodium experiment with hollow pipe and reported the results for thermal entrance region as well as fully developed region. He has concluded that the Reynolds number has an appreciable influence on the heat transfer to liquid sodium in the thermal entrance region and thermal entrance length for turbulent flow of liquid sodium is much greater than that for laminar flow. Also, the Prandtl number has only a little influence on the variation of local Nusselt number of liquid metal. An experimental study of intra subassembly (19 pin bundle) and inter subassembly (61 pin bundle) heat transfer during natural circulation decay heat removal in fast breeder reactors has been carried out by Kamide et al (1998). As the temperature distribution presented is for natural convection flow, this is not applicable for the forced convection flow considered in this thesis. A transient experiment on fast reactor core and a numerical analysis of intra subassembly and inter subassembly heat transfer has been carried out by Nishimura et al. (2000) using a simplified model for mixing of sodium due to wire wrap spacer in the 19 pin bundle developed by Chen and Todreas (1986b). A review of liquid metal heat transfer data and correlations for tube bundles has been carried out by Mikityuk et al. (2009). A useful Nusselt number correlation for sodium cooled pin bundle within a hexagonal sheath has been presented by Kazimi and Carelli (1980).

2.4 NUMERICAL STUDY BASED ON SUB-CHANNELS APPROACH

In order to determine the sodium flow distribution in the pin bundle with helical wire spacer and predict the temperature distribution including the maximum clad temperature to respect its permissible limit, detailed thermal hydraulic computations need to be carried out. Two calculation methods or geometrical modeling are generally used. The first one uses the sub-channel notion. The central sub-channels formed by the central pins are triangular in shape. The gap between the outer rows of the pins and hexagonal wrapper is divided into rectangular edge sub-channels and quadrilateral corner sub-channels. For each of these sub-channels, pressure, velocity and temperature are averaged on space. This approach requires physical models from theoretical and experimental data. These sub-channels are divided into a large number of divisions in the axial direction. The velocity and temperature distributions in the fuel subassembly are obtained by solving the conservation equations of mass, momentum and energy. The exchange of mass, momentum and energy among the various sub-channels is defined explicitly based on geometrical parameters of the pin bundle with the exchange coefficients derived from experimental data. These models do not offer detailed circumferential variations of flow and temperature around each and every fuel pin, which are essential for design optimization. Also, the sub-channel analysis cannot provide data on detailed flow and temperature distributions which are essential to have a realistic estimate of the parameters. Khan et al. (1975) developed a simplified porous body based computational tool. Later, Mikic et al. (1977) developed a graphical method to provide engineering estimates of temperature distributions in wire wrapped fuel subassemblies. The results of this analytical method compared well with numerical estimates of Khan et al. (1975). Simultaneously, several sub-channel based codes have been developed for thermal hydraulic analysis of LMFBR subassemblies, viz., COBRA (Rowe, 1973), ORRIBLE (Wantland,

1974) and SUPER-ENERGY (Chen and Todreas, 1986a). The evaluation of clad temperature for RAPSODIE, PHENIX and SUPER-PHENIX fuel pin bundles is achieved by calculation based on the simplified theoretical and experimental studies (Asty, 1993). These models are applicable only for forced convective flows and not suitable for natural / mixed convection conditions.

2.5 COMPUTATIONAL FLUID DYNAMICS STUDIES

The second approach based on Computational Fluid Dynamics (CFD) uses a refined mesh in the computational domain wherein flow and temperature fields are solved in the entire subassembly. This approach requires a large computer memory but is essential for a quantitative analysis. The thermal hydraulics within the subassembly has been studied either by a porous body model or by experiments. Both these classes of studies do not provide details of cross flow distribution in a fuel bundle with helically wound spacer wire. Determination of axial and transverse velocity distributions created by the helical wire wrap is also difficult to obtain from hydraulic experiments. The CFD based study attempts to fill this gap. The CFD based thermal hydraulic investigation of the pin bundle with accurate geometrical and physical models is akin to a practical experiment with measurement of parameters at every point of the pin bundle model. While there are no assumptions and simplifications, the complex thermal hydraulic characteristics of the subassembly are predicted from fundamental principles by numerically solving the 3-Dimensional conservation equations of mass, momentum and energy with a suitable turbulence model. CFD approach has got more maneuverability to alter the geometrical parameters of the bundle, when the geometry of the pin bundle undergoes irradiation induced dilation during its service in the core. The CFD model can be utilized to predict the thermal hydraulic characteristics under various possible conditions with ease, once the model is validated for one particular condition. CFD based models offer such a possibility for pin bundles of experimental reactors due to the advent of enhancements in computing power and advancement in CFD solution methodologies. Valentin (2000) presented details of modeling and qualification details of a new fuel subassembly concept by studying the thermal hydraulics of pin bundle with helical wire wrap spacer. His study focuses two main objectives: the first to achieve optimum performances of fuel subassembly and hence the whole core and the second to respect safety on the clad temperature (and the hexagonal sheath) to avoid mechanical failure. He brought out the fact that for implementing the new concepts in the fuel subassembly design, the physical modeling and the computer codes must be qualified. This qualification must address global and local thermal hydraulics of the pin bundle and mixing of the coolant due to wire warp spacer which imposes local thermal hydraulic couplings between sub-channels of the bundle. This warrants exact modeling of the fuel pin with helical wire with adequately refined meshing and solution of 3-D conservation equations, coupled with a suitable turbulence model. Numerical simulation for Pressurized water reactor fuel bundles with spacer grids have been attempted (Weber, 2005) with 64 million computational cells in parallel computing machines. The flow conditions normally encountered in a nuclear reactor core are highly turbulent. The complex physics of coolant flow through the fuel pin bundle requires advanced modeling techniques (Fanning et al. 2007). Hazi (2005) performed numerical studies to identify suitable turbulence model for the analysis of rod bundle. The cross flow encountered in rod bundle renders pipe flow correlations inaccurate when applied to rod-bundle geometry based on equivalent diameter. Large eddy simulation of flow around a wire wrapped fuel pin has been carried out by Fischer et al. (2007). The time averaged flow structures predicted by LES are found to be in good agreement with RANS (Reynolds Averaged Navier-Stokes model) simulation performed by Ahmad and Kim (2005), Chandra et al. (2009) and Chandra and Roelofs (2011). This indicates that numerical simulation of thermal hydraulics does not require complex turbulence models, as supported by the findings of Smith, et al. (2008) and Pointer, et al. (2008). The capabilities of the general purpose RANS based turbulence models for prediction of fluid dynamic characteristics in a wire wrap fuel assembly containing 7, 19 or 37 pins have been investigated by Smith et al. (2009). A Comparative Analysis of Flow and Convective Heat Transfer between 7-Pin and 19-Pin Wire-Wrapped Fuel assemblies has been carried out by Raza and Kim, (2008). The effects of wire spacer shape on thermal hydraulic performance of sodium coolant in a 7 pin wire wrapped fuel assembly has been studied by Wasim Raza and Kim, (2008). Three different cross-sectional shapes of wire spacer, namely, circle, hexagon and rhombus have been tested. It is found that circular shape wire spacer provides obvious advantages in overall pressure drop, maximum temperature and uniformity of temperature in the assembly in comparison with other two shapes. The effect of pin-wire contact modeling during flow over wire -wrapped pin bundle was studied by numerical simulation using LES by Merzari et al. (2012). It was found that the contact modeling is important from the point of view of hotspot factor. It was also found that CFD study using RANS based turbulence models are sufficient to predict the thermal hydraulics of the wire wrapped bundle. The use of standard k-ε type turbulence models, which are computationally efficient, is adequate for forced convective regime (Spalding and Launder, 1974).

In the case of liquid metals such as sodium, the molecular diffusion is very large. In comparison with the conventional fluids such as water and gas, liquid sodium has very low Prandtl number Viz. 0.005. In RANS model, the turbulent Prandtl number is assumed to be equal to unity for fluids whose Prandtl number (Pr) lies in the range $0.5 < Pr < 5$. For fully turbulent flows, Reynolds analogy is valid for sodium flows also. A constant value of 4 for turbulent Prandtl number is suggested for sodium pipe flows when $Pe < 1000$ (Fei Chen et al. 2013). As this is found to be much higher than 2 predicted by LES/DNS (Laurent Bricteux et al. 2010), the correct value of turbulent Prandtl number is still under research.

Three dimensional conjugate heat transfer calculation in a 7 pin wire wrap was performed by Peniquel et al. (2009) using unstructured and polyhedral meshes. The hydraulic and thermal performance of 19 pin with helical wire wrap is studied both by experiments and CFD simulation by Fricano et al. (2014). They have tested different turbulence models viz. high Reynolds number standard k-ε, the low Reynolds number version of the k-ε model and k-ω model by carrying a CFD study in 19 pin bundle and found that similar outlet temperature profiles were produced by all the models. Hence, the standard k-ε turbulence model was selected by him as reference model to validate the experimental results of 19 pin bundle. The CFD investigation of thermal hydraulic performance of helical wound wire wrap pin bundles with 7, 19 and 37 rods has been carried out with unstructured tetrahedral mesh using commercially available software with limited computer processing and memory capabilities (Gajapathy et al. 2007, 2009). The predicted friction factor values were compared with Rehme's experimental data and Novendstern's correlation. It was found that the wire wrap induces transverse velocity which makes the outlet coolant temperature distribution more uniform. The thermal hydraulic performance of 19 pin bundle using structured grid has been studied using commercially available software for various helical pitches by Natesan et al. (2010). A representative brief literature review on the thermal hydraulics of helical wire wrapped pin bundle is presented in Table. 2.1.

2.6 CLOSURE

A detailed literature survey indicates that thermal hydraulics within the subassembly has been studied by (a) experiments using water as the medium and in few cases using sodium as the medium, (b) porous body models for pin bundle and (c) 3-Dimensional CFD studies with limited number of pins viz. 7, 19 and 37 pins. It is seen that water experiments have been carried out to estimate pressure drop in wire-wrap bundle which can be adopted for hydraulics of sodium. But, only a limited number of sodium experiments have been reported for a 7 pin bundle. Traditionally, the sub channel model has been adopted for fast reactor thermal hydraulics to predict mean flow and temperature characteristics. The hotspots are accounted by using a hotspot factor approach. Although, CFD based numerical studies have been performed for bundles with limited number of pins, studies with large fuel pin bundle such as 217 pins are not reported. Also, correlations for Nusselt number as a function of helical wire parameters have not been reported. In this thesis, the thermal hydraulic analysis of 217 pin bundle which is used in commercial FBRs is carried out and correlations for friction factor and Nusselt number as a function of helical wire dimensions have been proposed. In addition, the hotspot and hot channel factors have been estimated for 217 pin bundle and available safety margin has been arrived at.

Table 2.1: Literature on thermal hydraulics analysis of helical wire-wrapped pin bundle

Reference	Focus of the study / Findings
Rehme, 1973 and 1987	The experimental results of hydraulic study of 7, 19 and 37 pin bundle with various helical pitch and wire parameters using water as the working fluid is presented.
Novendstern, 1972	Presented a pressure drop model developed by him using experimental data and ideas of Rehme .
Chen and Todreas,1986b, Chen et al. (2013, 2014)	Very useful friction factor correlations for laminar, transition and turbulent flow regimes and calculation of hydraulic diameter with wire-wrapped pin bundle have been presented. The transition regime correlations also have been modified.
Lorenz et al. 1974	Hydraulic experiments on a helical wire wrapped 91 pin bundle of 2/1 scale model of Fast Flux Test Facility (FFTF) FSA are presented.
Roychowdhury, et al 1998	Experimental data of Pressure drop in 217 pin wire wrap bundle has been reported.
Collingham et al. 1970	An experimental study of thermal hydraulics of sodium in an electrically heated 7 pin bundle had been carried out. It is observed that the coolant flow and mixing around a wire wrap was sufficient to prevent a severe hotspot beneath a wire wrap.
Khan et al. 1975	Developed a simplified porous body based computational tool.
Chen and Todreas, 1986a, Rowe 1973,	Several sub-channel based codes have been developed for thermal hydraulic analysis of LMFBR subassemblies, viz., COBRA, SUPER-ENERGY.
Fanning et al. 2007	Performed numerical studies to identify suitable turbulence model for rod bundle.
Fischer et al. 2007	Large eddy simulation of flow around a wire wrapped fuel pin has been carried out.
Ahmad and Kim, 2005 Smith et al. 2008.	The time averaged flow structures predicted by LES are found to be in good agreement with RANS simulation performed. This indicates that numerical simulation of flow hydraulics does not require complex turbulence models.
Gajapathy et al. 2007,2009	CFD studies of 7 pin bundle with and without wire-warp, comparison of 7, 19 and 37 pin bundles have been carried out.
Wasim Raza and Kim, 2008.	The effects of wire spacer shape on thermal hydraulic performance of sodium coolant in a 7 pin wire wrapped fuel assembly has been studied.
Natesan et al. 2010	The thermal hydraulic performance of 19 pin bundle using structured grid has been presented with grid sensitivity study and validation for friction factor and Nusselt number.
Mikityuk, et al. 2009	A review of liquid metal heat transfer data and correlations for infinite array of tube bundles has been presented
Kazimi and Carelli 1980, 2012	A Nusselt number correlation for sodium cooled pin bundle within a hexagonal sheath has been presented.

CHAPTER - 3

MATHEMATICAL MODEL AND SOLUTION METHOD

3.0 INTRODUCTION

The details of governing equations, associated boundary conditions, mesh generation, turbulence model and validation of the numerical model for the CFD investigation of helical wire-wrap fast reactor fuel pin bundle are presented in this chapter.

3.1 MESH GENERATION

The geometric complexity associated with line contact between the pin and wire is overcome by providing a radial offset of 0.05 mm for the wire towards the center of the pin. By this approximation, the line contact between the rod and the wire gets converted into surface contact and the point contact between the wire and the hexagonal sheath is converted into a minimum clearance region. This approximation does not alter the pressure drop and heat transfer characteristics of the wire-wrap bundle significantly (Gajapathy et al. 2007, Sreenivasalu et al. 2008). Structured computational mesh for the bundle has been generated using multi-block mesh generation approach. Meshes for a single pin with its wire-wrap along with a symmetric region surrounding the pin are formed by a combination of six multi-blocks to form a hexagonal block structure. These hexagonal blocks are then combined together to generate the structured mesh for the whole domain. Clustering of grid near the wall and smoothening are carried out to generate the final mesh structure used for the analysis. Fig. 3.1 (a) shows the computational mesh developed for a 7 pin bundle and its isometric view depicted in Fig. 3.1 (b). The structured mesh on a single pin with its wire-wrap is shown in Fig. 3.1 (c). Detailed view of the mesh structure surrounding a pin at an axial location where the wire comes closest to the neighboring pin is shown in Fig. 3.1 (d). The interference between the pin, its wire and neighboring pins is clearly evident from these figures. Figure 3.1 (e) shows the computational mesh developed for 217 pin bundle and its isometric view is shown in Fig. 3.1 (f).

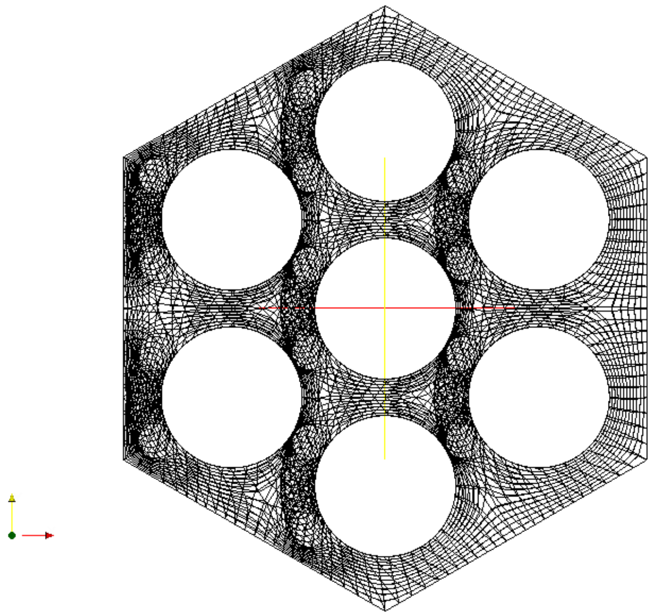

Fig.3.1 (a) Cross stream structured mesh for a 7 pin bundle.

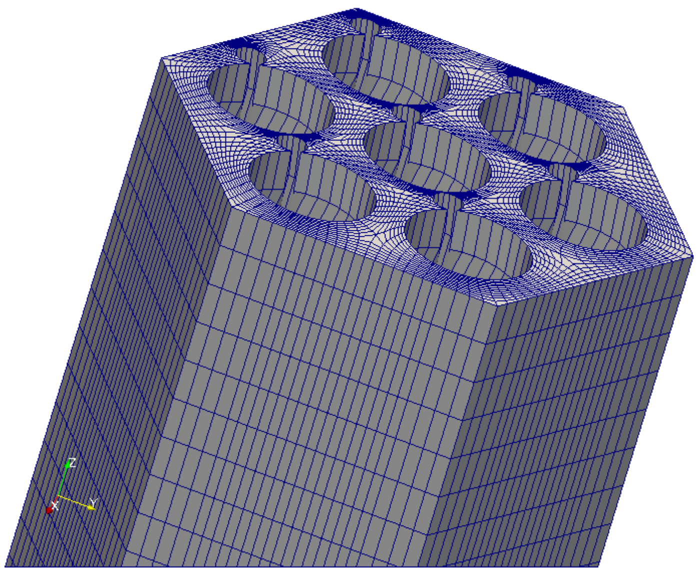

Fig. 3.1 (b) Isometric view of structured mesh pattern of 7 pin bundle

Fig. 3.1 (c) Structured mesh over the pins and helical wire

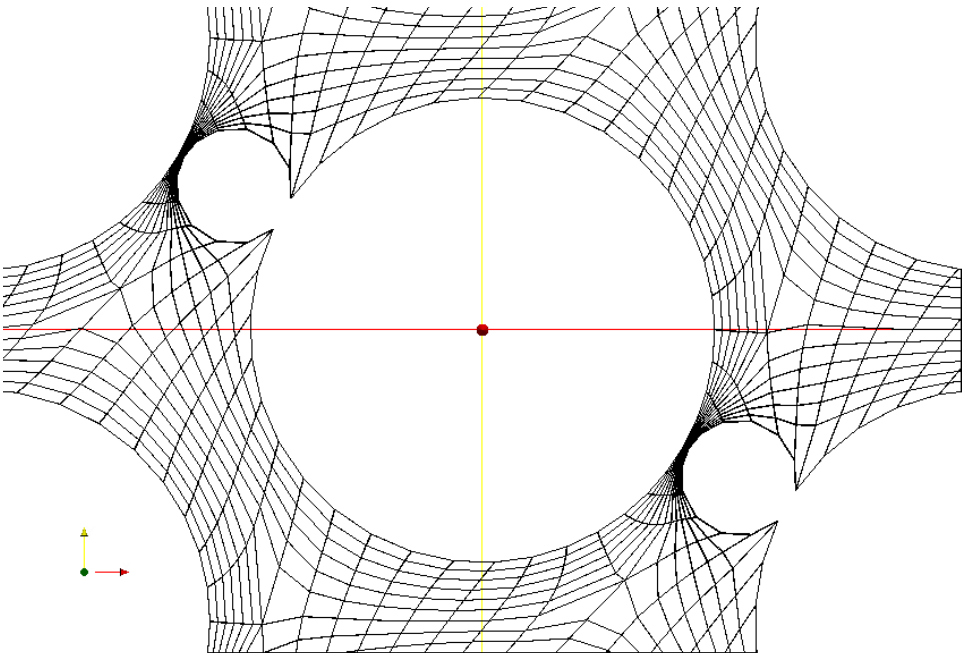

Fig. 3.1 (d) Mesh pattern in the vicinity of wire and pin in helical wire wrapped pin bundle

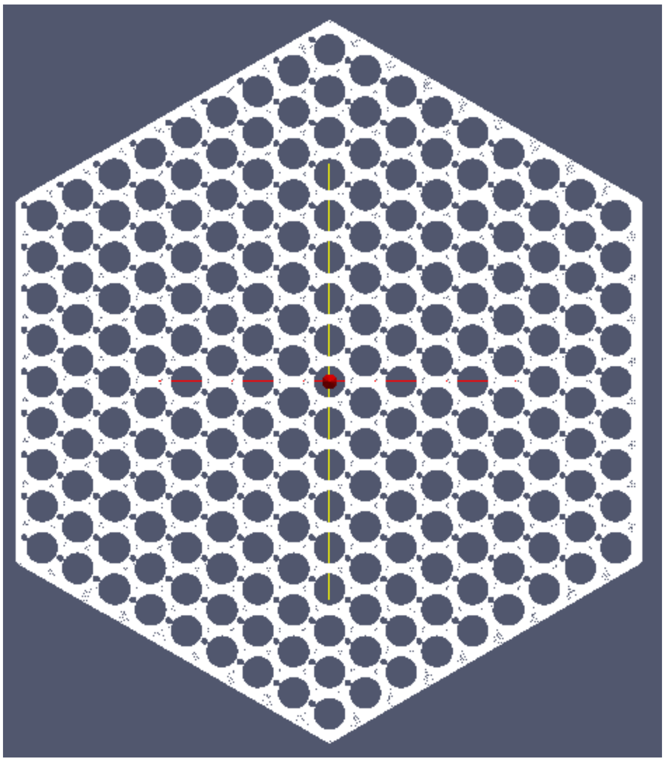

Fig. 3.1 (e) Cross stream structured mesh for a 217 pin bundle

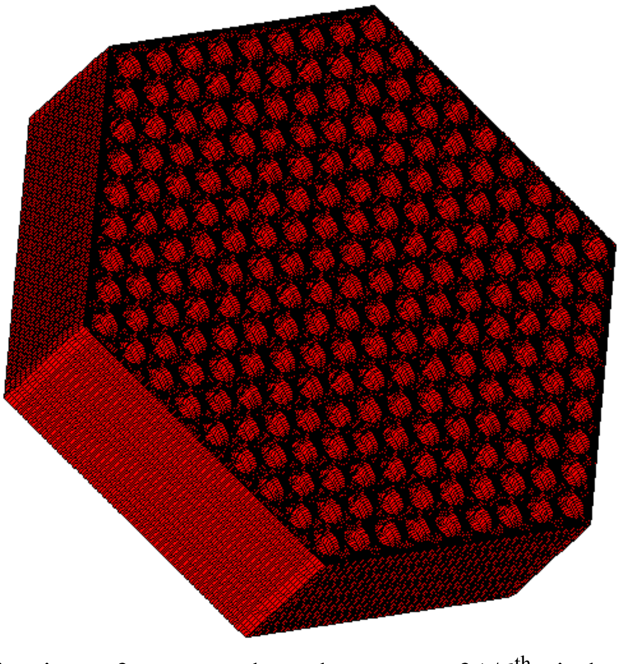

Fig. 3.1 (f) Isometric view of structured mesh pattern of 1/6th pitch of a 217 pin bundle

Models of 217 pin fuel bundle with various helical pitch of the spacer wire, viz., 100 mm, 200 mm and 300 mm have been obtained using customized mesh generation software GridZ (CFD EXPERT, 2008), by keeping the nominal pin diameter as 6.6 mm arranged in a triangular pitch of 8.28 mm. The nominal helical wire diameter is 1.65 mm with a nominal helical pitch of 200 mm. The helical pitch is varied from 100 mm to 300 mm. The helical wire diameter is varied from 1.25 mm to 2.0 mm. The number of cells for 7 pin bundle with a length of 200 mm is 0.1 million whereas for 217 pin bundle, it is 6.6 million.

3.2 GOVERNING EQUATIONS

The equations that govern steady state sodium flow and heat transfer process in the pin bundle are (Hughes and Gaylord, 1964):

Continuity

$$\frac{\partial}{\partial x_j}\left(\rho u_j\right)=0 \tag{3.1}$$

Momentum

$$\frac{\partial}{\partial x_j}\left(\rho u_j u_i-\tau_{ij}\right)=-\frac{\partial p}{\partial x_i} \tag{3.2}$$

where

$$\tau_{ij}=2\mu s_{ij}-\frac{2}{3}\mu\frac{\partial u_k}{\partial x_k}\delta_{ij}-\rho\overline{u_i^{'}u_j^{'}}$$

$$s_{ij}=\frac{1}{2}\left(\frac{\partial u_i}{\partial x_j}+\frac{\partial u_j}{\partial x_i}\right)$$

Energy

$$\frac{\partial}{\partial x_j}\left(\rho u_j c_p T-F_{h,j}\right)=0 \tag{3.3}$$

where

$$F_{h,j} = K\frac{\partial T}{\partial x_j} - \rho c_p \overline{u_j^{'}}\overline{T^{'}}$$

The turbulence is modeled with the standard k-ε model (Launder and Spalding, 1974) with wall functions in the present model. The details of selection of turbulence model is presented in section 3.6

The transport equation for turbulence parameters are:

Turbulent kinetic energy

$$\frac{\partial}{\partial x_j}\left[\rho u_j k - \left(\mu + \frac{\mu_t}{\sigma_k}\right)\frac{\partial k}{\partial x_j}\right] = -\rho\varepsilon - \frac{2}{3}\left(\mu_t\frac{\partial u_i}{\partial x_i} + \rho k\right)\frac{\partial u_i}{\partial x_i} \tag{3.4}$$

Turbulent dissipation rate

$$\frac{\partial}{\partial x_j}\left[\rho u_j \varepsilon - \left(\mu + \frac{\mu_t}{\sigma_\varepsilon}\right)\frac{\partial \varepsilon}{\partial x_j}\right] = C_{\varepsilon 1}\frac{\varepsilon}{k}\left[-\frac{2}{3}\left(\mu_t\frac{\partial u_i}{\partial x_i} + \rho k\right)\frac{\partial u_i}{\partial x_i}\right] - C_{\varepsilon 2}\rho\frac{\varepsilon^2}{k} \tag{3.5}$$

In this version of the turbulence model, the wall function approach is followed to capture the boundary layers adjacent to solid walls. This approach is computationally economical as it obviates the need for using fine mesh around the solid walls to resolve the steep velocity / temperature gradients within the laminar sub-layer and the buffer layer. In the present simulations, the following wall function treatment is adopted within the boundary layer:

$U^+ = Y^+$ for $Y^+ \le Y_m^+$ $\quad U^+ = \frac{1}{K}\ln(E^* Y_m^+)$ for $Y^+ > Y_m^+$

Where $Y_m^+ = \frac{1}{K}\ln(E^* Y_m^+)$ and $Y^+ = \frac{U_\tau \times Y}{\nu}$

$$U^+ = \frac{U}{U_\tau} \quad \text{Where} \quad U_\tau = \left(\frac{\tau_w}{\rho}\right)^{\frac{1}{2}} \quad \text{and} \quad \tau_w = \mu \frac{\partial u}{\partial y}$$

Various constants used in the turbulence model are presented in Table 3.1 and the meaning of various symbols is explained in Nomenclature.

Table 3.1 : Coefficients of the Standard k-ε Turbulence model

C_μ	σ_k	σ_ε	σ_m	σ_h	$C_{\varepsilon 1}$	$C_{\varepsilon 2}$	$C_{\varepsilon 3}$	$C_{\varepsilon 4}$	K	E
0.09	1.0	1.22	0.9	0.9	1.44	1.92	1.44	-0.33	0.419	9.0

As per this treatment, it is seen that the non-dimensional distance of near wall cell center from wall surface Y^+ lies in the range of 30 to 40. Second order up-wind scheme is adopted for combining convective and diffusive fluxes in all the transport equations. The above set of governing equations is solved by the finite volume based parallel solver CFD code FlowZ (CFDEXPERT 2008). The pressure-velocity coupling in the incompressible flow formulations is resolved using the SIMPLE algorithm (Patankar, 1980). To declare convergence, tolerance on the residual values for all the governing equations is set as 10^{-5}.

3.3 BOUNDARY CONDITIONS

The boundary conditions imposed on equations (3.1) - (3.5) for the study of thermal hydraulic analysis of 217 pin bundle are presented in Fig. 3.2. In the hydraulic study, the boundary conditions of no-slip (u = v = w = 0) on the surfaces of the pins and the hexagonal sheath are applied for flow modeling. The inlet is specified with uniform velocity and constant temperature of 670 K. While at the outlet, pressure boundary conditions are imposed. The inlet turbulence intensity and the eddy viscosity ratio are set equal to 2.0 and

10.0 respectively. The pressure drops are computed for different Reynolds number in the range of 2500 to 1, 00,000. For Reynolds numbers less than 2500, laminar model is used and for Reynolds numbers higher than 4000 high Reynolds number standard k-ε turbulence model is used with standard wall functions, Walter and Reynolds (1981). In the thermal study, by specifying heat flux over the fuel pins and no heat flux over the wire, sodium temperature distribution is found out. The hexagonal sheath is adiabatic. The pin surfaces are specified with constant heat flux of 1850 kW/m^2. This corresponds to the fuel subassembly at full power with 8.3 MW. The Peclet number corresponding to the flow of 38 kg/s is ~500. Sodium properties at mean temperature of the sodium coolant (773 K) are specified in the computations. Density = 850 kg/m^3, Kinematic viscosity = 0.29×10^{-6} m^2/s, Thermal conductivity = 60 W/m-K and Specific heat = 1.27 kJ/kg K. In all the studies with different helical pitch and wire diameters, the Reynolds number is kept constant and the fuel pin heat flux is specified in proportion to Reynolds Number. In the case of bundle with different wire diameters, the inlet velocity is different depending upon their equivalent diameter. Also, the heat flux value is varied to keep the outlet temperature constant.

3.4 CALCULATION OF FRICTION FACTOR AND NUSSELT NUMBER

In the hydraulic study, the equivalent diameter and friction factor for different flow regimes are calculated based on the sodium flow area in the pin bundle and the perimeters of the pins, wire and hexagonal sheath as prescribed by Chen et al (1986, 2014) in Appendix A. The hydraulic diameter of the 217 pin bundle with 1.65 mm wire diameter is 3.83 mm. This is same for various cases of helical pitch. The hydraulic diameter for wire diameters of 1.25 and 2.0 mm are 3.22 mm and 4.32 mm respectively. The ratio of triangular pitch to pin diameter for various wire diameters are 1.19, 1.255 and 1.314 for wire diameters of 1.25, 1.65

and 2.0 mm respectively. The hydraulic diameter of the 217 pin bundle without spacer wire is 5.0 mm. In the thermal study, in the case of annular duct with heated inner duct, the equivalent diameter is taken as the hydraulic diameter.

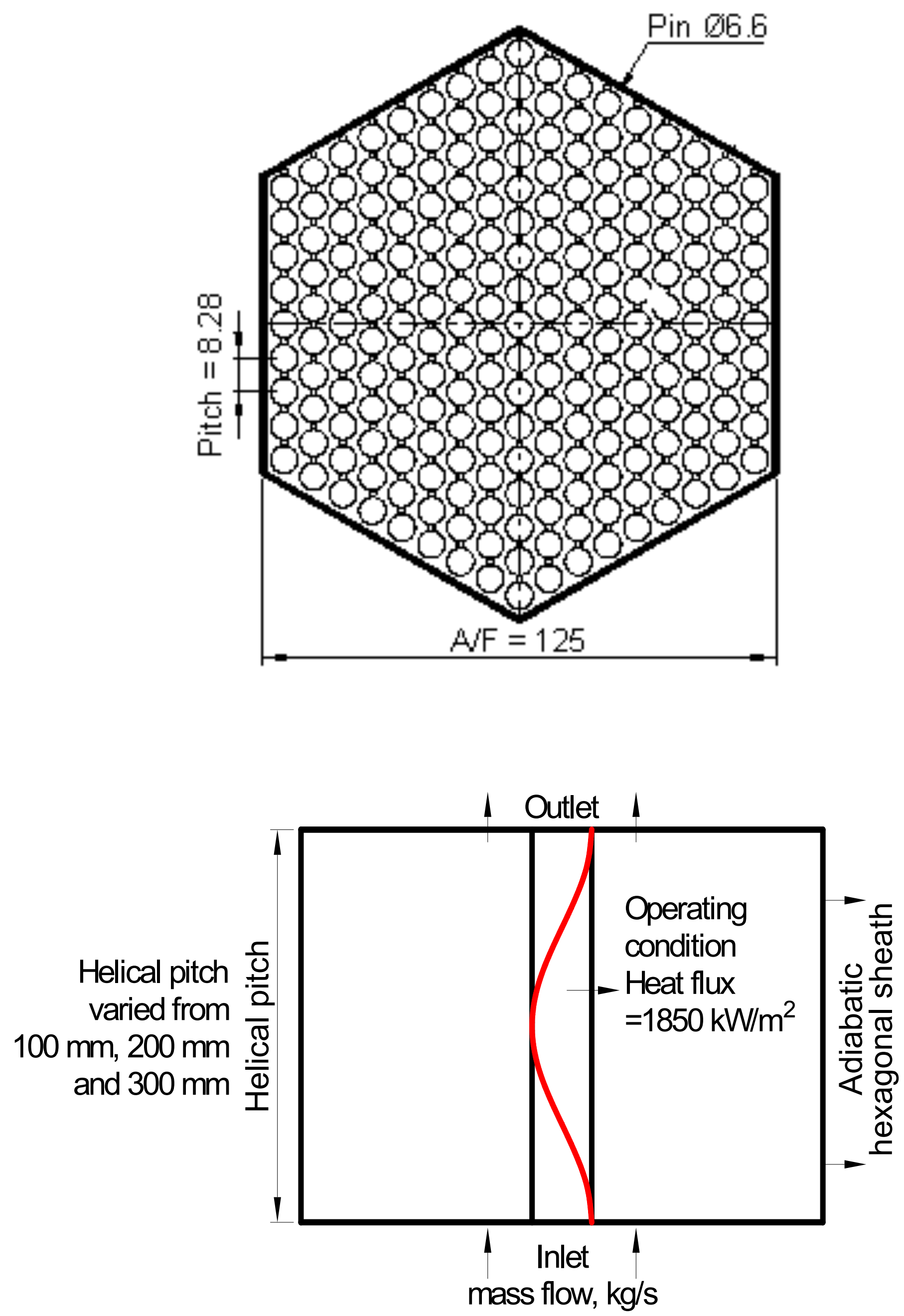

Fig. 3.2 Boundary conditions for the thermal hydraulic analysis of 217 pin fuel bundle.

For infinite array of bare pin bundle, the equivalent diameter is calculated based on the flow area of pins and the perimeter of the pins. But in the case of helical wire wrapped bundle with finite number of pins, the equivalent diameter is calculated same as that of hydraulic diameter. As the turbulence effects in a given sub-channel affect the adjacent sub-channels differently depending on the location of the sub-channels with respect to duct boundaries, the equivalent annulus concept provides an acceptable answer (Kazimi and Todreas, 2012). Also, the helical wire induces transverse flow and increases the turbulence effects in the sub channels similar to the duct boundary. Hence, in this thesis work, the equivalent diameter for thermal study is calculated based the sodium flow area in the pin bundle and the perimeters of the pins, wire and hexagonal sheath. The average Nusselt number at the outlet the pin bundle is calculated from the mean temperature of all the pins at the outlet and the mass weighted average coolant temperature in the sub-channel surrounding it at the outlet. Based on the above approach, the general equations for the calculation of equivalent diameter, Reynolds number, friction factor, heat transfer coefficient and the Nusselt number are given as follows.

The equivalent diameter is calculated as

$$d_{eq} = \frac{4 * flow\ area}{wetted\ perimeter}$$

The Reynolds is calculated as,

$$\mathrm{Re} = \frac{V\ d_{eq}}{\nu}$$

$$P_e = R_e * \mathrm{Pr}$$

$$\mathrm{Pr} = \mu * C_p / Kf_{cond}$$

Where Re – Reynolds number, Pe – Peclet number, Pr – Prandtl number

The Darcy friction factor is calculated from the pressure drop obtained for the pin bundle from the CFD study as

$$f = \frac{2\,\Delta P d_{eq}}{\rho l v^2}$$

The average heat transfer coefficient at the outlet is calculated as,

$$h = \frac{q''}{\Delta T}$$

Where $\Delta T = \overline{T_c} - \overline{T_f}$ where, $\overline{T_c}$ -Mean clad temperature of all pins at the outlet, $\overline{T_f}$ – Mean coolant outlet temperature.

The Nusselt number at the outlet is calculated based on the relation

$$Nu = \frac{h \times d_{eq}}{Kf_{cond}}$$

Experimental correlations for friction factor and Nusselt number for helical wire wrapped pin bundle for different flow regimes used for comparing with the calculated values of CFD studies are presented in the Appendix A.

3.5 VERIFICATION OF ADIABATIC BOUNDARY ASSUMPTION ON THE WIRE

In the reactor pin bundle, the nuclear heat generated within the fuel pin is transferred by conduction to the fuel pin clad through the gap between the fuel and clad. From the clad surface, it is then transferred to the sodium coolant by forced convection. The helical wire is in line contact with the fuel pin clad. Hence, there is no heat transferred to the wire from the fuel pin clad. But, in the present CFD modeling, the geometric complexity of line contact between the pin and wire is overcome by providing a radial offset of 0.05 mm for the wire towards the centre of the pin. By this approximation, the line contact between the pin and wire gets converted into surface contact. Due to this, heat conduction from the fuel pin clad to wire is possible. But, in the present CFD study, an adiabatic boundary condition is assumed on the helical wire surface while the clad surface is supplied with a constant heat flux. Hence, it is required to validate this assumption. Towards this, the 2-dimensional heat conduction equation in fuel pellet, clad and wire assembly is solved. Structured mesh has been generated for geometry of the pin, clad and wire-warp assembly with wire making surface contact with the clad. Volumetric heat generation rate in the pellet (1728 MW/m^3) and contact resistance between pellet and clad (0.45 W/m-K) have been considered. The outer surfaces of the clad and wire are provided with force convective boundary condition with a heat transfer coefficient of 1, 70, 000 W/m^2-K and sodium ambient temperature of 702 K. The finite volume mesh adopted is depicted in Fig. 3.3 (a). The predicted temperature distribution in the fuel pin, clad and wire-wrap assembly is presented in Fig. 3.3 (b). It is seen that the area averaged surface temperature of the clad and wire are 712.7 K and 702.7 K respectively. The total heat generated in the pellet is 37392 W. Out of this, the heat transfer from the surfaces of clad and wire are 36900 W and 492 W respectively. From this, it is estimated that the percentage of the total heat transfer from the fuel pin clad surface and wire are 98.6 % and 1.4 % respectively. Hence, this exercise justifies that the present assumption of constant heat flux on clad and adiabatic boundary condition on wire-wrap as valid.

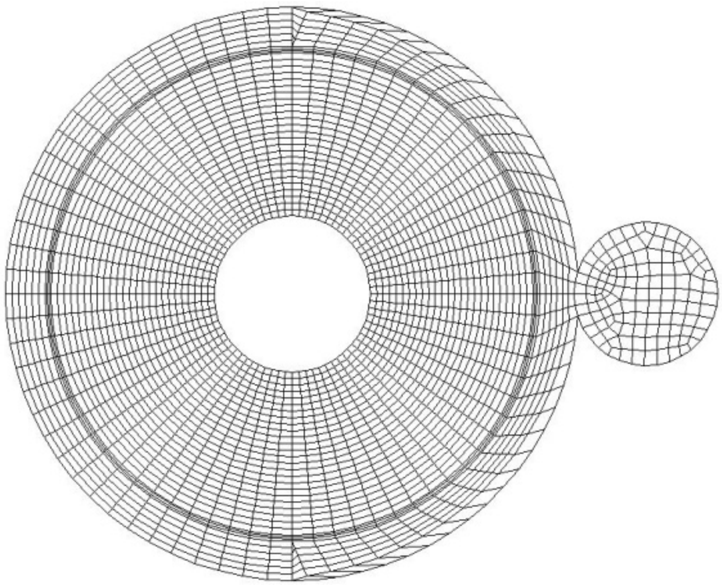

Fig. 3.3 (a) Finite volume mesh of fuel pellet, clad and wire

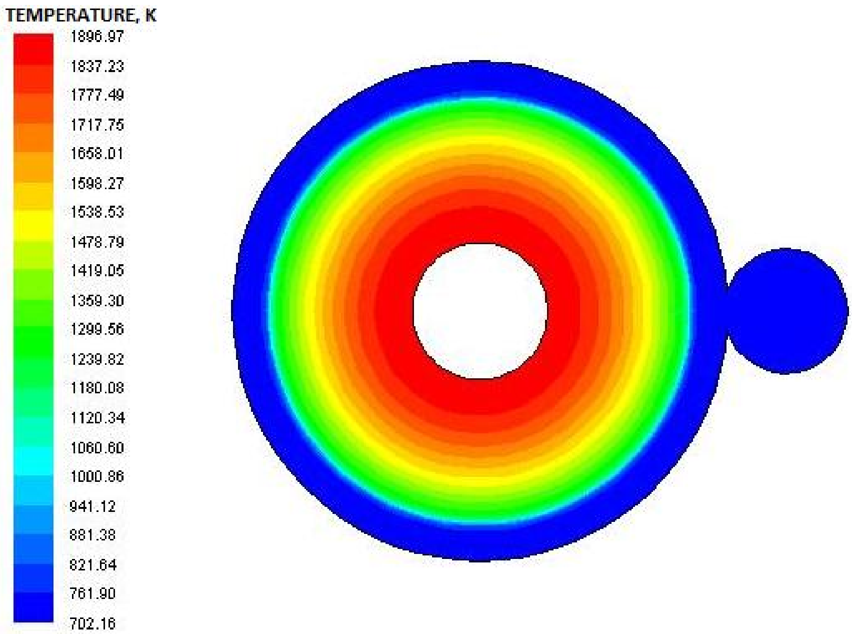

Fig. 3.3 (b) Temperature distribution in the fuel pellet, clad and wire assembly

3.6 STUDY OF VARIOUS TURBULENCE MODELS AND SELECTION OF HIGH REYNOLDS NUMBER k- ε MODEL

Several attempts have been made to solve the turbulence closure problem by the introduction of succession of turbulence models. The simplest one of them is Prandtl's mixing length model which is generally valid for plain two-dimensional flows. For a general case of three-dimensional flows higher order turbulence models are required. They utilize one or more partial differential equations derived from the modified Navier-Stokes equations for quantities like the turbulent kinetic energy k, the kinetic energy dissipation rate ε and the components of the turbulent stress tensor. The turbulence model employing a single partial differential equation for turbulent kinetic energy in conjunction with the algebraic expression for the turbulence length scale is referred as one equation model.

The low Reynolds number turbulence model to predict near wall flow and temperature fields does not employ wall functions. But, this requires very fine meshing near the wall which is very small to capture boundary layer near the wall. This will lead to a huge number of mesh points and requires enormous computer memory and time. The total number of cells used in the present helical wire wrapped 200 mm length 217 pin bundle is about 6.6 millions. If very fine meshing is adopted near the wall to suit low Reynolds number model, the total number of meshes will be of the order of billions and which is expected to make the CFD study impractical. Numerical simulation of the fine boundary layer features using low Reynolds number turbulence model even in a small pin bundle is highly challenging. But it is proposed to study the accuracy of Low Reynolds number turbulence model over High Reynolds number model in a small size 7 pin bundle in the future. Also, it is judged that the low Reynolds number turbulence model is required mainly to study the transition flow.

Another model, employing the partial differential equations for the turbulent kinetic energy and its dissipation rate is called the k- ε model. It is technically most often used and spread nearly throughout all commercial codes. Generally, applications of the k- ε model have made use of wall functions to treat the near wall region. Fortunately, in the case of liquid metals such as sodium, the molecular diffusion is very large. Hence, the use of standard k-ε type turbulence models, which are computationally efficient, is adequate in forced convective regime (Spalding et al. 1974). For fully turbulent flows, Reynolds analogy is valid for sodium flows also. The high Reynolds number turbulence model with standard wall functions fairly approximates the near wall boundary in the forced convective regime. Moreover, this model reduces the requirement of huge number of cells and makes the CFD study of pin bundle practical.

The other turbulence models employing the partial differential equations for the kinetic energy and Vorticity called k- ω model and the shear stress turbulence model (SST) which combines the advantages of the k- ω model and k- ε model, and takes care of the near wall region in the analytical solution are also explored.

Towards understanding the effect of turbulence model on the predicted solution, a CFD study of 7 pin bundle has been carried out with various turbulence models viz. k- ε, k- ω and SST. The friction factor and the Nusselt number predicted by these models are presented in Figs. 3.4 (a) - 3.4 (b) respectively. It is found that the k- ε model predicts friction factor closer to the experimental data and Chen et al (2014) correlation. It is also found that the Nusselt number predicted by k- ε turbulence model is the lowest and closer to experimental data. As the k- ε turbulence model predicts both friction factor and Nusselt number closer to experimental data, it is adopted for the present CFD study.

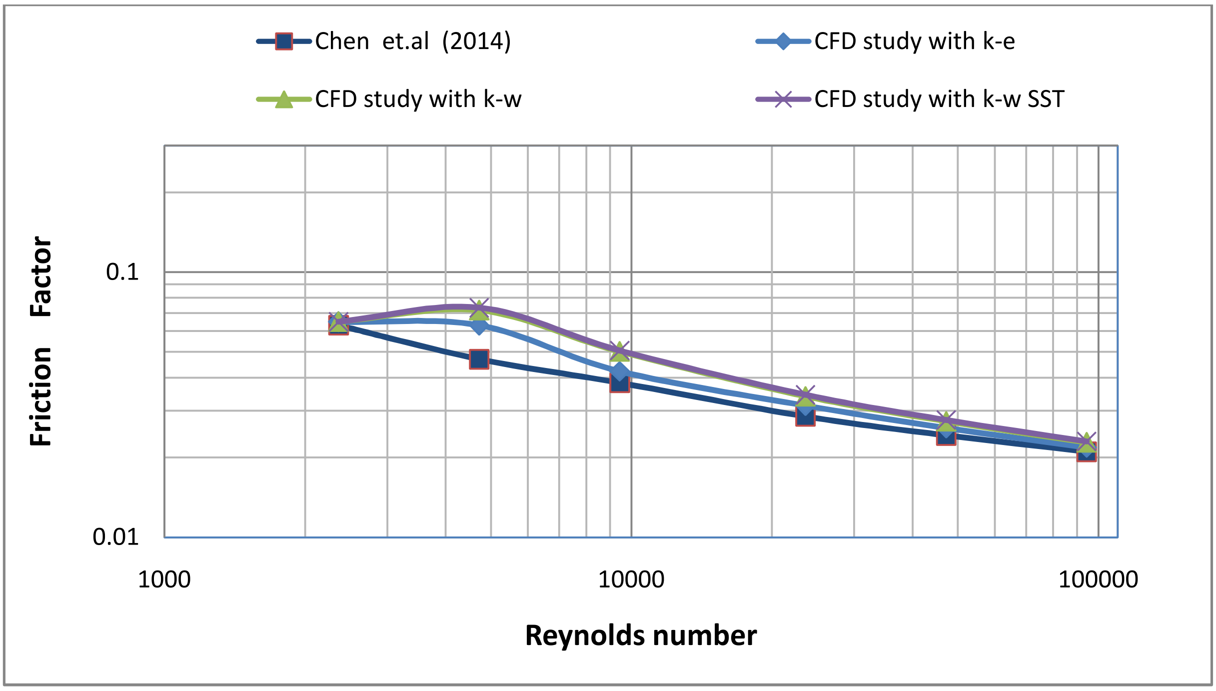

Fig. 3.4 (a) Prediction of friction factor for 7 pin bundle with different turbulence models for Re = 100000

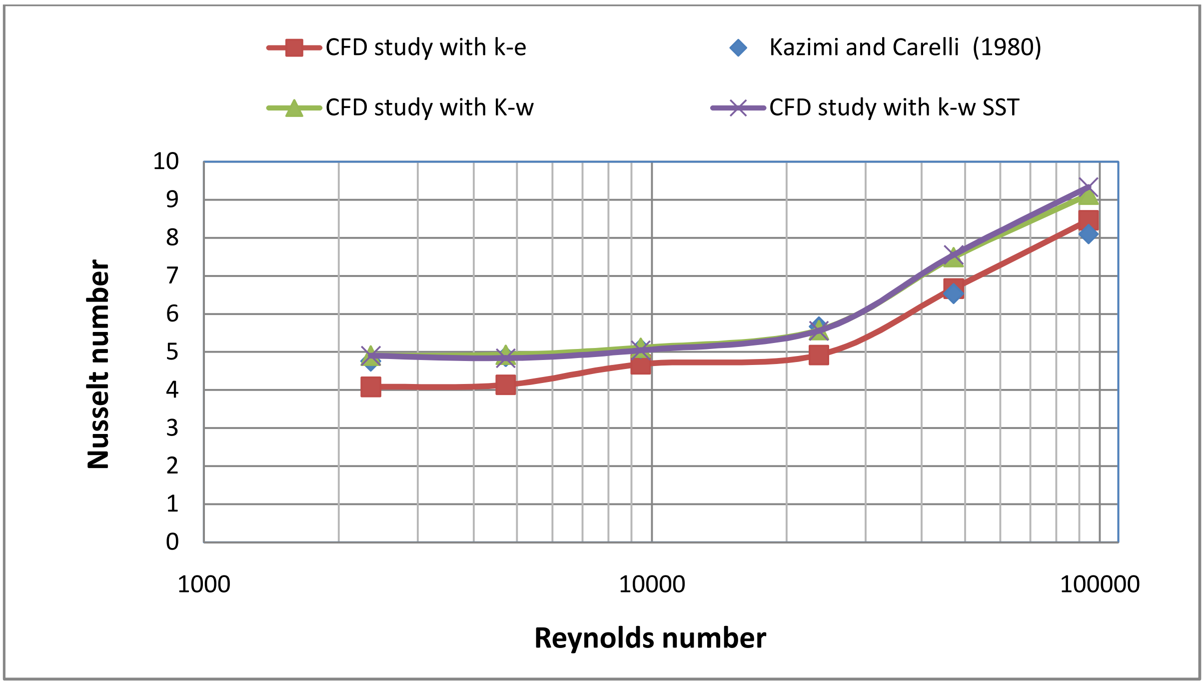

Fig. 3.4 (b) Prediction of Nusselt number for 7 pin bundle with different turbulence models for Re = 100000

3.7 GRID INDEPENDENCE STUDY

The reference grid contains 36 divisions around the pin, 12 divisions around the wire and 10 divisions between two pins. Sixty seven divisions are considered in the axial direction for a pitch of 200 mm. The mesh is refined near the wall to satisfy the Y^+ condition for the standard wall function used in the analysis. For the mesh adopted in the present study, a mesh independence study has been carried out with four different mesh patterns for Re= 10^5. The number of points around the pin and the wire are varied from 28 to 40 and 6 to 15. The grid model number 1 corresponds to 28 points on pin and 6 points on wire and so on. The values of the pin bundle pressure drop (which is used to calculate friction factor) and the area averaged clad temperature at the exit of the pin bundle (which is used to calculate Nusselt number) are presented in Figs. 3.5 (a) - 3.5 (b) respectively. It is found that these values at the bundle exit become insensitive after grid model number 3. Hence, 36 divisions around the pin and 12 divisions around the wire are judged to be adequate.

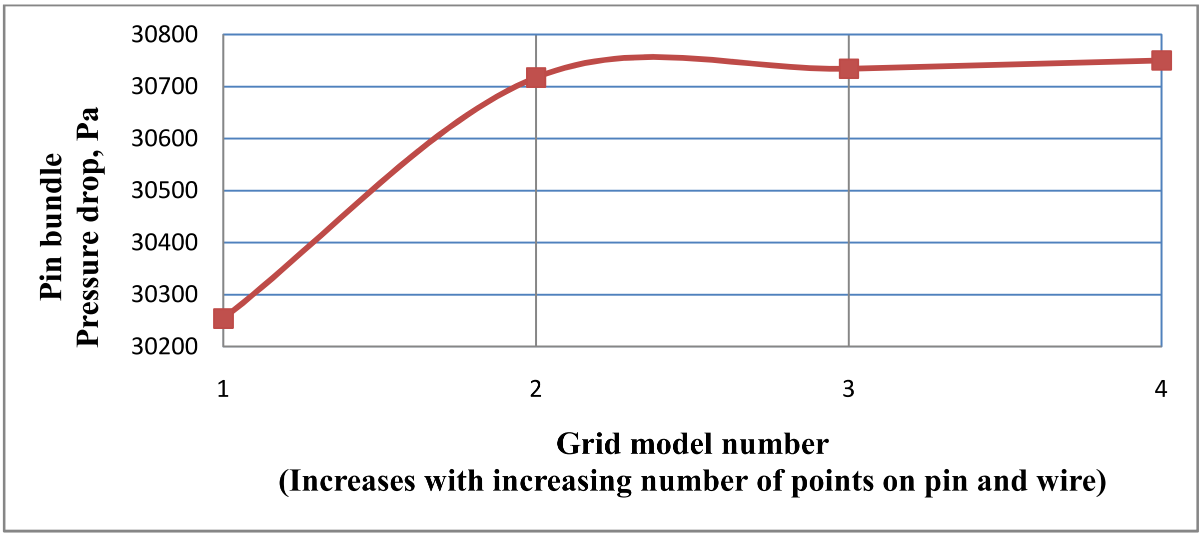

Fig. 3.5 (a) Pressure drop of pin bundle with various number points on pin and wire

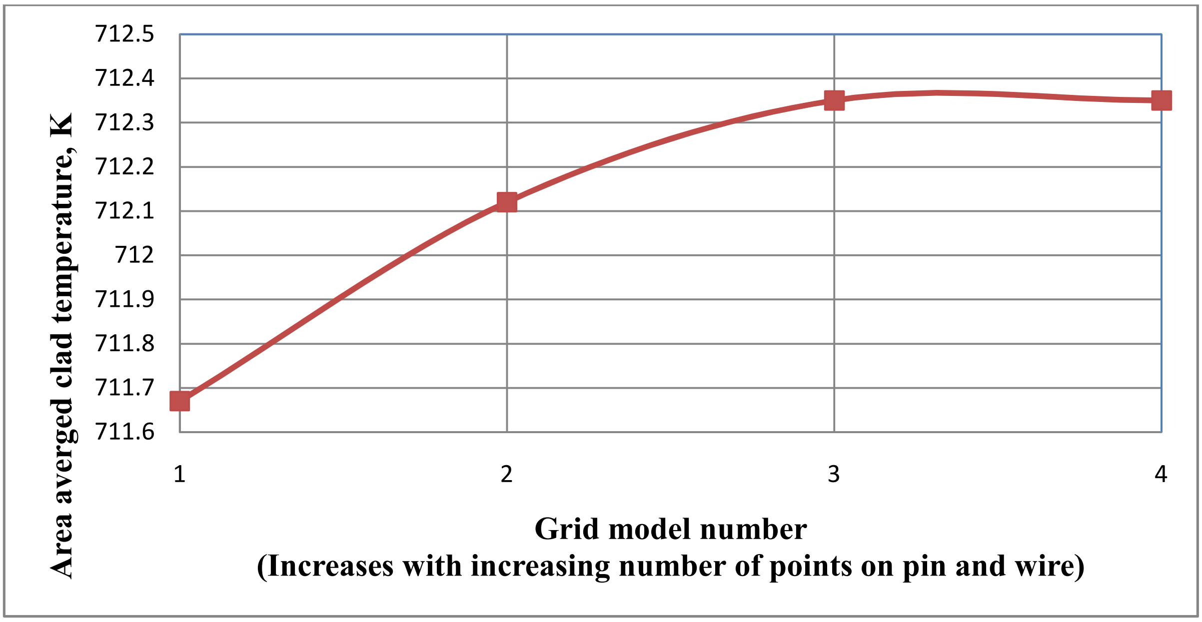

Fig. 3.5 (b) Area averaged clad temperature at the exit of the pin bundle with various number points on pin and wire

3.8 VALIDATION STUDIES

3.8.1 FRICTION FACTOR

The CFD results of friction factor in a 217 pin bundle is compared with the experimental results reported by Roychowdhury (1998) and the correlations proposed by Chen et al. (2014) in Fig 3.6 (a). It is seen that the friction factor values in the turbulent regime obtained by CFD analysis matches with that of the experimental values within 2 %. The friction factor values in the laminar regime obtained from CFD analysis are higher (15 %) than that of the experimental values. Hence, the present model appears to be well suited for turbulent flow. Also, in the present model the standard k-ε high Reynolds turbulence model is employed. Hence, the use of this turbulence model to predict turbulent flow friction factor in pin bundles is also validated.

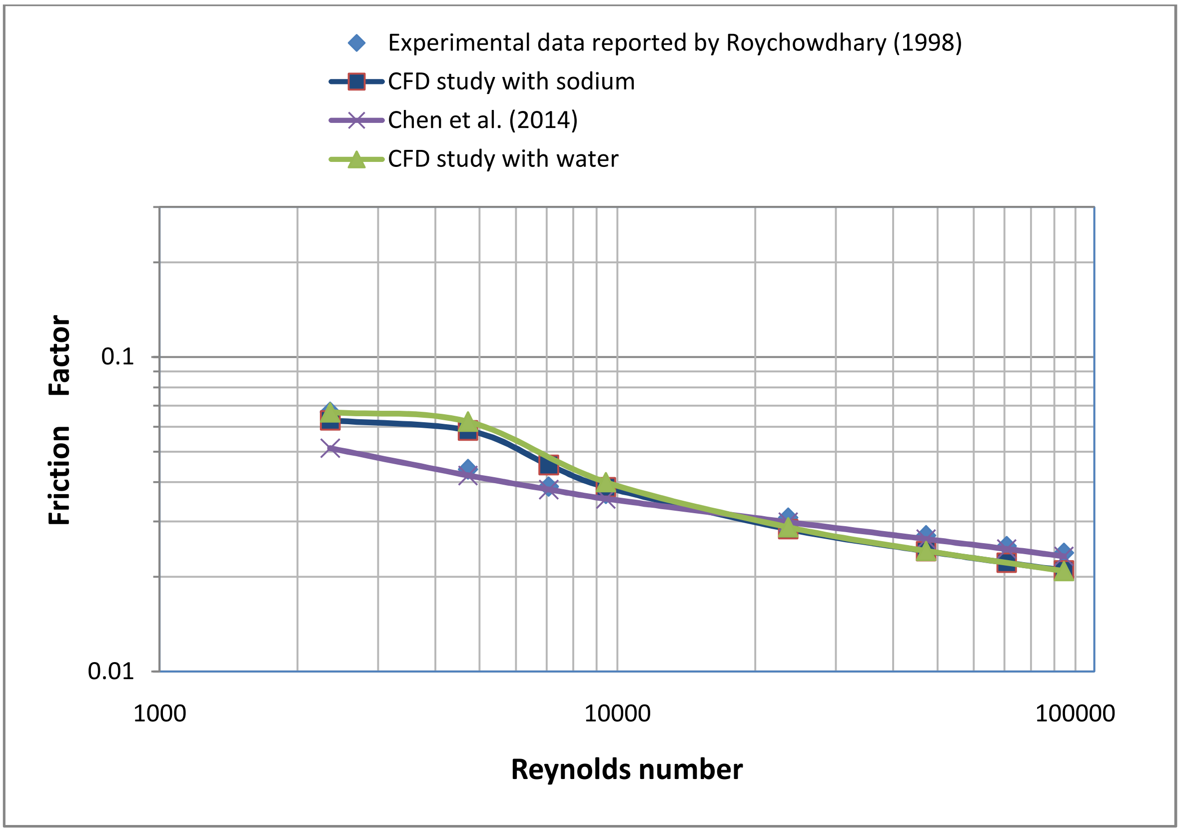

Fig. 3.6 (a) Comparison of friction factor of 217 pin bundle with experimental data and Chen et al (2014) correlation

3.8.2 NUSSELT NUMBER

The Nusselt number obtained for 217 pin bundle using sodium as coolant is compared with Kazimi and Carelli correlation (1980) for turbulent flow in Fig. 3.6 (b). The present CFD study using RANS model slightly over-predicts the Nusselt number as 10.0 for sodium flow through the pin bundle compared to 8.2 with the experimental correlation proposed by Kazimi and Carelli (1980) for turbulent flow (Re = 100,000 and Pe =500). The predicted Nusselt number in the turbulent regime is higher than the experimental correlation by 20 %. However, it matches with the correlation in the laminar regime. The higher value of predicted Nusselt number could be due to insufficient thermal development length of the pin bundle (200 mm) simulated. The Nusselt number at the outlet of the bundle obtained using water flow has been compared with the experimental correlation obtained by Fenech (1985)

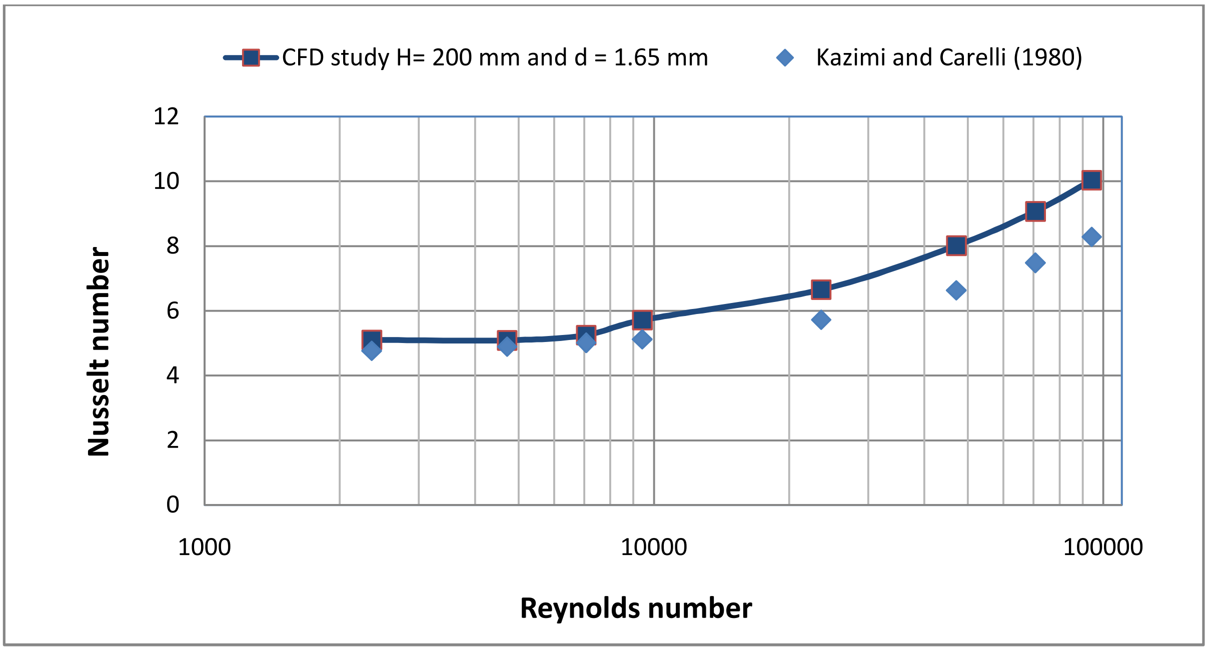

Fig. 3.6 (b) Comparison of Nusselt number at the exit of 217 pin bundle with experimental correlation

in Fig. 3.6 (c). It is found that the Nusselt number predicted for water flow matches very well with the experimental correlation.

3.9 CLOSURE

For the CFD study of fuel pin bundle, the structured mesh has been generated for the fuel pin bundles and is used for solving 3 – D conservation equations using commercially available parallel CFD software. The equations for the calculation of equivalent diameter of bare and helical wire-wrap pin bundle, Reynolds number and Nusselt number are detailed. The boundary conditions for the hydraulic and thermal study of heat generating fuel pin bundle has been explained. The heat transfer from the surfaces of clad and helical wire has been estimated by a 2-dimensional heat conduction analysis of fuel pellet, clad and wire-warp assembly and found that the heat transfer from the wire surface is only 1.4 % of the total heat transfer.

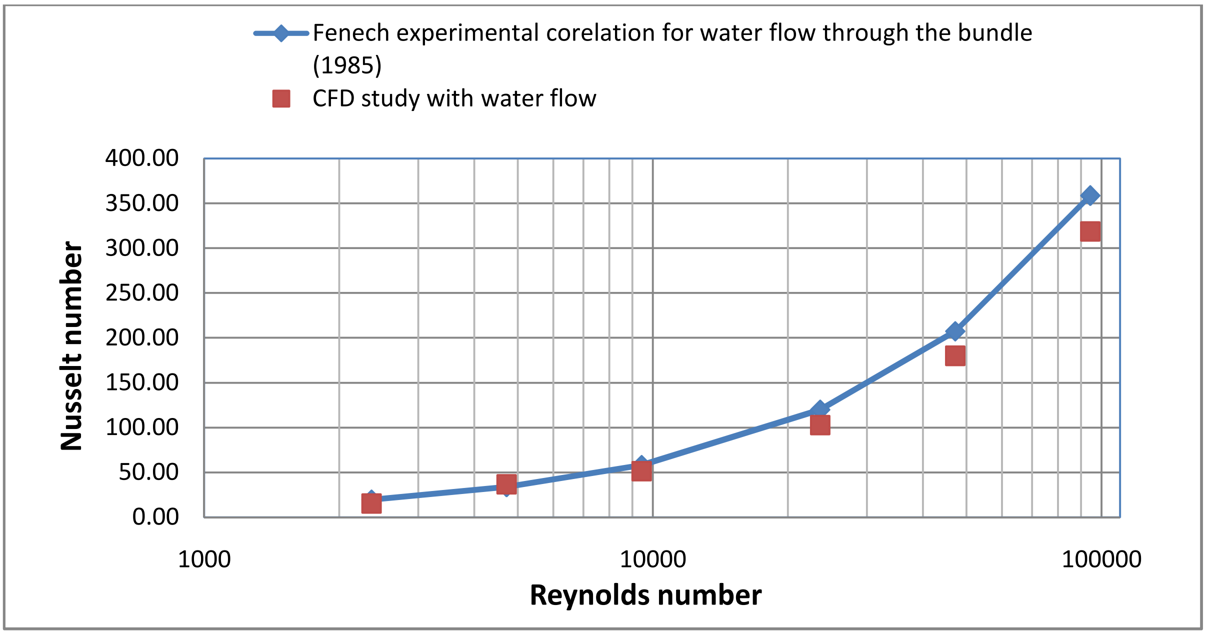

Fig. 3.6 (c) Coparison of Nusselt number at the exit of 217 pin bundle with experimental correlation for water flow through the bundle.

Thus, the adiabatic boundary assumption on the wire which makes surface contact with the fuel pin in the CFD modeling is verified. For the mesh adopted in the present study, a mesh independence study has been carried out with four different mesh patterns for Re = 10^5. The number of points on the pin and the wire are varied It is found that the pin bundle pressure drop and average clad temperature at the outlet of the bundle are constant for more than 36 meshes for pin, 12 meshes for wire meshes. This confirms that the above meshes which fairly approximates the circular surfaces of the pin and wire and their boundary layer. Also, this confirms the grid independence of the present mesh for the numerical solution of the pin bundle with helical wire-wrap. The 7 pin bundle CFD model has been studied with various turbulence models like k-ω and Shear Stress Turbulence model and the high Reynolds k- ε turbulence is found to be in close agreement with the experimental results. The CFD results are validated against both experimental results and published correlations and are found to be in good agreement with them.

CHAPTER - 4

THERMAL HYDRAULICS WITHIN 7 PIN BUNDLE

4.0 INTRODUCTION

The development of transverse velocity in the 7 pin bundle and its variation with helical pitch, friction factor of the 7 pin bundle, sodium temperature development in the 7 pin bundle and the thermal benefits of the transverse velocity are presented in this chapter.

4.1 DEVELOPMENT OF TRANSVERSE VELOCITY

The Reynolds number for this simulation is 100,000 with an axial velocity of 7.53 m/s. The heat flux on the clad surface is 1.85 MW/m^2. The inlet temperature of sodium to the pin bundle is 670 K. The nominal helical wire diameter is 1.65 mm and the nominal helical pitch is 200 mm. The distribution of cross-stream velocity at the various elevations of the bundle is presented in Figs. 4.1 (a) - 4.1 (g). The magnitude of cross stream velocity is typically about 0.77 m/s. The activity of the secondary flow is maximum in the vicinity of the spacer wire. This swirl flow occurring at the peripheral sub-channels is found to be periodic and is found to be a function of wire position. As we move upwards in the axial direction, the wire moves anti-clockwise. As a consequence of this, the circumferential flow is developed in anti-clock wise direction. The velocity is maximum in the peripheral sub-channels which are diametrically opposite to the channels where a spacer wire blocks the sub-channel. This flow developed due to the helical wire is very important from the thermal hydraulics point of view, as it enhances mixing of the coolant which is required to obtain a fairly uniform coolant temperature at the exit of the bundle. It also increases the level of turbulence which promotes good mixing of the coolant and better uniformity of the temperatures. Also, it is seen that the flow has got developed within 33 mm from the inlet of the bundle after which the changes in the flow is marginal.

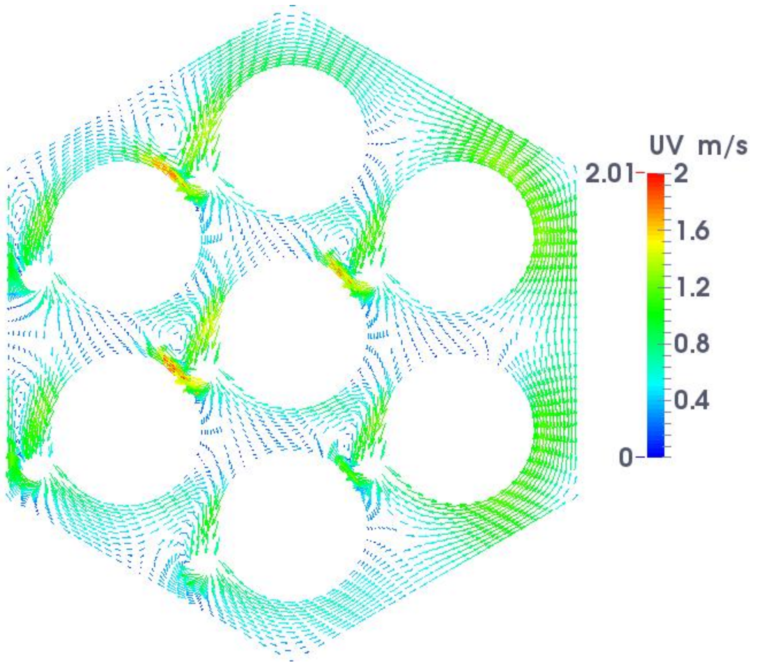

Fig. 4.1 (a) Transverse velocity field at 33 mm from the inlet of helical wire wrap 7 pin bundle

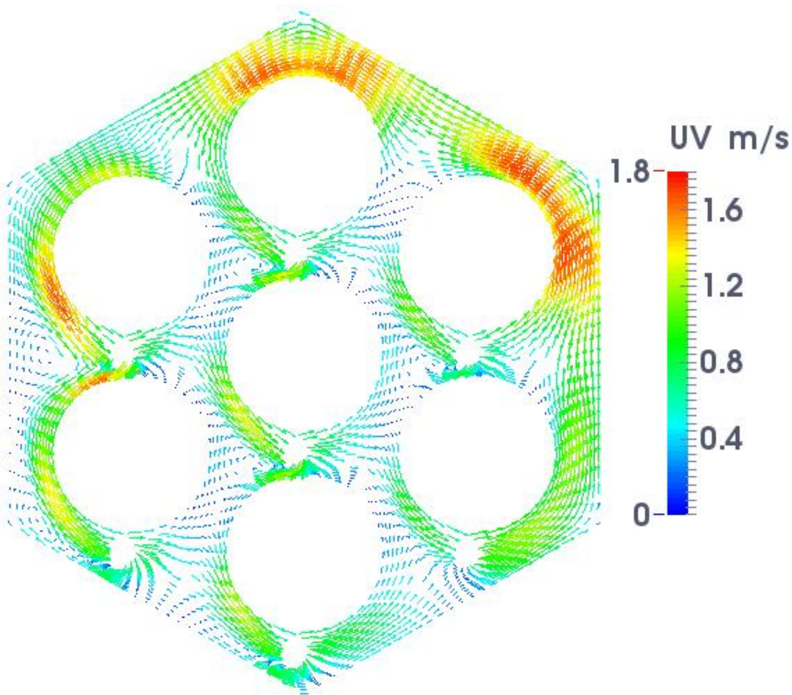

Fig. 4.1 (b) Transverse velocity field at 66 mm from the inlet of helical wire wrap 7 pin bundle

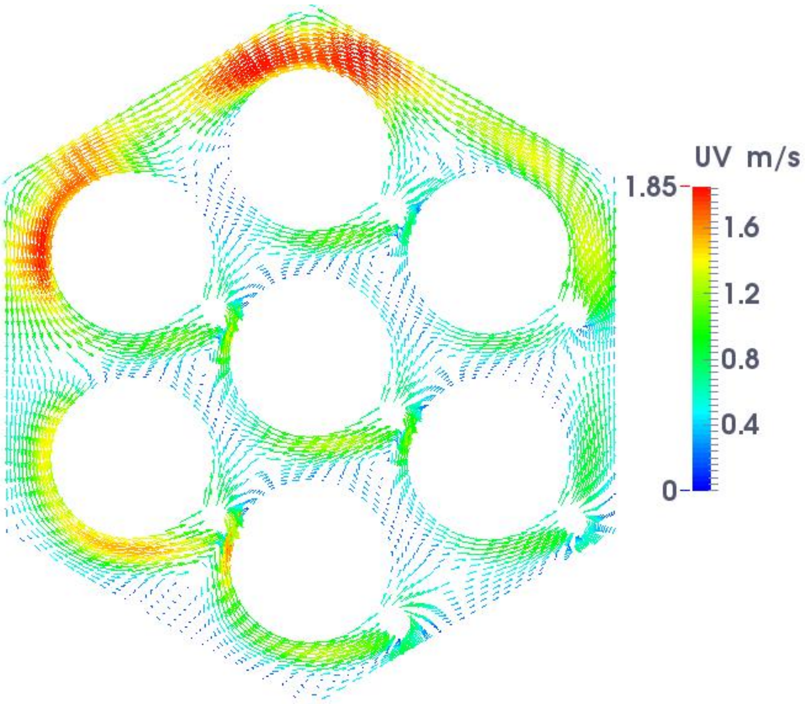

Fig. 4.1 (c) Transverse velocity field at the 99 mm from the inlet of helical wire wrap 7 pin bundle

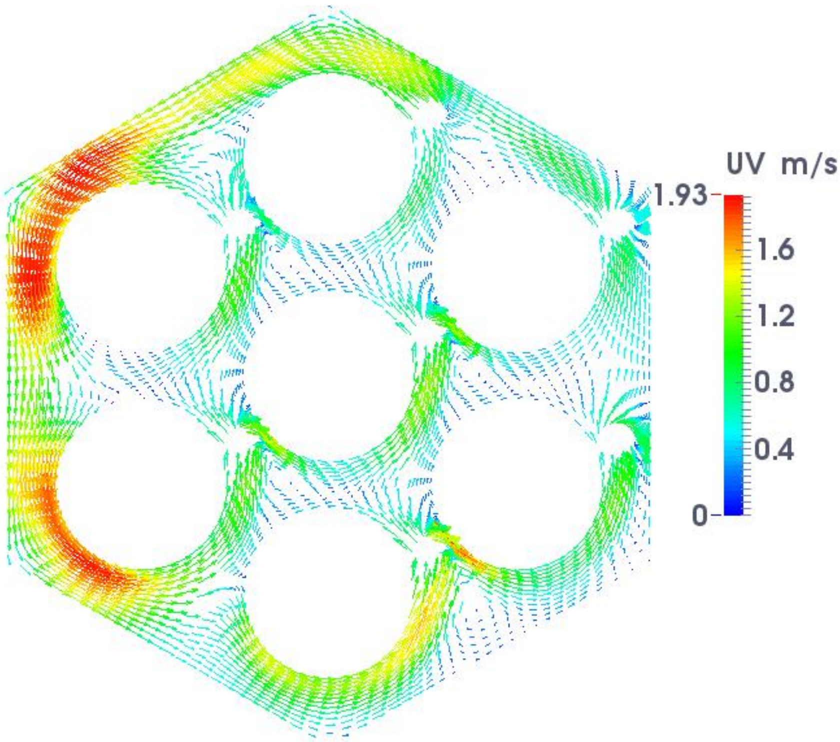

Fig. 4.1 (d) Transverse velocity field at the 133 mm from the inlet of helical wire wrap 7 pin bundle

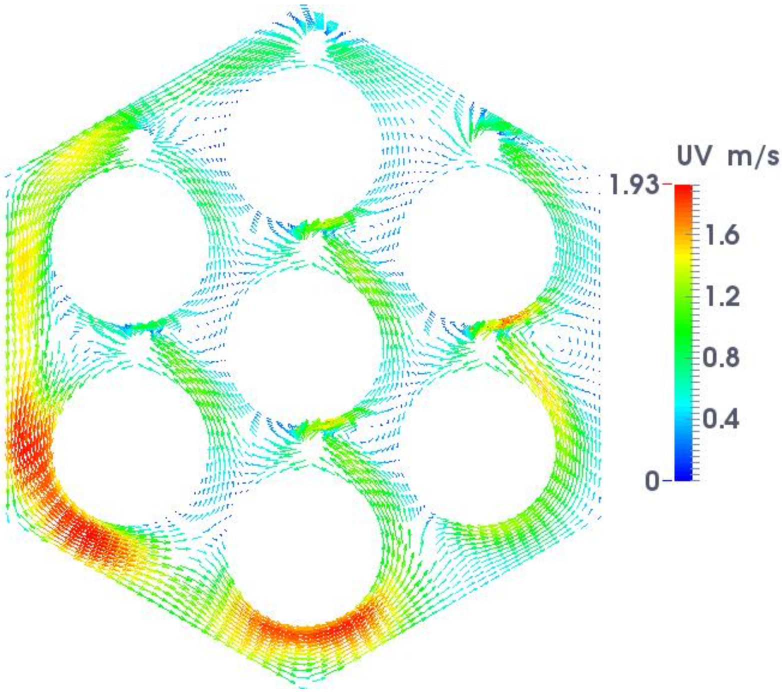

Fig. 4.1 (e) Transverse velocity field at the 166 mm from the inlet of helical wire wrap 7 pin bundle

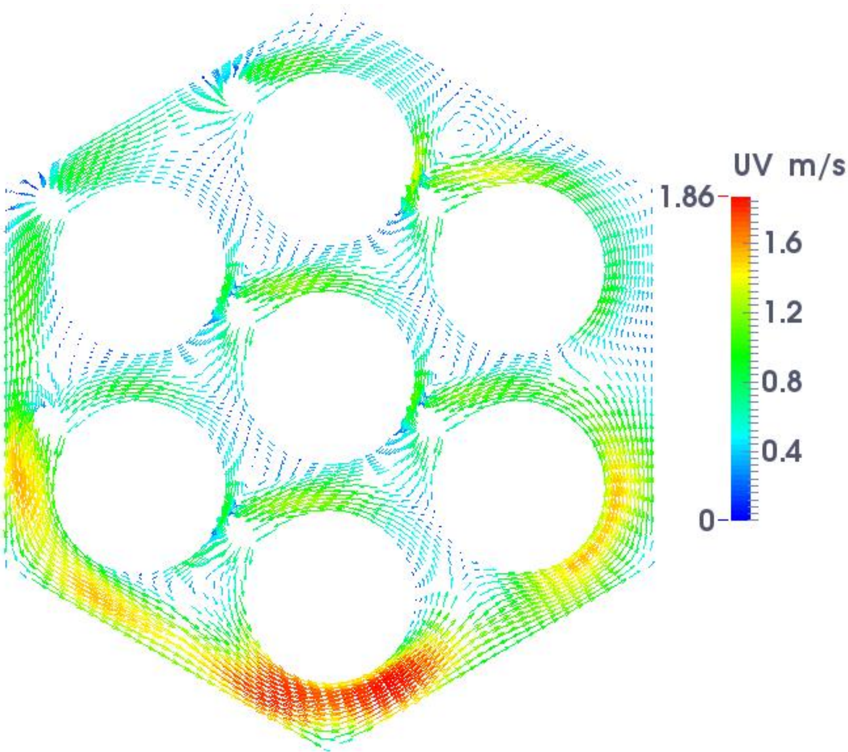

Fig. 4.1 (f) Transverse velocity field at the exit of helical wire wrap 7 pin bundle

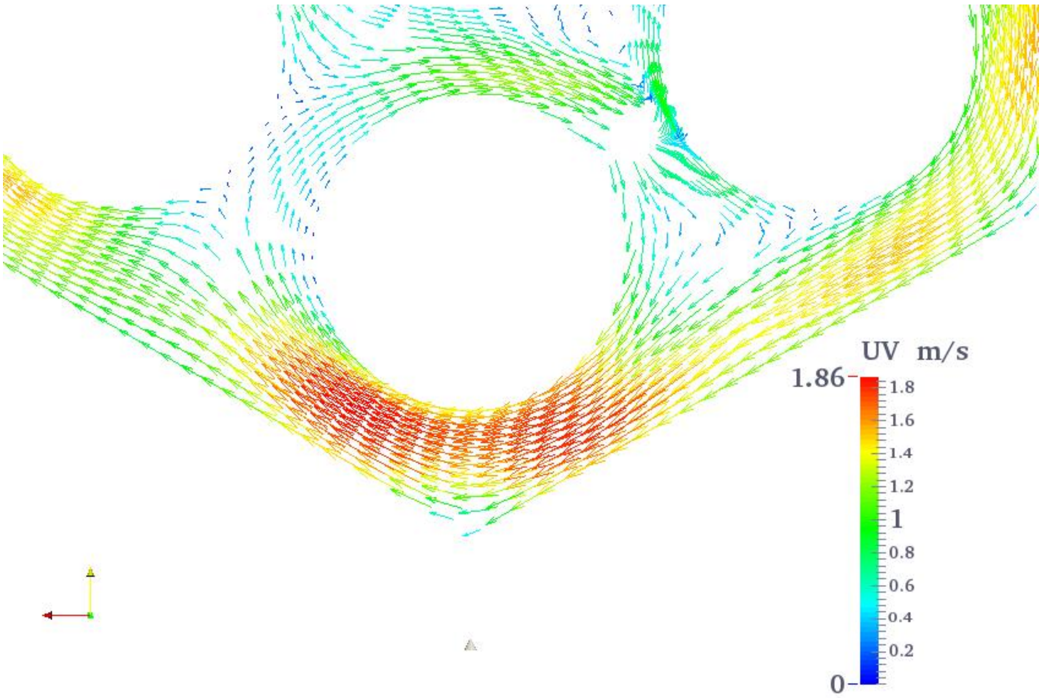

Fig. 4.1 (g) Close-up view of transverse velocity field at the exit of helical wire wrap 7 pin bundle in X-Y plane.

4.2 VARIATION OF TRANSVERSE VELOCITY WITH HELICAL PITCH

The local transverse velocity is defined as,

$$V_T = \sqrt{{V_x}^2 + {V_y}^2}$$

The mass averaged transverse velocity is defined as,

$$\overline{V_T} = \frac{\int \mathrm{V_z}\ V_T\ dA}{\int \mathrm{V_z}\ \mathrm{dA}}$$

Where V_T = local transverse velocity, V_x – component of velocity in the x- direction, V_y– component of velocity in the y- direction, V_z– component of velocity in the z- direction, $\overline{V_T}$ – mass averaged transverse velocity, dA- elemental flow area.

The variation of mass weighted average transverse velocity with helical pitch of the wire is presented in Fig. 4.2 (a). It is seen that the transverse velocity drastically reduces and becomes negligible when helical pitch increases to 1500 mm as it approaches that of the straight wire pin bundle where no transverse velocity is possible. The ratio of maximum axial velocity (V_z = 7.53 m/s) to the transverse velocity (Average V_T= 0.77 m/s) is about 9.8 for the geometry under study. This is nearly equal to the tangent of the rolling up angle ($\theta = 85^o$) of the helical wire. That is,

$$Tan\ (\theta) = \frac{V_z}{V_T} = \frac{H/2}{(D+d)}$$

The variation of rolling up angle of the wire with helical pitch is presented in the Fig. 4.2$_{A}$(b). It is seen that when the helical pitch becomes 1500 mm, the rolling up angle becomes nearly equal to 90^o which is a straight wire.

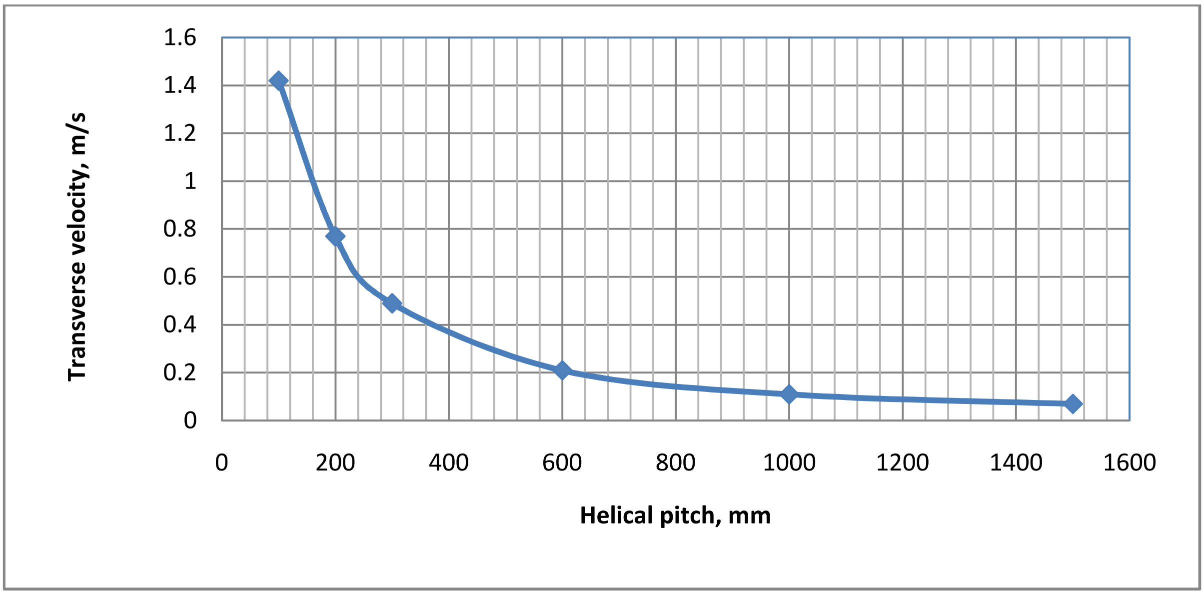

Fig. 4.2 (a) Variation of transverse velocity with helical pitch of the spacer wire.

The ratio of axial velocity to transverse velocity for various helical pitches and the corresponding rolling up angle of the helical wire are presented in Table.4.1. It is seen from the table that the ratio of axial velocity to transverse velocity is nearly equal to the tangent of the rolling up angle of the helical wire. The Table 4.1 shows that for higher value of helical pitch, the rolling up angle becomes very close to 90^{o} for which the ratio of transverse velocity to axial velocity becomes infinity as the transverse flow becomes negligible for straight wire case.

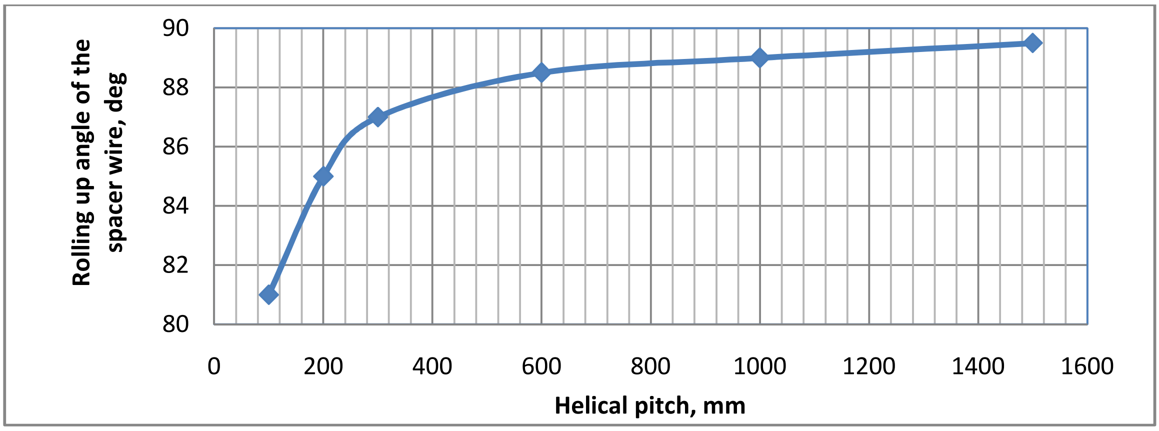

Fig. 4.2 (b) Variation of rolling up angle with helical pitch of the spacer wire

4.3 VARIATION OF AXIAL VELOCITY

The contours of axial velocity at various axial planes along the flow direction are depicted in Figs. 4.3 (a) – 4.3 (f). The uniform axial velocity after entering the pin bundle distorts significantly. The distortion is such that the velocity is high in the peripheral sub channels. Among the various peripheral sub channels, the velocity is high in the sub channels having spacer wire. This is true especially close to the entrance within half helical pitch length. Further, the position of the sub channel (with peak axial velocity) changes along the flow direction. In fact, it rotates anti-clockwise as the flow moves upwards. The ratio of maximum velocity to average velocity increases from unity at the entry and reaches 1.2 at the exit.

Table 4.1 The ratio of axial velocity to transverse velocity transverse velocity and the rolling up angle for various helical pitches

Helical pitch	Transverse velocity	Ratio of axial velocity to Transverse velocity (a)	Rolling up angle of the helical wire # (b)	Tan^{-1}(a)	Tan^{-1}(b)
100	1.42	5.30	6.73	79.3	81
200	0.77	9.78	13.46	84	85
300	0.49	15.36	20.20	86	87
600	0.21	35.85	40.40	88	88.5
1000	0.11	68.45	67.34	89	89
1500	0.07	107.6	90.90	89.5	89.5

Ratio of half of helical pitch to sum of pin diameter and wire diameter.

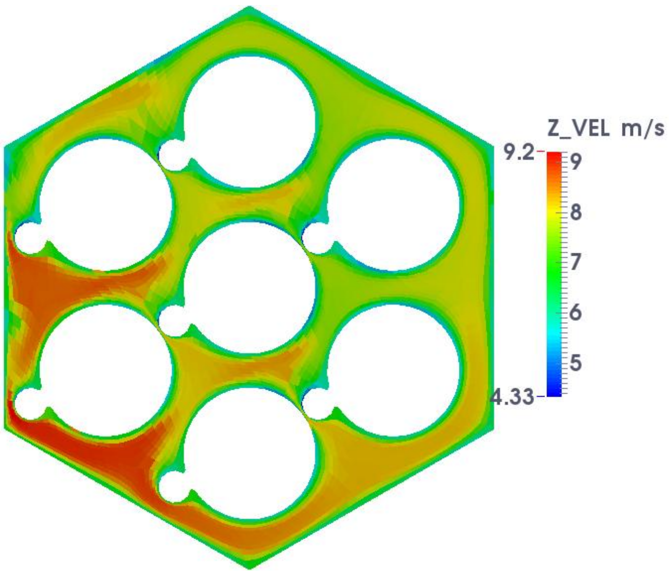

Fig. 4.3 (a) Axial velocity field at 33 mm from the inlet of helical wire wrap 7 pin bundle

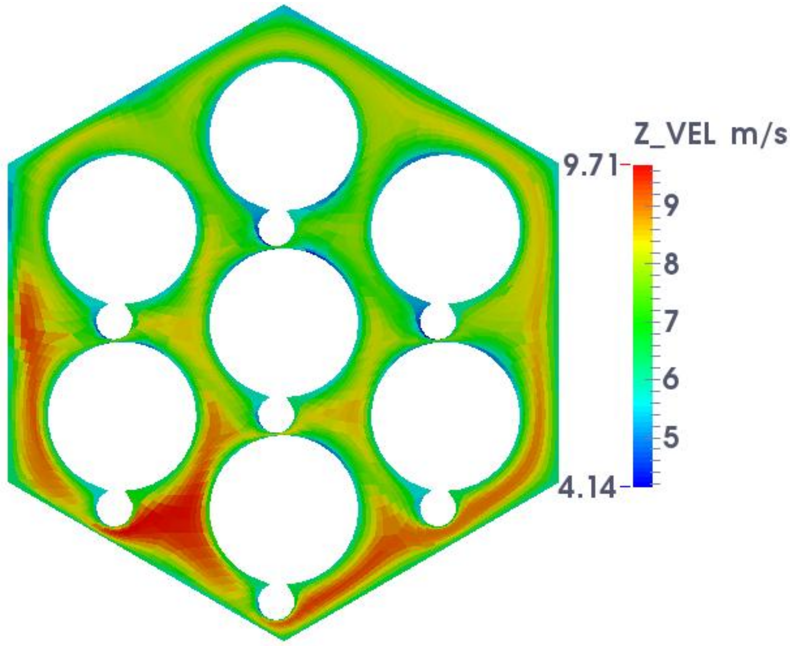

Fig. 4.3 (b) Axial velocity field at 66 mm from the inlet of helical wire wrap 7 pin bundle

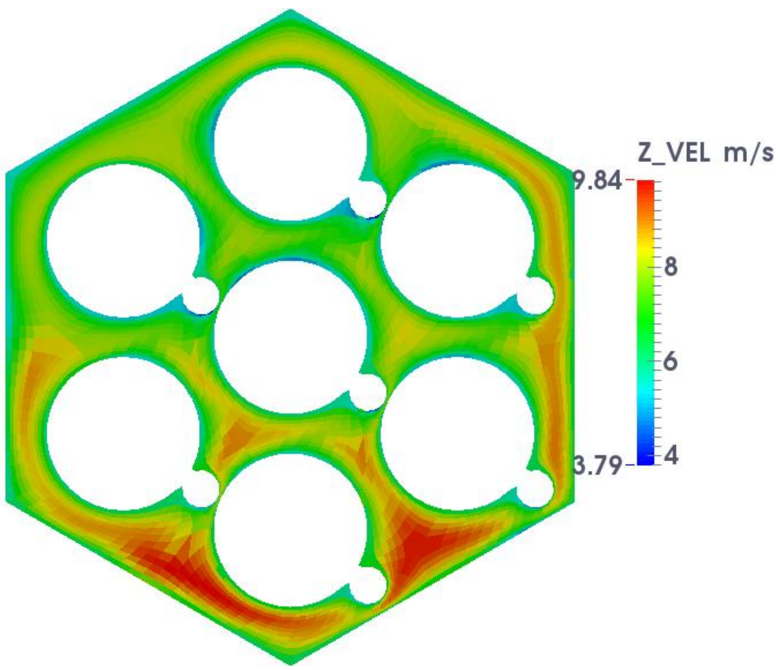

Fig. 4.3 (c) Axial velocity field at 99 mm from the inlet of helical wire wrap 7 pin bundle

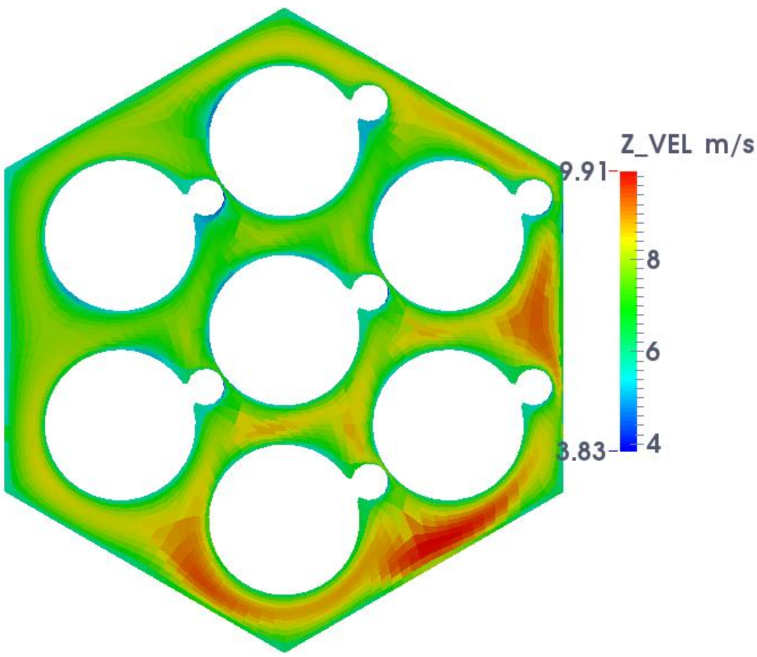

Fig. 4.3 (d) Axial velocity field at 133 mm from the inlet of helical wire wrap 7 pin bundle

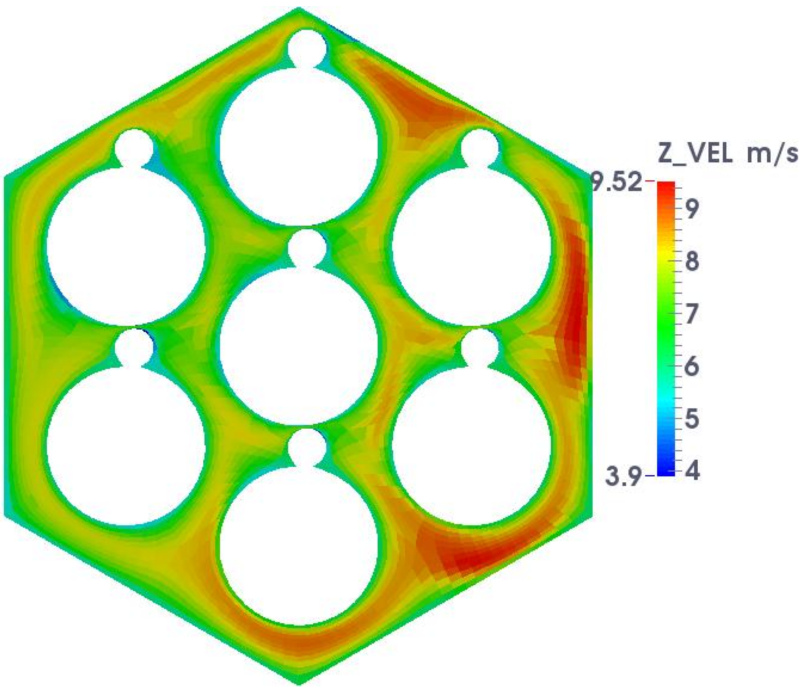

Fig. 4.3 (e) Axial velocity field at 166 mm from the inlet of helical wire wrap 7 pin bundle

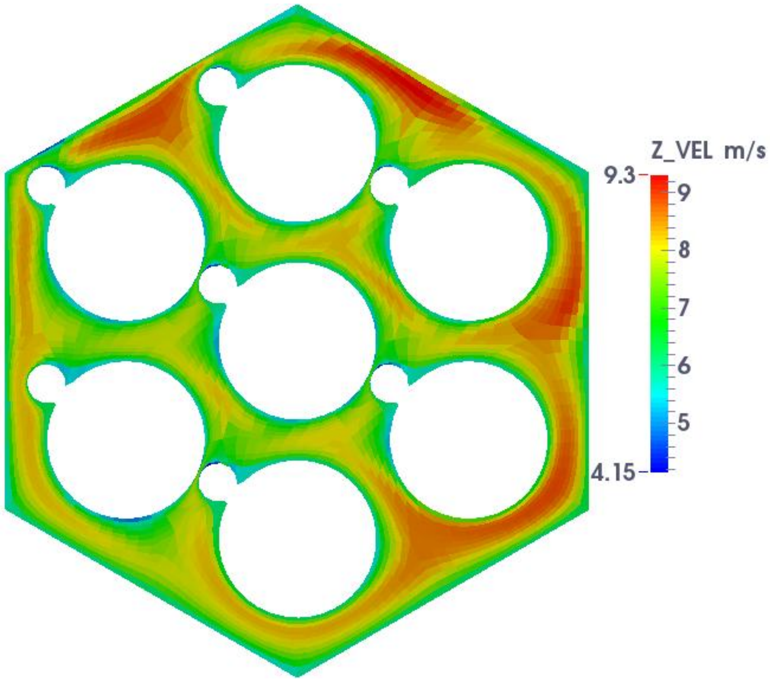

Fig. 4.3 (f) Axial velocity field at the exit of helical wire wrap 7 pin bundle

4.4 VELOCITY DISTRIBUTION IN STRAIGHT WIRE PIN BUNDLE

The velocity distribution in straight wire pin bundle is marked by the insignificant transverse flow, Fig.4.4 (a). The mass average transverse velocity is 5 mm/s. This indicates that the there is no cross flow within the bundle. The outlet axial velocity distribution for this case is presented in Fig. 4.4 (b). The velocity in the gap between wire and pin is 0.08 m/s whereas the same is 4.15 m/s in the case of helical wire. This shows that the velocity field is stagnant in this gap between wire and pin but the same is active in the case of helical wire which can enhance heat transfer in this gap and reduces the hotspot.

4.5 FRICTION FACTOR IN 7 PIN BUNDLE

One of the engineering parameters of interest is the friction factor. The value of friction factor predicted in the present study for 7 pin bundle with helical wire for various Reynolds number is compared with Chen et al (2014) correlation in Fig. 4.5 (a). It is seen that the agreement is very good with a maximum deviation of 15 %. The CFD model is seen to over predict the friction factor in the laminar regime while the same is under predicted in the turbulent regime.

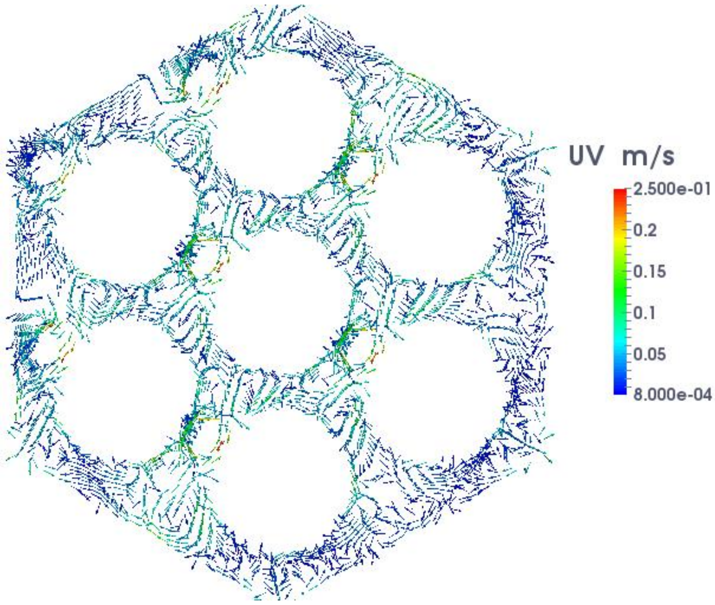

Fig. 4.4 (a) Transverse velocity field in straight wire wrap 7 pin bundle

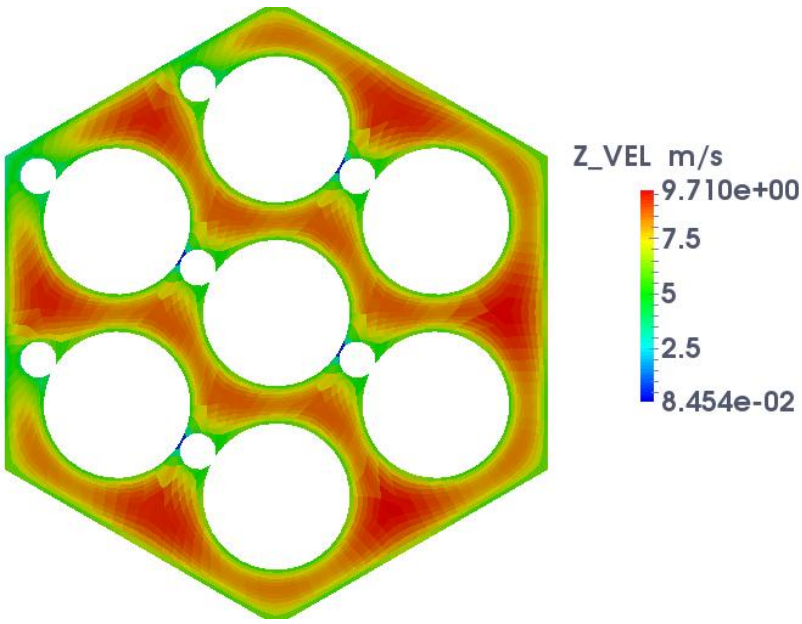

Fig. 4.4 (b) Axial velocity field in straight wire wrap 7 pin bundle

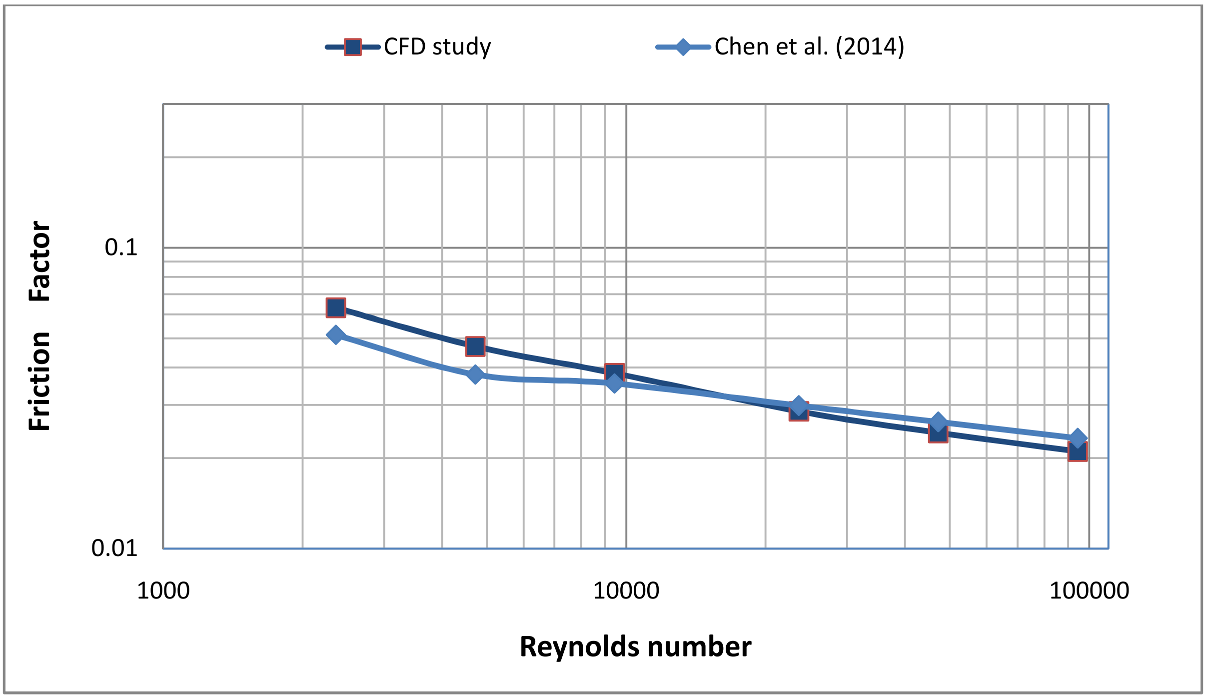

Fig. 4.5 (a) Comparison of friction factor of 7 pin bundle with Chen et al. (2014) correlation

Comparison of friction factor with helical spacer wire and straight spacer wire is presented in Fig.4.5 (b). It is seen that the friction factor with helical spacer wire is higher than that of straight spacer wire. The value of friction factor for straight wire smooth pin bundle is 0.018 from Blasius correlation (1913).

The variation of friction factor with helical pitch is plotted and presented in the Fig. 4.5 (c). It is seen that friction factor drastically reduces from 0.033 for 100 mm helical pitch to 0.0175 for 600 mm helical pitch.

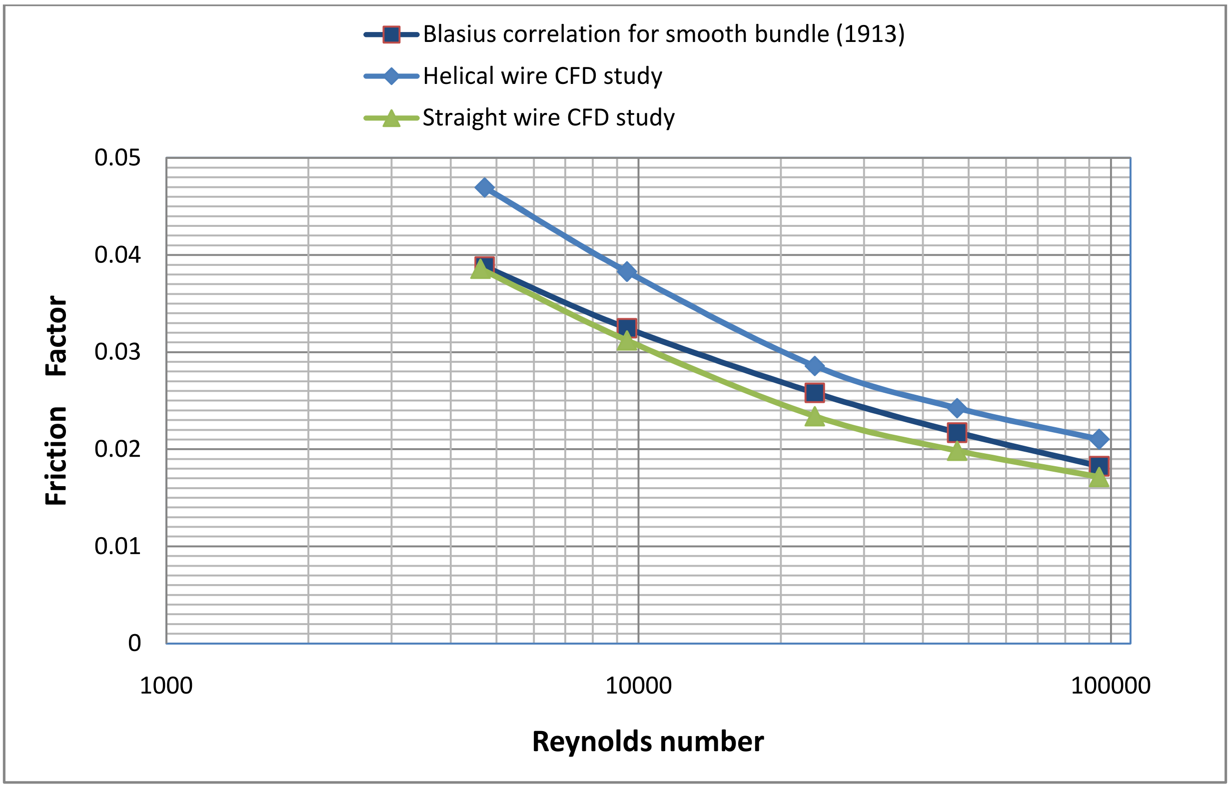

Fig. 4.5 (b) Comparison of friction factor of helical and straight wire pin bundle with Blasius correlation

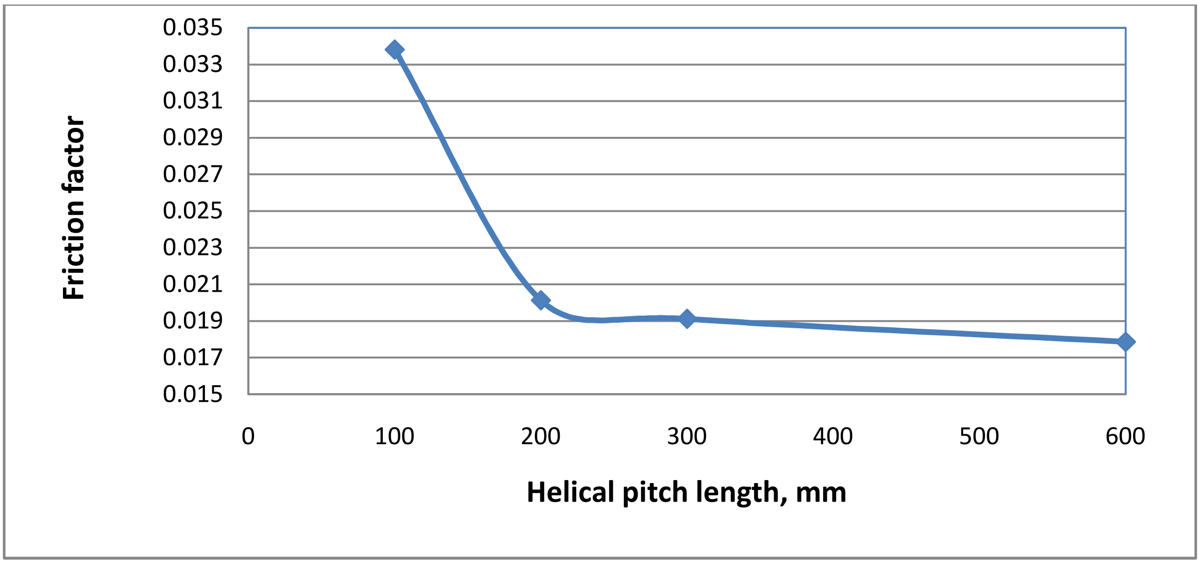

Fig. 4.5 (c) Variation of friction factor with helical pitch length for 7 pin bundle

4.6 SODIUM TEMPERATURE DISTRIBUTION WITH HELICAL WIRE 7 PIN BUNLDE

The sodium temperature distribution in the pin bundle with spacer wire is depicted in Figs. 4.6 (a) – 4.6 (f) in the form of contours at various axial planes. These results are for an axial entry velocity of 7.53 m/s and Reynolds number 100,000. It is observed that the sodium temperature increase is higher in the central sub-channels, as sodium flowing in these sub-channels is heated all-around, because these channels are formed by fuel pins. The sodium temperature increase is less in the peripheral sub-channels since the heat input per unit length in these channels are less due to the presence of hexagonal sheath which is adiabatic. The bulk temperature increase of sodium between the inlet and the outlet is 32 K, satisfying the heat balance requirement. The temperature field at any elevation depends on the wire position. The temperature is maximum at the outlet where wire position is facing the hexagonal sheath. The temperature is minimum in the position which is diametrically opposite to the maximum temperature region.

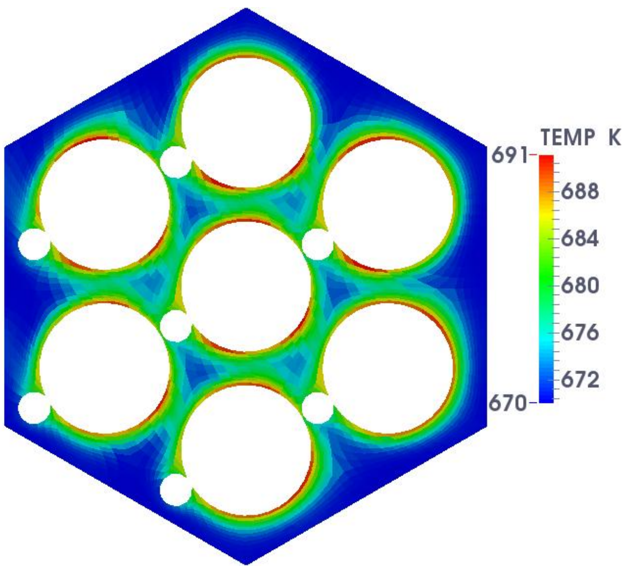

Fig. 4.6 (a) Temperature field at 33 mm from the inlet of helical wire wrap 7 pin bundle

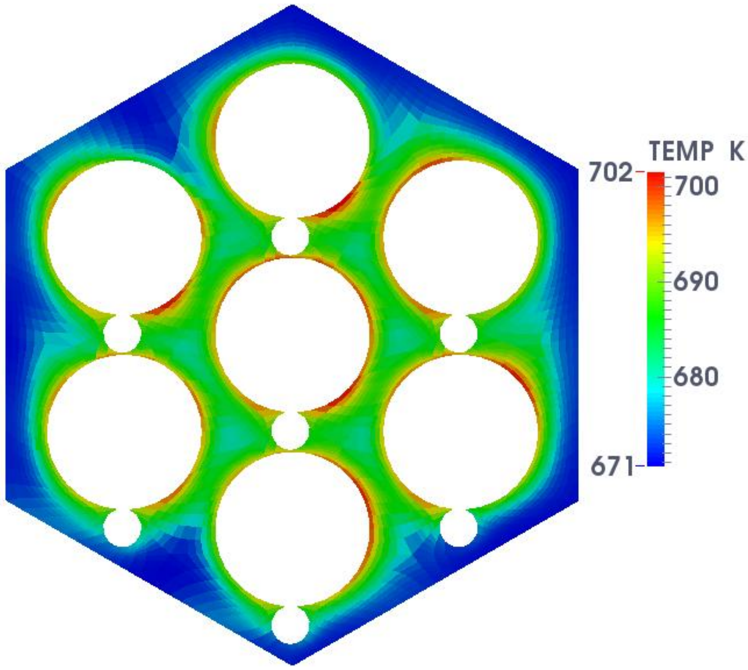

Fig. 4.6 (b) Temperature field at 66 mm from the inlet of helical wire wrap 7 pin bundle

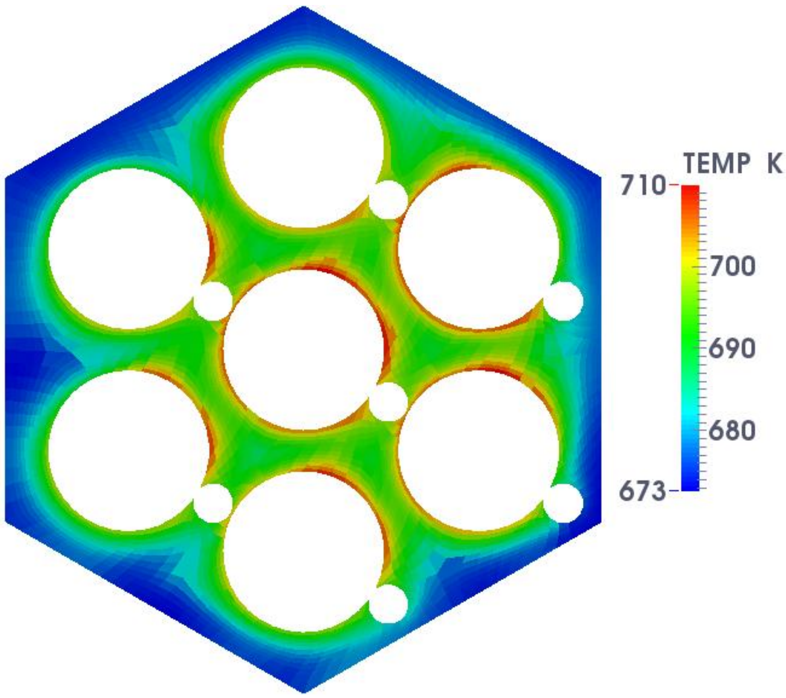

Fig. 4.6 (c) Temperature field at 99 mm from the inlet of helical wire wrap 7 pin bundle

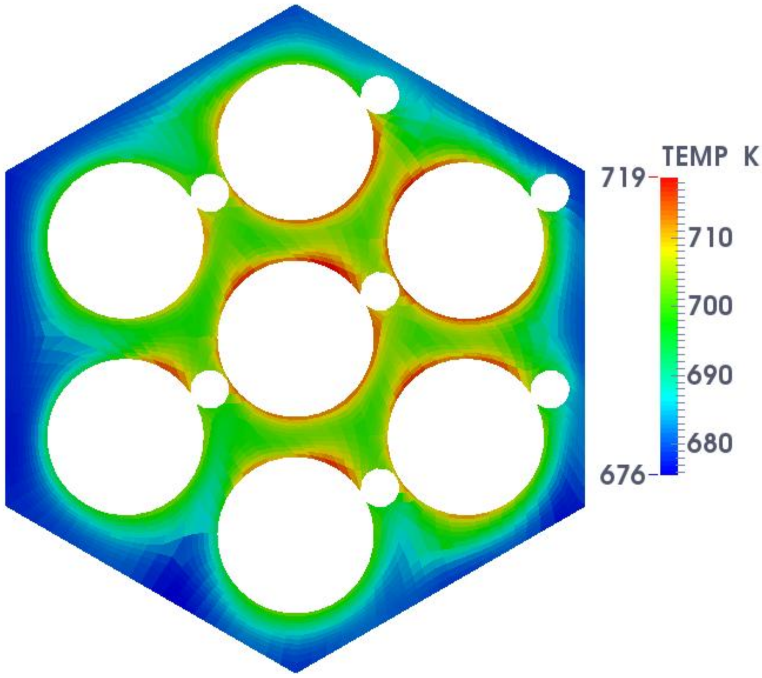

Fig. 4.6 (d) Temperature field at 133 mm from the inlet of helical wire wrap 7 pin bundle

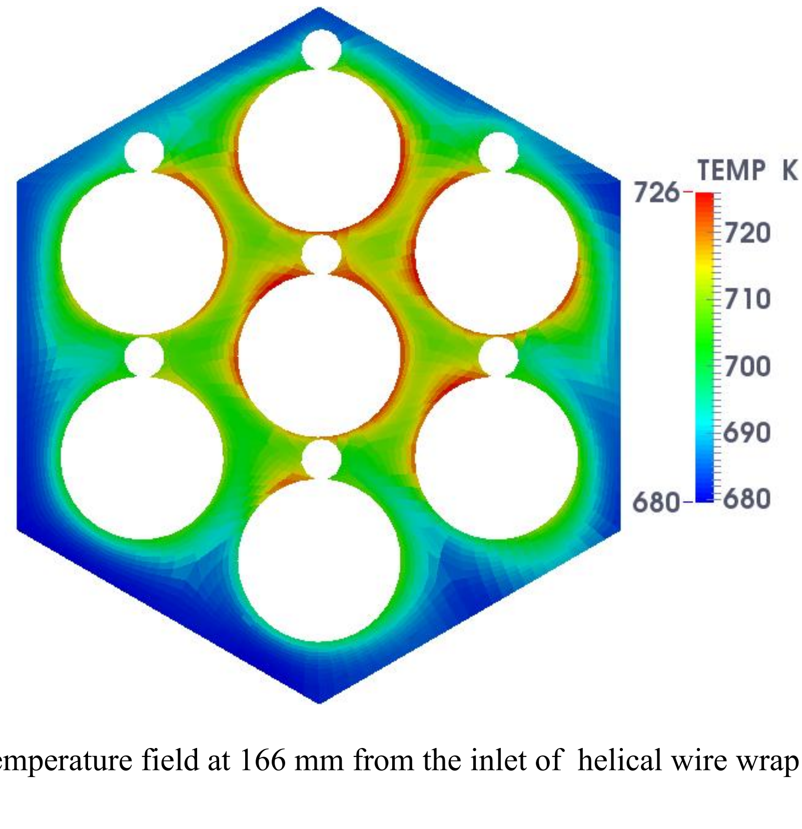

Fig. 4.6 (e) Temperature field at 166 mm from the inlet of helical wire wrap 7 pin bundle

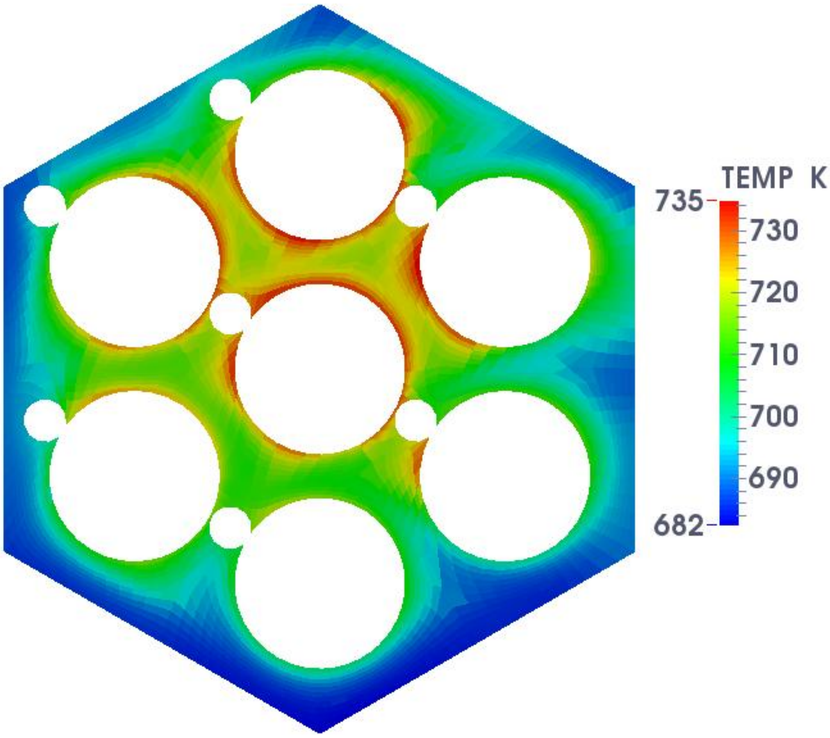

Fig. 4.6 (f) Temperature field at the exit of helical wire wrap 7 pin bundle

4.7 COMPARISON OF SODIUM TEMPERATURE DISTRIBUTION IN STRAIGHT WIRE PIN BUNDLE WITH HELICAL WIRE PIN BUNDLE

The sodium temperatures at the exit of straight wire and helical wire pin bundle are presented in Figs. 4.7 (a) – 4.7 (b) for comparison. From Fig. 4.7 (a), it is seen that the maximum clad temperature is 765 K and the same for helical wire is 735 K. The maximum clad temperature is higher in the case straight wire bundle due to the absence of transverse flow. The maximum temperature occurs at the location of the gap between pin and wire. The ΔT between the bulk sodium in the central sub-channel and peripheral sub-channel is 38 K for straight wire and the same for helical wire is 22 K. The difference in bulk sodium temperature between the central and peripheral sub-channels is less in the case with helical wire than the case of straight pin bundle due to the presence of secondary flow. Hence, the outlet temperature is more uniform in the case of helical wire bundle. The helical wire forces the hot sodium from the central sub-channels to move out to peripheral sub-channels to mix with the relatively cold sodium and direct the relatively cold sodium at the periphery towards the center. These inward and outward flows create good mixing of the hot sodium at the central sub-channels with the relatively colder sodium at the periphery, rendering a more uniform temperature profile across the pin bundle and reduced hot spot on the pin. The average sodium temperature at the outlet in both the cases is 702 K. The bulk temperature increase of sodium between the inlet and the outlet is 32 K satisfying the heat balance requirement.

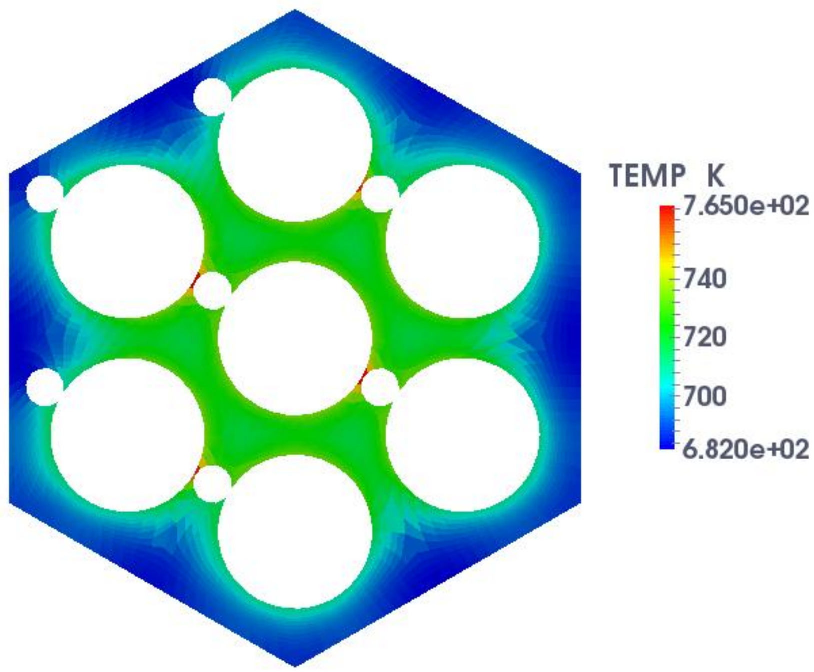

Fig. 4.7 (a) Temperature field at the exit of straight wire 7 pin bundle

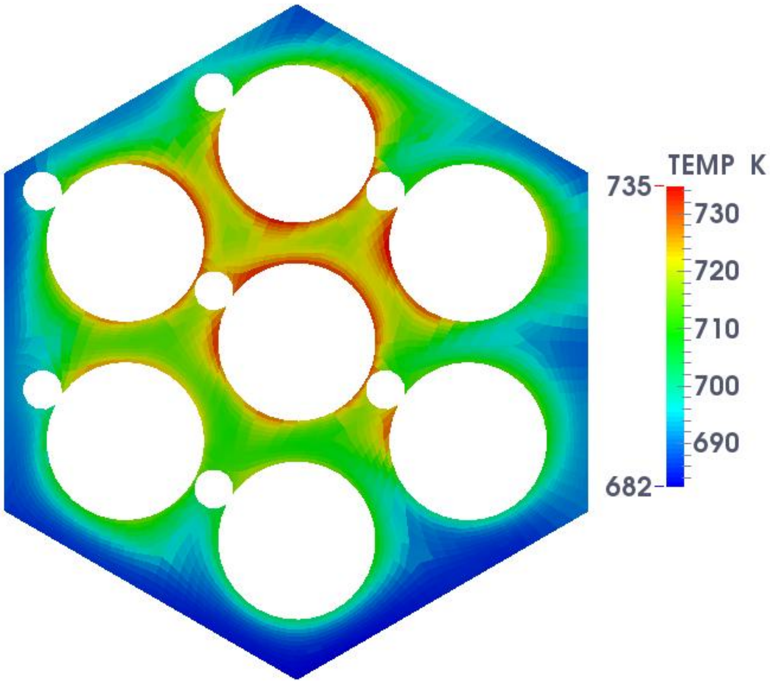

Fig. 4.7 (b) Temperature field at the exit of helical wire 7 pin bundle

4.8 NUSSELT NUMBER IN HELICAL AND STRAIGHT WIRE BUNDLE

The Nusselt number at the exit of helical wire wrapped and straight wire 7 pin bundle for Re = 100, 000 is presented in Fig. 4.8 along with the correlation based on experimental data. It is seen that the Nusselt for helical wire wrapped bundle is 15 % higher than that of the straight wire bundle in the turbulent regime (Re > 4000) and nearly equal in the laminar regime (Re < 2500). It is also seen that the Nusselt number predicted by the present CFD study is higher than the experimental data in the turbulent regime. This is due to the increased heat transfer coefficient due to helical wire which is probably not considered in the experimental correlation.

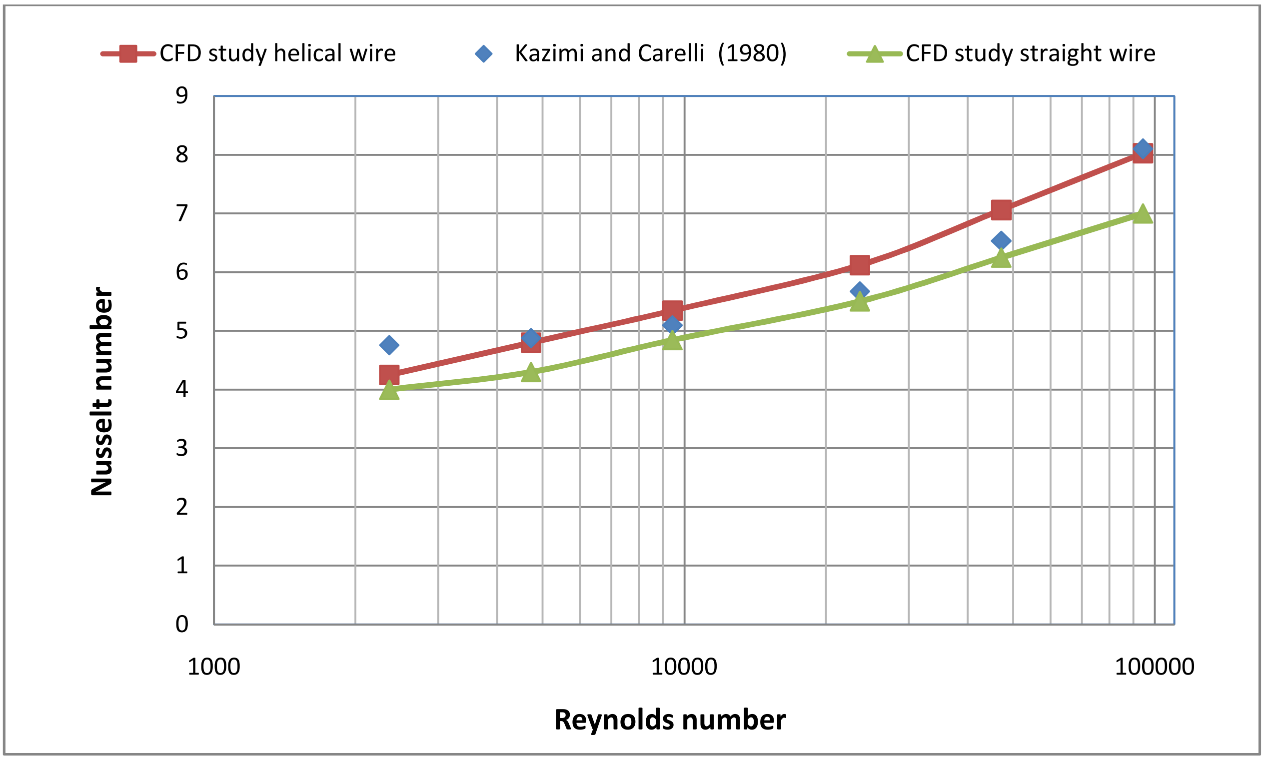

Fig. 4.8 Comparison of Nusselt number at the bundle exit of helical and straight wire 7 pin bundle with experimental correlation

4.9 THERMAL BENEFITS OF TRANSVERSAL FLOW DUE TO HELICAL WIRE

There are three advantages realized due to the transversal flow created by helical spacer wire. One is the sodium outlet temperature has become more uniform due to the fact that the temperature difference (ΔT) between sodium in the central sub-channels and in the periphery sub-channels is reduced. The low value of ΔT leads to lower levels of fluctuation in the readings of core monitoring thermocouples which is essential for online monitoring. The second advantage is that the clad temperature has become more uniform in the circumferential direction due to the circulating flow created by helical wire. The coolant is made to impinge and sweep the corners formed by the junction of the pin and spacer wire. This sweeping prevents possible hot spot beneath the wire wrap. The third advantage is that the fuel subassembly can be designed to generate a larger power without exceeding the temperature limits of clad and sodium.

4.10 CLOSURE

The friction factor of the pin bundle with helical wire and straight wire obtained from the present study is seen to agree well with the reported experimental data. It is observed that the helical wire induces a secondary swirl in the pin bundle which promotes cross stream mixing of the coolant to make its temperature more uniform. The transverse flow reduces the sodium temperature difference between the inner and outer sub-channels to 22 K (in the case of helical wire pin bundle) from 38 K (in the case of straight wire pin bundle).

CHAPTER - 5

THERMAL HYDRAULICS WITHIN 19, 37 AND 91 PIN BUNDLES

5.0 INTRODUCTION

In the earlier chapter, it was observed that the central sub-channels of 7 pin bundle are directly in communication with peripheral sub-channels. Hence, it is essential to understand the dependence of thermal hydraulic features on the number of pins in the bundle. Towards this, the thermal hydraulics characteristics of 19, 37 and 91 pin bundles have been predicted. This chapter is devoted for discussion of these results. For the results presented in this chapter, the helical pitch of the spacer wire is 200 mm. The pin diameter, wire diameter and triangular pitch are 6.6 mm, 1.65 mm and 8.28 mm respectively.

5.1 TRANSVERSE VELOCITY IN 19, 37 AND 91 PIN BUNDLES

The transverse velocity fields at the outlet of 19, 37 and 91 pin bundles for Reynolds number of 100,000 are presented in Figs. 5.1 (a) – 5.1 (f). The transverse velocity distributions are similar pattern to that of 7 pin bundle. The variation of average transverse velocity with number of pins in the bundle is presented in Fig. 5.1 (g). It is seen that the transverse velocity first decreases with increase in number of pins and then increases for higher number of pins. As the number of pins increases in the bundle, the number of rows between the central pin and peripheral pins increases. The equivalent diameter of the pin bundle with different number of pins in the bundle is presented in the Fig. 5.1 (h). The equivalent diameter decreases with number of pins in the bundle. This blocks the free communication between the sub-channels and establishes increased resistance to cross flow. The variation of inlet axial velocity with number of pins in the bundle which is a boundary condition is presented in Fig. 5.1 (i). The inlet velocity increases with number of pins in the bundle as the equivalent diameter decreases with increasing number of pins to keep the Reynolds number constant at 100,000. For higher number of pins, the axial velocity itself increases. Consequently, the transverse velocity is also increasing. As a result, the average transverse velocity is in the range of 0.76 – 0.67 m/s for 7 to 217 pins in the pin bundle respectively. The variation of ratio of axial velocity to transverse velocity is presented in Fig. 5.1 (j). It is seen that the ratio increases with increase in the number of pins and reaches a constant value. This is due to the combined effect of increased resistance to cross flow with increase in the number of pins in the bundle and increase in the inlet axial velocity to the bundle with number of pins.

5.2 AXIAL VELOCITY IN 19, 37 AND 91 PIN BUNDLES

The axial velocity fields at the outlet of 19, 37 and 91 pin bundles for the same Reynolds number of 100,000 are presented in Figs. 5.2 (a) – 5.2 (c). It is seen that the maximum axial velocity increases with number of rows of pins. The ratio of normalized axial velocity (ratio of maximum axial velocity to inlet velocity) for the central and peripheral sub channels are also indicated in the figures. It is noted that from 19 pin bundle onwards, the locations of maximum normalized velocities are in IV and V zones. The minimum normalized peripheral velocity zones (I and II) are located diametrically opposite to the maximum normalized velocity zones. In general, in all the pin bundles, the maximum axial velocities are in the zones where the wire is in the sub-channel. The minimum normalized axial velocities are in the zones which are diametrically opposite to the respective zones of maximum velocities.

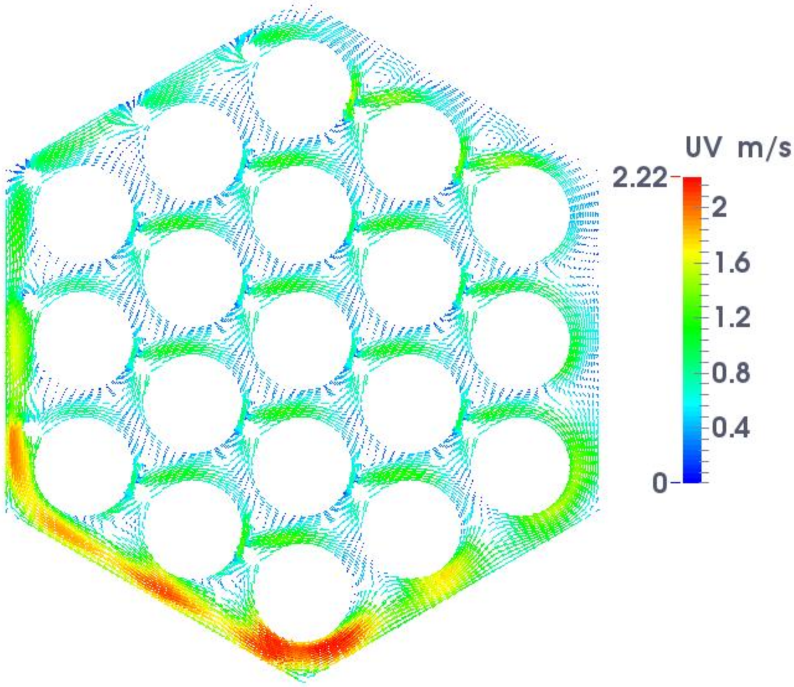

Fig. 5.1 (a) Transverse velocity field at the exit of helical wire wrap 19 pin bundle

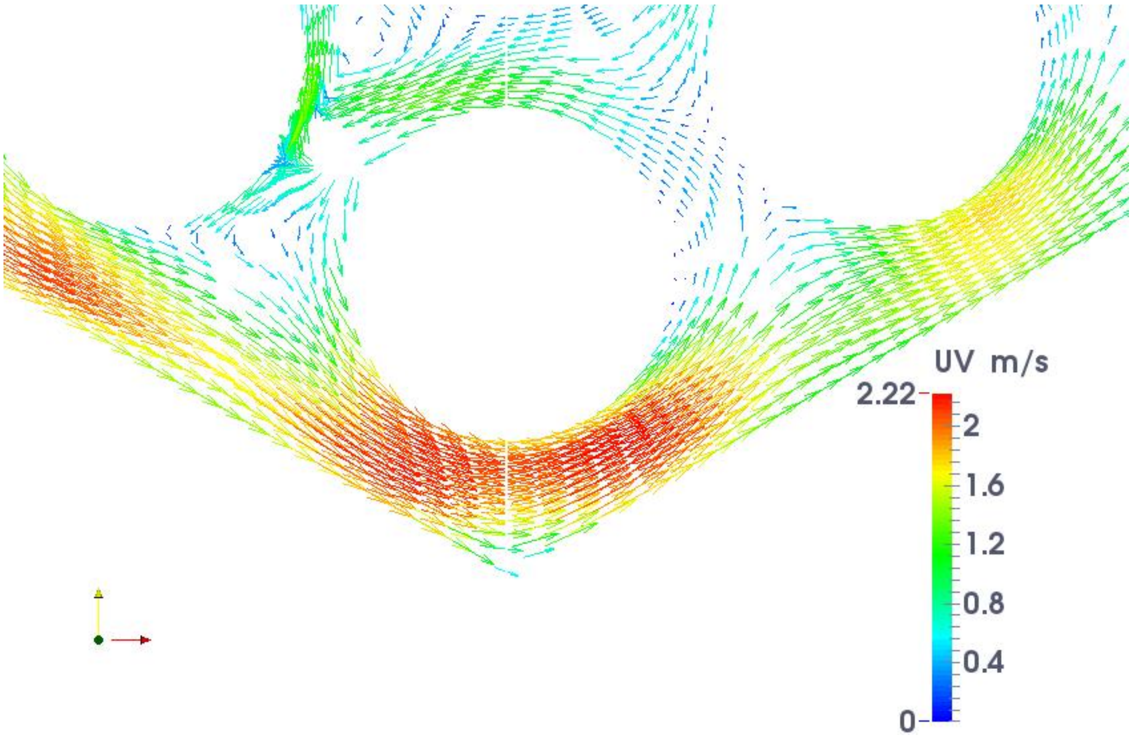

Fig. 5.1 (b) Close-up view of transverse velocity field at the exit of helical wire wrap 19 pin bundle in X-Y plane.

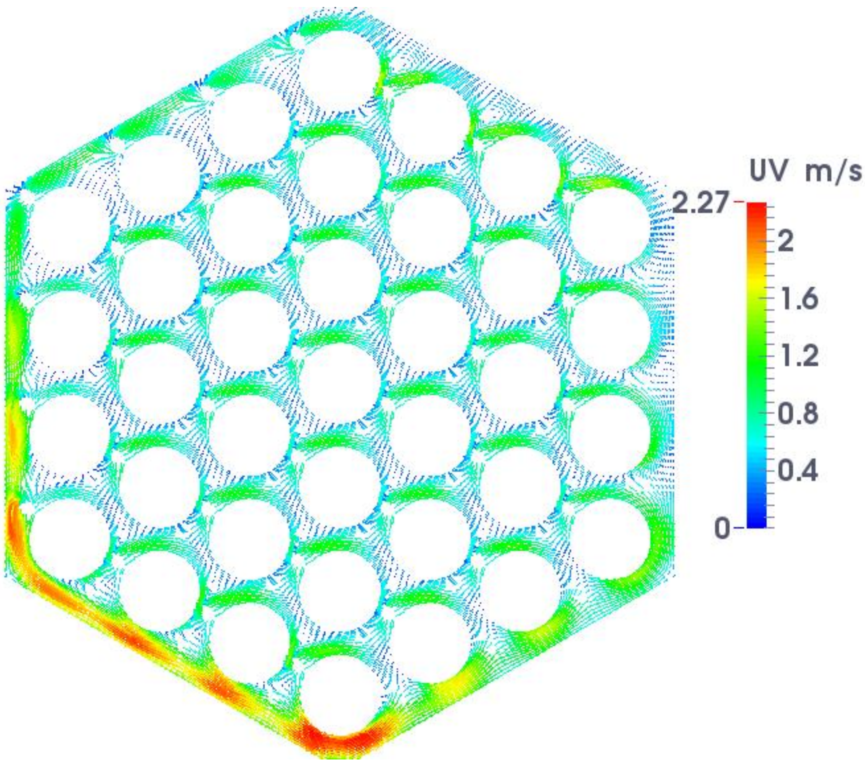

Fig. 5.1 (c) Transverse velocity field at the exit of helical wire wrap 37 pin bundle

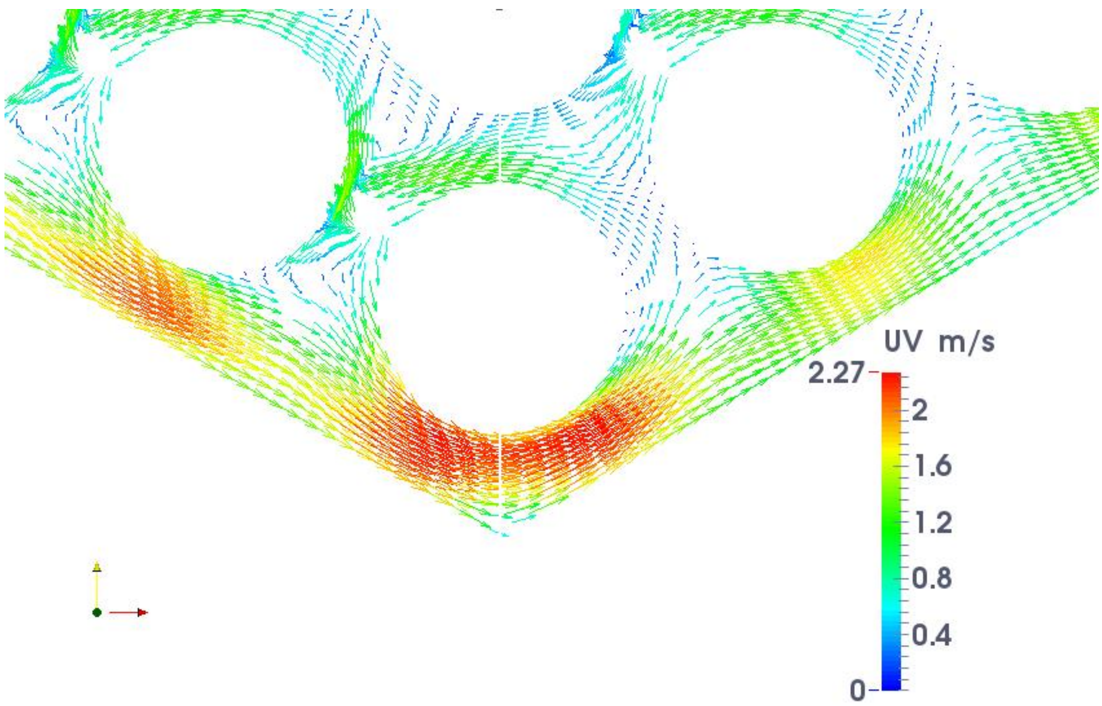

Fig. 5.1 (d) Close-up view of transverse velocity field at the exit of helical wire wrap 37 pin bundle in X-Y plane.

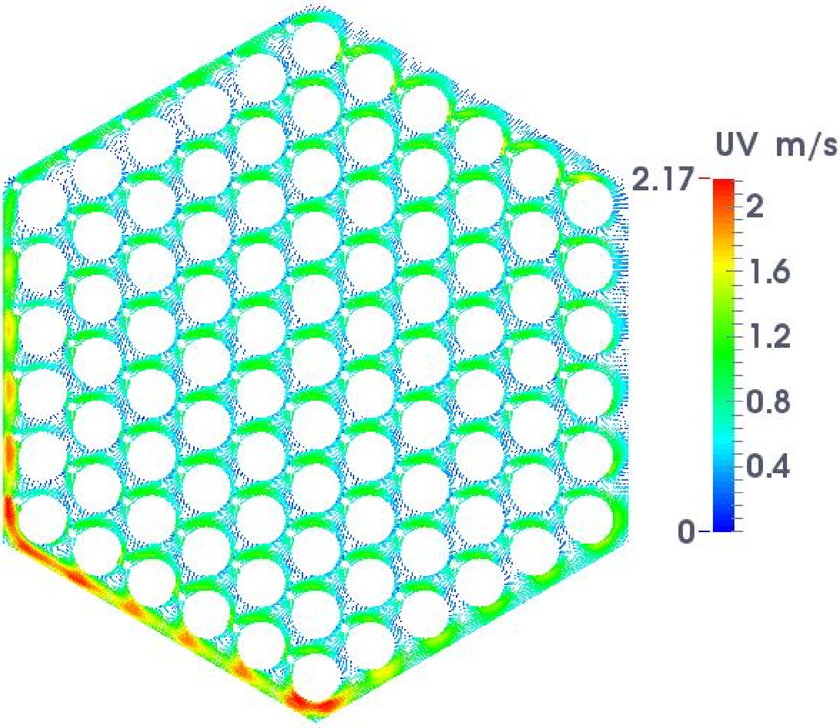

Fig. 5.1 (e) Transverse velocity field at the exit of helical wire wrap 91 pin bundle

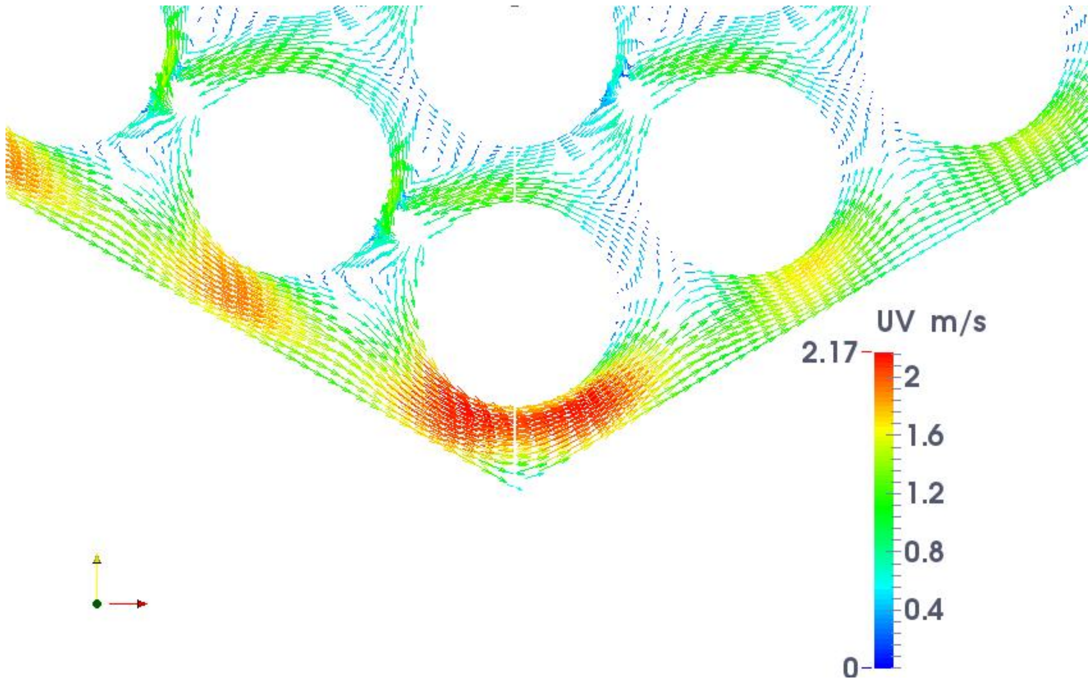

Fig. 5.1 (f) Close-up view of transverse velocity field at the exit of helical wire wrap 91 pin bundle in X-Y plane.

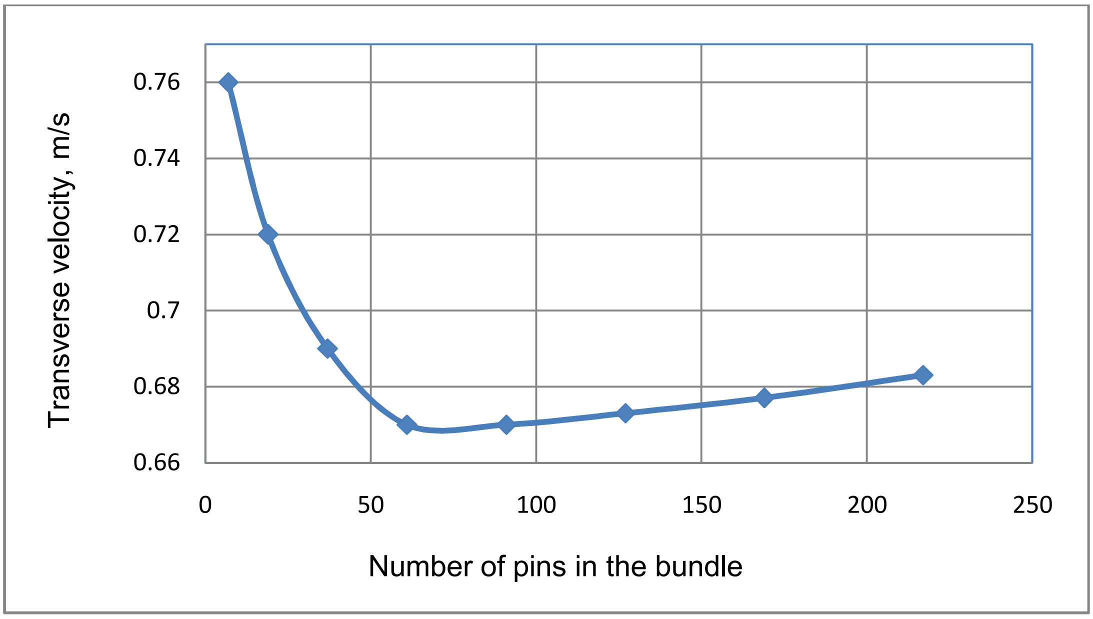

Fig. 5.1 (g) Variation of transverse velocity with number of pins in the bundle

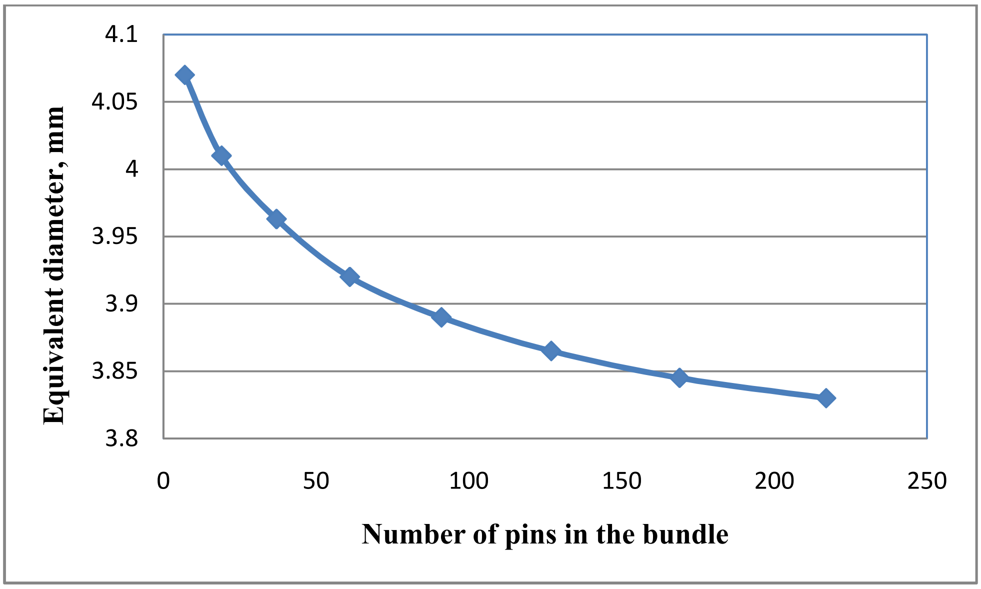

Fig. 5.1 (h) Variation of equivalent diameter with number of pins in the bundle

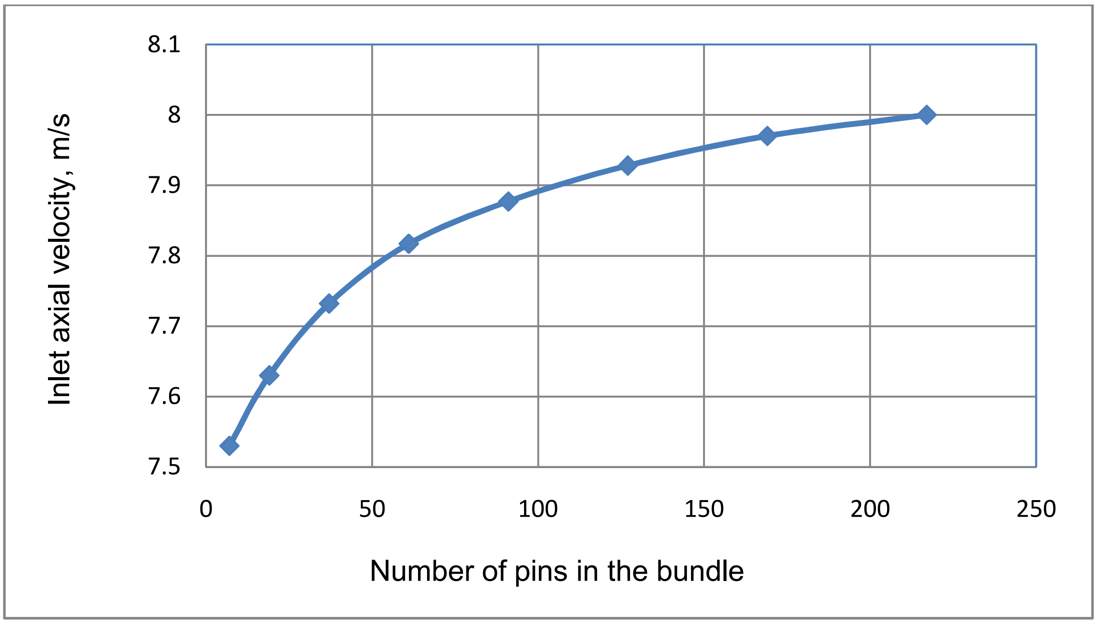

Fig. 5.1 (i) Variation of inlet axial velocity with number of pins in the bundle

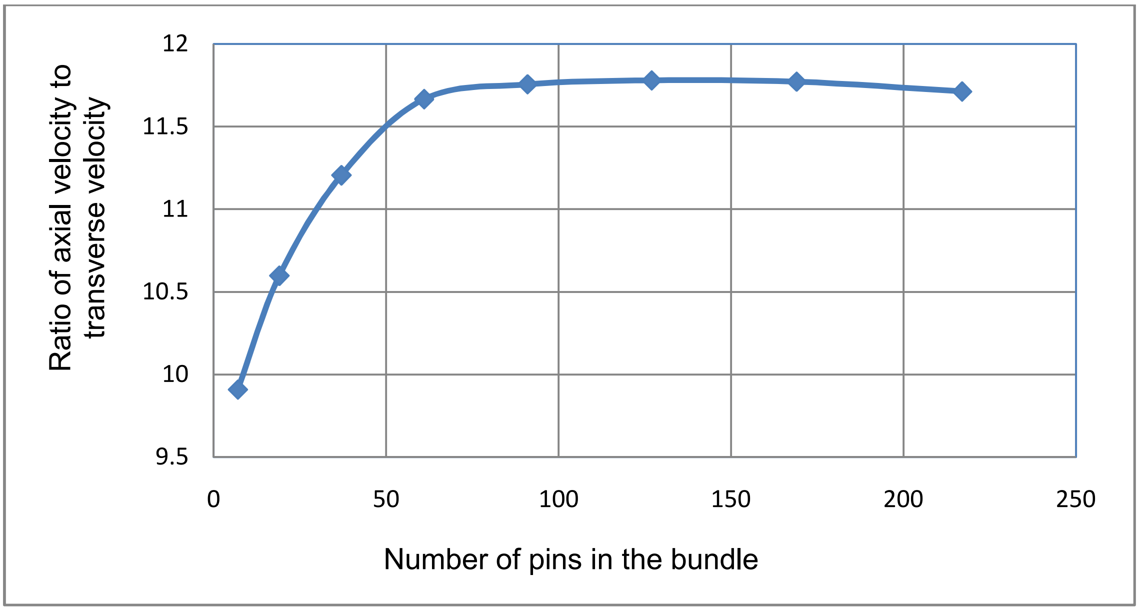

Fig. 5.1 (j) Variation of ratio of axial velocity to transverse velocity with number of pins in the bundle

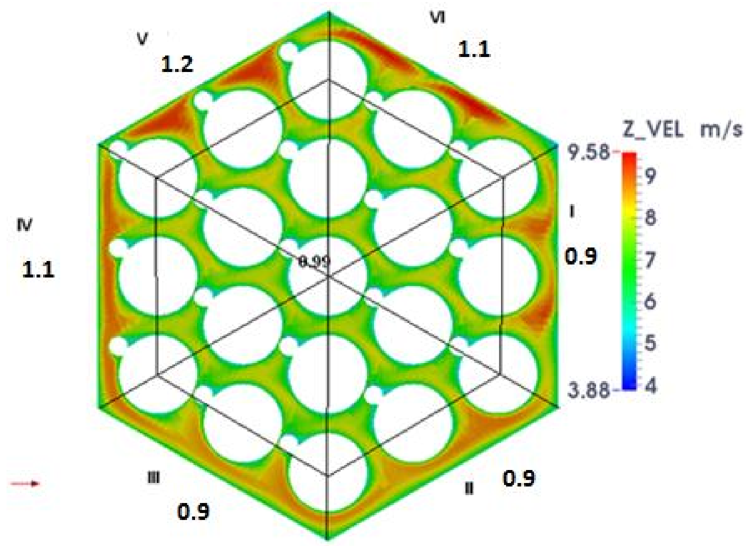

Fig. 5.2 (a) Axial velocity field at the exit of helical wire wrap 19 pin bundle indicating the values of normalized velocity at the central and peripheral sub channels

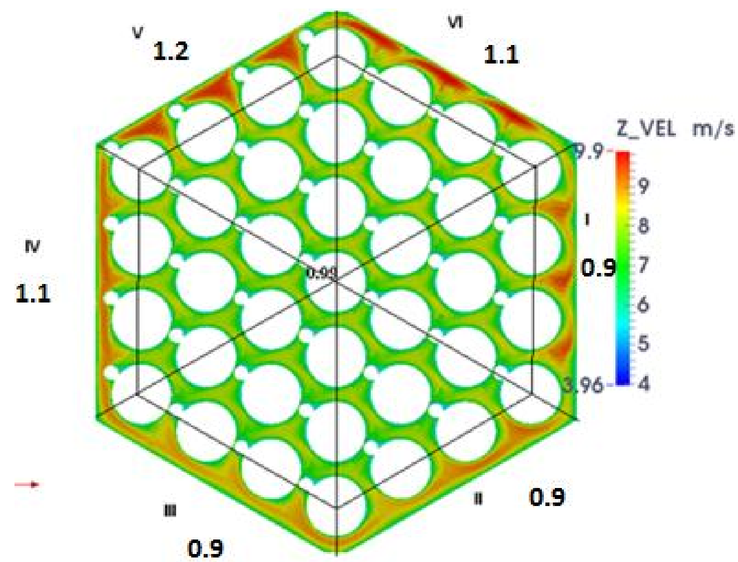

Fig. 5.2 (b) Axial velocity field at the exit of helical wire wrap 37 pin bundle indicating the values of normalized velocity at the central and peripheral sub channels

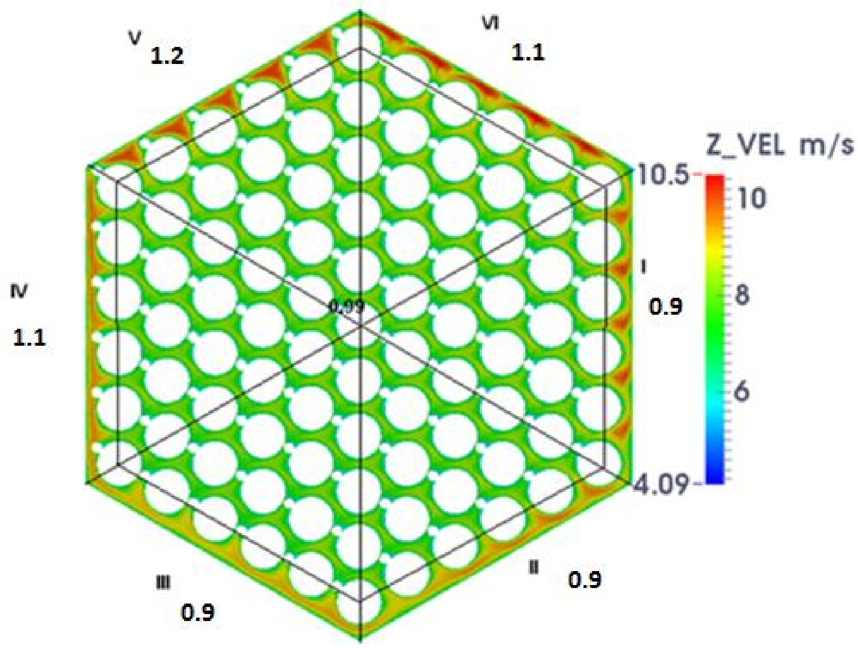

Fig. 5.2 (c) Axial velocity field at the exit of helical wire wrap 91 pin bundle indicating the values of normalized velocity at the central and peripheral sub channels

5.2.1 CFD Simulation of 91 Pin Water Model

Hydraulic experiments on a helical wire wrapped 91 pin bundle of 2/1 scale model of Fast Flux Test Facility (FFTF) fuel subassembly are presented by Lorenz. et al. 1974. The pin diameter is 12.7 mm. The pitch to diameter ratio is 1.24. The pitch of the helical wire is 610 mm. The Reynolds number is in between 9000 and 24000. The results are summarized as follows. The sub-channel velocities are normalized with respect to the bundle velocity (Fig. 5.2 (d)). The velocity measurements obtained reveal that the average sub-channel velocities for both the edge and the central sub-channels are nearly equal to the average bundle velocity. The edge sub-channel velocity is the maximum when a wire wrap is in the sub-channel and minimum when it is far away from the sub-channel. The edge sub-channel velocities vary from 0.85 and 1.1. It is also reported that the maximum normalized peripheral velocities are in the IV and V zones and minimum velocities are in I and II zones (Fig. 5.2 (d)). The present CFD results of axial velocities for 19, 37 and 91 pin bundles compare favorably with the experimental findings in 91 pin bundle. It can be seen that the present predictions of average velocity in the central zones match very well the experimental findings, with a maximum deviation of about 5%. In the peripheral zones, while the trend of the results matches, the absolute values in the numerical simulations are over-predicted by a maximum of 10 %. This is attributed to the marginal difference in gap between the outermost pins and the hexagonal sheath considered in the numerical and experimental simulations.

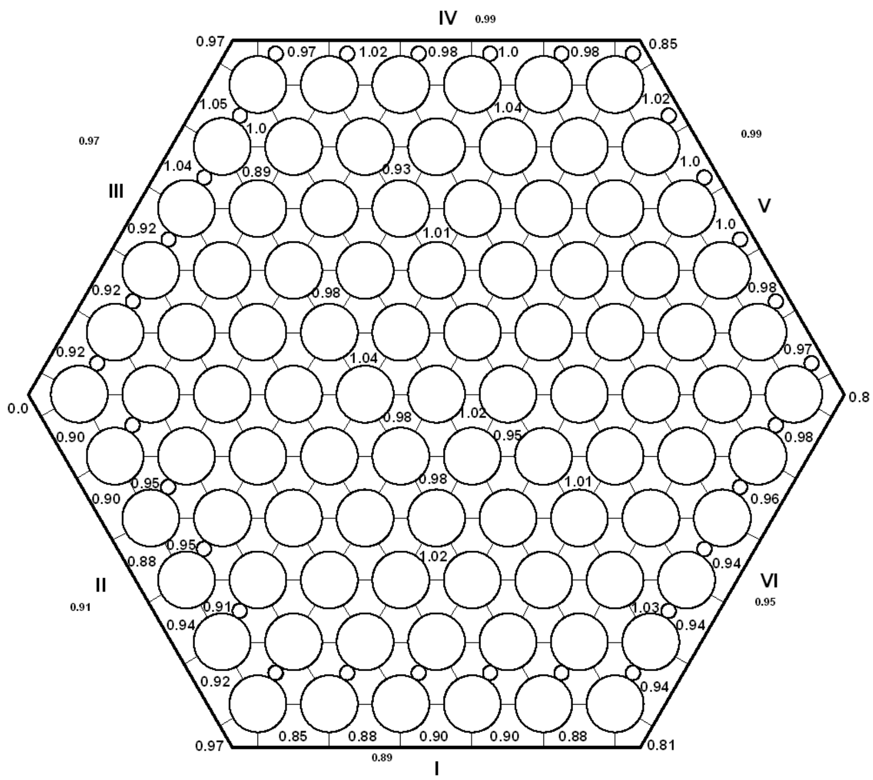

Fig. 5.2 (d) Experimental axial velocity field at the exit of helical wire wrap 91 pin bundle indicating the values of normalized velocity at the central and peripheral sub channels

5.3 COMPARISON OF FRICTION FACTOR IN 19, 37 and 91 PIN BUNDLES

The values of friction factors obtained from the CFD study for 19 and 37 pin bundles are compared with those obtained using Chen et al. (2014) correlation for friction factor in Fig. 5.3 for various values of Reynolds number. It is seen that the agreement is very good with a maximum deviation of 15 %, with the CFD model in the laminar regime consistently over-predicting the friction factor.

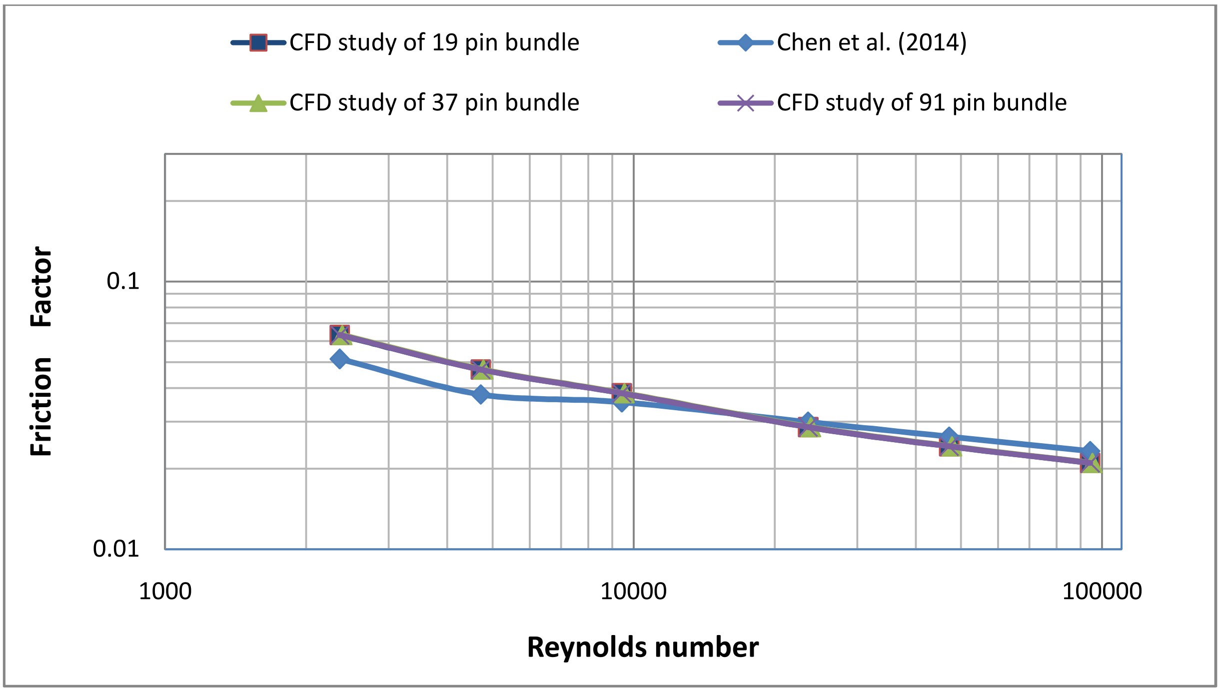

Fig. 5.3 Comparison of friction factor of various pin bundles with Chen et al (2014) correlation

It is seen that the friction factor marginally increases with number of pins as the ratio of axial velocity to transverse velocity increases marginally with number of pins with fixed Reynolds number condition. The turbulence increases with increase in number of pins in the pin bundle which leads to increase in friction factor.

5.4 SODIUM TEMPERATURE DISTRIBUTION IN 19, 37 and 91 PIN BUNDLES

The temperature field at the outlet of 19, 37 and 91 pin bundles for the same Reynolds number of 100, 000 and same mean outlet temperature of 702 K are presented in Figs. 5.4 (a) – 5.4 (c). From the hydraulic analysis, it is seen that the axial velocity is higher in the zones where spacer wire is present. In the thermal analysis, it is observed that in general the sodium temperature is also higher in these zones, which is contrary to the normal expectation. This is because of the fact that although the velocity is high, the flow area is less due to the presence of the spacer wires in these hot zones, leading to lower mass flow rate compared to the heat deposited in the peripheral zones. Incidentally, the cross-flow velocity is minimum in these zones. The temperature is minimum in the peripheral zones where the circumferential flow is large. This happens in the peripheral zones where there is no spacer wire between the pin and the hexagonal sheath leading to larger mass flow rate around the pins despite lower axial velocities. CFD simulation is capable of bringing out such intricate flow physics. The minimum, maximum and average temperatures in these zones either increase or remain insensitive to the number of pins. Also, due to the action of transverse velocity, the difference between the bulk sodium temperatures of the central and peripheral zones are 20 and 19.5 and 18.5 K respectively for 19, 37 and 91 pin bundles. The helical wire forces the hot sodium from the central sub-channels to move out to peripheral sub-channels to mix with the relatively cold sodium and direct the relatively cold sodium at the periphery towards the center. These inward and outward flows create good mixing of the hot sodium at the central sub-channels with the relatively colder sodium at the periphery hence giving a more uniform temperature profile.

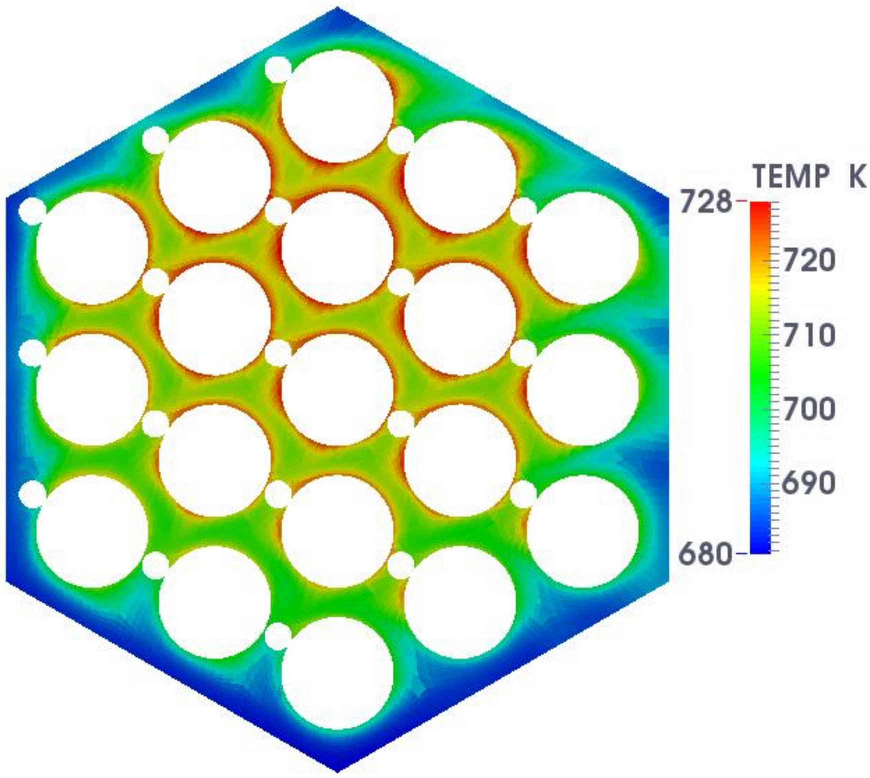

Fig. 5.4 (a) Temperature field at the exit of helical wire wrap 19 pin bundle

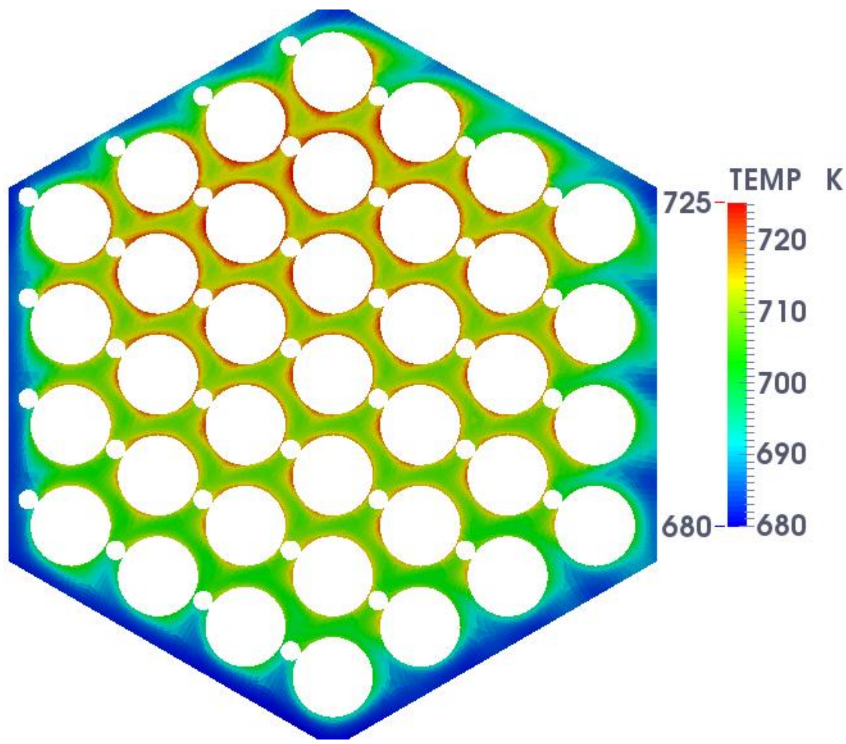

Fig. 5.4 (b) Temperature field at the exit of helical wire wrap 37 pin bundle

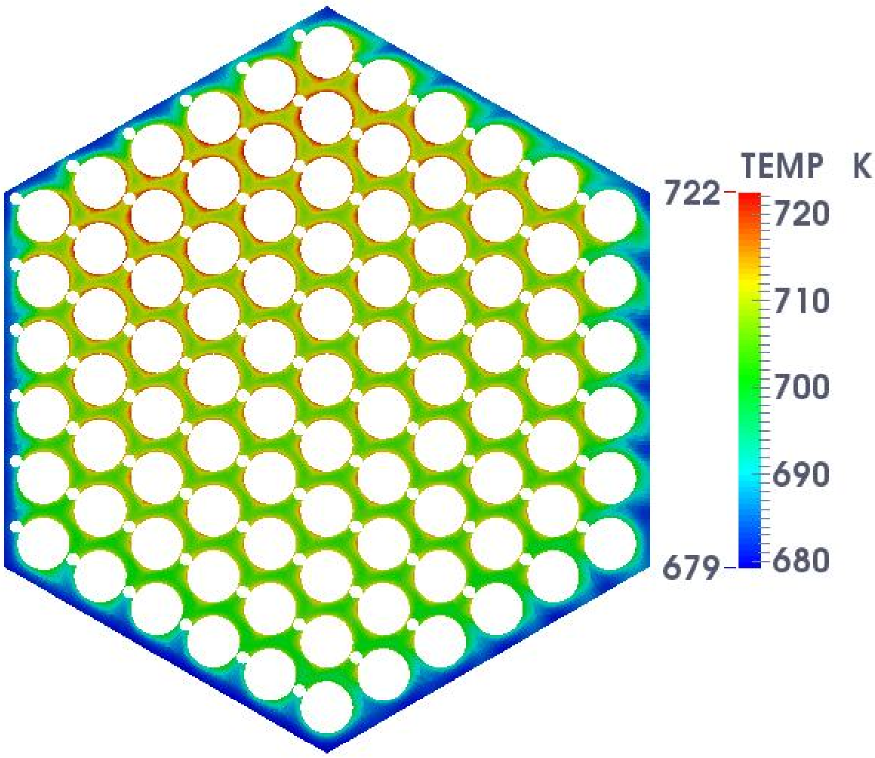

Fig. 5.4 (c) Temperature field at the exit of helical wire wrap 91 pin bundle

5.5 COMPARISON OF NUSSELT NUMBER IN 19, 37 and 91 PIN BUNDLES

The Nusselt number at the exit of various helical wire wrapped pin bundles and for various values of Reynolds number is presented in Fig. 5.5 (a) along with the experimental data. The Nusselt number for a particular Re = 100, 000 is presented in Fig. 5.5 (b) as a function of number of pins. It is seen that the Nusselt number marginally increases with number of pins in the bundle with its dependence on number of pins is more in the turbulent regime as compared to that in the laminar regime due to increased turbulent mixing with more number of pins. It is seen that the Nusselt number predicted by CFD study is higher than the experimental data in the turbulent regime. This is due to the increased heat transfer coefficient due to helical wire which is probably not considered in the experimental correlation.

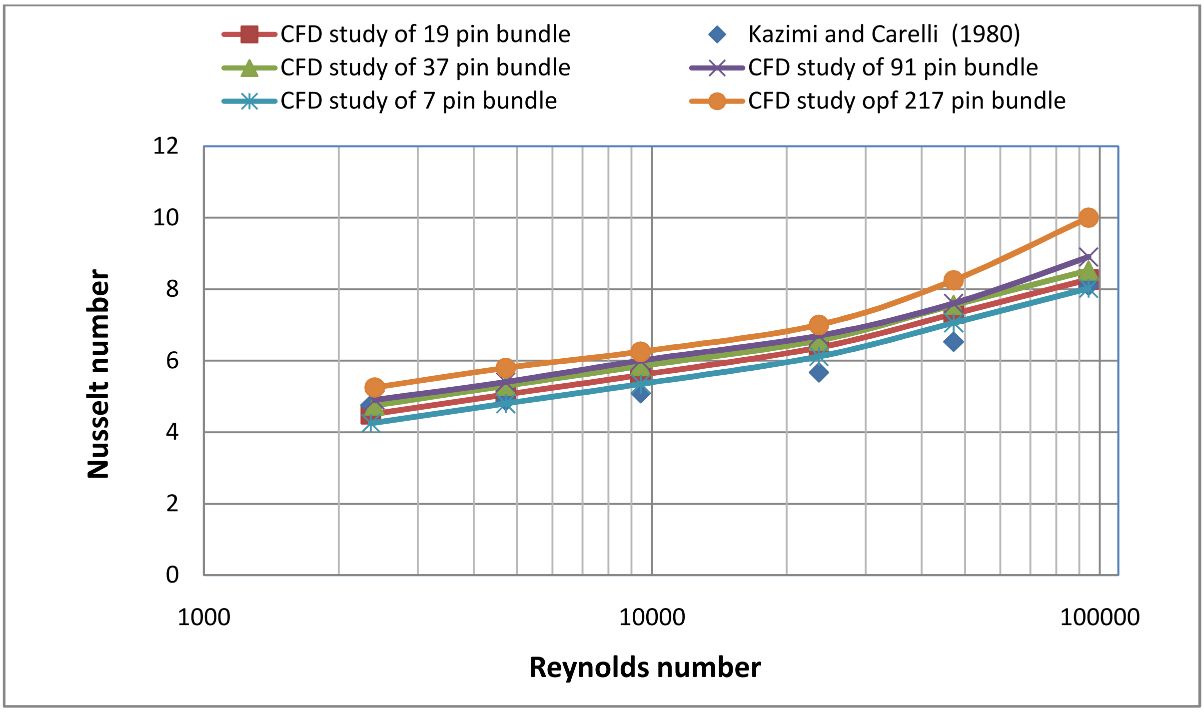

Fig. 5.5 (a) Comparison of Nusselt number for various pin bundles with Kazimi and Carelli correlation (1980)

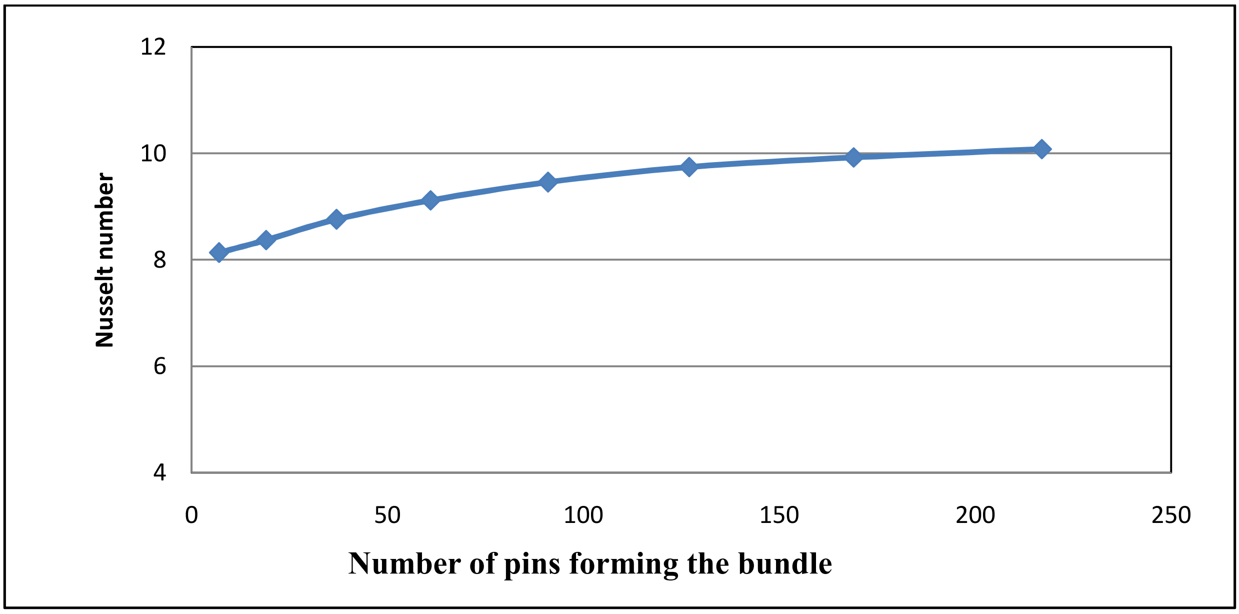

Fig. 5.5 (b) Variation of Nusselt number with number of pins for Re = 100,000

5.6 CLOSURE

It is seen that the axial velocity is maximum in the peripheral zone where spacer wires are located between the pins and the hexagonal sheath. The velocity is minimum in the zone which is diametrically opposite to the respective zone of maximum velocity. The average normalized axial velocities of the peripheral and central zones vary from 1.1 to 0.9 for all the bundles. This is in good agreement with the experimental measurements of 1.1 and 0.85 for a 91 pin bundle. The friction factor values of the pin bundles obtained from the present study are seen to agree well with the values derived from reported experimental correlations. The turbulence increases with increase in number of pins in the pin bundle which leads to marginal increase in the pressure drop and friction factor. The sodium temperature is higher in the zones where the flow area and hence the mass flow rate are less due to the presence of the spacer wires though the axial velocity is higher. The sodium temperature is minimum in the wall sub-channels where the circumferential flow is larger, leading to larger mass flow rate around the pins despite the lower axial velocities. The transverse flow reduces the sodium temperature difference between the central and peripheral sub-channels in the pin bundles. It is seen that the Nusselt number predicted by CFD study is higher than the experimental data in the turbulent regime. This is due to the increased heat transfer coefficient due to helical wire which is not considered in the experimental correlation. It is seen that the Nusselt number marginally increases with number of pins in the bundle with its dependence on number of pins is more in the turbulent regime as compared to that in the laminar regime due to increased turbulent mixing with more number of pins.

CHAPTER - 6

THERMAL HYDRAULICS WITHIN 217 PIN BUNDLE

6.0 INTRODUCTION

The thermal hydraulics within 217 pin fuel bundle has been studied in detail. The geometrical dimensions are depicted in Fig. 1.2 (a). The thermal hydraulics effect of helical wire spacer over the straight wire spacer is studied to ascertain the effect of helical wire in 217 pin bundle. One of the parameters that require detailed assessment is the ligament gap between the spacer wire of the outermost row of pins and the hexagonal sheath. For the purpose of tolerance allowance, this gap is kept as 0.1 mm. It is required to see the thermal hydraulics effect of reducing this nominal gap of 0.1 mm to 0.03 mm which is the minimum value feasible. Hence, the study of 217 pin bundle with this two different ligament gaps has been carried out. The nominal length of the heat generating portion of the 217 fuel pin bundle is 1000 mm which is equal to 5 pitch length of the helical wire (one pitch length of the helical wire is 200 mm). Hence, the 217 pin bundle is also studied for 1000 mm length. The results of all the above studies are discussed in this chapter.

6.1 EFFECT OF HELICAL WIRE SPACER OVER THE STRAIGHT WIRE SPACER

The cross stream velocity distributions at the exit of 217 pin bundle with helical wire and with straight wire for the same Re = 100,000 are presented in Figs.6 1 (a) - 6.1 (c). It is seen that the cross-stream velocity is active with helical wire wrap with maximum and average velocity of 2.2 and 0.683 m/s respectively and is absent in the case of straight wire-wrap bundle. The maximum transverse velocity is only 9 mm/s with straight wire case.

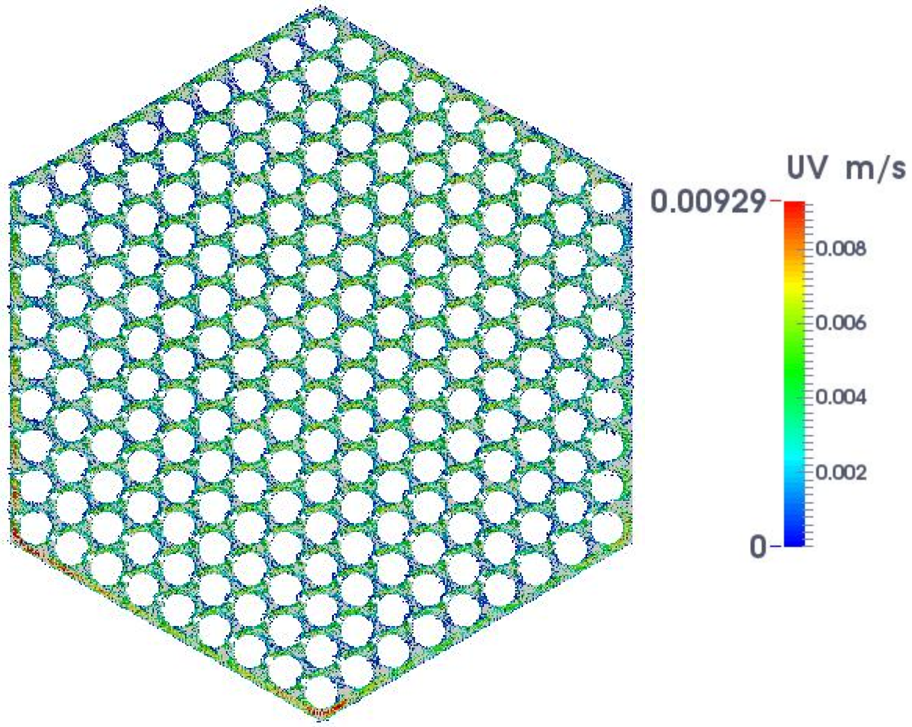

Fig. 6.1 (a) The transverse velocity field at the exit of straight wire wrap 217 pin bundle

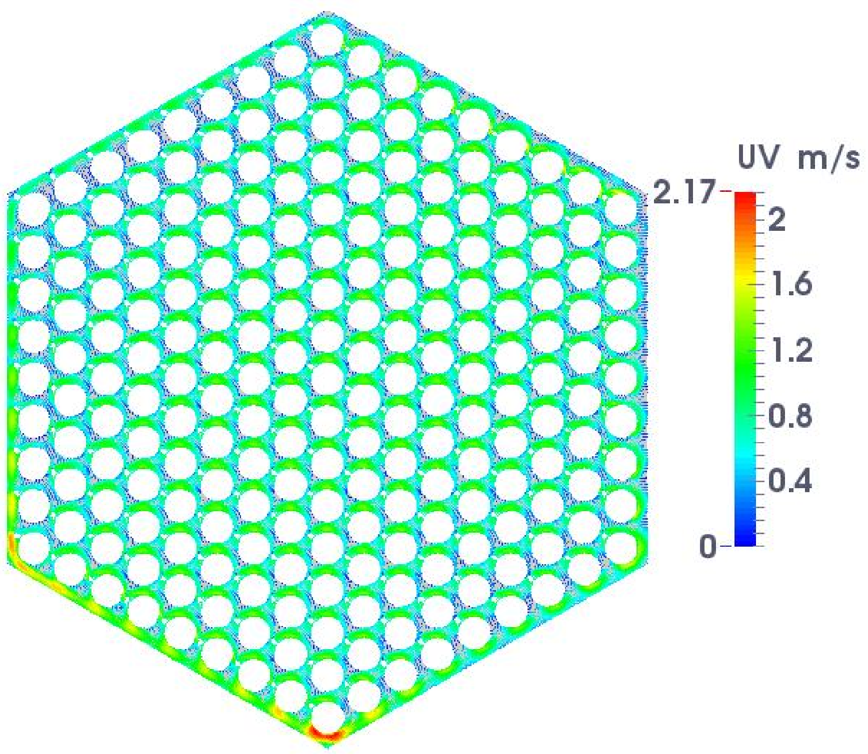

Fig. 6.1 (b) The transverse velocity field at the exit of helical wire wrap 217 pin bundle

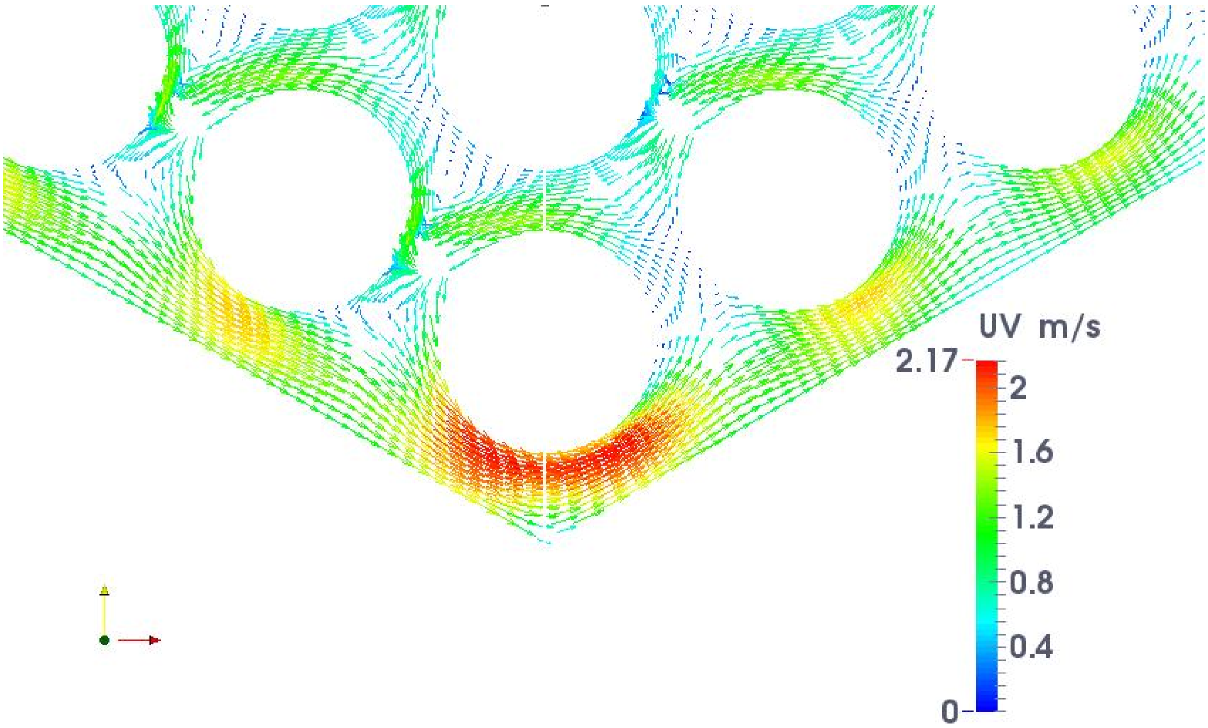

Fig. 6.1 (c) Close-up view of transverse velocity field at the exit of helical wire wrap 217 pin bundle in X-Y plane.

The axial velocity distributions at the exit of 217 pin bundle with helical wire and straight wire for the same Re = 100,000 are presented in Figs.6 1 (d) - 6.1 (e). It is seen that the axial velocity is uniform in all the central sub-channels as well as in the peripheral sub-channels at the outlet in the case of straight wire bundle with the maximum axial velocity of 9.7 m/s. The maximum axial velocity in helical wire wrap bundle is 10.9 m/s. The central zone has uniform axial velocity nearly equal to that of the inlet velocity (8 m/s). The maximum peripheral axial velocity is in the zone where helical wire is present. The increase in axial velocity in the case of helical wire wrap bundle is due to transverse velocity induced by the helical wire.

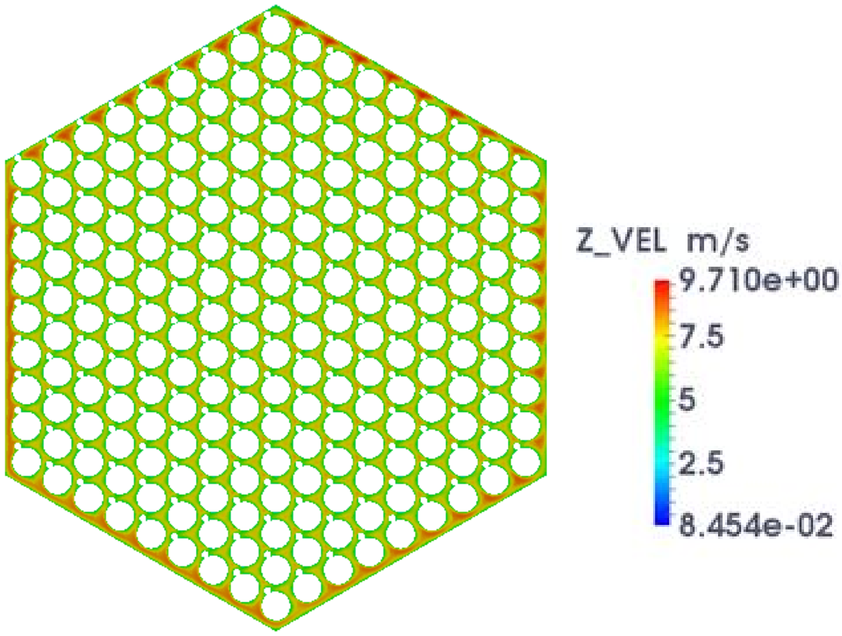

Fig. 6.1 (d) The axial velocity field at the exit of straight wire wrap 217 pin bundle

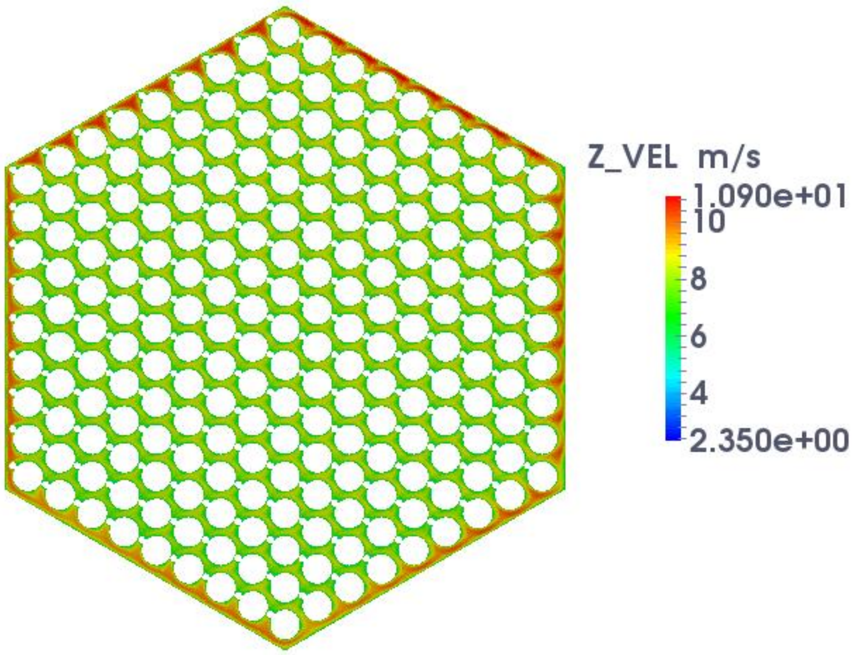

Fig. 6.1 (e) The axial velocity field at the exit of helical wire wrap 217 pin bundle

The temperature distributions at the exit of 217 pin bundle with straight wire and helical wire for the same Re = 100,000 and for the same outlet temperature of 702 K, are presented in Figs.6 2 (a) - 6.2 (b). These results are at 200 mm from the inlet. In the straight wire bundle, the temperature distribution is nearly symmetrical. In the helical wire-wrap bundle, there is asymmetric distribution of sodium temperature. The maximum temperature is in the central zone adjacent to the peripheral zone where wire is present. It is seen that the maximum clad temperature is 750 K for straight wire case and the same for helical wire is 720 K. The maximum clad temperature is higher in the case straight wire bundle due to the absence of transverse flow. The maximum temperature occurs at the location of the gap between pin and wire. In the case of helical wire-wrap pin bundle, the maximum clad temperature which occurs at the location of the gap between pin and wire is only 720 K which is much lower than the straight wire wrap 7 pin bundle. This enhanced reduction of hot spot is due to the more number of pins with helical wire-wrap in 217 pin bundle. The ΔT between the bulk sodium in the central sub-channel and peripheral sub-channel is 30 K for straight wire and the same for helical wire is 18 K. The difference in bulk sodium temperature between the central and peripheral sub-channels is less in the case with helical wire than the case of straight pin bundle due to the presence of secondary flow. Hence, the outlet temperature is more uniform in the case of helical wire bundle. The helical wire forces the hot sodium from the central sub-channels to move out to peripheral sub-channels to mix with the relatively cold sodium and direct the relatively cold sodium at the periphery towards the center. These inward and outward flows create good mixing of the hot sodium at the central sub-channels with the relatively colder sodium at the periphery, rendering a more uniform temperature profile across the pin bundle and reduced hot spot on the pin. Due to the transverse flow induced by the helical wire, the Nusselt number is higher for helical wire-wrap bundle (10.4) than the straight wire-wrap bundle (9.4).

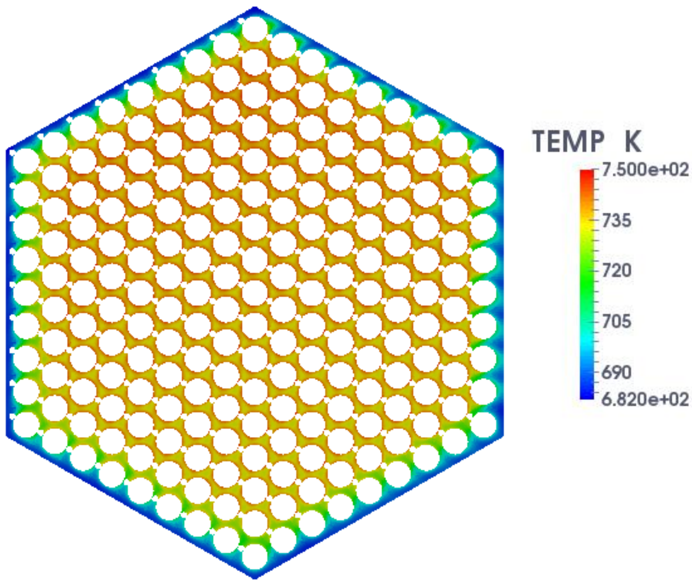

Fig. 6.2 (a) The temperature field at the exit of straight wire 217 pin bundle (200 mm from the inlet)

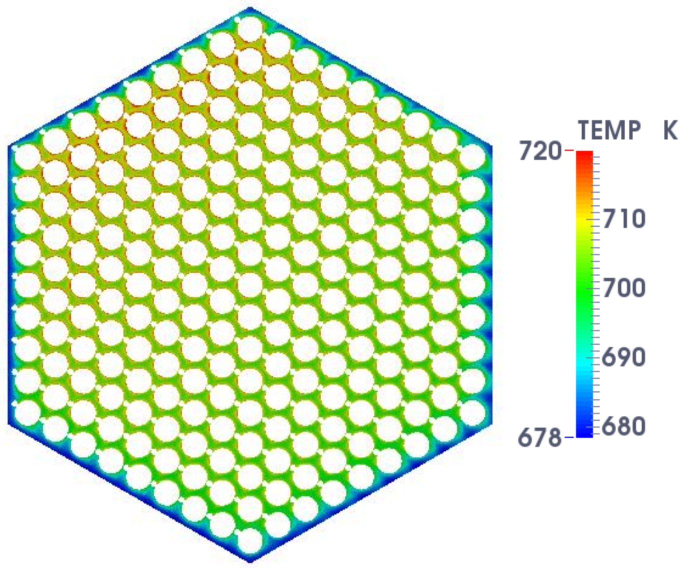

Fig. 6.2 (b) The temperature field at the exit of helical wire 217 pin bundle (200 mm from the inlet)

The comparison of 217 pin bundle with straight and helical wires is summarized in the Table.6.1. It is seen that the helical wire provides increase in friction factor and Nusselt number in the 217 pin bundle due to transverse velocity induced by the helical wire.

Table 6.1 Comparison of friction factor and Nusselt number at the exit for helical and straight wire pin bundles

	Maximum transverse velocity, m/s	Maximum axial velocity, m/s	Friction factor	Nusselt Number
Straight wire	0.009	9.7	0.0185	9.1
Helical wire	2.2	10.8	0.0215	10.4

6.2 THE EFFECT OF LIGAMENT GAP

For the nominal gap of 0.1 mm between the last row of pins and the hexagonal wrapper, the flow fraction through the central and the peripheral sub-channels in 217 pin bundle is 77.4 % and 22.6 % respectively for Reynolds number of 100,000. When the gap is reduced to 0.03 mm, the flow fraction through the central sub-channels has increased to 77.7 % and that of the peripheral sub-channels is decreased to 22.3 % respectively for the same Reynolds number of 100,000. The friction factor has increased marginally from 0.0210 to 0.0211 and the Nusselt number has increased from 10.4 to 10.75. As there is not much increase in the friction factor and Nusselt number at the exit, it is recommended that the ligament gap of 0.1 mm kept from the consideration of tolerance allowance can be retained.

6.3 FRICTION FACTOR

The values of friction factor for a 217 pin bundle with 200 mm helical pitch and 1.65 mm helical wire diameter at the bundle exit for various Reynolds numbers obtained by the CFD analysis is compared with the experimental data reported by Roychowdhary et al. (1998) and presented in Fig. 6.3. It is seen that the overall variation of friction factor obtained by the CFD analysis compares well with the experimental values. The friction factor values in the turbulent regime obtained by CFD analysis matches with that of the experimental values within 2 %. The friction factor values in the laminar regime obtained by CFD analysis are higher (15 %) than that of the experimental values.

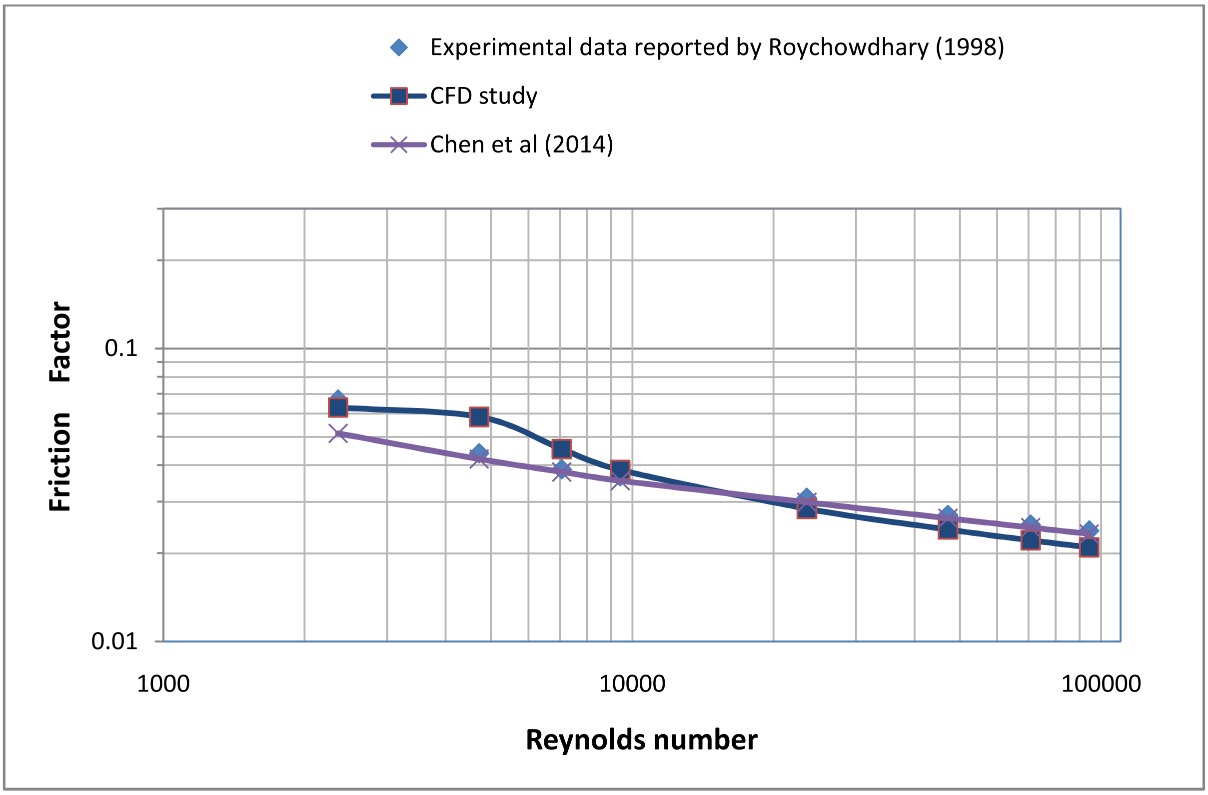

Fig. 6.3 Comparison of friction factor of 217 pin bundle with experimental data and Chen et al correlation (2014).

6.4 DEPENDENCE OF TRANSVERSE VELOCITY ON REYNOLDS NUMBER

The variation of transverse velocity at the outlet of the pin bundle as a function of Reynolds number is presented in Figs. 6.4 (a) - 6.4 (e). The variation of minimum, maximum and transverse velocity for various Reynolds number is presented in Table 6.2. It is seen that the minimum, maximum and transverse velocity drastically decreases from high Reynolds number to low Reynolds number. It is seen that the transverse velocity decreases from a maximum value of 2.17 m/s with Reynolds number and becomes 0.06 m/s for Reynolds number equals to 2500. The cross stream velocity is seen to be directly proportional to Reynolds number. This is because for identical geometry, Reynolds number is proportional to inlet axial velocity. This suggests that the flow distribution within the bundle is a weak function of Reynolds number in the turbulent regime.

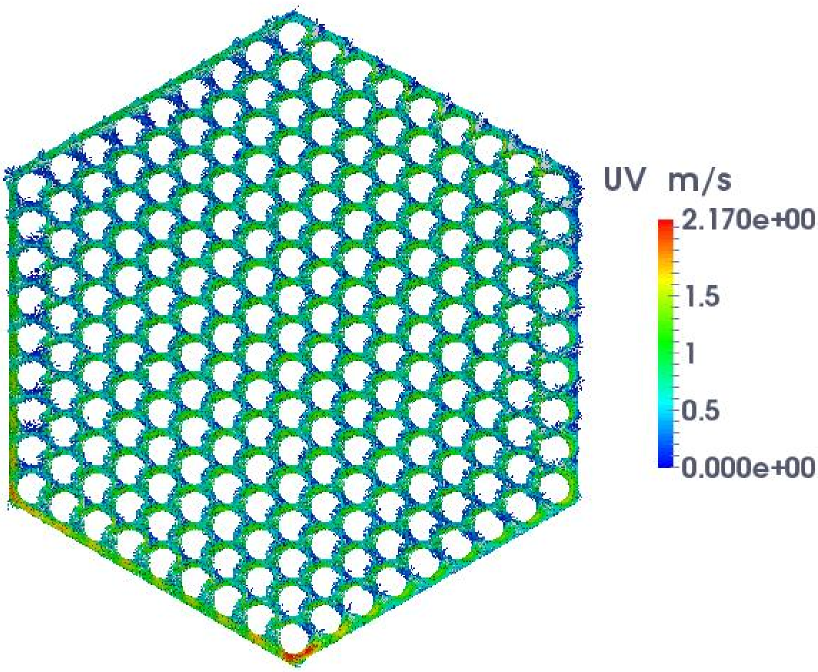

Fig. 6.4 (a) Transverse velocity field at the exit of helical wire wrap 217 pin bundle for Reynolds number = 100000

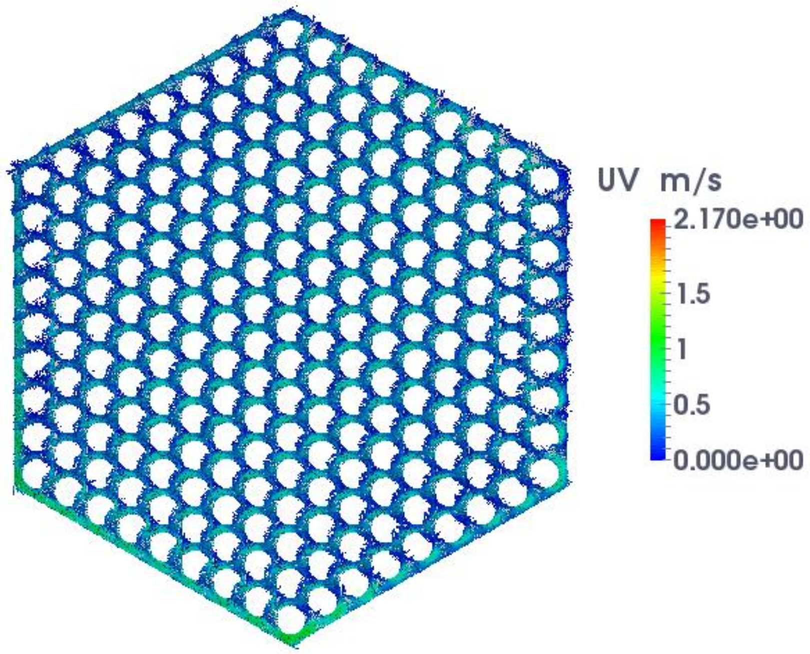

Fig. 6.4 (b) Transverse velocity field at the exit of helical wire wrap 217 pin bundle for Reynolds number = 50000

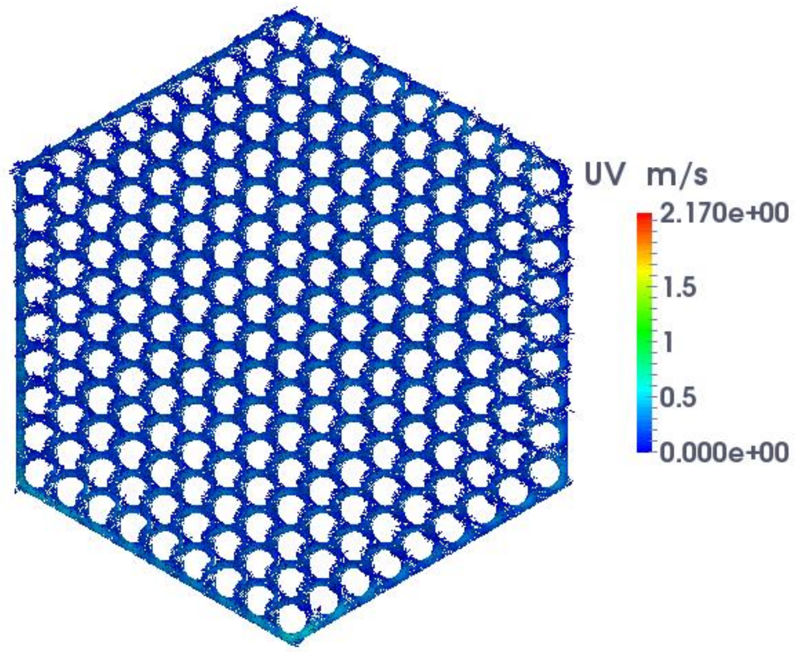

Fig. 6.4 (c) Transverse velocity field at the exit of helical wire wrap 217 pin bundle for Reynolds number = 25000

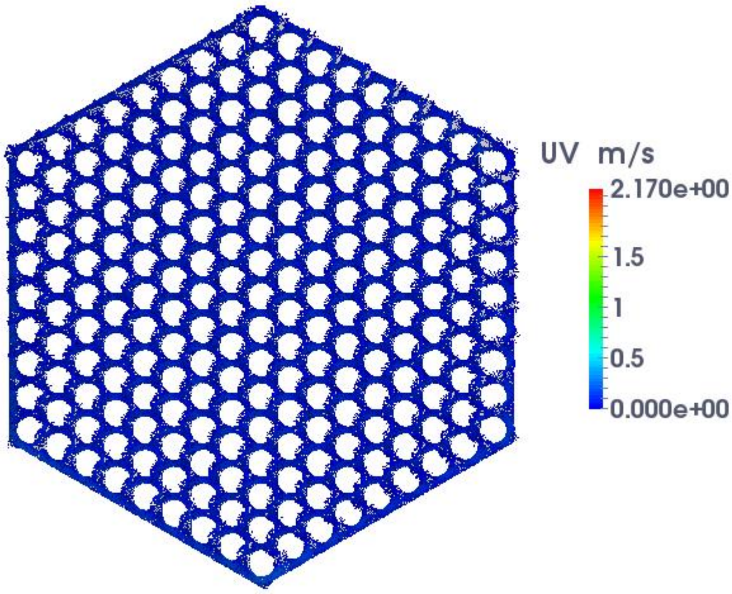

Fig. 6.4 (d) Transverse velocity field at the exit of helical wire wrap 217 pin bundle for Reynolds number = 10000

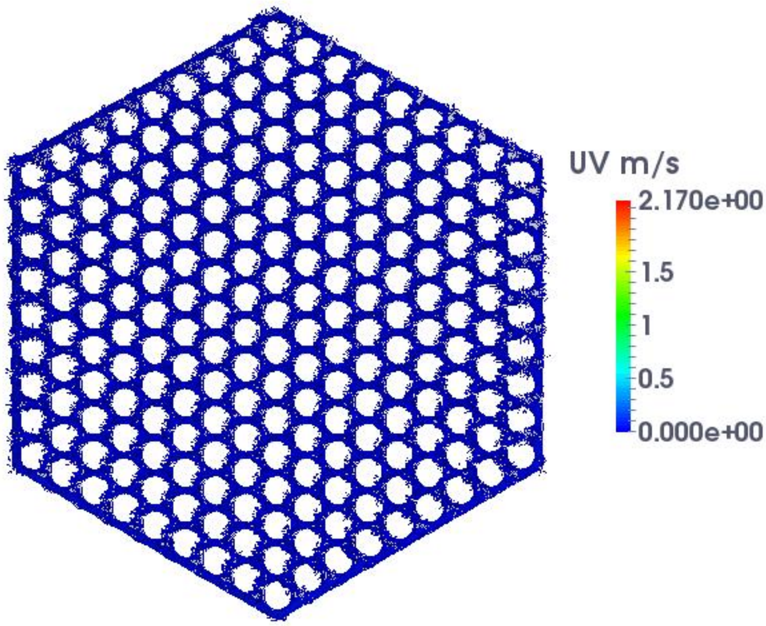

Fig. 6.4 (e) Transverse velocity field at the exit of helical wire wrap 217 pin bundle for Reynolds number = 2500

Table 6.2 Variation of Minimum, maximum and average transverse velocity as a function of Reynolds number

Reynolds number	Minimum Transverse velocity, m/s	Maximum Transverse velocity, m/s	Average Transverse velocity, m/s
1,00,000	0.002	2.17	0.68
50,000	0.0012	1.06	0.34
25,000	0.0005	0.52	0.17
10,000	0.0002	0.2	0.067
5,000	7.5e-5	0.1	0.033
2,500	1.5e-5	0.06	0.018

The variation of average transverse velocity at the outlet of the pin bundle with various Reynolds number is presented in Fig. 6.4 (f). It is seen that the transverse velocity decreases drastically from an average value of 0.68 m/s with Reynolds number equals to 1, 00, 000 and becomes 0.018 m/s for Reynolds number equals to 2500 (Table 6.1).

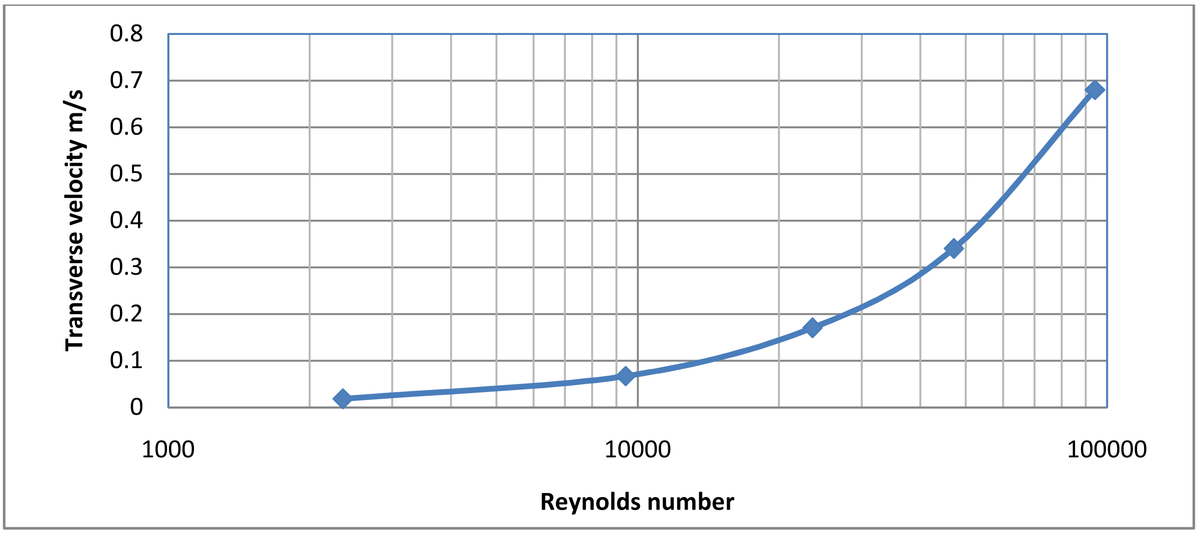

Fig. 6.4 (f) Variation of average transverse velocity at the outlet of 217 pin bundle with Reynolds number

6.5 DEVELOPMENT OF TEMPERATURE DISTRIBUTION ALONG THE LENGTH OF THE BUNDLE

The temperature distributions at various elevations of the 217 pin bundle with helical wire are presented in Figs. 6 5 (a) - 6.5 (f). It is seen that the temperature of cold sodium flowing in the periphery increases with the length of the bundle as the transverse velocity induced by the helical wire drives the sodium in and out of the sub channels. The sodium temperature is higher in the zones where the flow area and hence the mass flow rate are less due to the presence of the spacer wires. The sodium temperature is minimum in the wall sub-channels.

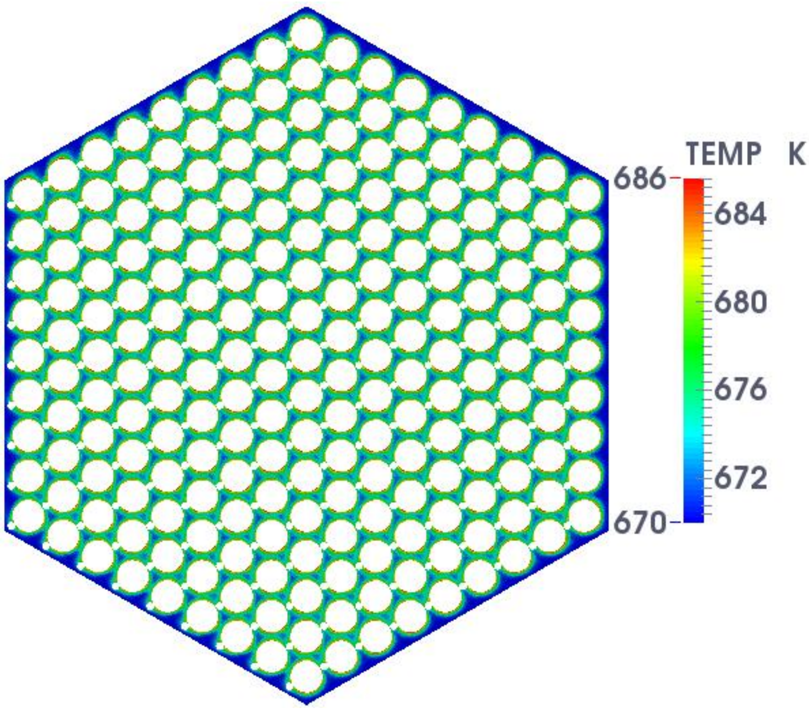

Fig. 6.5 (a) The temperature field at 33 mm from the inlet of helical wire wrap 217 bundle

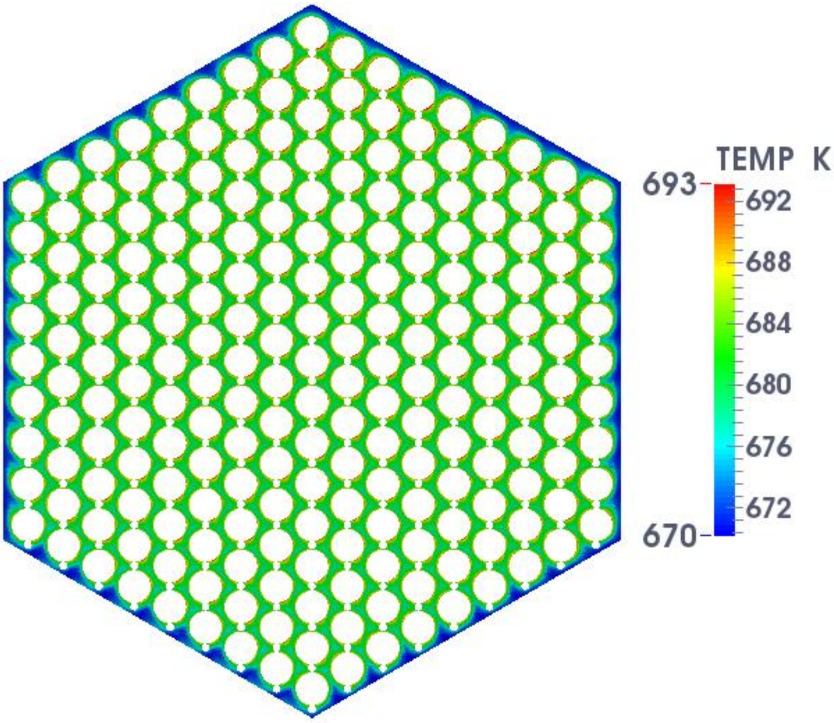

Fig. 6.5 (b) The temperature field at 66 mm from the inlet of helical wire wrap 217 bundle

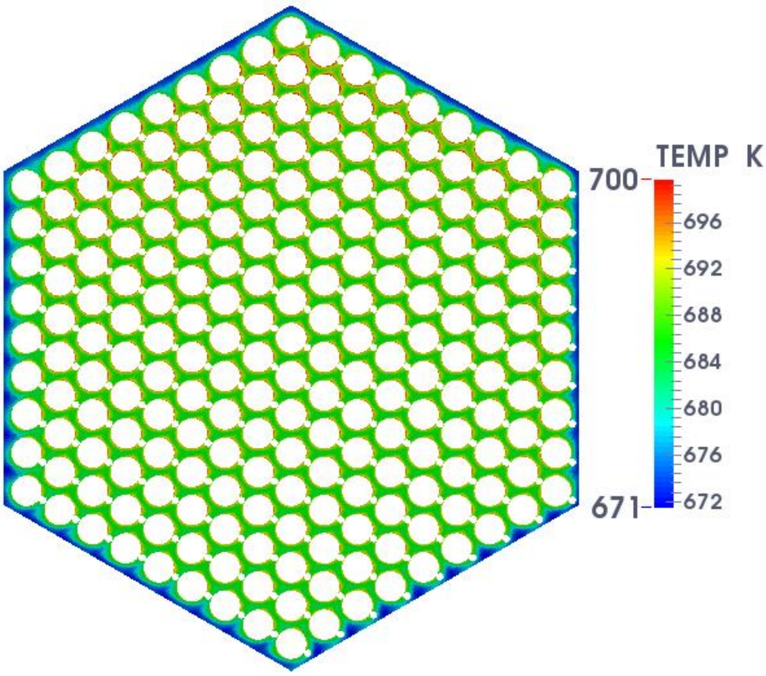

Fig. 6.5 (c) The temperature field at 99 mm from the inlet of helical wire wrap 217 bundle

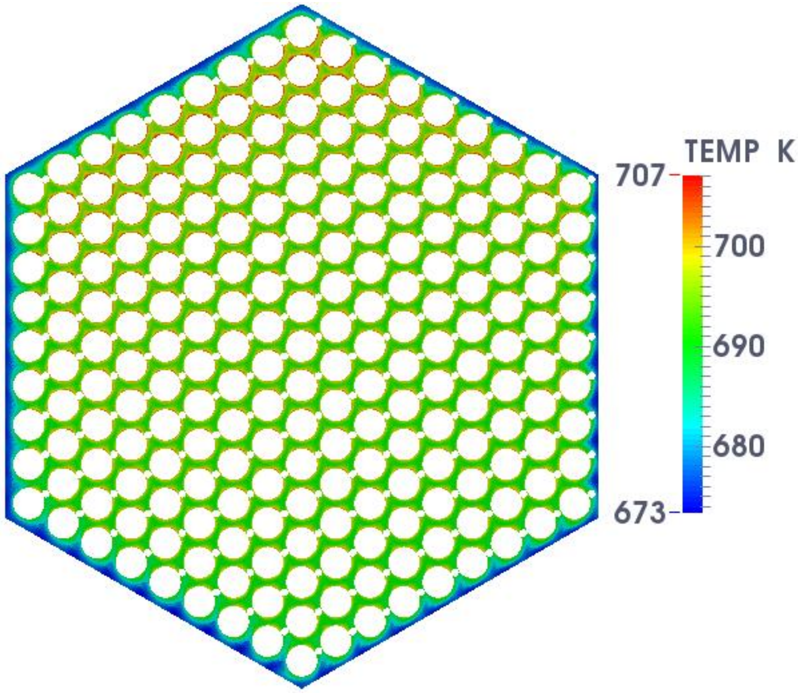

Fig. 6.5 (d) The temperature field at 133 mm from the inlet of helical wire wrap 217 bundle

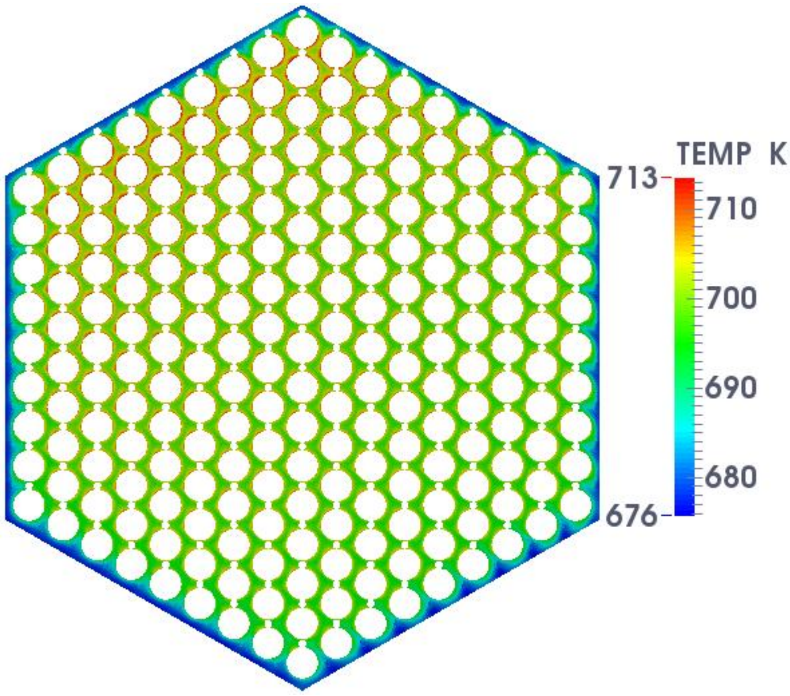

Fig. 6.5 (e) The temperature field at 166 mm from the inlet of helical wire wrap 217 bundle

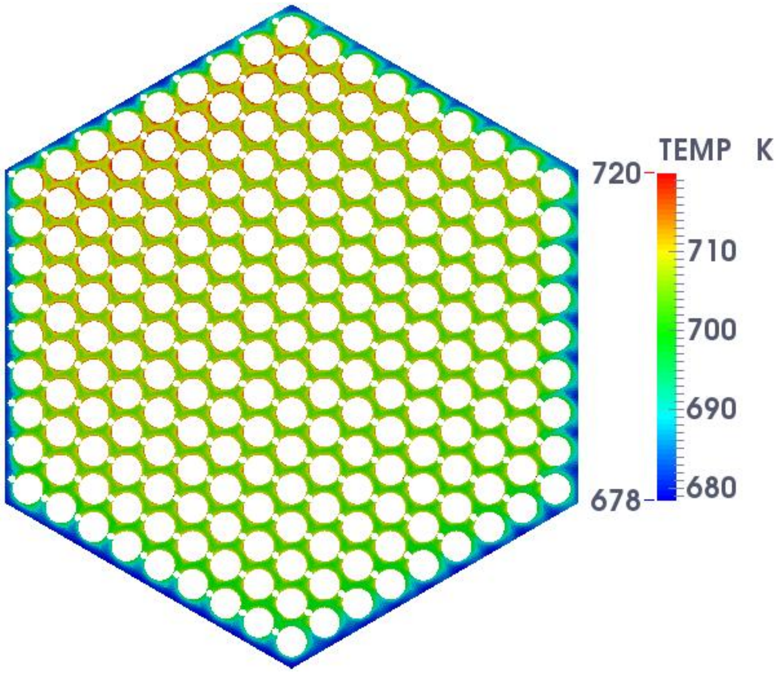

Fig. 6.5 (f) The temperature field at the exit of helical wire wrap 217 bundle

6.6 DEPENDENCE OF TEMPERATURE FIELD ON REYNOLDS NUMBER

The variation of temperature at the outlet of the pin bundle as a function of Reynolds number is presented in Figs. 6.6 (a) - 6.6 (e). By varying the heat flux proportional to the flow, the average outlet temperature is kept constant at 702 K. The minimum and maximum temperatures as a function of Reynolds number is presented in the Table 6.3. It is seen that the peak temperature decreases from a maximum value of 720 K at Reynolds number of 1, 00, 000 and reaches 708 K at Reynolds number equals to 2500. Similarly, the minimum temperature increases from 678 K in the peripheral sub channels at Reynolds number equal to 1, 00,000 to 688 K at Reynolds number equal to 2500. This, the minimum and maximum temperatures increase and decreases with the Reynolds number respectively. This suggests that the temperature distribution becomes more uniform at lower Reynolds number.

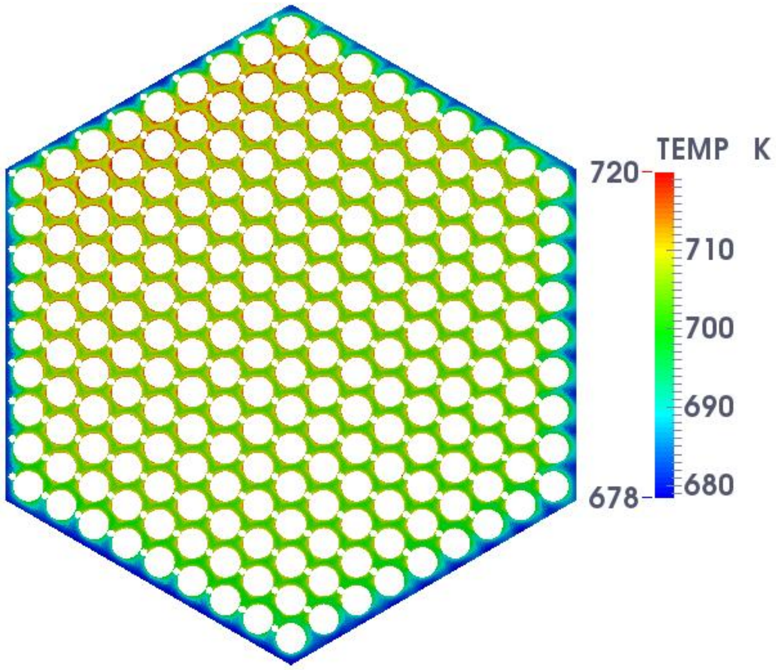

Fig. 6.6 (a) The temperature field at the exit of helical wire wrap 217 pin bundle for Reynolds number = 100,000

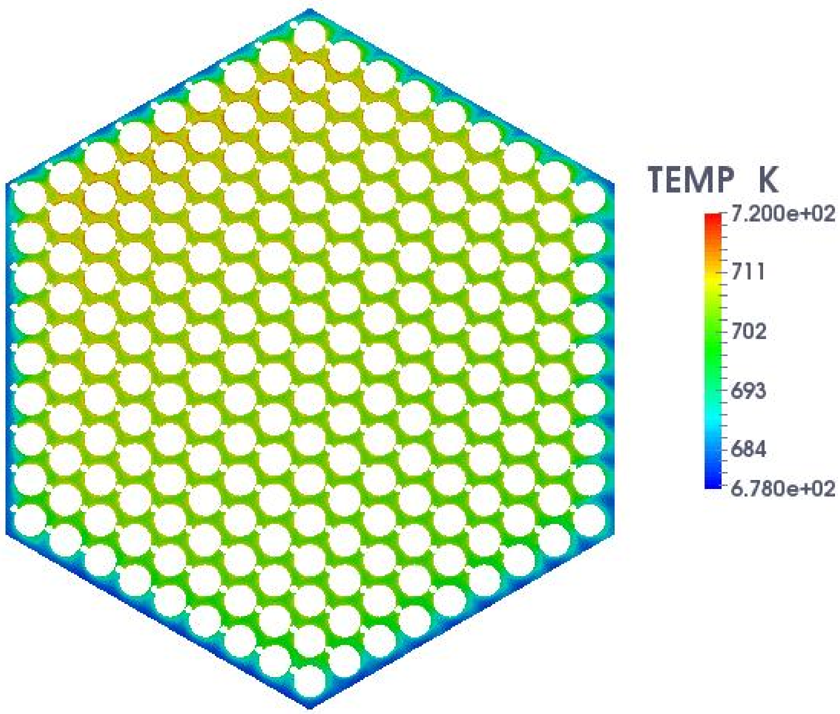

Fig. 6.6 (b) The temperature field at the exit of helical wire wrap 217 pin bundle for Reynolds number = 50000

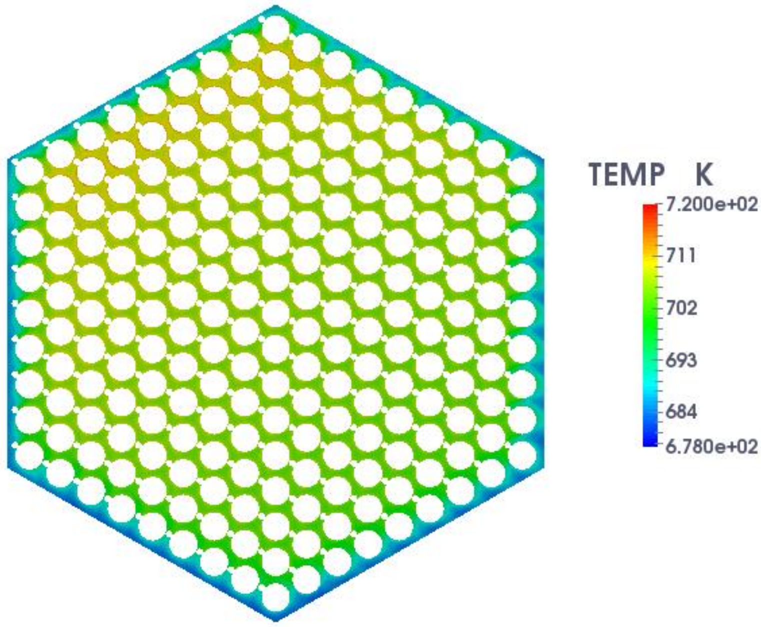

Fig. 6.6 (c) The temperature field at the exit of helical wire wrap 217 pin bundle for Reynolds number = 25000

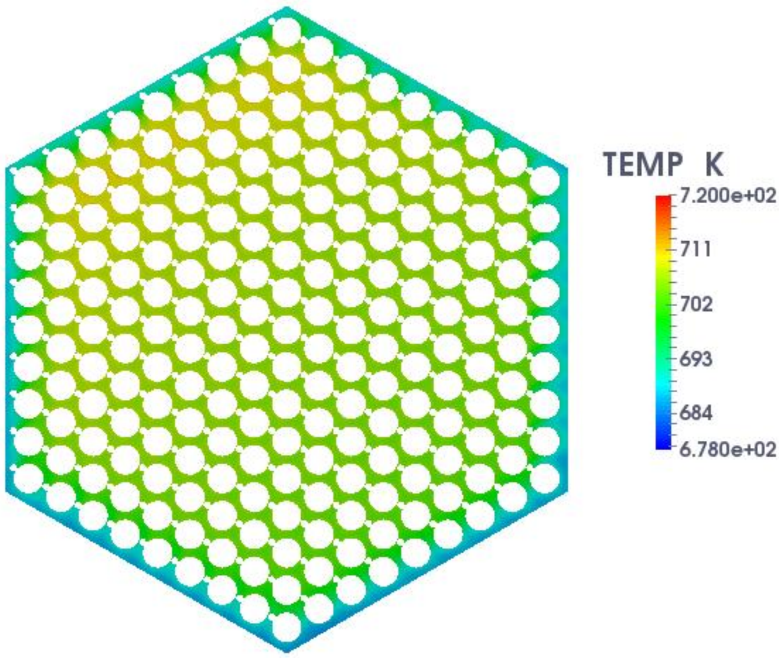

Fig. 6.6 (d) The temperature field at the exit of helical wire wrap 217 pin bundle for Reynolds number = 10000

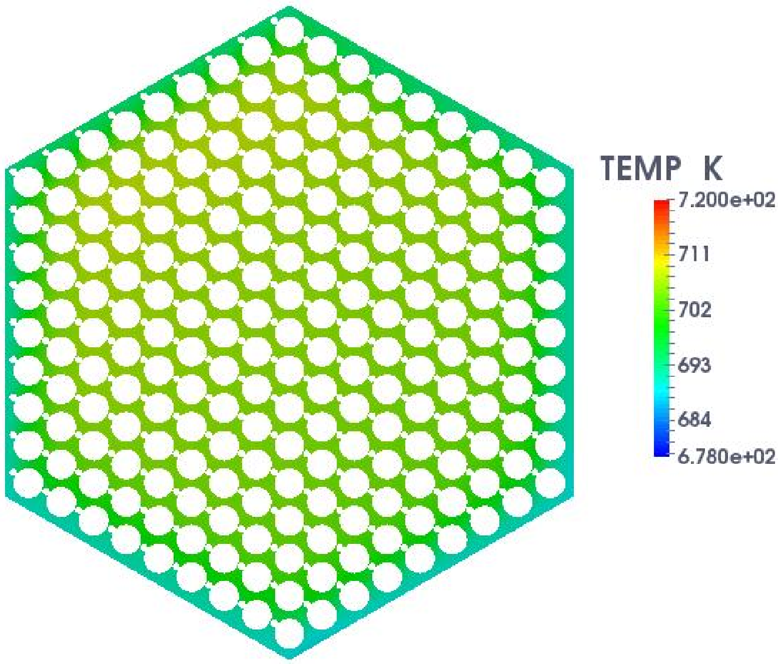

Fig. 6.6 (e) The temperature field at the exit of helical wire wrap 217 pin bundle for Reynolds number = 2500

Table 6.3 Variation of Minimum, maximum temperatures as a function of Reynolds number

Reynolds number	Minimum Temperature, K	Maximum Temperature, K
1,00,000	678	720
50,000	681	716
25,000	682.5	712.8
10,000	684.5	711.2
5,000	686	710.2
2,500	688	708

6.7 DEPENDENCE OF NUSSELT NUMBER ON REYNOLDS NUMBER

The variation of Nusselt number at the outlet of the pin bundle (200 mm length) with Reynolds number is presented in Fig. 6.7. It is seen from the outlet temperature field presented in Fig. 6.5 (f) that there exits two major temperature regions in the bundle. The one which is at high temperature is of the central sub channels up to the row of peripheral pins. The other which is at low temperature is of the peripheral sub channels between the last peripheral row of pins and the hexagonal sheath. The Nusselt number decreases with decrease in Reynolds number and is validated against the experimental correlation suggested by Kazimi and Carelli et al. (1980). As explained already, the higher values of predicted Nusselt number in the turbulent regime are due to the helical wire induced heat transfer from the pins which are probably not considered in the experimental correlation and also could be due to insufficient thermal development length of the pin bundle (200 mm) simulated.

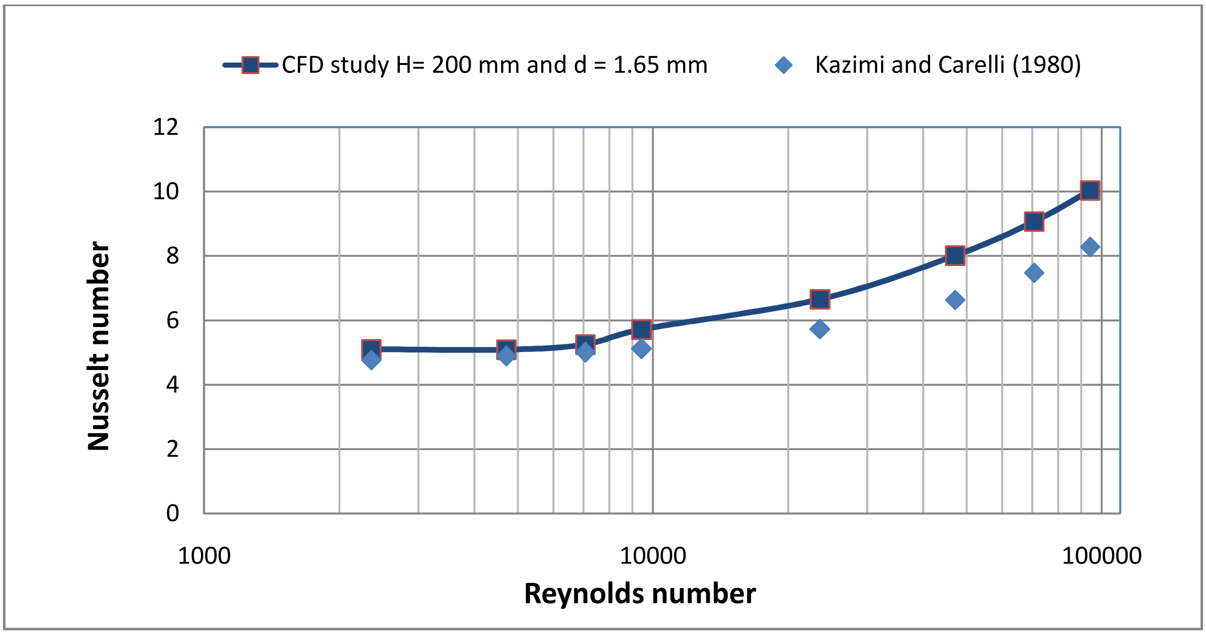

Fig. 6.7 Comparison of Nusselt number at the exit of 217 pin bundle with experimental Correlation.

6.8 THERMAL HYDRAULICS OF HELICAL WIRE 217 PIN BUNDLE WITH 5 PITCHES

The thermal hydraulic study has been carried out for a full heat generation length of 1000 mm (5 pitches) of the bundle to obtain the results which is directly useful for the reactor.

6.8.1 Transverse Velocity Distribution

The transverse velocity at the exit of the bundle 217 pin bundle with 5 pitches is presented in Figs. 6.8 (a) – 6.8 (b). It is seen that the value of maximum transverse velocity is 2.2 m/s. This value compares well with that at the exit of one-pitch (see, Figs. 6.1 (b) and 6.1 (c)). Further, this velocity magnitude and distribution are very similar to that seen in the case of pin bundle with less number of fuel pins (Figs. 4.1 (f) - 4.1 (g), Figs. 5.1 (a) -5.1 (f). Thus, it can be surmised that the cross stream velocity in a bundle nearly develops within one helical pitch, probably due to small hydraulic diameter of the pin bundle. Further, the flow field in the bundle is characterized by two zones, viz., central sub-channels and peripheral sub-channels. This characteristic is independent of the number of pins.

6.8.2 Axial Velocity Distribution

The axial velocity at the exit of the bundle is presented in Fig. 6.9. It is seen that the value of maximum axial velocity is 10.8 m/s. The central zone has a nearly uniform axial velocity equal to the inlet velocity (8 m/s). The maximum axial velocity in the peripheral sub-channel is in the zone where helical wire is present.

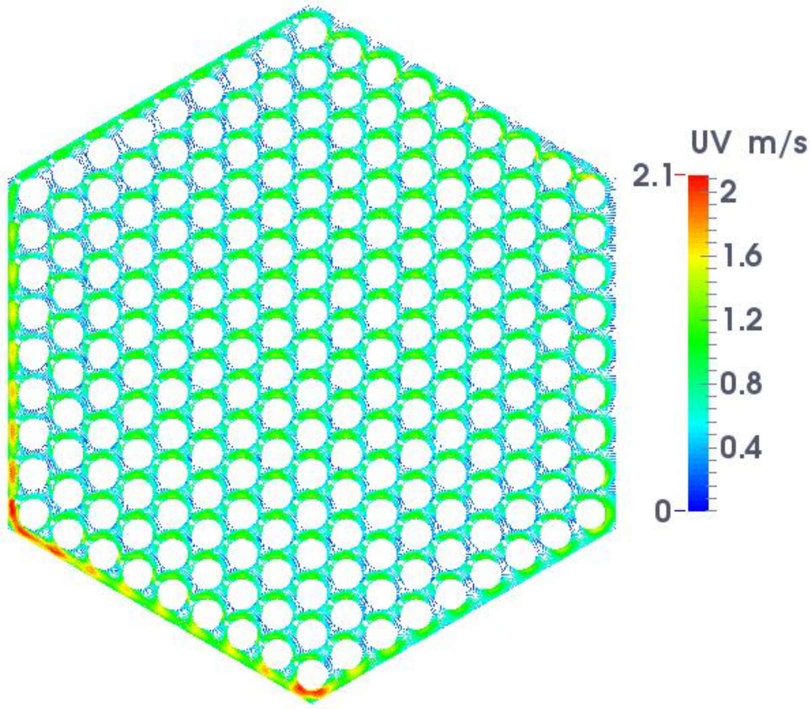

Fig. 6.8 (a) The transverse velocity field at the exit of 1000 mm length of helical wire 217 pin bundle

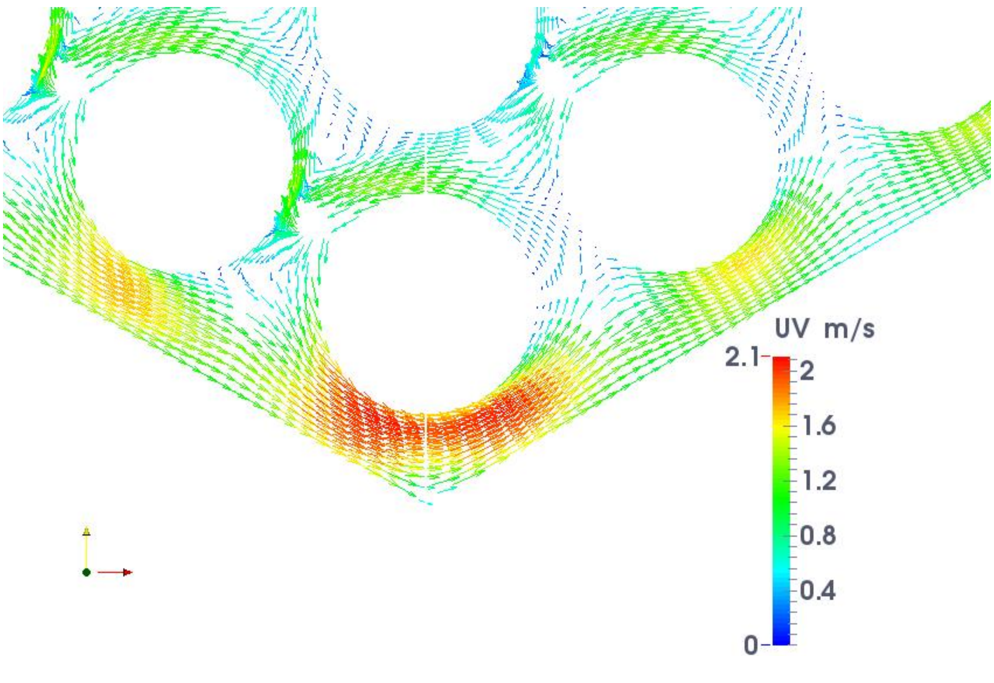

Fig. 6.8 (b) Close-up view of transverse velocity field at the exit of 1000 mm length of helical wire 217 pin bundle in X – Y plane

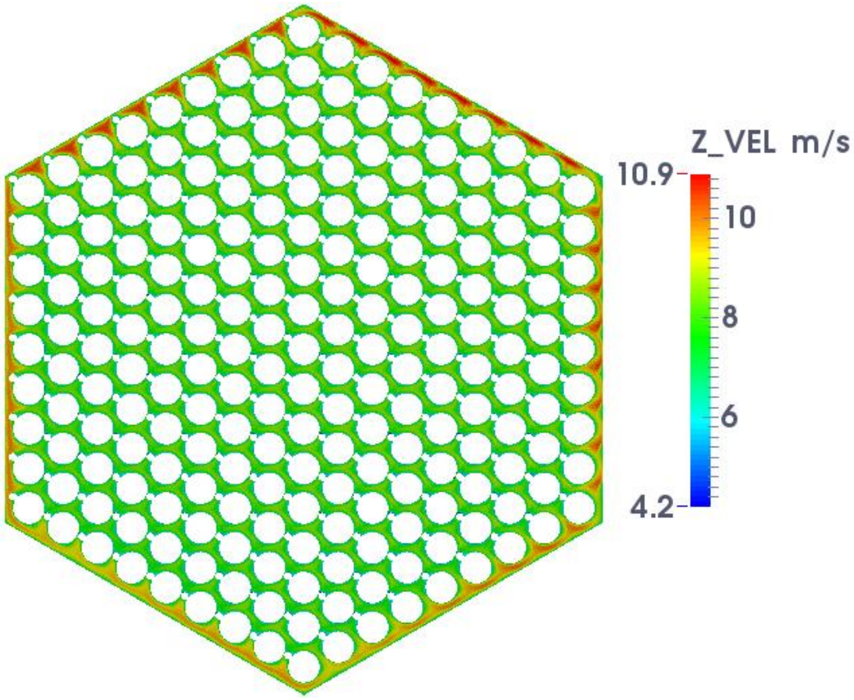

Fig. 6.9 The axial velocity distribution at the exit of 1000 mm length of the bundle

6.8.3 Temperature Distribution

The temperature field at various elevations of the 1000 mm length bundle and Re = 100,000 is presented in Figs. 6.10 (a) – 6.10 (e). It is seen that maximum temperature increases with height of the bundle as expected. The sodium temperature is higher in the zones where the flow area and hence the mass flow rate are less due to the presence of the spacer wires though the axial velocity is higher. The sodium temperature is minimum in the wall sub-channels where the circumferential flow is larger, leading to larger mass flow rate around the pins despite the lower axial velocities. It is seen from Fig. 6.10 (e) that the temperature at the exit of the bundle has three regions. The hottest region comprises of central sub channels where the temperature is almost uniform. The coldest region comprises of peripheral sub channels. The intermediate region is in between these two sub channels. The temperature difference between clad and sodium increases with the length of the bundle.

At any cross section, it can be said that the temperature field exhibits significant asymmetry. The sodium temperature is maximum in the sector which coincides with the direction pointed by spacer wire. This feature is very similar to that observed in bundles with less number of pins also (see Figs 5.4 (a) - 5.4 (c))

6.8.4 Development of Nusselt number

The development of Nusselt number along the 1000 mm length of the bundle at Re = 100,000 is presented in Fig. 6.11. It is seen that the Nusselt number drastically decreases from a high value at the entry of the bundle due to the development of boundary layer and the associated heat transfer resistance and keep gradually decreasing along the length of the bundle. It appears that the boundary layer growth is nearly completed in about 35 mm length from the entry. This axial length is about 10 times the hydraulic diameter of the pin bundle.

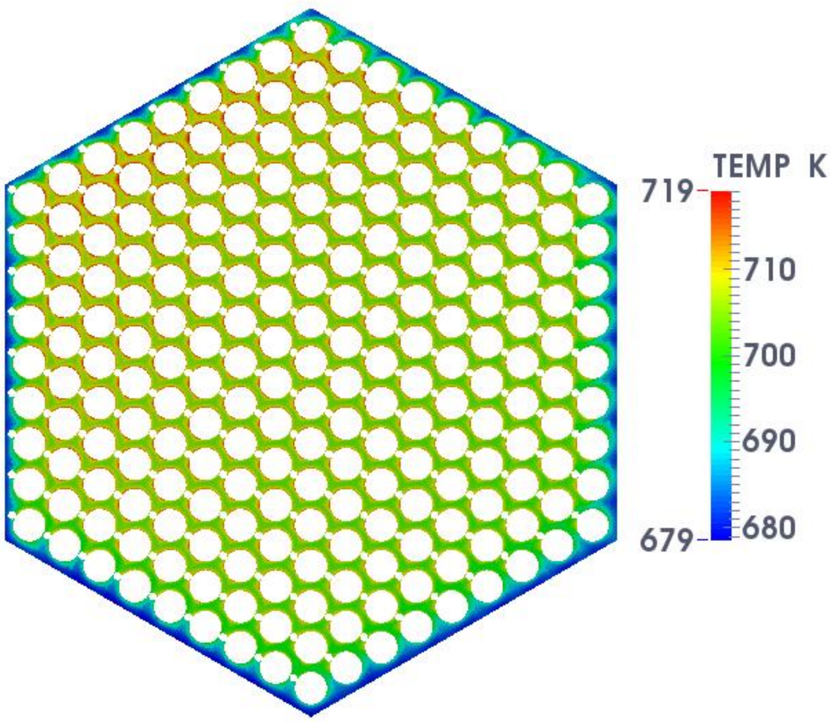

Fig. 6.10 (a) The temperature field at 200 mm from the inlet of helical wire wrap 217 pin bundle

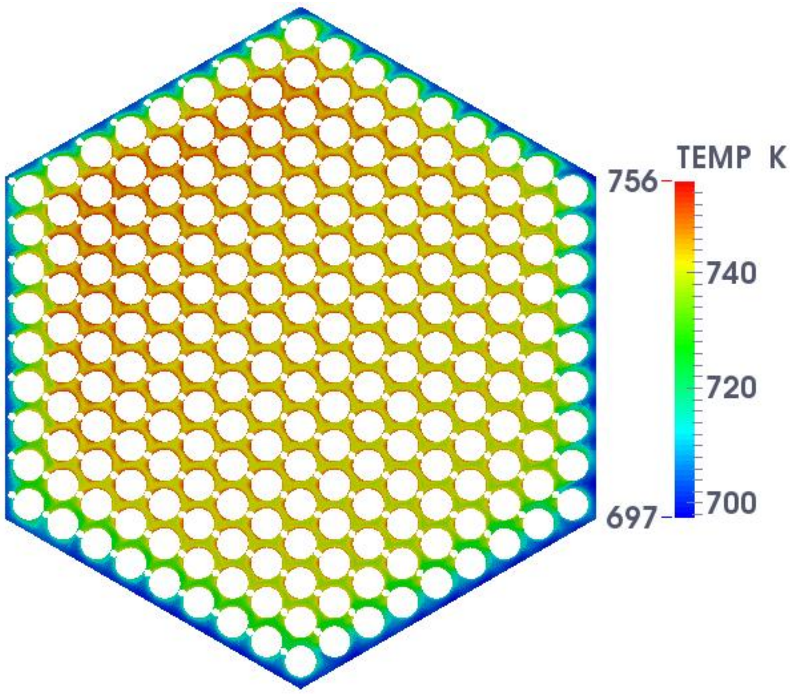

Fig. 6.10 (b) The temperature field at 400 mm from the inlet of helical wire wrap 217 pin bundle

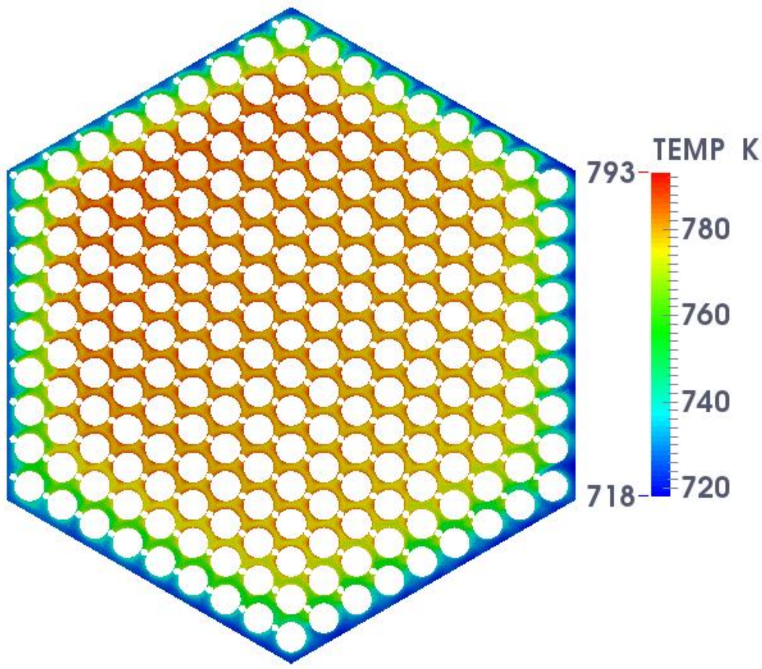

Fig. 6.10 (c) The temperature field at 600 mm from the inlet of helical wire wrap 217 pin bundle

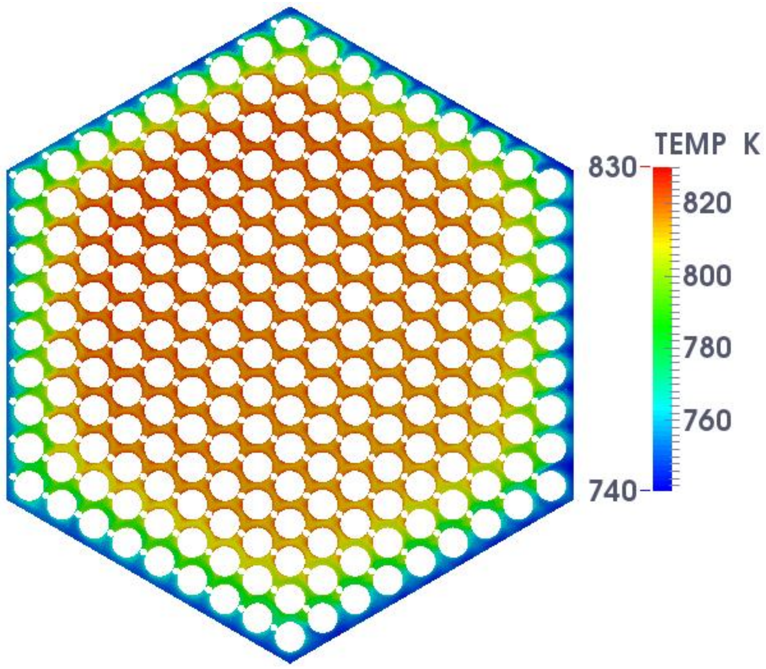

Fig. 6.10 (d) The temperature field at 800 mm from the inlet of helical wire wrap 217 pin bundle

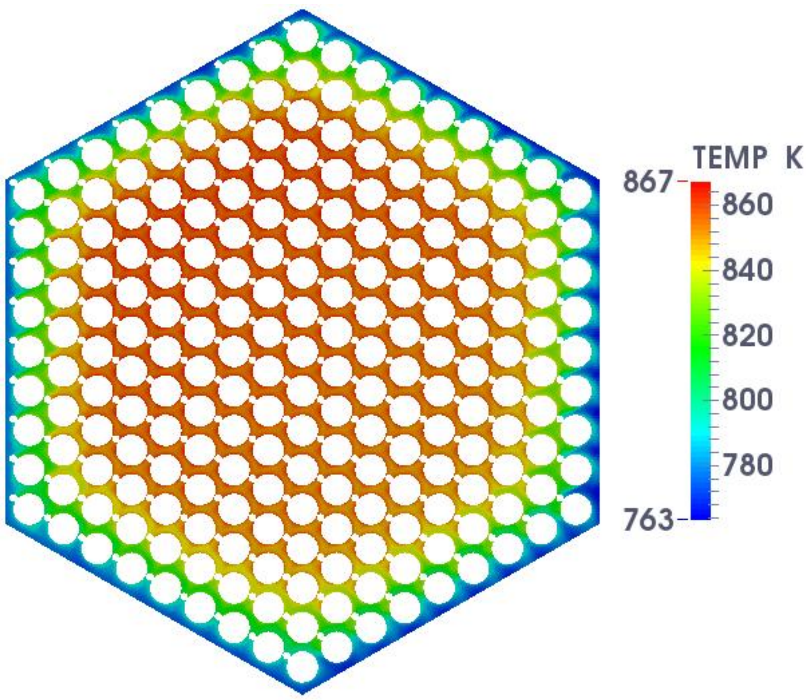

Fig. 6.10 (e) The temperature field at the exit (1000 mm) of helical wire wrap 217 bundle

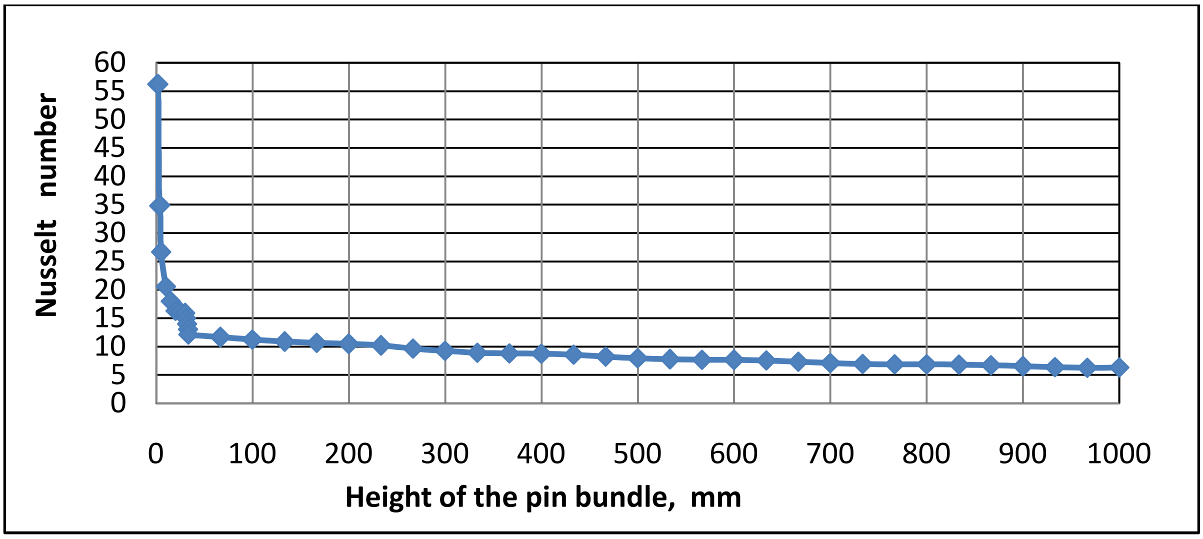

Fig. 6.11 Development of Nusselt number along the length of 217 pin bundle

6.9 CLOSURE

The thermal hydraulics of helical wire wrapped 217 bundle with 200 mm length is compared with that of the straight wire wrapped pin bundle for the same Reynolds number. Due to the transverse flow induced by the helical wire, the Nusselt number is higher for helical wire-wrap bundle than the straight wire-wrap bundle. The effect of reducing the ligament gap from nominal value to minimum value is found to be insignificant. It is seen that the overall variation of friction factor obtained by the CFD analysis compares well with the experimental values. The friction factor values in the turbulent regime obtained by CFD analysis matches with that of the experimental values within 2 %. The friction factor values in the laminar regime obtained by CFD analysis are higher (15 %) than that of the experimental values. The Nusselt number decreases with decrease in Reynolds number and is validated against the experimental correlation suggested by Kazimi and Carelli et al. (1980). The thermal hydraulics within 217 pin bundle for the full length of the fuel region has been studied. The flow and temperature fields at various axial lengths along the bundle suggest that the flow field is nearly independent of axial position beyond one helical pitch suggesting completion of cross-flow development. Also, for identical Reynolds number, the flow field is found to be similar for all bundles with varying number of pins. Similar characteristics were noticed in the case of temperature field also. The temperature field is far from symmetry in the zones. It is seen from the sodium temperature distribution at the outlet of the bundle (i.e.) at 1000 mm from the sodium entry, there exist three temperature regions, viz. hottest, coldest and intermediate becomes more distinct with the increase in the length of the bundle and becomes more uniform. It is seen that the difference in maximum to average clad temperature also remains unaltered with the increase in the length of the bundle. But, the location of the pin having maximum clad temperature moves towards the center with the increase in the length of the bundle.

CHAPTER - 7

EFFECT OF HELICAL WIRE PARAMETERS IN 217 PIN BUNDLE

7.0 INTRODUCTION

Since the helical wire increases the friction factor and Nusselt number in the pin bundle by inducing transverse velocity, it is very essential to estimate its effect for various helical wire parameters like its helical pitch and wire diameter. Towards this, the helical wire pitch is varied in the range of 100 – 300 mm. Similarly, the wire diameter is varied in the range of 1.25 – 2.0 mm. Based on detailed parametric studies, correlations for Nusselt number are proposed.

7.1 DEPENDENCE OF TRANSVERSE VELOCITY ON HELICAL PITCH

The distribution of cross-stream velocity fields and an enlarge view of velocity vectors at the bundle exit for the cases of 100, 200 and 300 mm helical pitch are presented in Figs. 7.1 (a) – 7.1 (f) respectively. These results are for an axial entry velocity of 8 m/s and the corresponding Reynolds number is 100,000. It is seen that the transverse velocity decreases with increase in helical pitch. The values of transverse velocity as function of helical wire pitch are presented in Table 7.1. It is seen that the transverse velocity is highest for 100 mm helical pitch and the values decrease with increase in the helical pitch. The transversal flow induced by the helical wire in the 217 fuel pin bundle is dependent upon the helical pitch and is inversely proportional to it. Thus, the intensity of transverse velocity is more with shorter helical pitch. The ratio of transverse velocity to axial velocity is higher for shorter helical pitch.

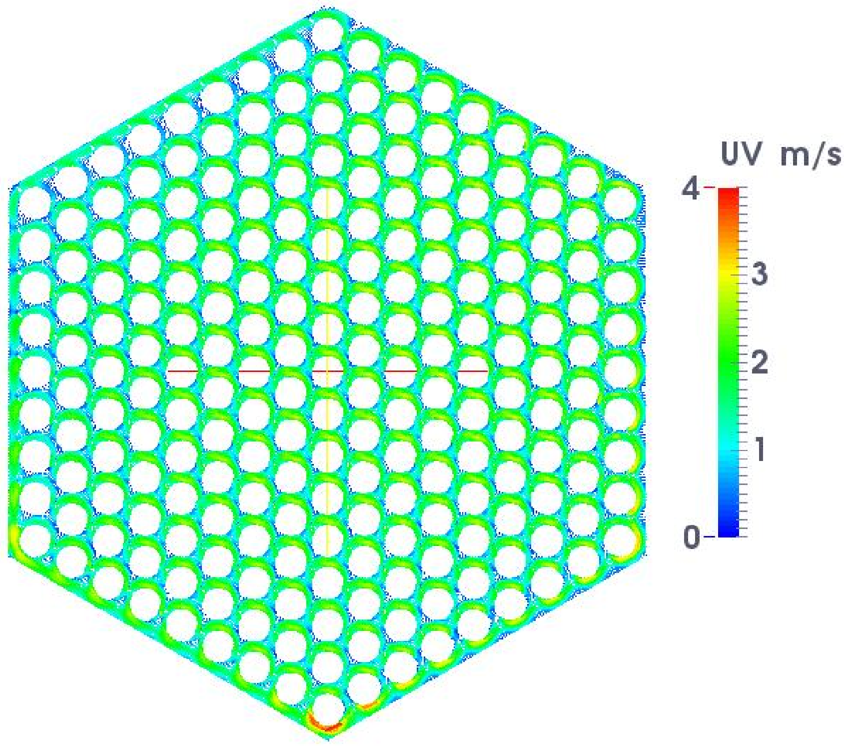

Fig. 7.1 (a) The transverse velocity field at the exit of 100 mm helical pitch wire wrap 217 pin bundle

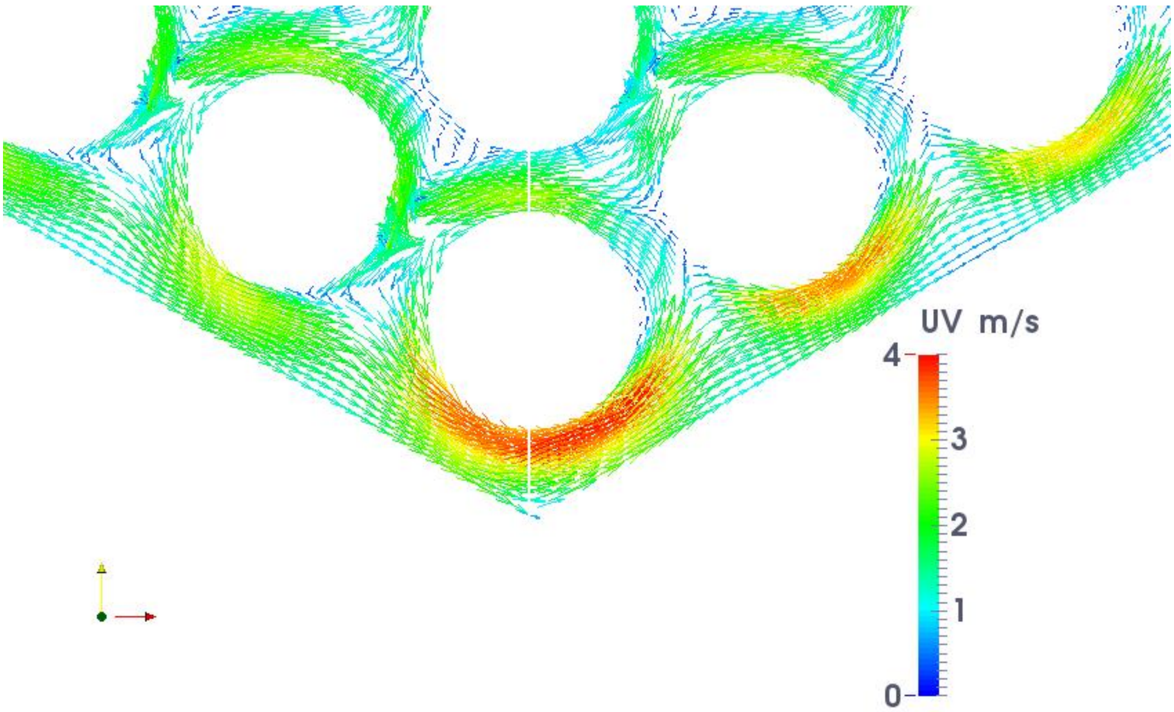

Fig. 7.1 (b) Close-up view of the transverse velocity field at exit of 100 mm helical pitch wire wrapped 217 pin bundle in X-Y plane.

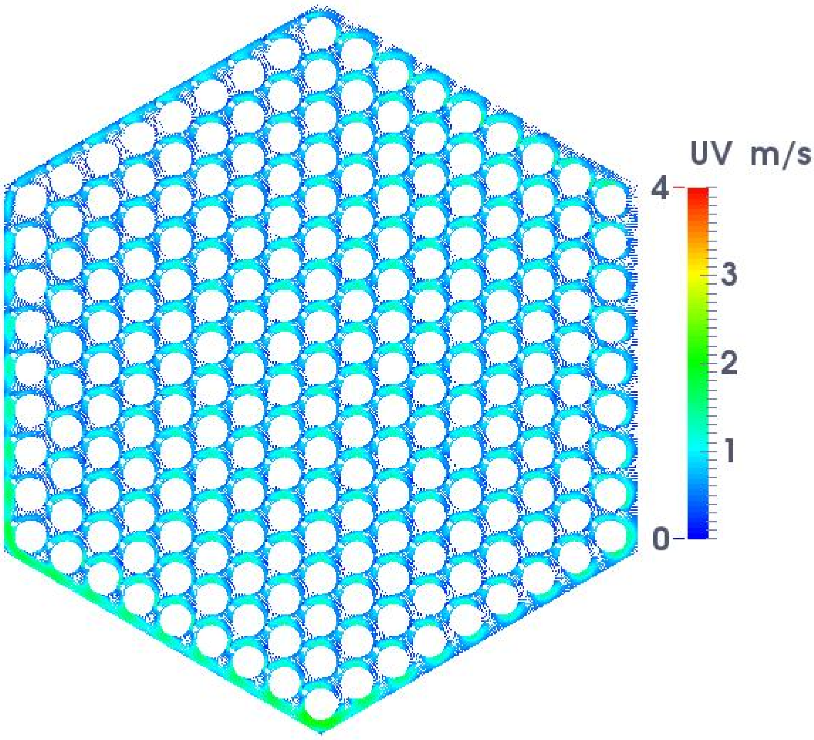

Fig. 7.1 (c) Transverse velocity field at the exit of 200 mm helical pitch wire wrap 217 pin bundle

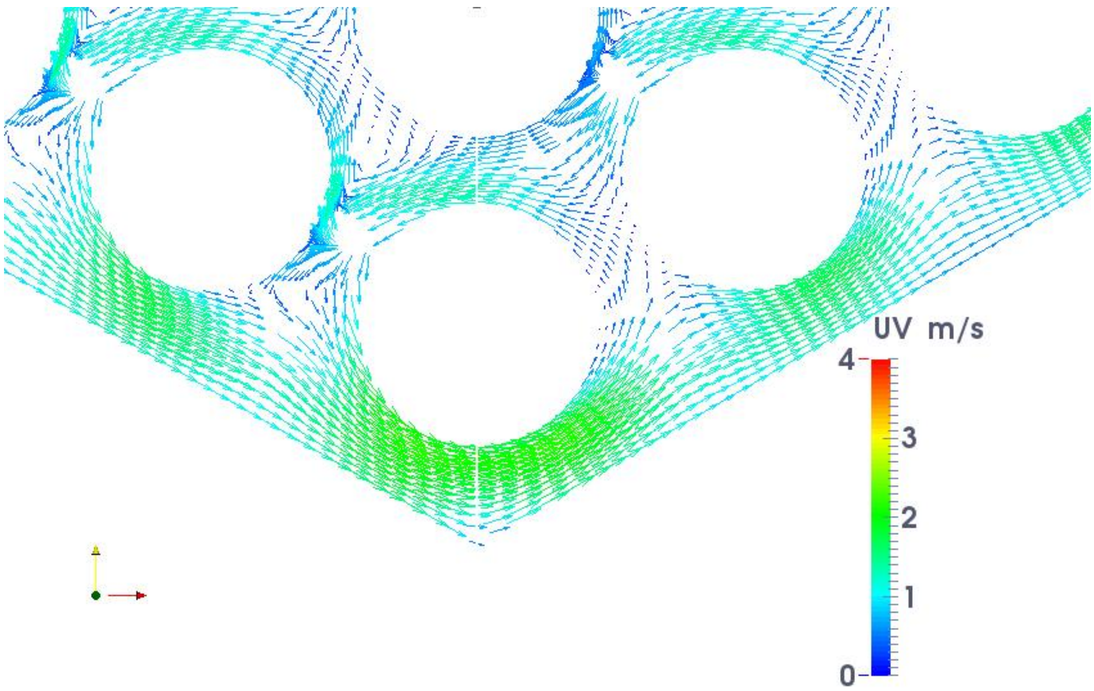

Fig. 7.1 (d) Close-up view of the transverse velocity field at exit of 200 mm helical pitch wire wrapped 217 pin bundle in X-Y plane.

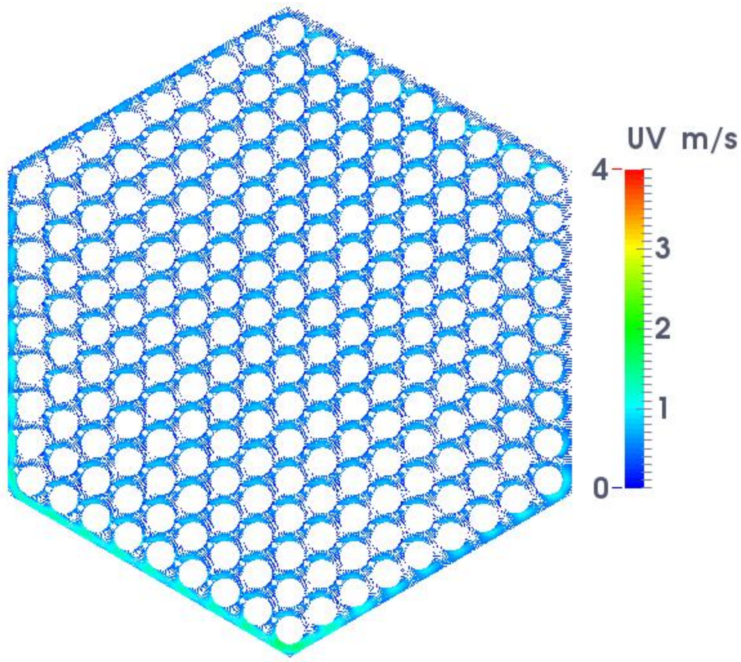

Fig. 7.1 (e) The transverse velocity field at the exit of 300 mm helical pitch wire wrap 217 pin bundle

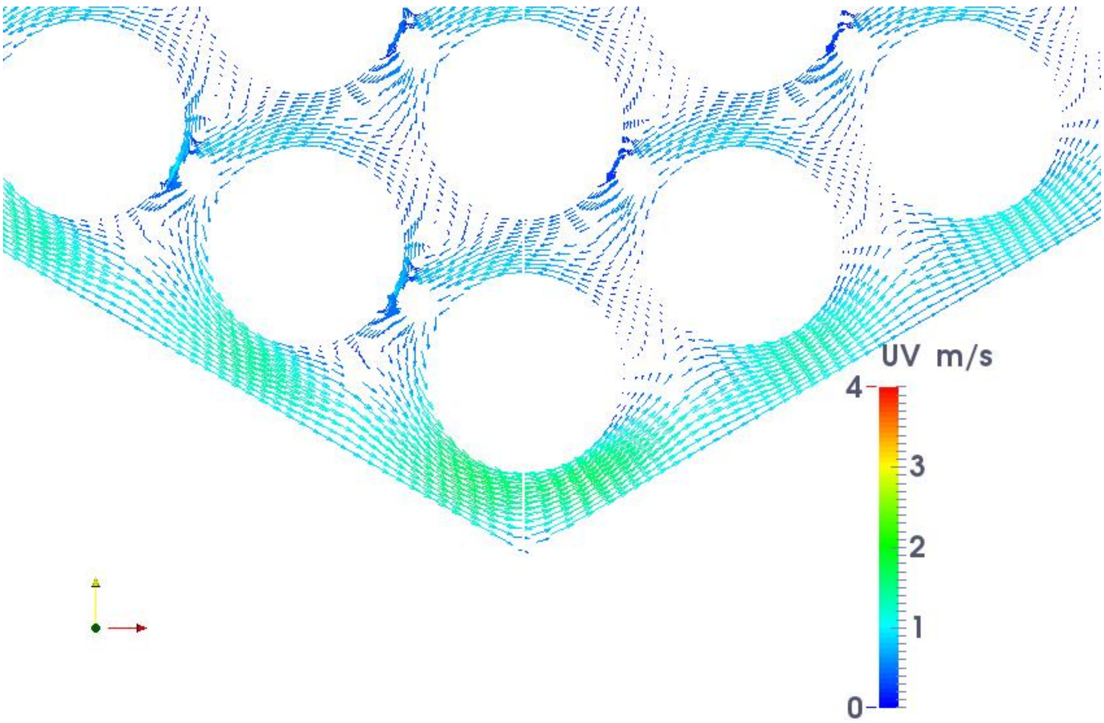

Fig. 7.1 (f) Close-up view of the transverse velocity field at exit of 300 mm helical pitch wire wrap 217 pin bundle in X-Y plane.

Table. 7.1 Transverse velocity as a function of helical pitch for Re =100,000

Helical pitch, mm	Average transverse velocity, m/s	Maximum transverse velocity, m/s	Ratio of Transverse velocity to Average axial velocity
100	1.47	4.0	0.18
200	0.68	2.2	0.08
300	0.42	1.7	0.05

7.2 DEPENDENCE OF TRANSVERSE VELOCITY ON HELICAL WIRE DIAMETERS

In order to compare the velocity vector field for different wire diameters, the velocity vector fields at the bundle exit for the same Reynolds number of 100,000 is presented in Figs. 7.2 (a) – 7.2 (f) for wire diameters of 1.25, 1.65 and 2.0 mm respectively. The values of transverse velocity as function of wire wrap parameters are presented in Table 7.2. The cross–stream velocity appears to be nearly insensitive to the wire diameter for identical Reynolds number. When the wire diameter changes, the flow area occupied by the wire also changes. But, the change in flow area due to change in size of the hexagonal sheath is significant. Hence, the equivalent diameter increases with wire diameter due to the cumulative changes in wire area and the cross sectional area of hexagonal sheath. Hence, the inlet velocity is more for smaller wire diameter as its equivalent diameter is small. Consequently, the ratio of cross stream velocity to mean axial velocity is less for small wire diameter, due to larger cross flow resistance.

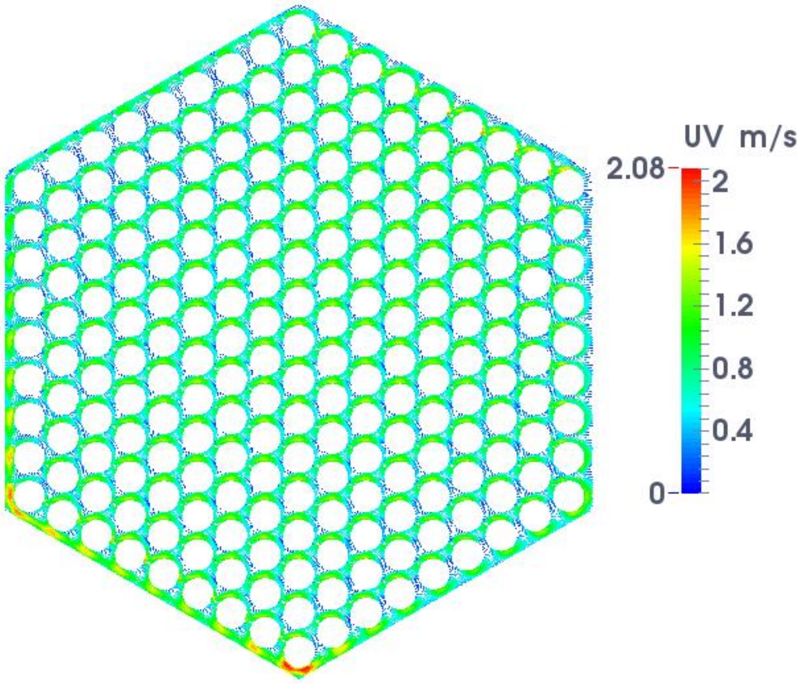

Fig. 7.2 (a) The transverse velocity field at the bundle exit of 1.25 mm diameter helical wire wrap 217 pin bundle

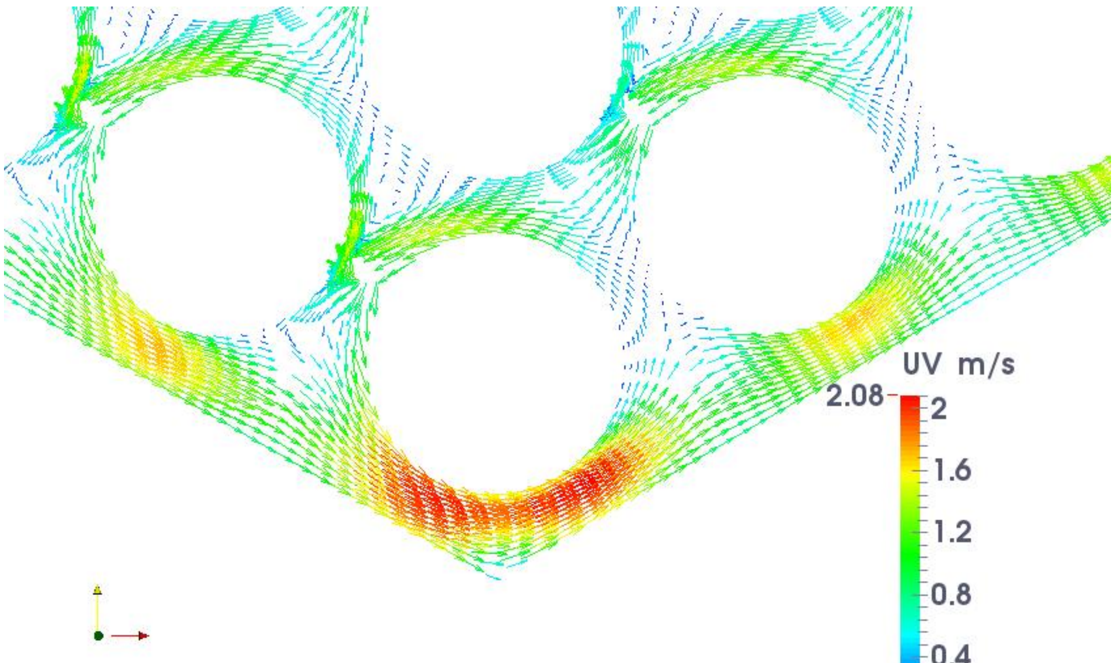

Fig. 7.2 (b) Close-up view of transverse velocity field at the bundle exit of 1.25 mm diameter helical wire wrap 217 pin bundle in X-Y plane.

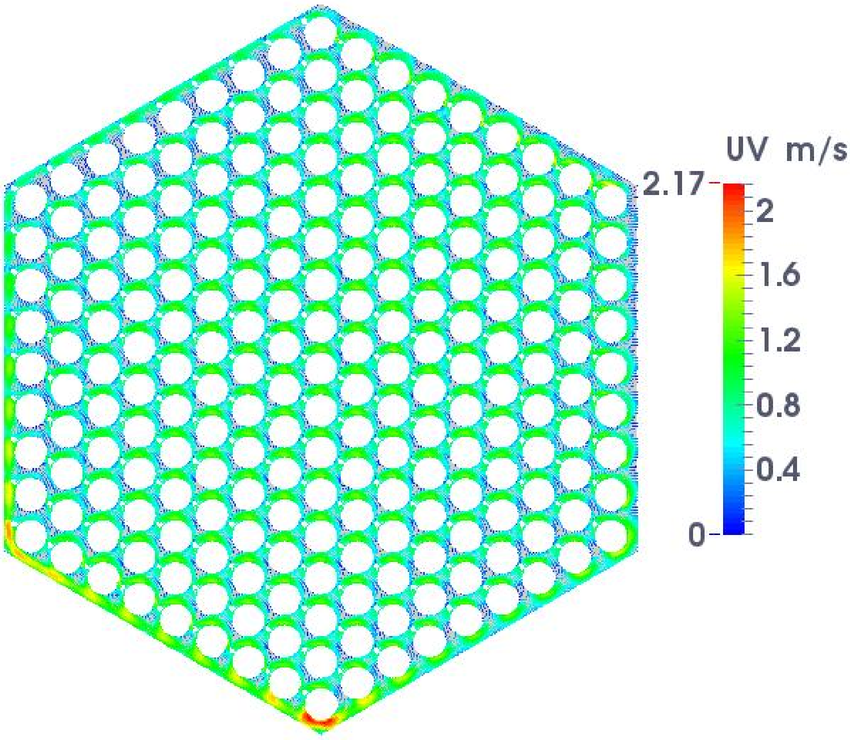

Fig. 7.2 (c) The transverse velocity field at the bundle exit of 1.65 mm diameter helical wire wrap 217 pin bundle

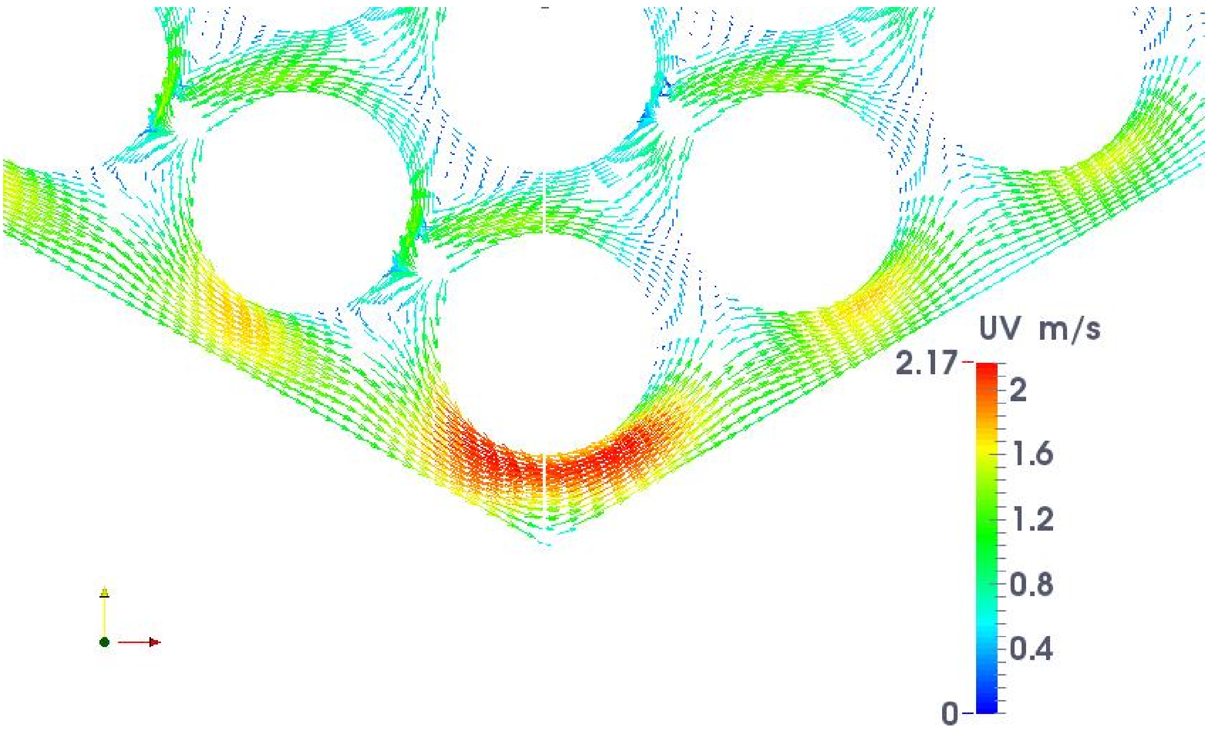

Fig. 7.2 (d) Close-up view of the transverse velocity field at the bundle exit of 1.65 mm diameter helical wire wrap 217 pin bundle in X-Y plane.

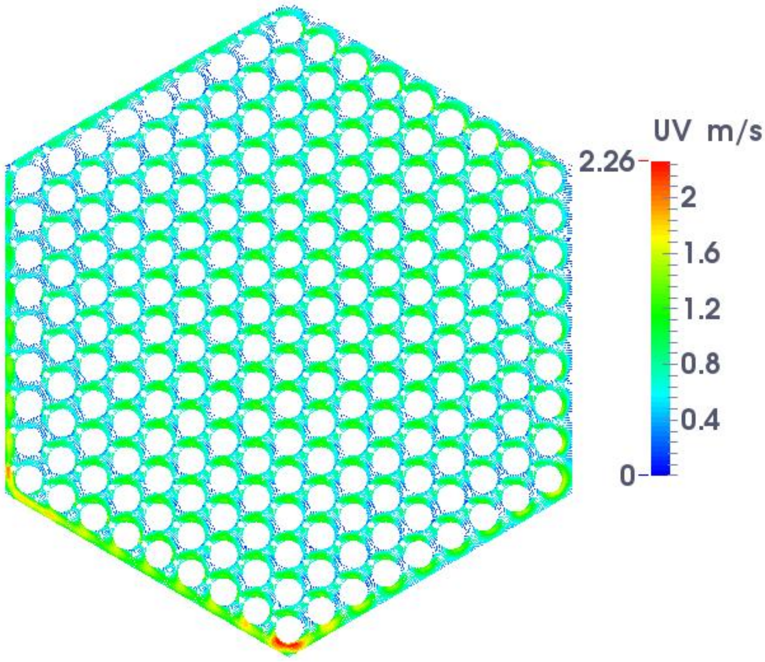

Fig. 7.2 (e) The transverse velocity field at the bundle exit of 2.0 mm diameter helical wire wrap 217 pin bundle

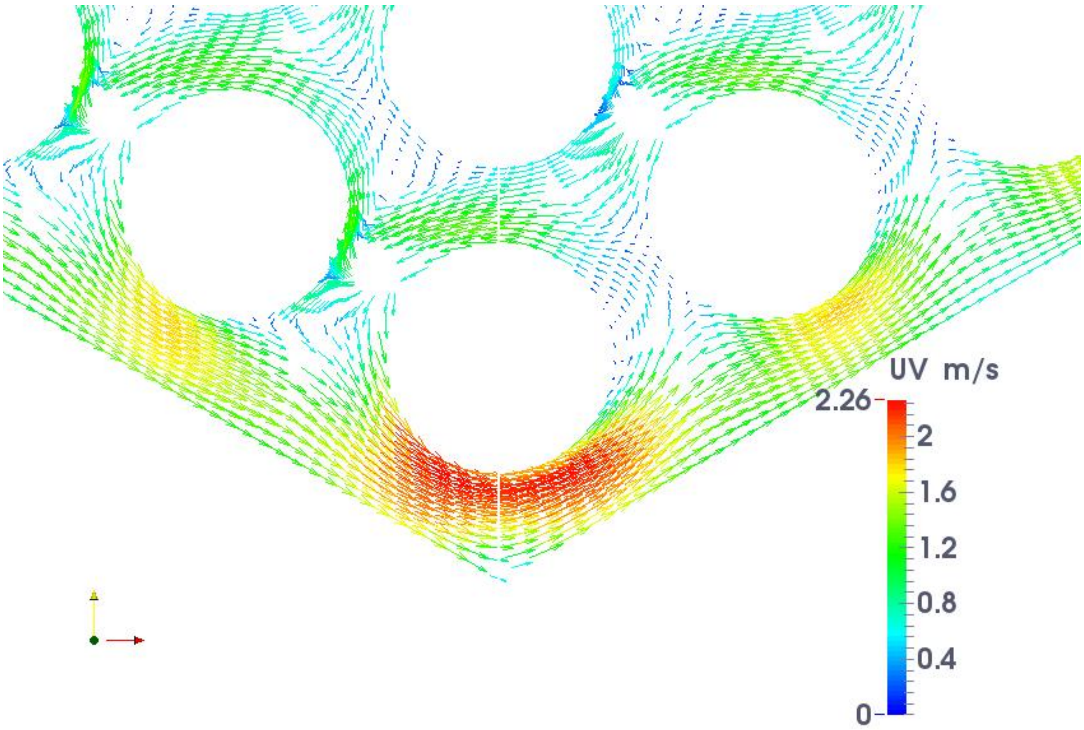

Fig. 7.2 (f) Close-up view of transverse velocity field at the bundle exit of 2.0 mm diameter helical wire wrap 217 pin bundle in X-Y plane.

Table 7.2 Transverse velocity as a function of helical wire diameter for Re = 100,000

Helical wire diameter, mm	Average transverse velocity, m/s	Maximum transverse velocity, m/s	Ratio of Transverse velocity to Average axial velocity
1.25	0.66	2.13	0.07
1.65	0.68	2.2	0.08
2.0	0.69	2.27	0.098

7.3 DEPENDENCE OF AXIAL VELOCITY ON HELICAL PITCH

The contours of axial velocity for 100, 200 and 300 mm helical pitch models with a fixed wire diameter of 1.65 mm and with a ratio of the triangular pitch distance to pin diameter (P/D) of 1.255 are presented at the bundle exit in Figs.7.3 (a) - 7.3 (c). These results are for an axial entry velocity of 8 m/s and the corresponding Reynolds number is 100,000. The values of axial velocity at the bundle exit as function of helical wire pitch are presented in Table 7.3. The equivalent diameter of the pin bundle and the average velocity are same for all values of helical pitch. But, maximum values are higher for shorter helical pitches due to distortion by the transverse velocity.

7.4 DEPENDENCE OF AXIAL VELOCITY ON HELICAL WIRE DIAMETERS

In order to compare the velocity field for 1.25, 1.65 and 2.0 mm diameter pins (the P/D ratios are 1.307, 1.255 and 1.194) for a fixed 200 mm helical pitch, the axial velocity fields at the bundle exit for the same Reynolds number are presented in the Figs. 7.4 (a) – 7.4 (c).

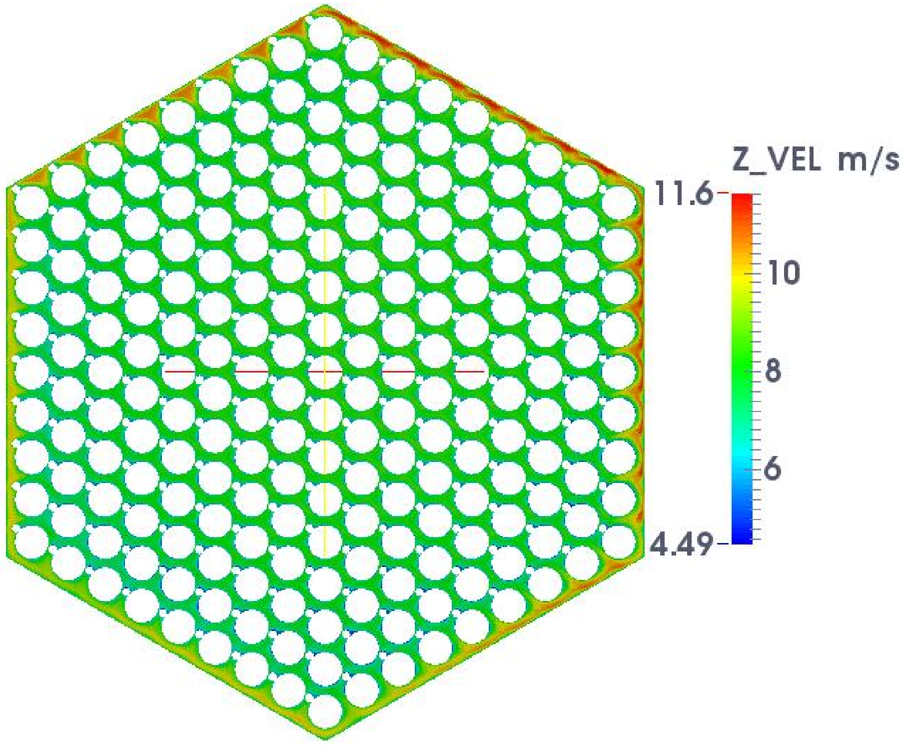

Fig. 7.3 (a) The axial velocity field at the bundle exit of 100 mm helical pitch wire wrap 217 pin bundle

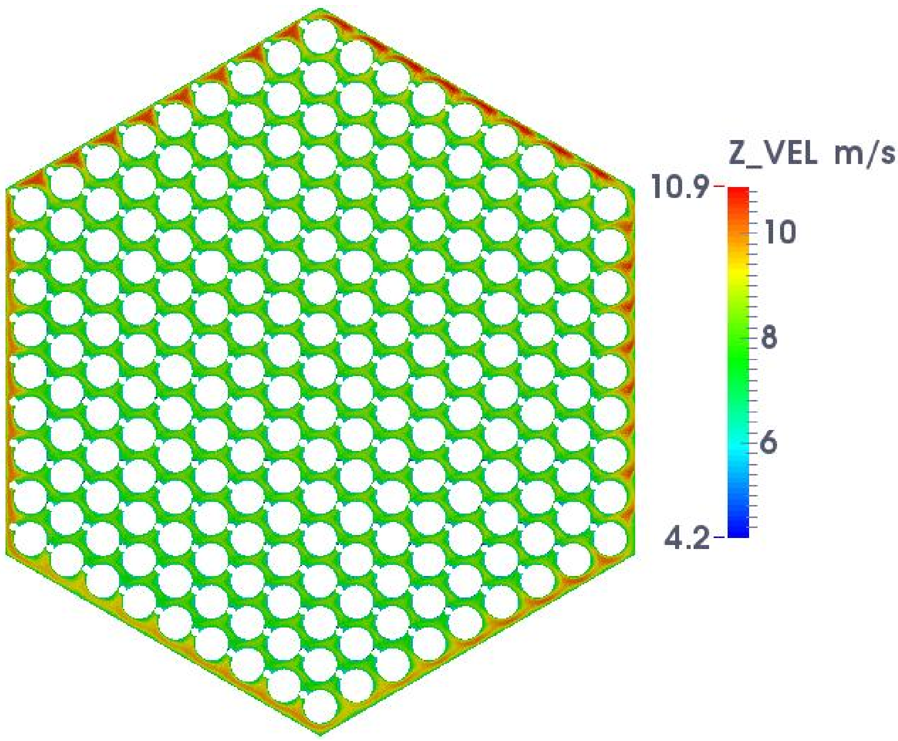

Fig. 7.3 (b) The axial velocity field at the bundle exit of 200 mm helical pitch wire wrap 217 pin bundle

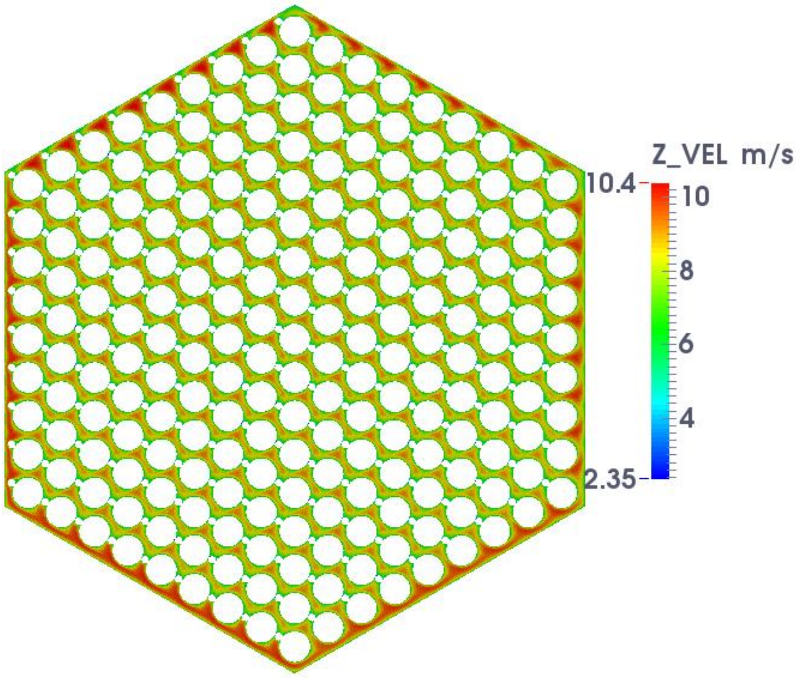

Fig. 7.3 (c) The axial velocity field at the bundle exit of 300 mm helical pitch wire wrap 217 pin bundle

Table 7.3 Axial velocity as a function of helical pitch for Re = 100,000

Helical pitch, mm	Average axial velocity, m/s	Maximum axial velocity, m/s
100	8.0	11.6
200	8.0	10.8
300	8.0	10.4

The values of axial velocity as function of wire wrap parameters are presented in Table 7.4. As the wire diameter increases, the equivalent diameter of the bundle increases. So, the axial flow velocity is correspondingly reduced to keep the Reynolds number same. It is seen that the average and maximum values of axial velocity decrease with increase in wire diameter.

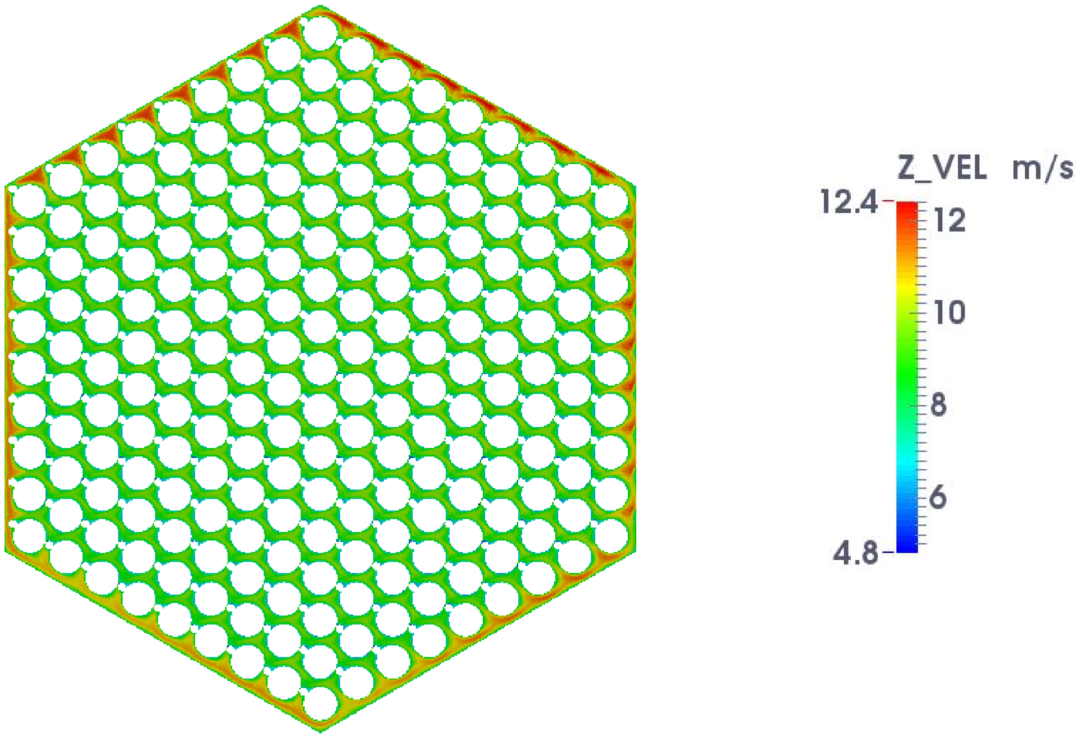

Fig. 7.4 (a) The axial velocity field at the bundle exit of 1.25 mm diameter helical wire wrap 217 pin bundle

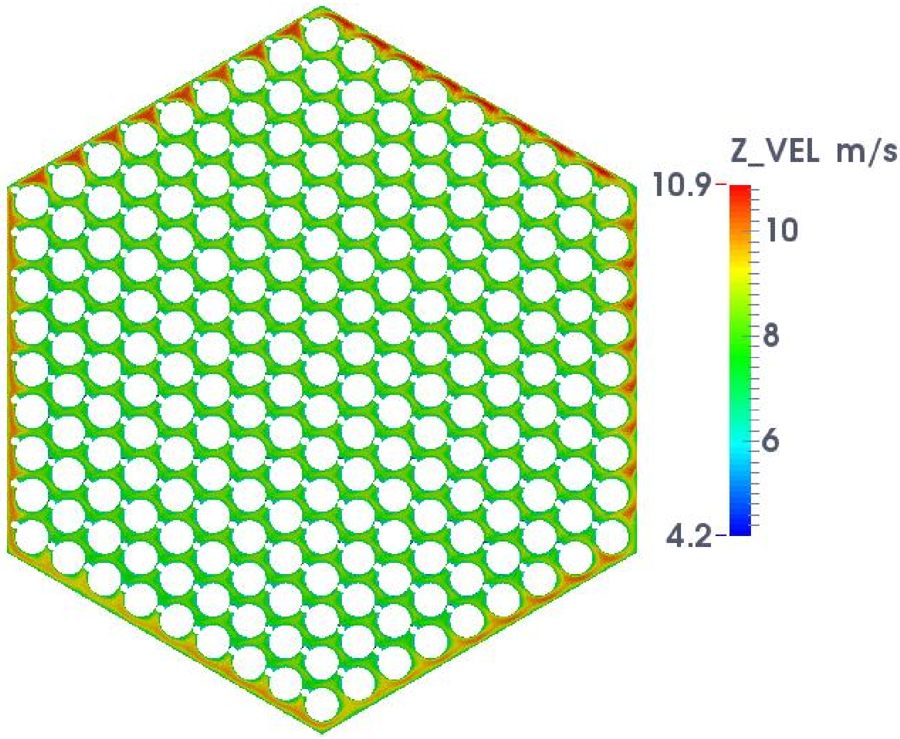

Fig. 7.4 (b) The axial velocity field at the bundle exit of 1.65 mm diameter helical wire wrap 217 pin bundle

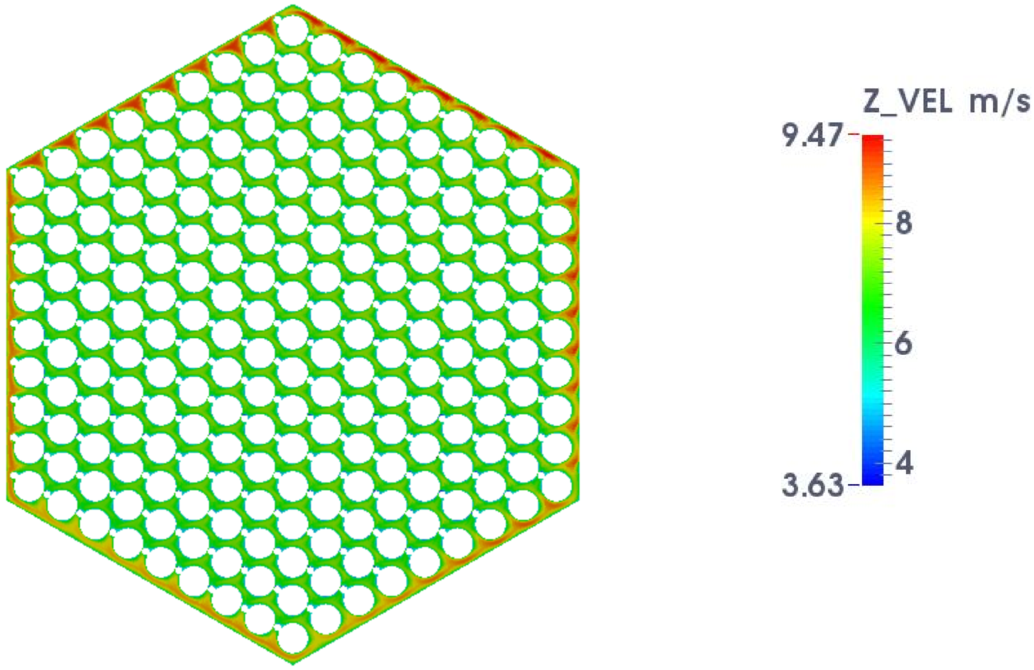

Fig. 7.4 (c) The axial velocity field at the bundle exit of 2.0 mm diameter helical wire warpped 217 pin bundle

Table 7.4 Axial velocity as a function of helical wire diameter for Re = 100,000

Helical wire diameter, mm	Average axial velocity, m/s	Maximum axial velocity, m/s
1.25	9.5	12.4
1.65	8.0	10.9
2.0	7.03	9.47

7.5 INFLUENCE OF HELICAL PITCH ON FRICTION FACTOR

The dependence of friction factor on helical pitch is depicted in Fig. 7.5 (a) for Re = 100,000. It is seen that friction factor decreases from 0.03 for 100 mm helical pitch and approaches a constant value of 0.0175 for helical pitches 600 mm and above. When the length of the helical pitch increases, the friction factor approaches as that of Blasius correlation for internal flow, as expected.

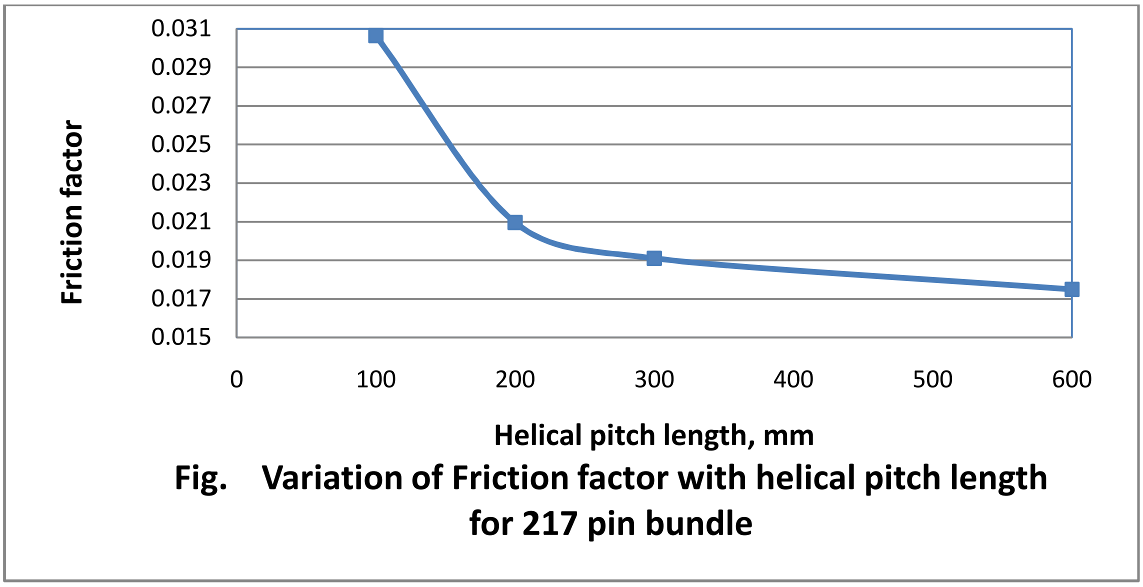

Fig. 7.5 (a) Variation of friction factor of 217 pin bundle with helical pitch

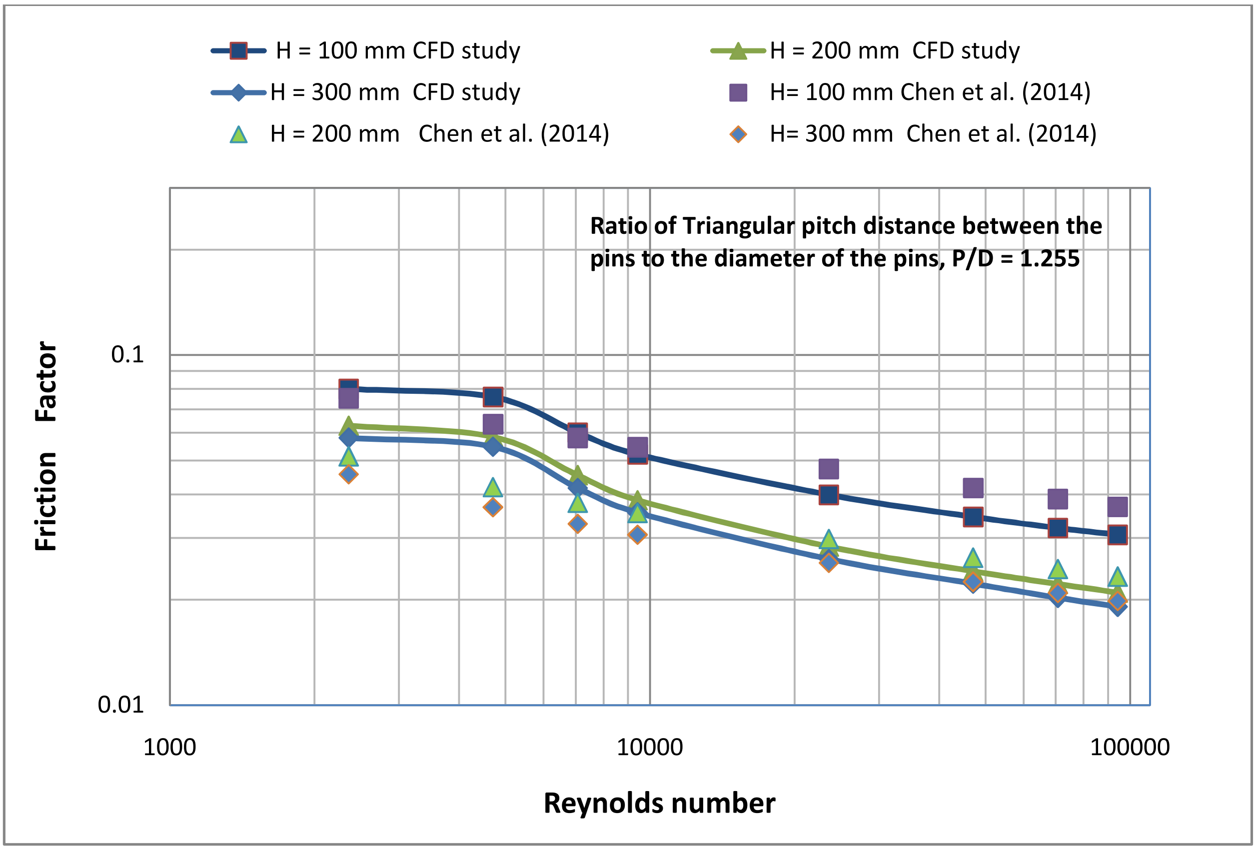

Fig. 7.5 (b) Dependence of friction factor of 217 bundle on helical pitch for various Reynolds number

The dependence of friction factor on helical pitch for various Reynolds numbers, both in the laminar and turbulent regimes is depicted in Fig. 7.5 (b). It is seen that the friction factor is inversely proportional to the Reynolds number for all values of helical pitch, as in any internal flow. Also, as the helical pitch decreases, the friction factor increases due to enhancement in cross flow induced by short helical pitches.

The average percentage increase in friction factor when the helical pitch decreased from 200 mm to 100 mm is around 50 % whereas it is only 5 % when the helical pitch is decreased from 300 mm to 200 mm. From the Chen and Todreas correlation for friction factor with different helical pitch, it is seen that the friction factor is higher for shorter helical pitch with which the present CFD results agree well.

7.6 INFLUENCE OF HELICAL WIRE DIAMETER ON FRICTION FACTOR

The predicted dependence of friction factor on P/D is depicted in Fig. 7.6 for various values of Reynolds number. The friction factor is seen to increase with P/D. Due to change in diameter of the helical wire, the triangular pitch distance between the fuel pins will get changed but velocity of flow is correspondingly changed to keep the Reynolds number same as that of the bundle with wire diameter 1.65 mm. When the wire diameter is reduced, the resistance to cross flow is increased. As a result of this, the relative magnitude of cross flow reduces leading to reduction in friction factor in small wire diameter bundles. The friction factor is seen to be a weak function of P/D for the pin bundle dimensions considered. The average percentage increase in friction factor when the helical wire diameter decreased from 1.65 mm to 1.25 mm is around 5 % whereas it is only 3 % when it is decreased from 2.0 mm to 1.65 mm. From the Chen et al (2014) correlation for friction factor with different helical wire diameter, it is observed that the friction factor is higher for larger P/D ratio (i.e. for larger helical wire diameter) with which the present CFD results for 217 pin bundle agree.

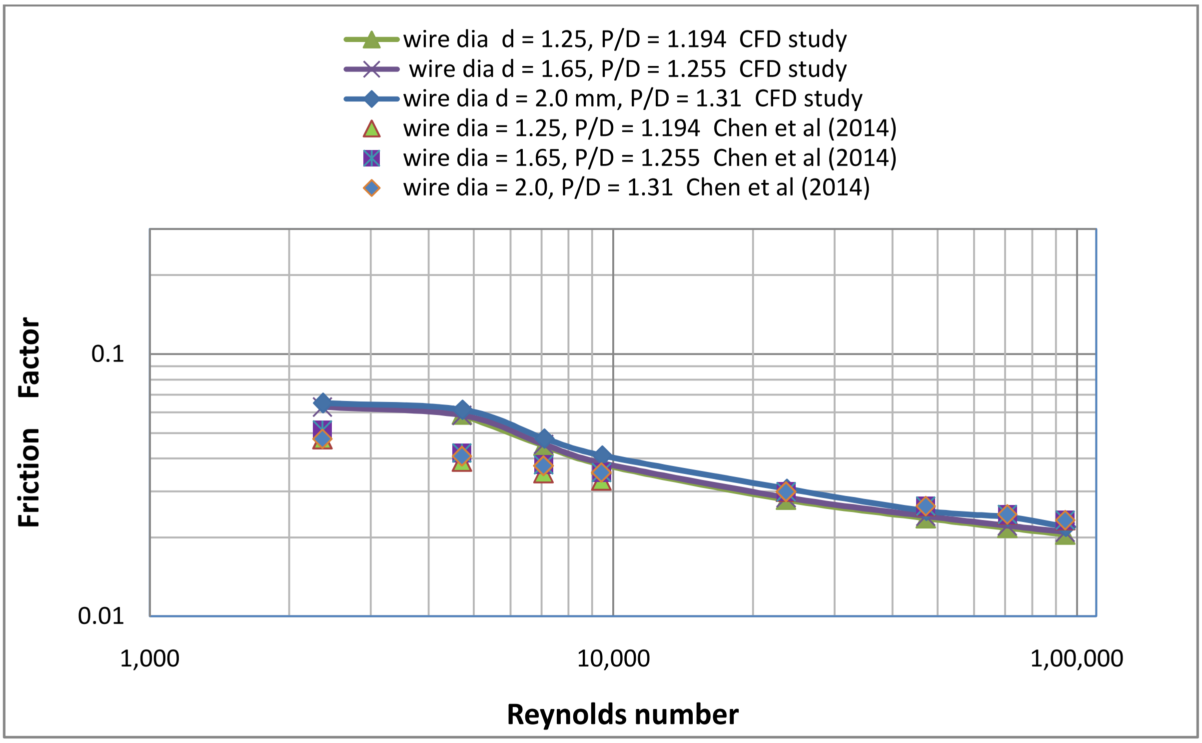

Fig. 7.6 Dependence of friction factor of 217 bundle on helical wire diameter for various Reynolds number

7.7 INFLUENCE OF HELICAL PITCH ON TEMPERATURE DISTRIBUTION

The temperature fields for a fixed Reynolds number of ~ 100000 in a 217 pin bundle with 100, 200 and 300 mm helical pitch values are presented at a distance of 100 mm from the bundle entry in Figs. 7.7 (a) – 7.7 (c). While the average sodium temperature at the exit of 100 mm is same (686.2 K) for all the cases, the average clad temperature is 694.4 K, 694.9 K and 695.4 K respectively for 100, 200 and 300 mm helical pitch pin bundles. Hence, it is seen that the clad temperature is lower for 100 mm helical pitch and higher for 300 mm helical pitch. It is also seen that the maximum temperature occurs in different regions of the bundle, as the helical wire completes one full turn for 100 mm helical pitch, half turn for 200 mm and one third turn for 300 mm helical pitch pin bundles.

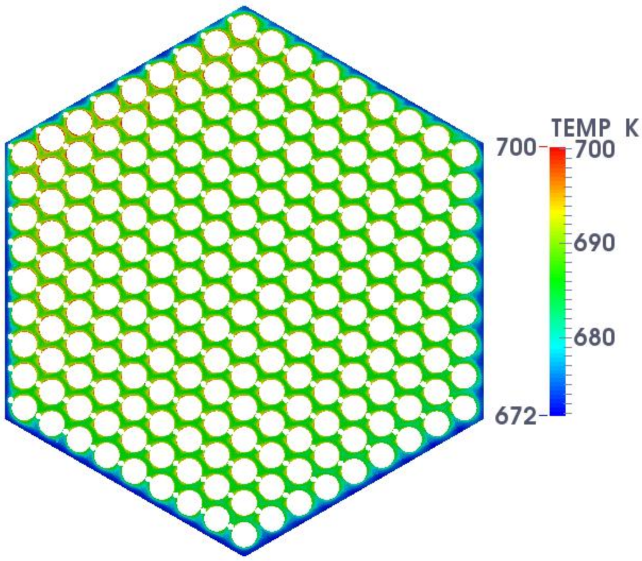

Fig. 7.7 (a) Temperature field at 100 mm elevation for 100 mm helical pitch wire wrap 217 pin bundle

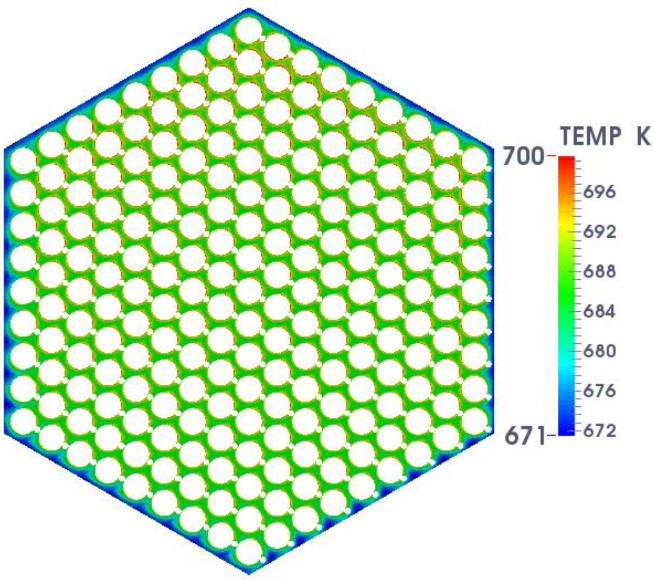

Fig. 7.7 (b) Temperature field at 100 mm elevation for 200 mm helical pitch wire wrap 217 pin bundle

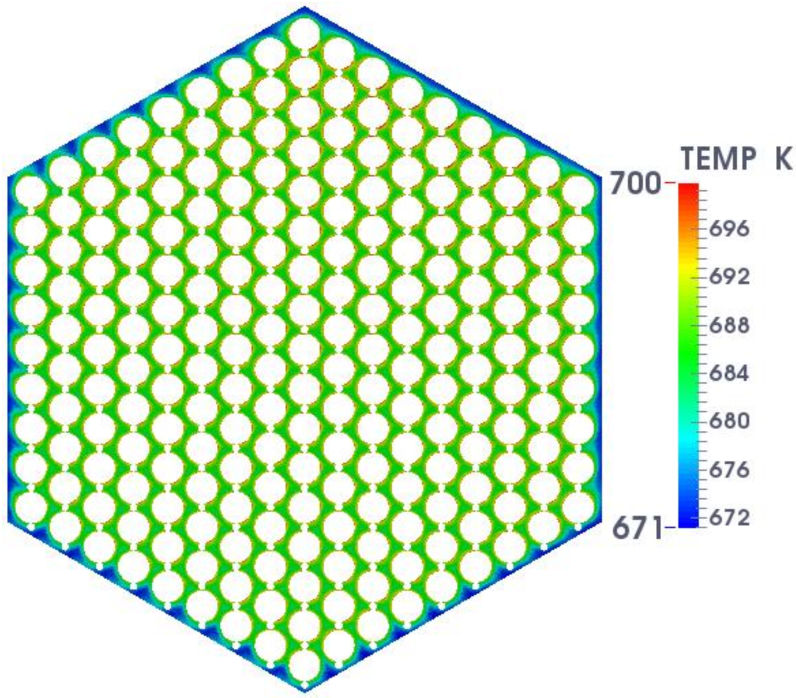

Fig. 7.7 (c) Temperature field at 100 mm elevation for 300 mm helical pitch wire wrap 217 pin bundle

Table 7.5 Effect of helical pitch on clad to sodium temperature difference

Helical pitch (mm)	Clad temperature, K		Sodium temperature, K		Clad to Sodium temperature difference, (K)	
	Maximum	Minimum,	Maximum	minimum	Maximum	Minimum
100	699	691	692	685	7	6
200	699	691	691	685	8	6
300	699	692	689	686	10	6

The effect of helical pitch on clad to sodium temperature difference is presented in Table 7.5. It is seen that the hot spot location is only about 6 - 8 K higher than the local bulk temperature for nominal helical pitch of 200 mm. In other words, the clad temperature is fairly uniform in the circumferential direction due to the circulating fluid flow created by the helical wires. The coolant is made to impinge and sweep the corners formed by the junction of the pin and spacer wire. Hence, wire wrap promotes cross stream flow to prevent excessively high temperature around the wire wrap.

7.8 INFLUENCE OF HELICAL WIRE DIAMETER ON TEMPERATURE DISTRIBUTION

The sodium temperature field for 217 pin bundle at a Reynolds number of ~ 100000 with different helical wire diameters of 1.25, 1.65 and 2.0 mm at the bundle exit of 200 mm travel in the bundle is presented in Fig. 7.8 (a) – 7.8 (c). The temperature field contains both the clad and sodium temperatures. It is seen that the temperature is lower for smaller wire diameter as the heat flux is kept lower to obtain a fixed sodium outlet temperature of 702 K. The temperature distribution becomes more uniform when wire diameter increases.

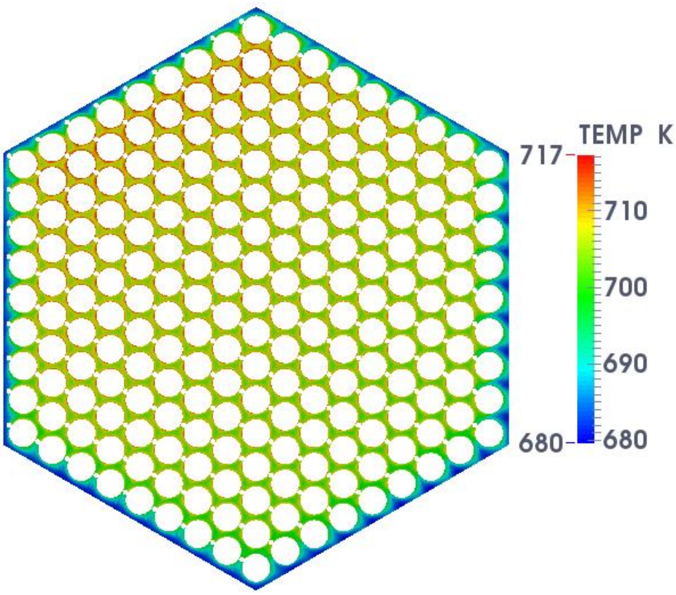

Fig. 7.8 (a) Temperature field at the exit of 1.25 mm diameter helical wire wrap 217 pin bundle

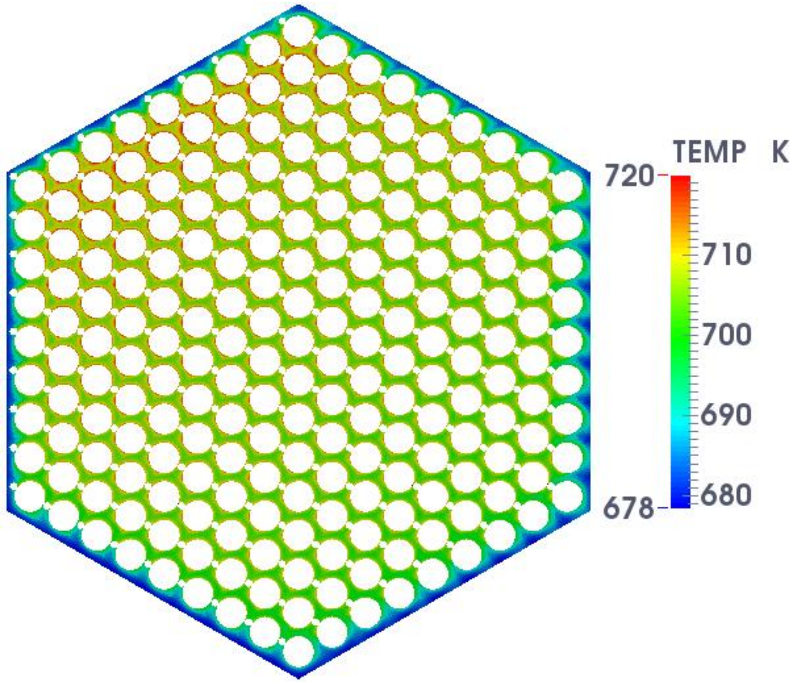

Fig. 7.8 (b) Temperature field at the exit of 1.65 mm diameter helical wire wrap 217 pin bundle

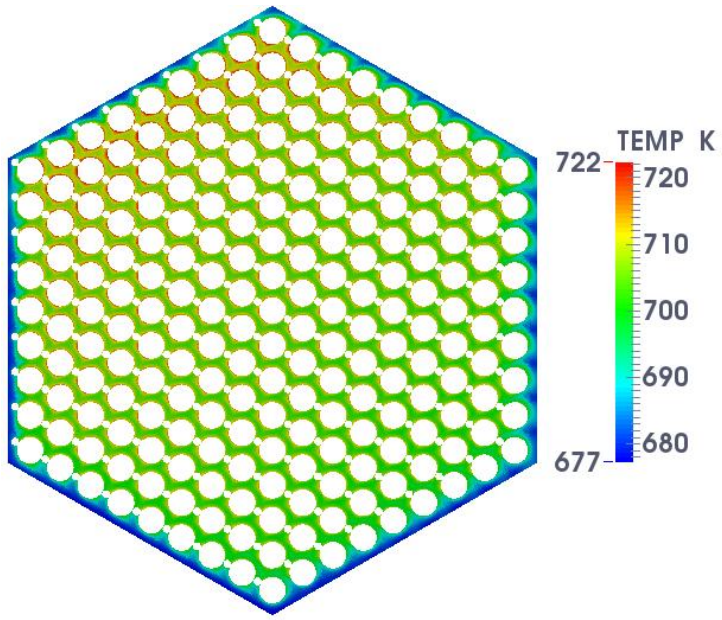

Fig. 7.8 (c) Temperature field at the exit of 2.0 mm diameter helical wire wrap 217 pin bundle

7.9 INFLUENCE OF HELICAL PITCH ON NUSSELT NUMBER

It is found that the temperature difference between the clad and coolant increases with helical pitch suggesting lower values of Nusselt number for longer helical pitches. This is due to the fact that when the helical pitch is increased, the helical wire induced cross flow decreases. The predicted dependence of Nusselt number on helical pitch is depicted in Fig. 7.9 for various values of Reynolds number. In the turbulent regime, the Nusselt number is higher if the helical pitch is shorter. This trend is in line with the dependence of friction factor on helical pitch as expected. However, in the laminar regime, The Nusselt number does not exhibit any perceptible dependence on helical pitch.

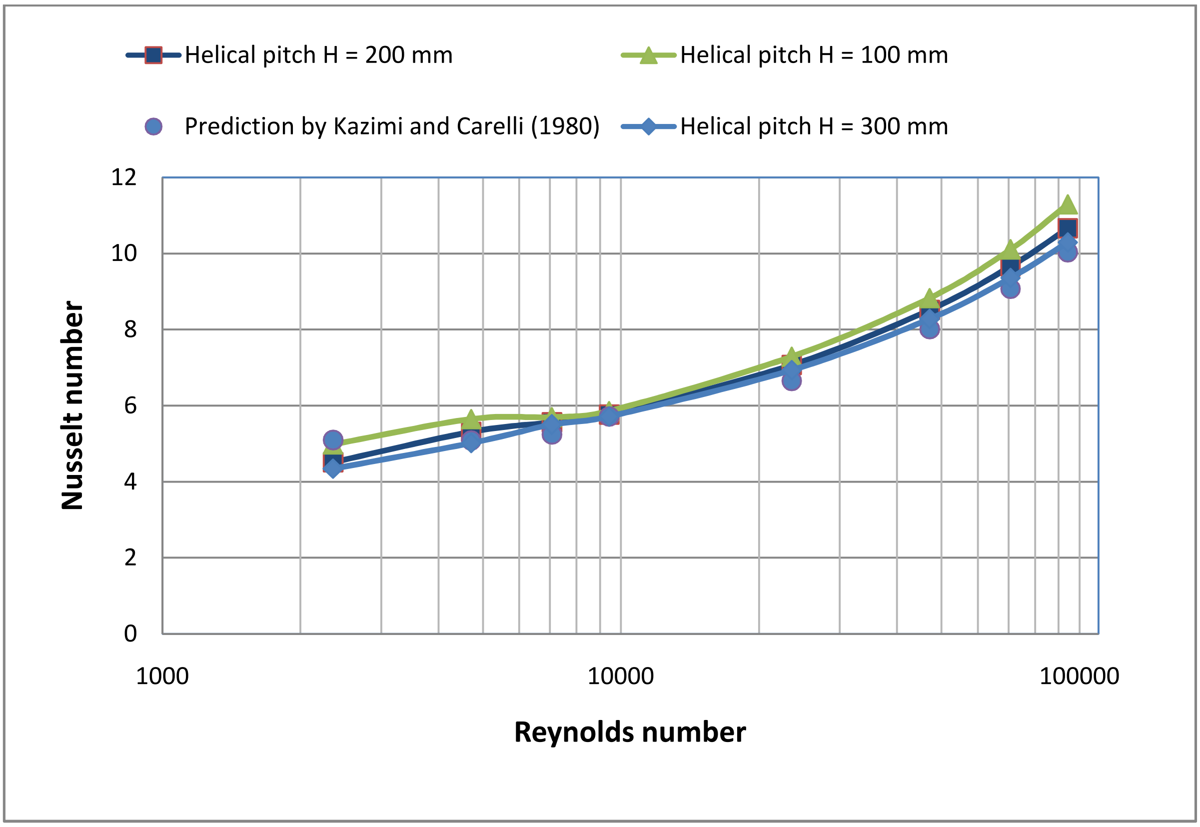

Fig. 7.9 Comparison of Nusselt number at 100 mm from the inlet of 217 fuel pin bundle for various helical pitch

7.10 INFLUENCE OF HELICAL WIRE DIAMETER ON NUSSELT NUMBER

When the wire diameter increases, the axial velocity of flowing fluid decreases and heat flux is increased to keep the Reynolds number and outlet temperature constant. It is found that the temperature difference between the clad and coolant increases with helical wire diameter indicating lower values of heat transfer coefficient for larger wire diameter. This is due to the fact that when wire diameter increases, the axial velocity of sodium decreases though the relative cross flow velocity increases. As a consequence of this, as well as increase in hydraulic diameter, the Nusselt number increases with wire diameter. This is in line with dependence of friction factor on wire diameter. The estimated variation of Nusselt number with respect to diameter is depicted in Fig. 7.10 for various values of Reynolds number. It is seen that larger the helical wire diameter, larger is the Nusselt number.

7.11 DEVELOPMENT OF NUSSELT NUMBER CORRELATIONS

Correlations for Nusselt number at the bundle exit based on CFD study are proposed for 217 pin bundle with different helical pitches and helical wire diameter and for a range of Reynolds number.

7.11.1 For Various Helical Pitches

The following empirical correlation is valid for a pin diameter of 6.6 mm, helical pitch from 100 to 300 mm and constant wire diameter of 1.65 mm. The sodium flow should be in turbulent regime with Reynolds number in the range of 20000 to 100000 and Peclet number from 100 to 500 respectively.

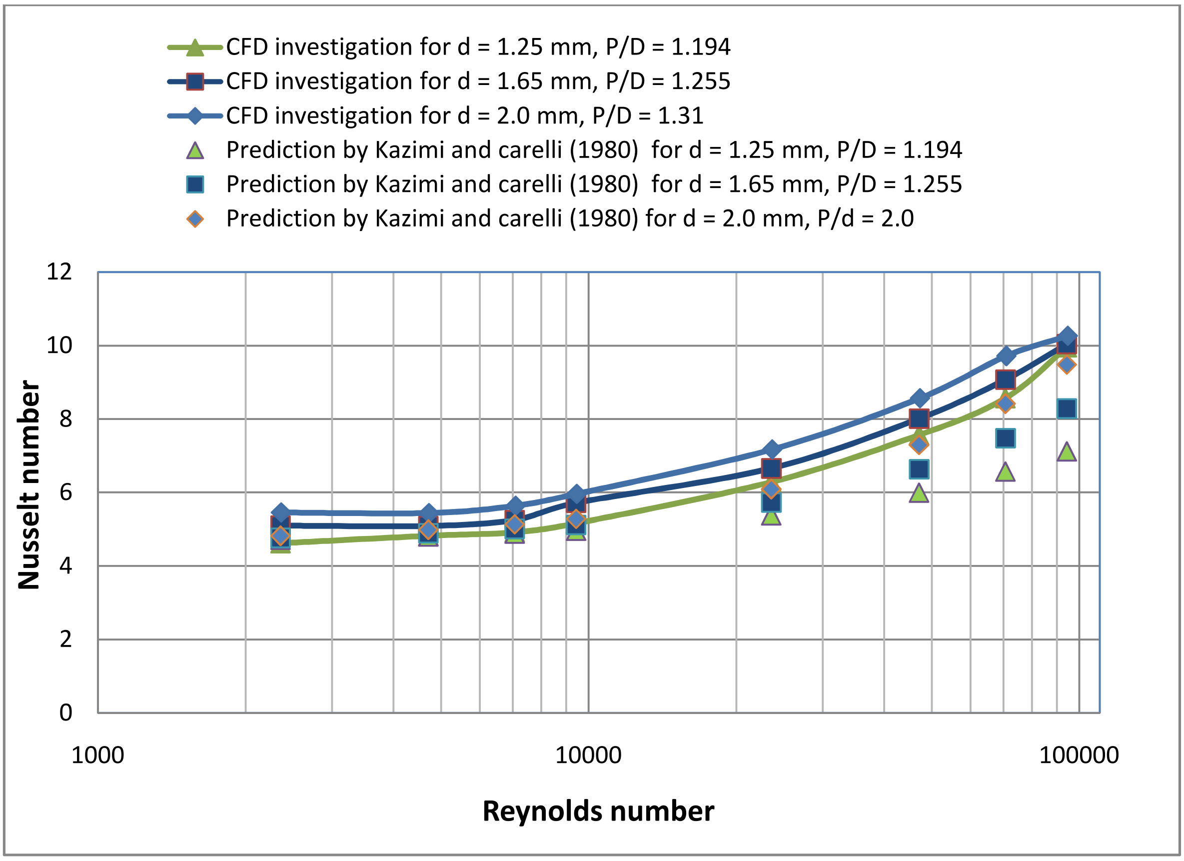

Fig. 7.10 Comparison of Nusselt number at the exit of 217 fuel pin bundle for various helical wire diameter

$$Nu = 2.293 \times \left(\frac{H}{D}\right)^{-0.06} \times (Pe)^{0.283}$$

The following correlation is valid for Reynolds number 2000 to 20000 and Peclet number from 10 to 100 respectively.

$$Nu = 3.246 \times \left(\frac{H}{D}\right)^{-0.05} \times (Pe)^{0.201}$$

7.11.2 For Various Helical Wire Diameter

The following correlation is valid for a pin diameter of 6.6 mm, constant helical pitch of 200 mm and wire diameter from 1.25 to 2.0 mm. The Reynolds number range is 20000 to 100000 and Peclet number from 100 to 500 respectively.

$$Nu = 2.133 \times (\frac{d}{D})^{0.283} \times (Pe)^{0.315}$$

The following correlation is valid for Reynolds number from 2000 to 20000 and Peclet number ranges from 10 to 100 respectively.

$$Nu = 5.893 \times (\frac{d}{D})^{0.224} \times (Pe)^{0.065}$$

Where d - diameter of the wire, D – diameter of the pin, H – Helical pitch of the wire.

The method of deducing the constants and exponents of the proposed correlations and the analysis of data scatter and the estimation maximum possible error in the proposed correlations is presented in Appendix B. It is seen that the proposed correlations are best fitted against the actual values of Nusselt number obtained from the CFD study. The maximum possible error is 10 %.

7.12 CLOSURE

The intensity of transverse velocity is found to be inversely proportional to the helical pitch. Hence, the values of friction factor and Nusselt number are larger for shorter helical pitch for all values of Reynolds number. As the wire diameter increases, the equivalent diameter of the whole bundle increases. The relative transverse velocity is found to be directly proportional to the wire diameter and the values of friction factor are smaller for smaller values of helical wire diameter. The Nusselt number is seen to increase with increase in wire diameter. Based on parametric study, correlations for Nusselt number at the bundle exit are proposed for 217 pin bundle with different helical pitches and helical wire diameter as a function of Peclet number.

CHAPTER - 8

INVESTIGATION OF CLAD AND SODIUM TEMPERATURE DISTRIBUTIONS

8.0 INTRODUCTION

One of the purposes of pin bundle thermal hydraulics is to obtain the clad temperature distribution on the surface of each and every pin of the 217 pin bundle. The sodium temperature distribution in each and every sub channel of the pin bundle is also equally important. As the clad and sodium temperatures are the highest at the outlet of the bundle, their circumferential distributions are presented here at the outlet of the 217 pin bundle. Based on these distributions, the heat transfer from the clad to sodium can be ascertained on the surface of every pin and in every sub channel. From the maximum values of clad and sodium temperatures, the hot spot factors and the hot channel factors which are important from safety analysis of the core can be evaluated (Chapter 10).

8.1 PIN NUMBERING OF THE 217 PIN BUNDLE

For the purpose of identifying the pins and for obtaining corresponding circumferential clad temperature distribution, the 217 pin bundle is numbered as shown in Fig 8.1 (a). From the pin numbering, it can be seen that the central pin is numbered as No.1. Also, the sub-channels enclosed by three pins in the triangular pitch in the case of central sub-channels, and the peripheral sub-channels enclosed by the pins and the hexagonal sheath can be identified. The angular locations of the sub-channels of the nine hexagonal rows can also be identified. For example, the angular location of the sub-channel of the first hexagonal row (surrounded by the central pin) from 0^o to 60^o are 1_2_3. The pins and the sub channels within the hexagonal sheath are divided into six zones as shown in Fig. 8.1 (a). Thus, zone I consists of pins and sub channels in the $1/6^{th}$ quadrant between $\theta = 240^o$ to 300^o. The definition of the angle along the circumference of the pin is also shown in Fig 8.1 (b) for the purpose of studying clad temperature distribution.

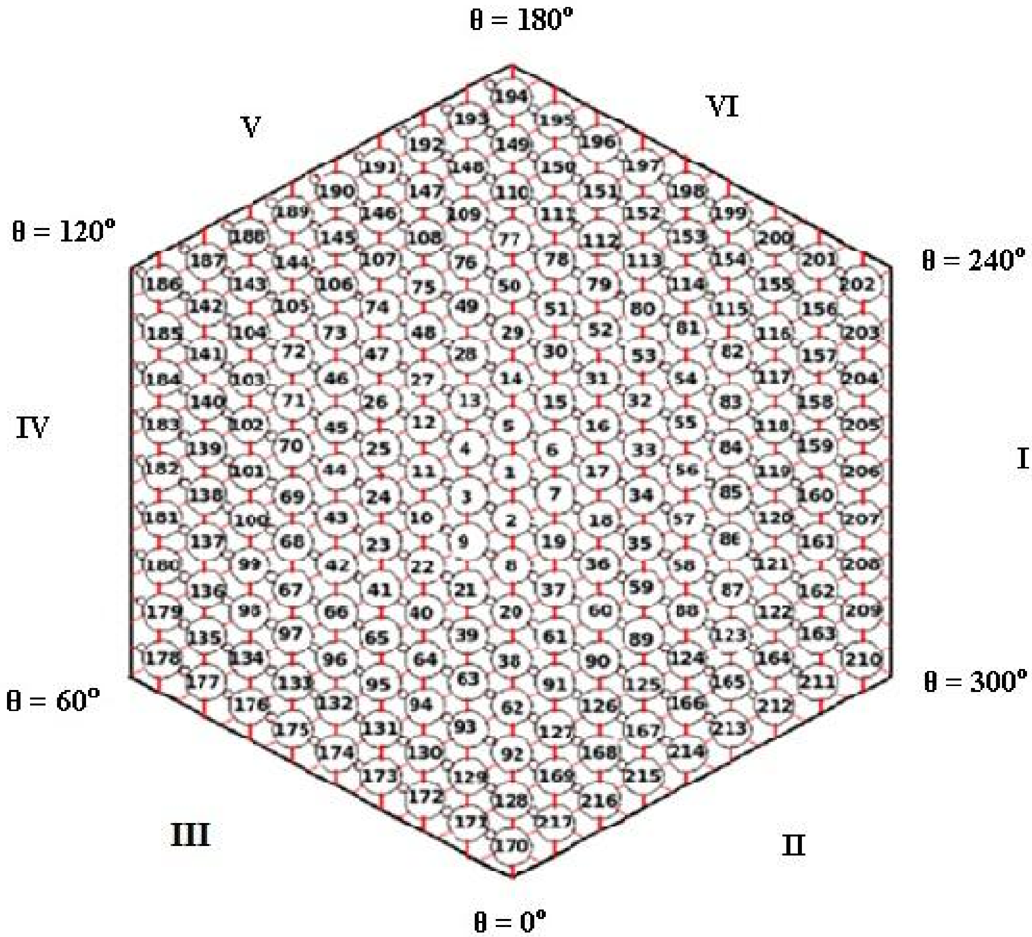

Fig. 8.1 (a) Pin numbering of the 217 pin bundle and angular locations of the sub-channels of various hexagonal rows.

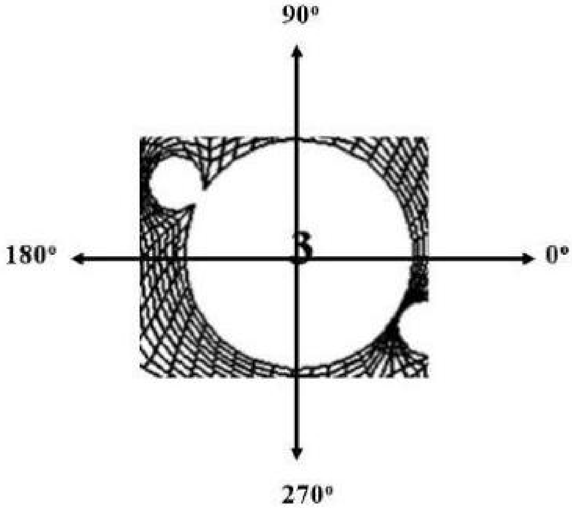

Fig 8.1 (b) Definition of angle along the circumference of the pin

8.2 EFFECT OF BUNDLE LENGTH ON CLAD TEMPERATURE DISTRIBUTION IN 217 PIN BUNDLE

Figure 8.2 (a) shows the clad temperature distribution around the central and peripheral pins at 200 mm length from the entry of the bundle. Fig 8.2 (b) shows the same at the outlet of the bundle (i.e.) at 1000 mm from the entry of the bundle. The circumferential variation in clad temperature exhibits intense distribution with alternate crests and troughs which remains unaltered with increase in the length of the bundle. But, the location of the pin having maximum clad temperature moves towards the center with the increase in the length of the bundle. This is due to the three distinct sodium temperature regions viz. hottest, coldest and intermediate becoming more distinct and uniform with the increase in the length of the bundle due to the transverse velocity induced by the helical wire.

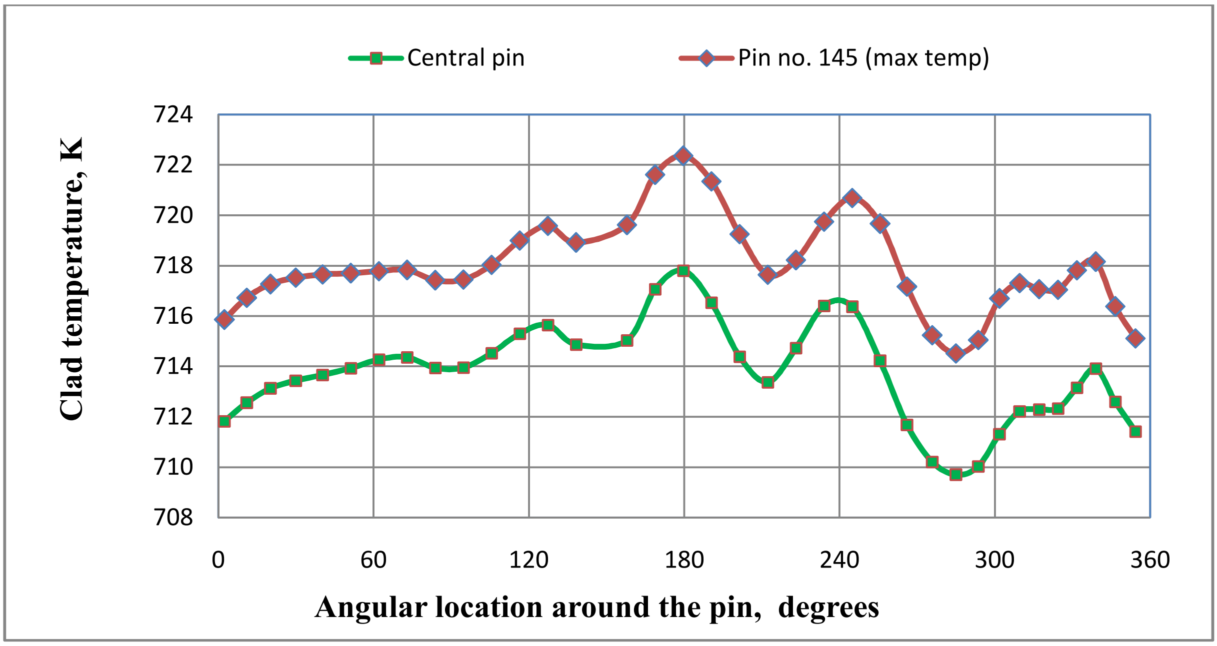

Fig. 8.2 (a) Clad temperature distribution around the central and peripheral pins at 200 mm from the inlet.

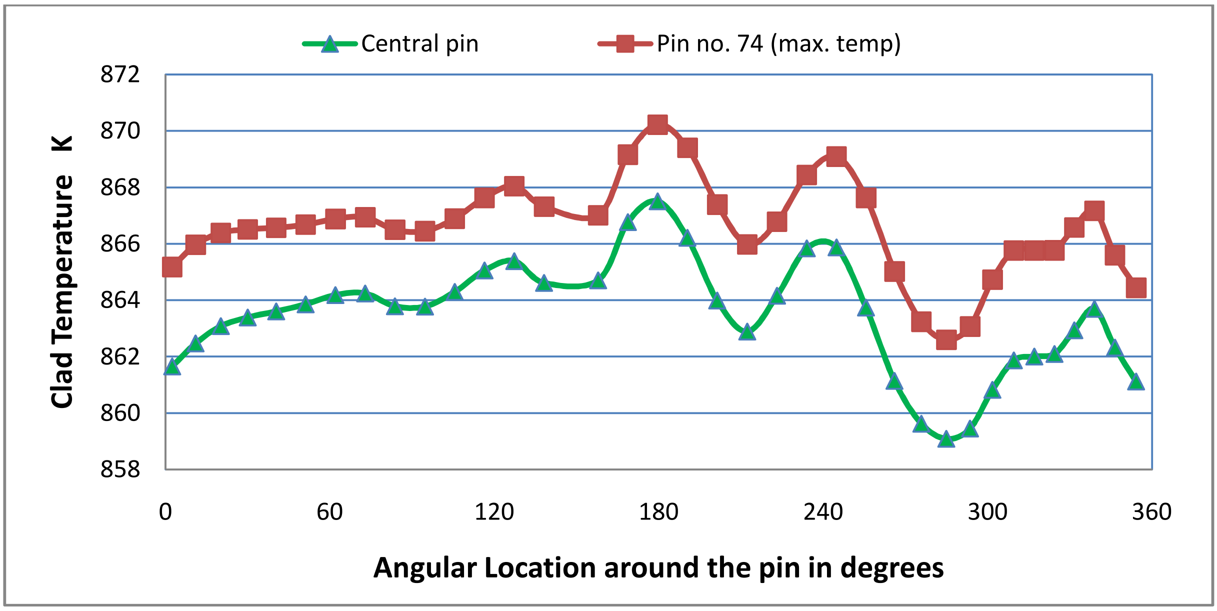

Fig. 8.2 (b) Clad temperature distribution around the central and peripheral pins at the outlet (1000 mm from the inlet).

8.3 EFFECT OF BUNDLE LENGTH ON SUB-CHANNEL SODIUM TEMPERATURE DISTRIBUTION IN 217 PIN BUNDLE

It is of interest to know the average outlet temperature of each sub-channel in the pin bundle. The average outlet temperature of sodium in the first row is obtained from each of the six sub-channels surrounded by the pin number 1 (i.e.) 1_2_3, 1_3_4, 1_4_5, 1_5_6, 1_6_7 and 1_7_2. This is plotted against the angular location of the hexagonal rows corresponding to the sub-channels. Similarly, the average outlet temperature of sodium in all other rows is obtained from each of the sub-channels surrounded by the subsequent row of pins in the pin bundle.

Figure 8.3 (a) shows the sodium temperature distribution in the nine rows of the sub-channels at 200 mm length from the entry of the bundle. Fig. 8.3 (b) shows the same at the outlet of the bundle (i.e.) at 1000 mm from the entry of the bundle. It is seen that the three temperature regions, viz. hottest, coldest and intermediate becomes more distinct with the increase in the length of the bundle and becomes more uniform. In addition, the temperature distribution in each row becomes closer to one another reducing the average temperature difference between them. Thus, the transverse velocity induced by the helical wire is able to reduce the temperature difference between the central and peripheral sub channels significantly due to the enhance heat transfer coefficient due to the helical wire induced transverse velocity along the length of the bundle and makes the sodium outlet temperature more uniform.

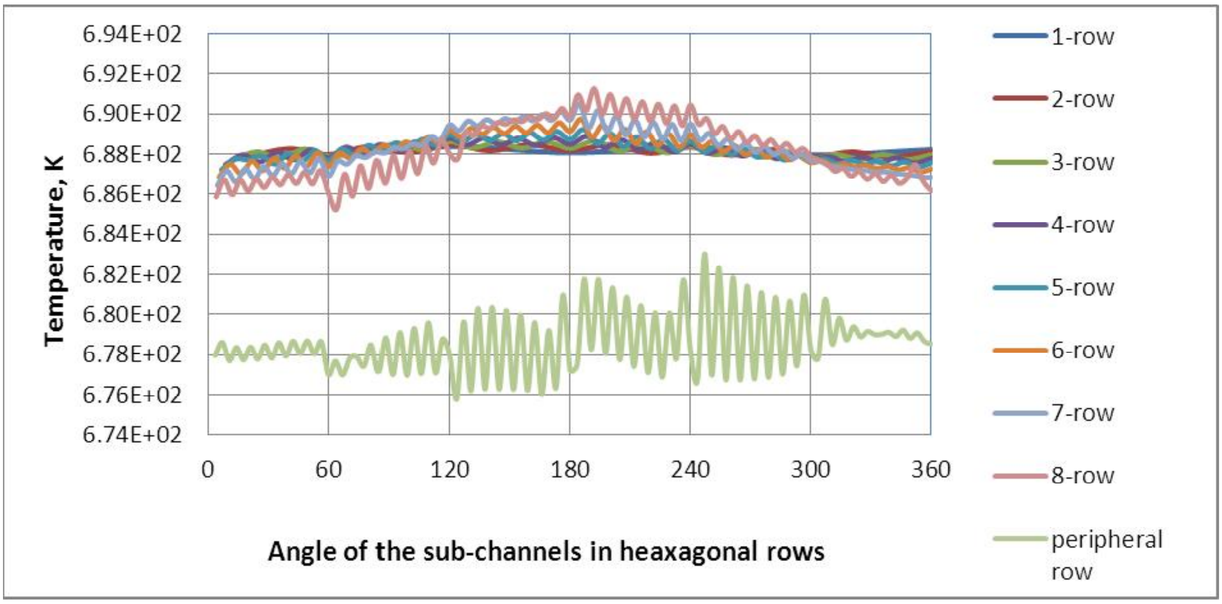

Fig. 8.3 (a) Sodium temperature distribution at 200 mm from the inlet of 217 pin bundle

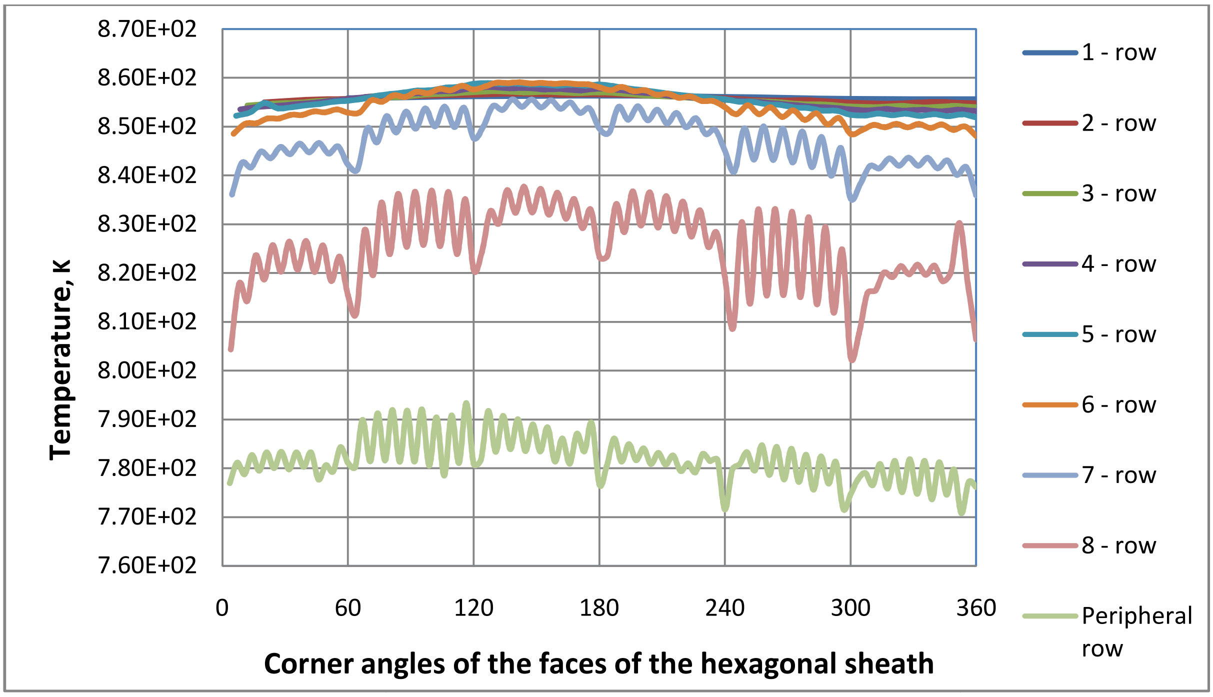

Fig. 8.3 (b) Sodium temperature distribution at 1000 mm from the inlet of 217 pin bundle

8.4 EFFECT OF HELICAL WIRE PARARAMETERS ON CLAD TEMPERATURE DISTRIBUTION IN 217 PIN BUNDLE

As it is not possible to present the temperature distribution on the surface of each and every pin, a representative pin in each of the six zones is presented here. It is seen from the temperature fields at the outlet of 217 pin bundle presented in Chapter 7, the temperatures of clad and sodium are maximum in zones IV and V where wire is present in the peripheral sub-channels. The temperatures are minimum in the zones I and II which are diametrically opposite to maximum temperature zones.

8.4.1 Influence of Helical Pitch

Figures 8.4.1 (a) – 8.4.1 (g) show the clad temperature distribution at 100 mm from the bundle entry for different helical pitches of 100 mm, 200 mm and 300 mm for representative pins in each zone with pin numbers No. 1 (central pin), No.145 (zone IV), No.152 (zone III), No. 160 (zone II), No. 166 (zone I), No.131 (zone II) and peripheral pin No.217. The clad temperature around the pin decreases with decrease in helical pitch for central pin as the transverse flow increases the heat transfer coefficient in the central sub-channels. The circumferential variation in clad temperature exhibits intense distribution with alternate crests and troughs. These crests and troughs are strongly influenced by (i) the radial gap between the pin under consideration and the neighboring pin and (ii) cross flow velocity induced by the spacer wire. While a smaller radial gap increases the clad temperature, larger cross stream velocity reduces the clad temperature. The clad temperature increases with decrease in helical pitch for the 7th row of pins due to the fact that the cross flow direction in different cases are different due to variation in helical pitch length.

In the peripheral pins, the decrease in clad temperature with decrease in helical pitch is more. This is because of the enhanced mixing due to higher cross flow in the peripheral sub-channels for shorter helical pitch. Also, the sodium temperature is less in the peripheral sub-channels since the heat input per unit length in these channels are less due to the presence of adiabatic hexagonal sheath. The clad temperature for 100 mm helical pitch is higher from 0^o-180^o which is facing the central pins and the same is lower from 180^o-360^o which is facing the hexagonal sheath. The clad temperatures for 200 and 300 mm helical pitch are higher due to reduced transverse velocities.

8.4.2 Influence of Helical Wire Diameter

Figures 8.4.2 (a) - 8.4.2 (c) show the normalized clad temperature distribution at the bundle exit for different helical wire diameters of 1.25 mm, 1.65 mm and 2.0 mm for representative pins in the central, 7^{th} row and peripheral pins.

The clad temperature is normalized as follows,

$$T_{nor.clad} = Kf_{cond} \times ((T_c - T_f) / (q'' \times d_{eq})$$

Where $T_{nor\ clad}$ – Normalized clad temperature, Kf_{cond} –Thermal conductivity of sodium, T_c – Mean clad temperature at the bundle exit, T_f - Mean sodium temperature at the bundle exit, q'' pin surface heat flux, W/m^2, d_{eq} – Equivalent diameter of the pin bundle.

It is seen that the normalized clad temperature decreases with increase in helical wire diameter for central pin and 7^{th} row of pins as the transverse flow increases the heat transfer coefficient in the central sub-channels. In the peripheral pins, the normalized clad temperature also decreases with increase in wire diameter as the transverse flow is higher in the peripheral sub-channels. The peripheral pin clad temperature for all helical wire diameters is higher in the region 0^o - 180^o which is facing the central pins and the same is lower from 180^o – 360^o which is facing the hexagonal sheath.

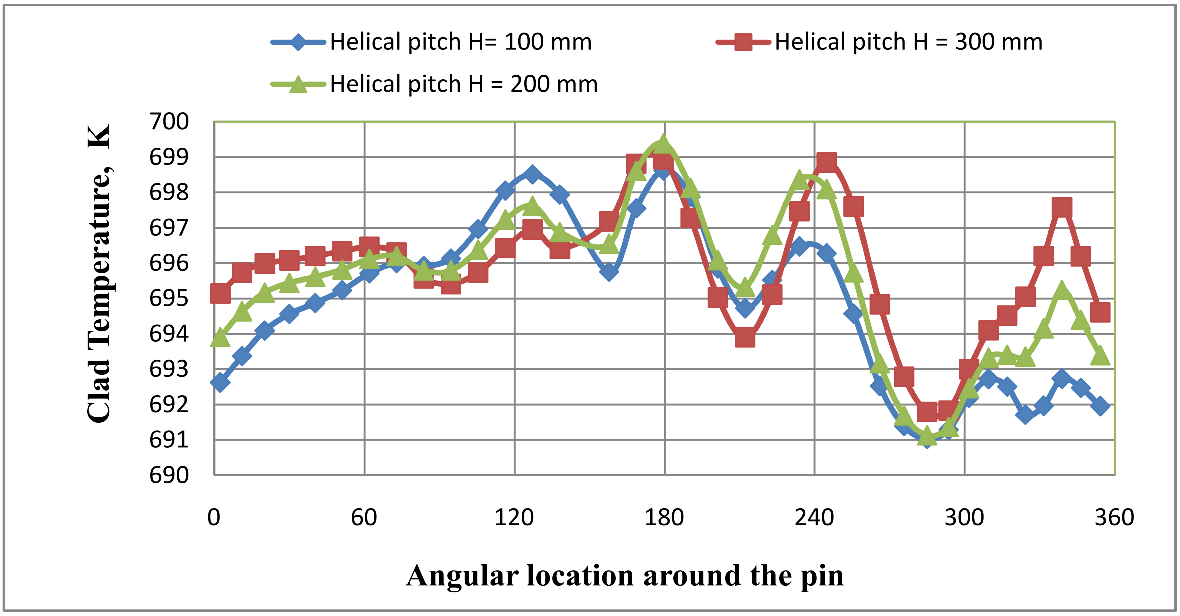

Fig. 8.4.1 (a) Clad temperature around the central pin for different helical pitches

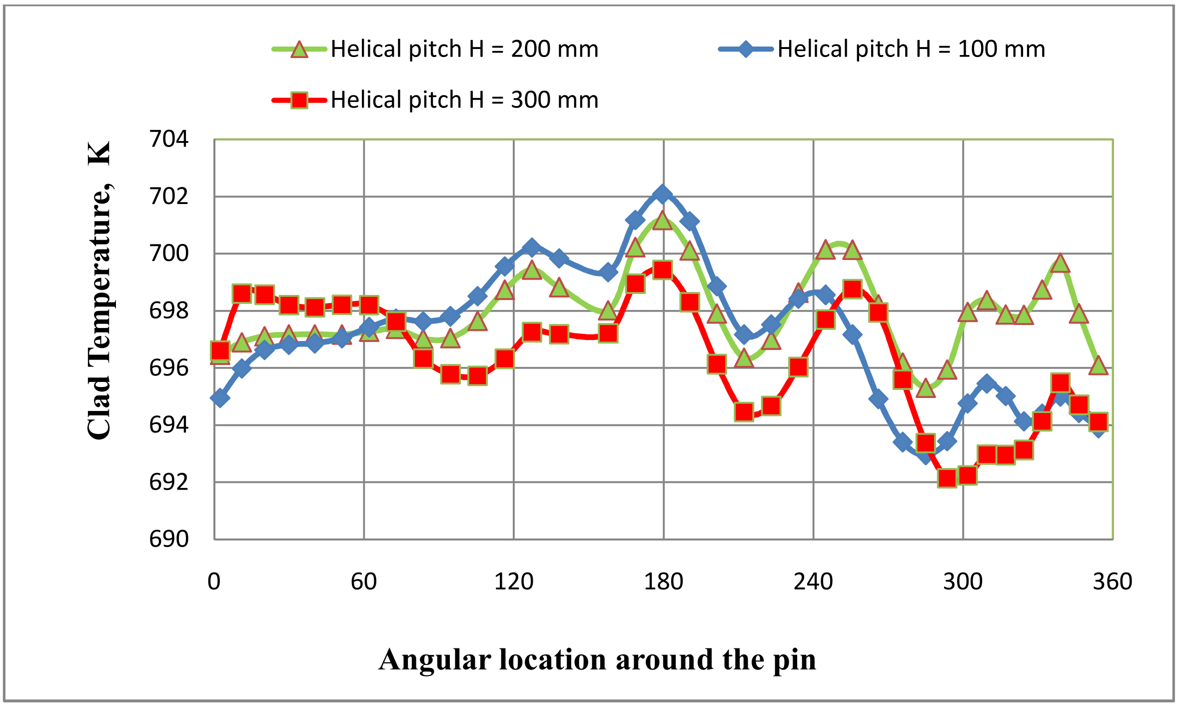

Fig. 8.4.1 (b) Clad temperature around the pin no. 145 located at the 7th row for different helical pitches

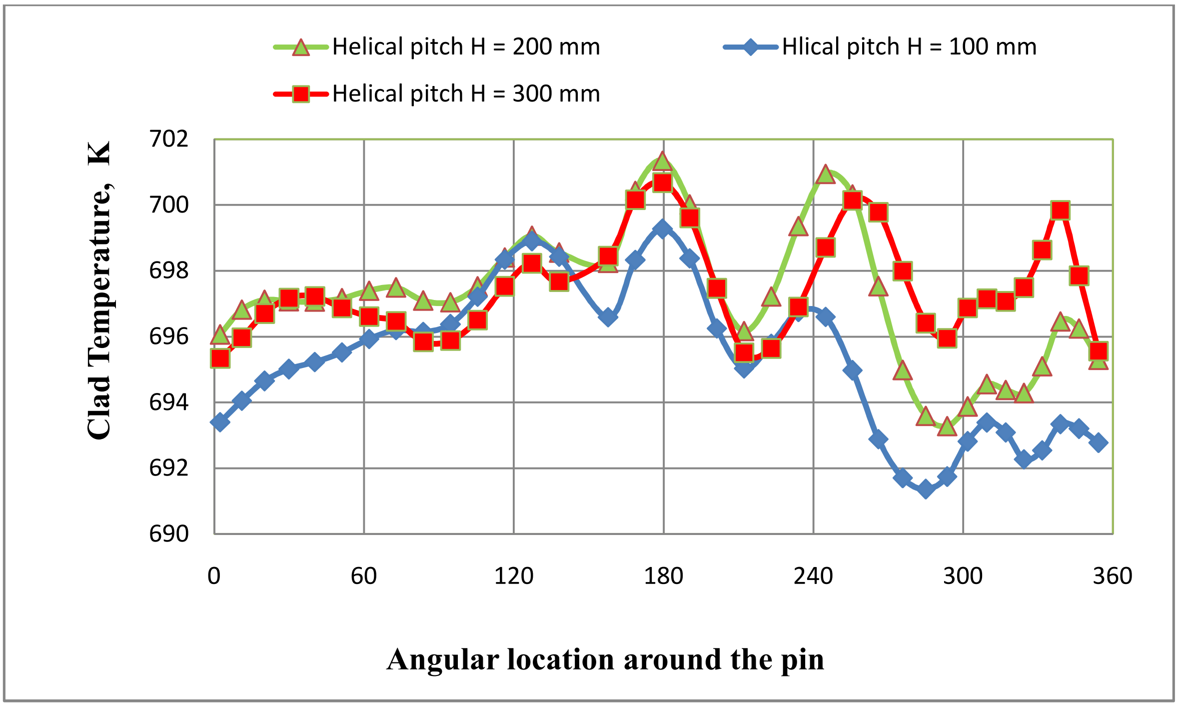

Fig. 8.4.1 (c) Clad temperature around the pin no. 152 located at the 7th row for different helical pitches

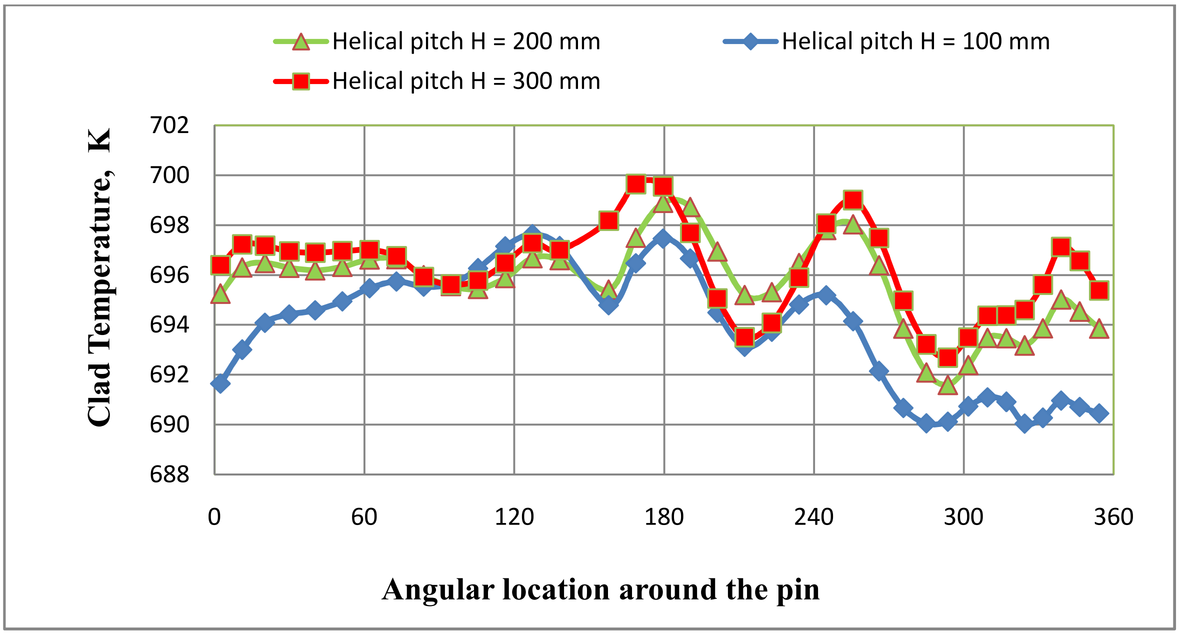

Fig. 8.4.1 (d) Clad temperature around the pin no. 160 located at the 7th row for different helical pitches

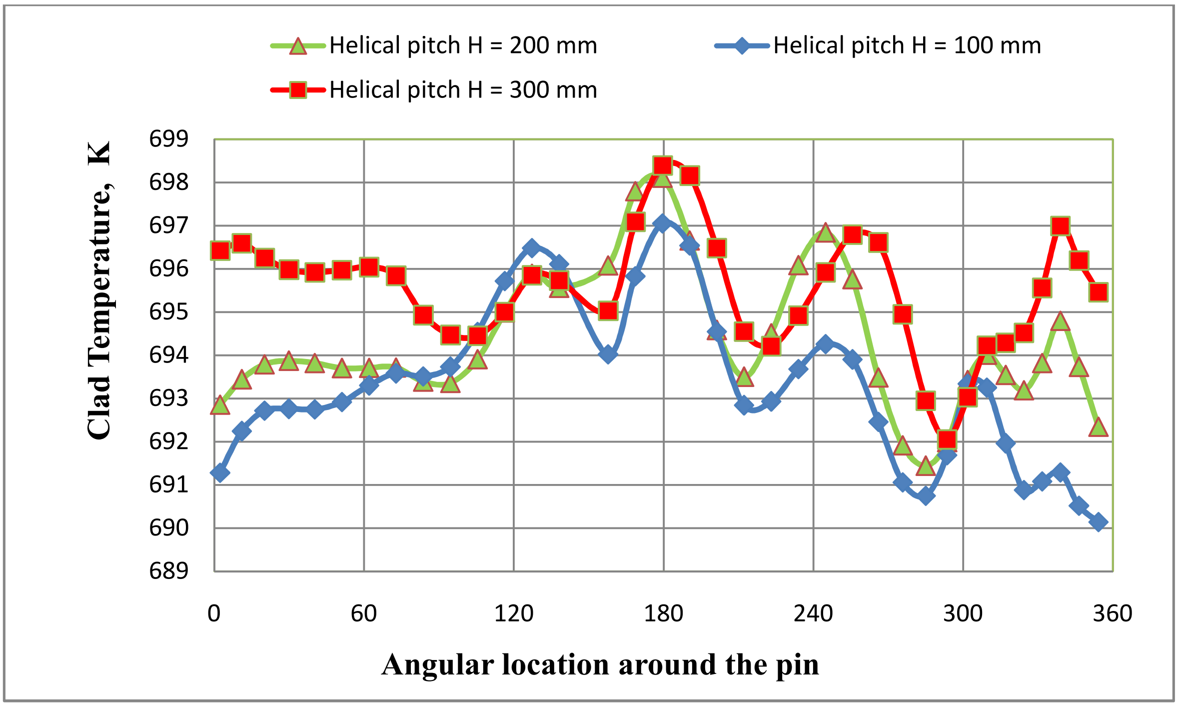

Fig. 8.4.1 (e) Clad temperature around the pin no. 166 located at the 7th row for different helical pitches

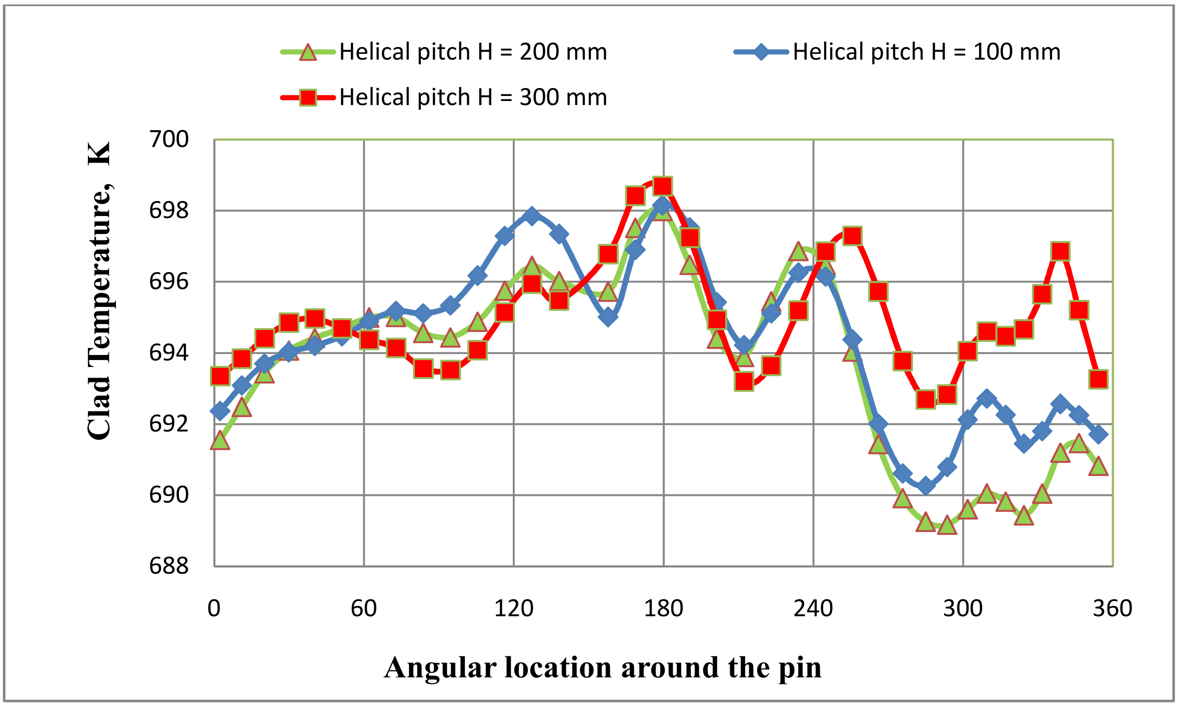

Fig. 8.4.1 (f) Clad temperature around the pin no. 131 located at the 7th row for different helical pitches

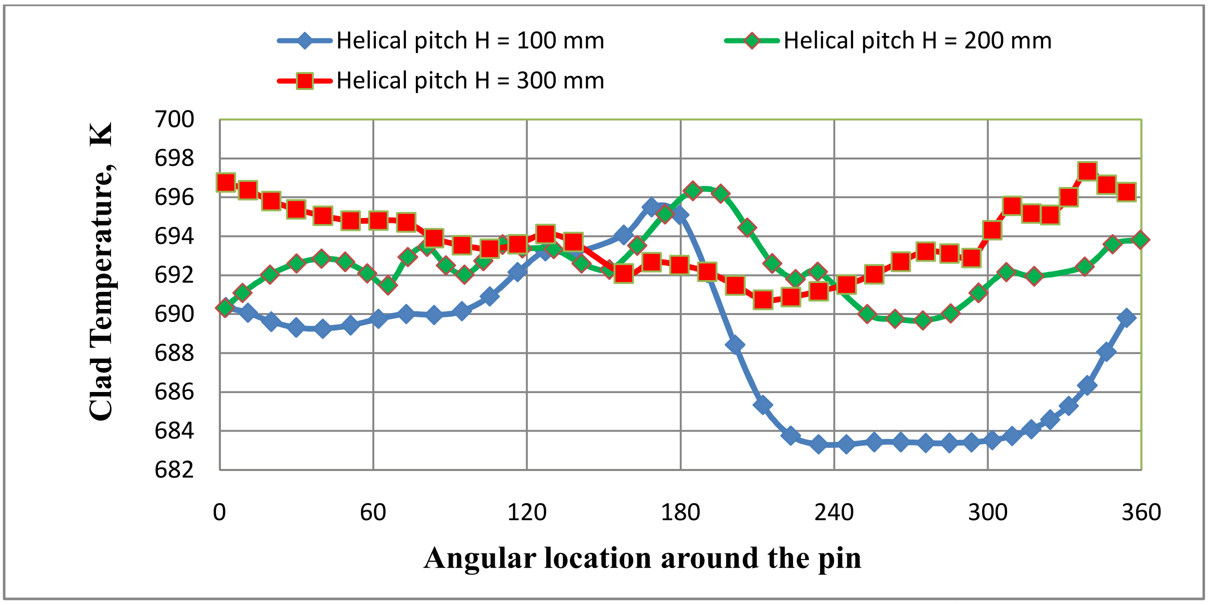

Fig. 8.4.1 (g) Clad temperature around the pin no. 217 located at the peripheral row for different helical pitches

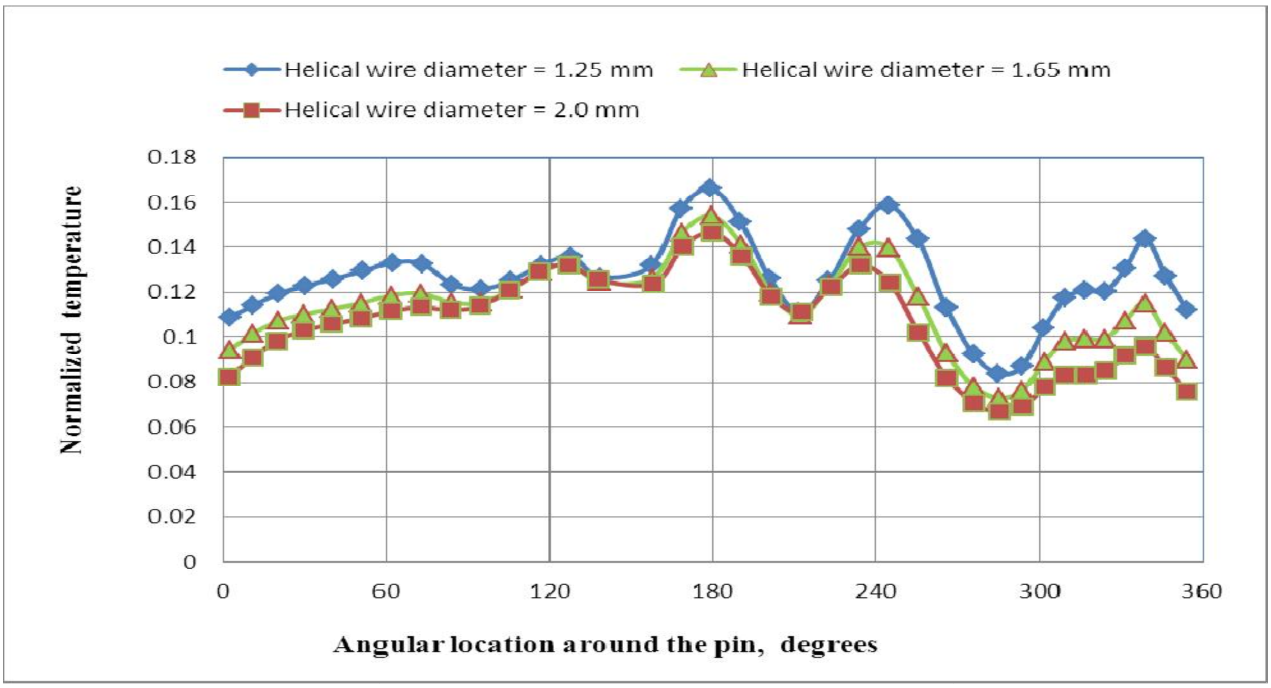

Fig. 8.4.2 (a) Clad temperature around the central pin for different wire diameters

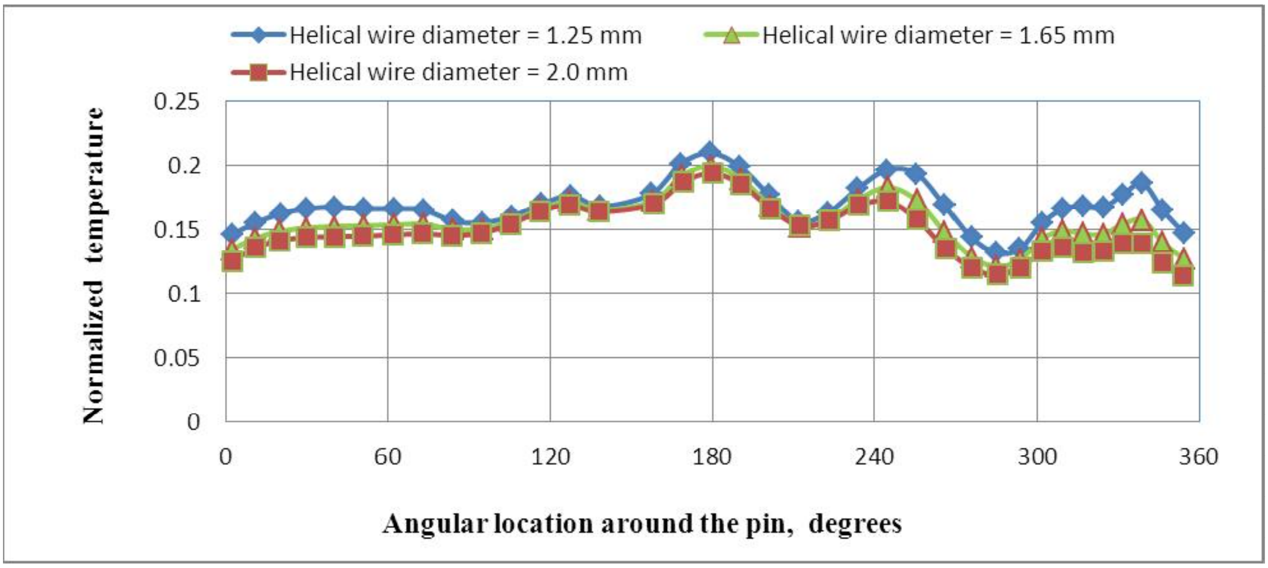

Fig. 8.4.2 (b) Clad temperature around the pin no. 145 located at the 7th row for different wire diameters

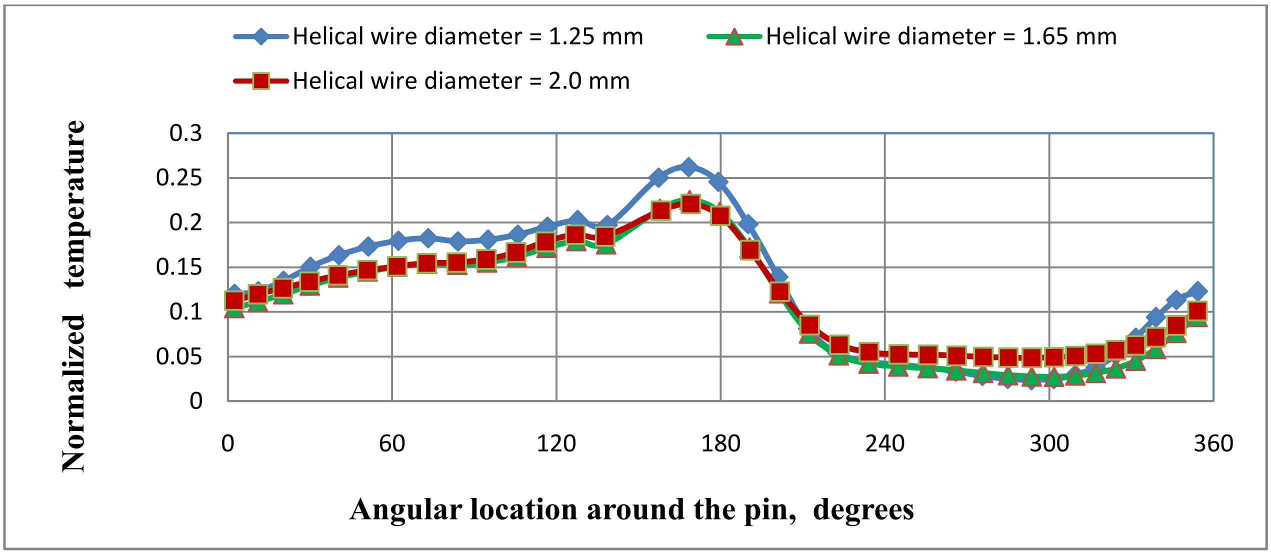

Fig. 8.4.2 (c) Clad temperature around the pin no. 217 located at the peripheral row for different wire diameters

8.5 EFFECT OF HELICAL WIRE PARARMETERS ON SUB-CHANNEL SODIUM TEMPERATURE DISTRIBUTION IN 217 PIN BUNDLE

8.5.1 Influence of Helical Pitch

Figures 8.5.1 (a) - 8.5.1 (c) show the sodium temperature distribution at 100 mm from the bundle entry in the nine rows of the sub-channels of the bundle for various helical pitches of 100 mm, 200 mm and 300 mm respectively. It is seen that the sodium outlet temperature distribution in all the central sub-channels are uniform except in the eighth row which is adjacent to the peripheral row. The peripheral sub-channel sodium temperature is much lower and non-uniform than that of the central sub-channels. The sodium temperature is higher in the central sub-channels, as these are formed by the fuel pins and consequently the rate of heat addition per unit length of the channel is more. For similar reason, the sodium temperature is less in the peripheral sub-channels since the heat input per unit length in these channels are less due to the presence of hexagonal sheath which is adiabatic. It is seen that the sodium temperature difference between the central sub-channels in the eight rows of pin bundle and the peripheral sub-channels at the same hexagonal face is lower for shorter helical pitch which is attributed to the enhanced mixing due to higher cross flow in the shorter helical pitch case. The maximum sodium temperature occurs at the location beneath the wire wrap as well as in the minimum gap between the wire wrap and the neighboring fuel pin.

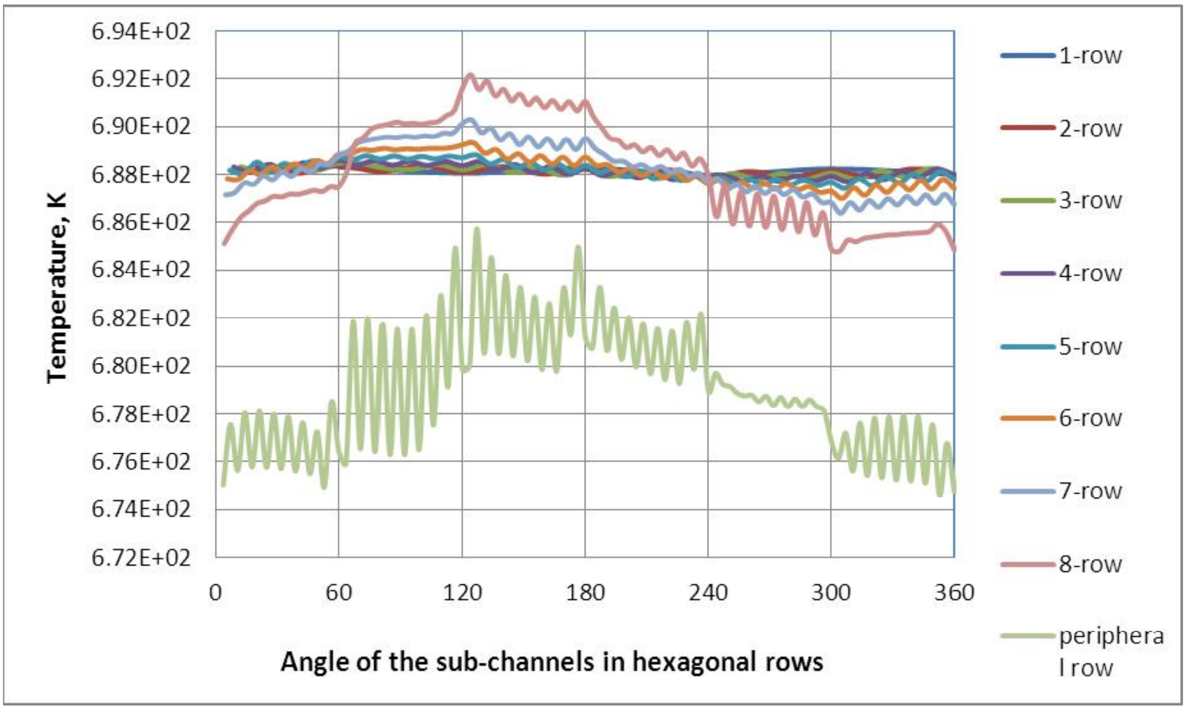

Fig. 8.5.1 (a) Sodium temperature at 100 mm elevation of 217 pin bundle helical pitch = 100 mm

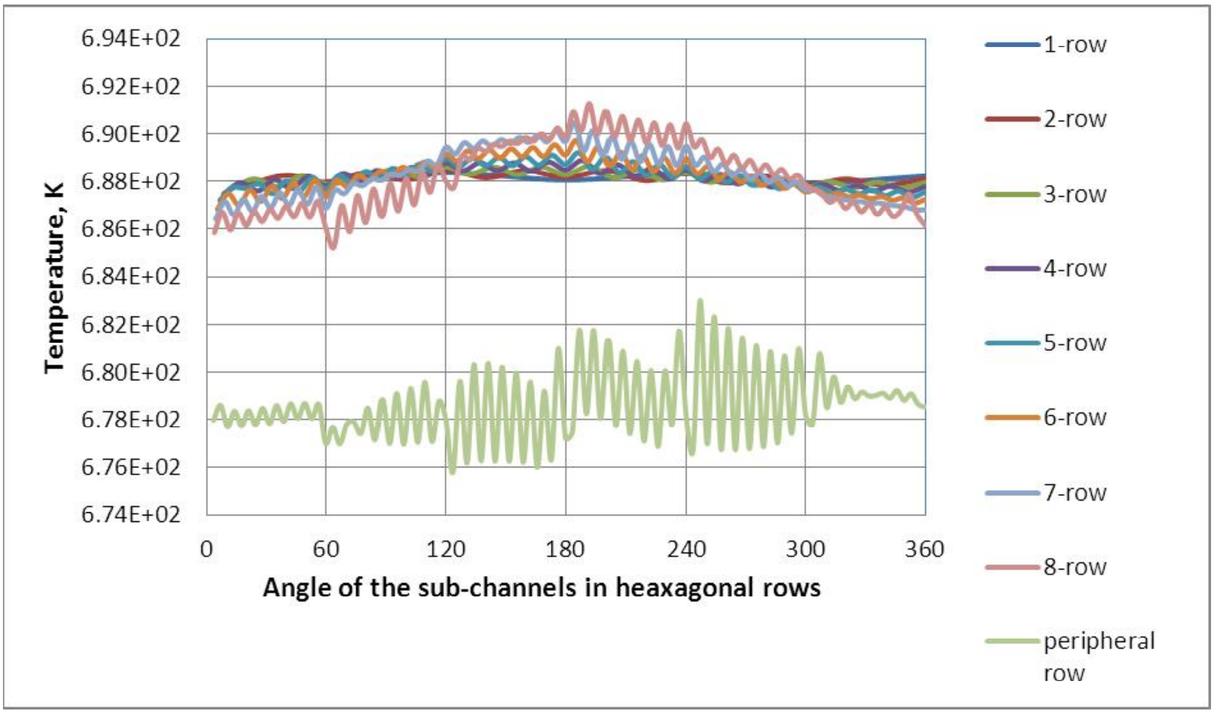

Fig. 8.5.1 (b) Sodium temperature at 100 mm elevation of 217 pin bundle : helical pitch = 200 mm

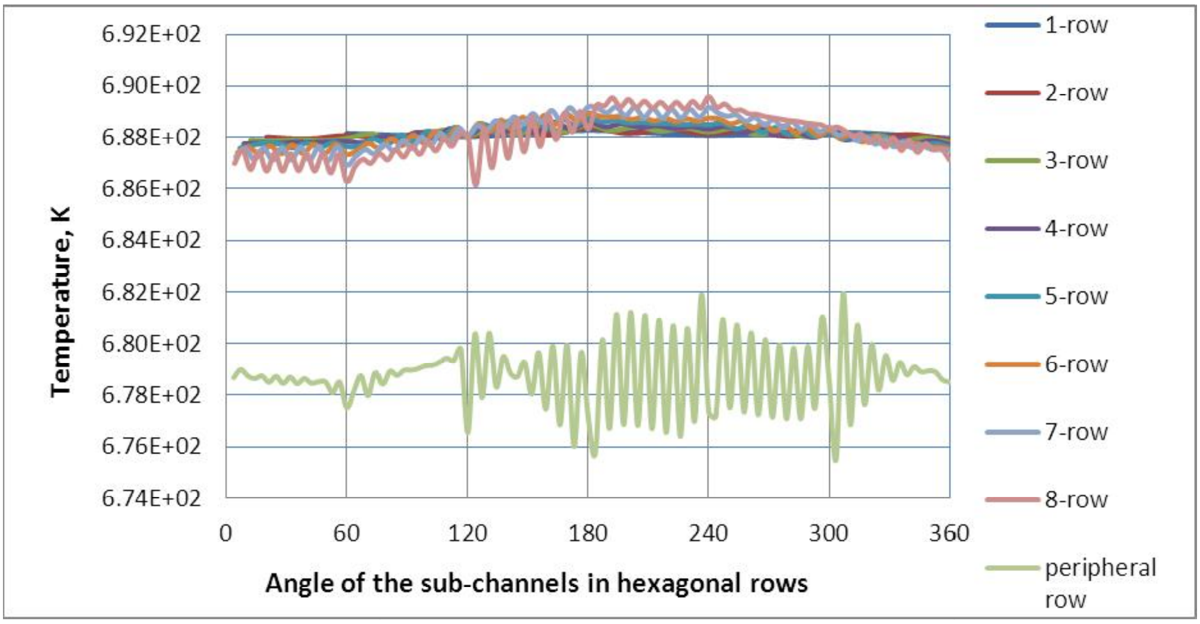

Fig. 8.5.1 (c) Sodium temperature at 100 mm elevation of 217 pin bundle : helical pitch = 300 mm

8.5.2 Influence of Helical Wire Diameter

Figures 8.5.2 (a) – 8.5.2 (c) show the sodium temperature distribution at the bundle exit in the nine rows of the sub-channels of the bundle for helical wire diameter of 1.25 mm, 1.65 mm and 2.0 mm respectively. It is seen that the sodium temperature distribution is similar in all the cases due to fixed outlet temperature. Further, the sodium temperature distribution in the sub-channels in the various rows of pin bundle is not varying much for smaller helical wire diameter which is attributed to the lower cross flow. Whereas, the sodium temperatures in the sub-channels of various rows of pin bundle are varying with increase in helical wire diameter which is attributed to the increased cross flow.

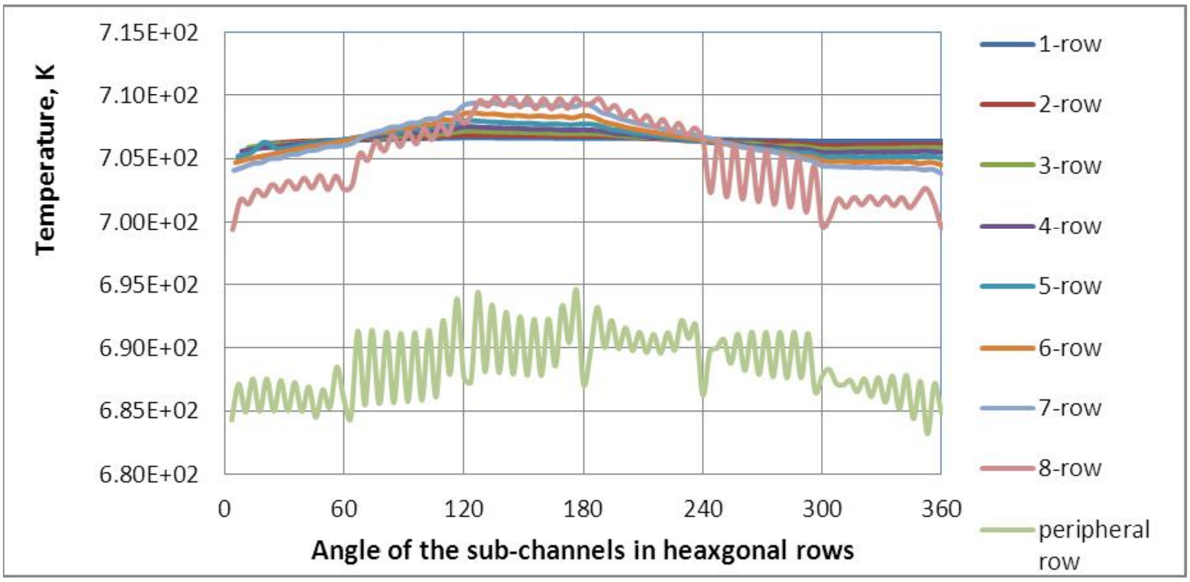

Fig. 8.5.2 (a) Sodium temperature distribution at the outlet of 217 pin bundle : Helical wire diameter = 1.25 mm

Fig. 8.5.2 (b) Sodium temperature distribution at the outlet of 217 pin bundle : Helical wire diameter = 1.65 mm

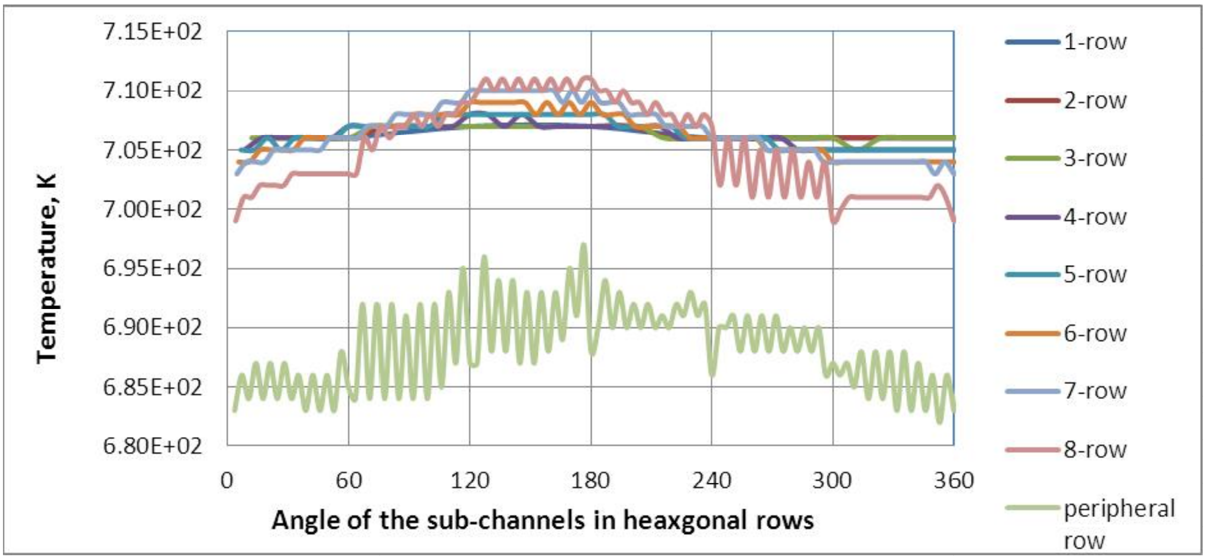

Fig. 8.5.2 (c) Sodium temperature distribution at the outlet of 217 pin bundle : Helical wire diameter = 2.0 mm

8.6 SELECTION OF ECONOMICAL HELICAL PITCH AND WIRE DIAMETER

The helical wire basically serves as a spacer between the pins and provides support for pins. Unlike grid spacers, it induces a transverse flow in the pin bundle which increases the heat transfer coefficient of sodium flow through the pin bundle. It reduces the hot spots and makes the outlet sodium temperature more uniform. But, it increases the pressure drop in the bundle. As the performance of helical wire increases with Reynolds number, it is much preferred in the turbulent flow regime compared to transition, laminar regime and buoyant flow regime. As the friction factor and Nusselt number increases with decrease in helical pitch, it is always economical to keep the helical pitch above 100 mm but below 300 mm. The wire diameter should be above 1.25 mm and below 2.0 mm. Hence, the optimum helical pitch and wire diameter are 200 mm 1.65 mm. These helical wire parameters are found to be economical and the fuel pins wound over with this wire is found to be easy to manufacture.

8.7 CLOSURE

The clad temperature decreases with decrease in helical pitch for central pin as the transverse flow increases the heat transfer coefficient in the central sub-channels. The circumferential variation in clad temperature exhibits intense variation with alternate crests and troughs. These crests and troughs are strongly influenced by (i) the radial gap between the pin under consideration and the neighboring pin and (ii) cross flow velocity induced by the spacer wire. While a smaller radial gap increases the clad temperature, large cross stream velocity reduces the clad temperature. In the peripheral pins, clad temperature decreases with decrease in helical pitch as the transverse flow increases the heat transfer coefficient in this row of pins. The sodium temperature is higher in the central sub-channels and the same is lower in the peripheral sub-channels. It is seen that the sodium temperature difference between the central sub-channels in the eight rows of pin bundle and the peripheral sub-channels at the same hexagonal face is lower for shorter helical pitch which is attributed to the enhanced mixing due to higher cross flow in the shorter helical pitch case. With larger wire diameters, the normalized clad temperature around the pin is lower due to higher cross flow because of increased wire size and reduced cross flow resistance.

CHAPTER - 9

STUDY OF HOTSPOT AND HOTCHANNEL FACTORS

9.0 INTRODUCTION

In the preceding sections, it was noticed that thermal hydraulics of fast reactor subassembly exhibits large scale 3-dimensional variations. Further, 3-dimensional computation for prediction of clad and coolant temperatures demand a large computational time and memory, even for steady state conditions. However, safety analysis of the reactor requires transient temperature variations in the pins. To circumvent this difficulty, traditionally, safety analysis is performed by one dimensional codes. Such codes predict only transient variation of mean temperature of the clad. To compute the peak value of clad temperature from mean clad temperature, hot spot factors (Walter and Reynolds, 1981) are used. These factors are evaluated from the experimental and theoretical predictions. From the results of the CFD study, some of these factors are found out for 217 fuel pin bundle and they are compared with the factors used in safety analysis.

9.1 CLAD HOTSPOT FACTOR

This hot spot factor is defined as follows

$$\zeta = \frac{T_{max-clad} - T_{Bulk-Na}}{T_{av-clad} - T_{Bulk-Na}} \qquad (9.1)$$

Where $T_{max-clad}$ is the maximum clad temperature in the pin bundle, $T_{av-clad}$ is the average clad temperature of all the pins and $T_{Bulk-Na}$ is the bulk sodium temperature at the outlet of the bundle.

Once the value of ζ is found from CFD study, the peak clad temperature is determined from mean clad temperature evaluated by one dimensional analysis, as follows,

$$T_{max-clad} = \zeta * (T_{av-clad} - T_{Bulk-Na}) + T_{Bulk-Na} \qquad (9.2)$$

The variation of clad hot spot factor with number of pins in the bundle obtained from CFD study is presented in Fig. 9.1(a). It is seen that the hotspot factor increases from a value of 1.87 (for a 19 pin bundle) to 2.05 (for a 217 pin bundle) with one axial pitch of the bundle (200 mm). This is due to the fact that both maximum and average clad temperatures decrease with increase in the number of pins in the bundle with the decrease in average clad temperature slower than the maximum clad temperature.

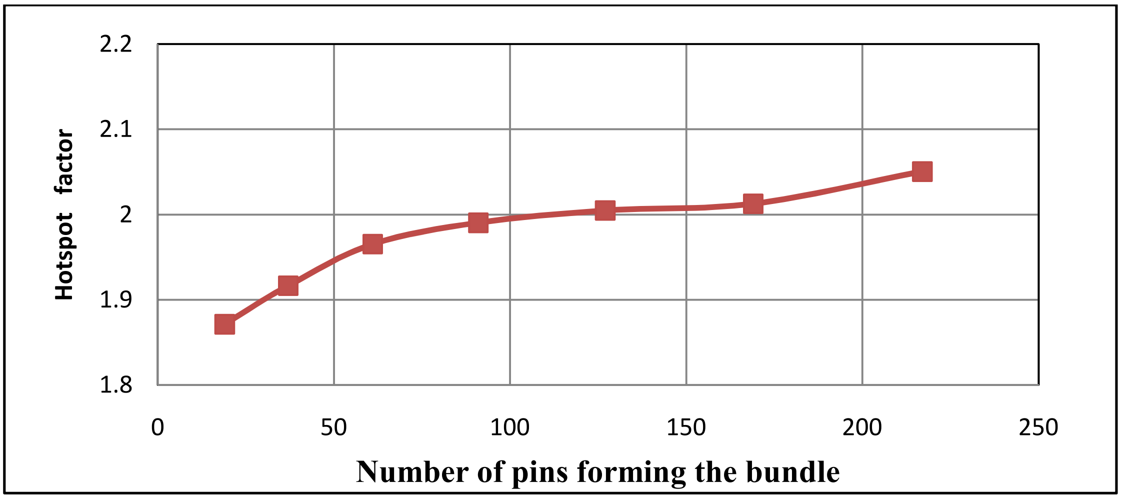

Fig. 9.1 (a) Variation of hotspot factor with number of pins

The variation of hotspot factor along the length of the 217 bundle for an axial length of 5 pitches (viz. 1000 mm) obtained from CFD study is presented in Fig. 9.1 (b). The hotspot factor increases from 2.1 at the exit of 200 mm to 2.6 at the exit of 1000 mm. The increase is monotonic. The initial low value of hotspot factor is due to the large heat transfer coefficient at the entrance. As the flow develops, the Nusselt number decreases (Fig. 9.1 (c)). As a consequence, the circumferential variation in the pin temperature increases which eventually leads to marginal increase in the hotspot factor.

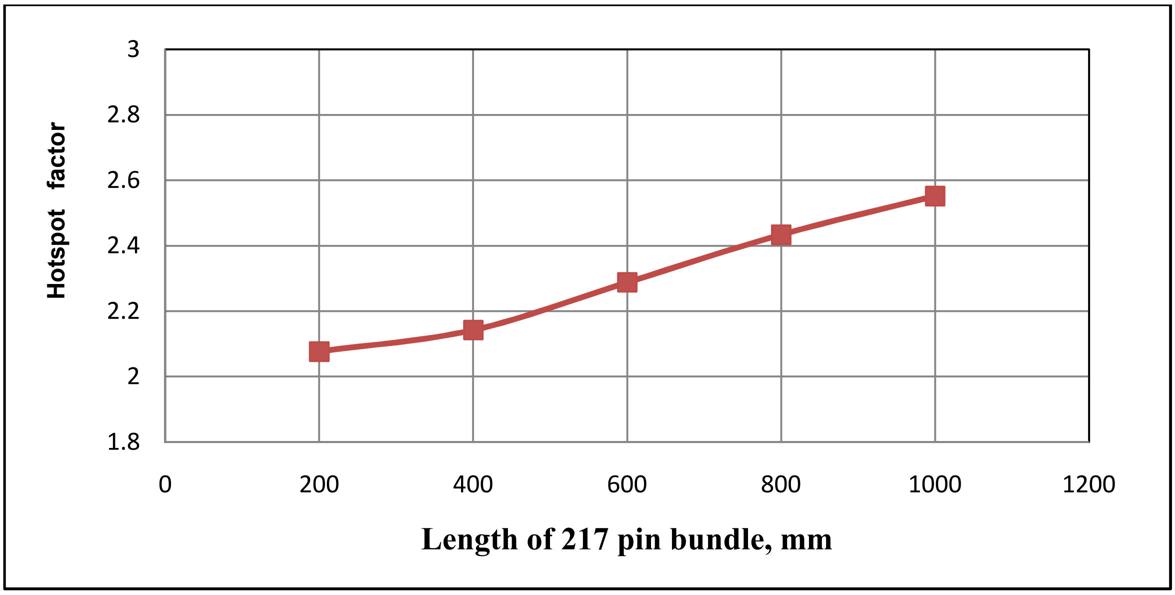

Fig. 9.1 (b) Variation of hotspot factor with length of the bundle of 1000 mm

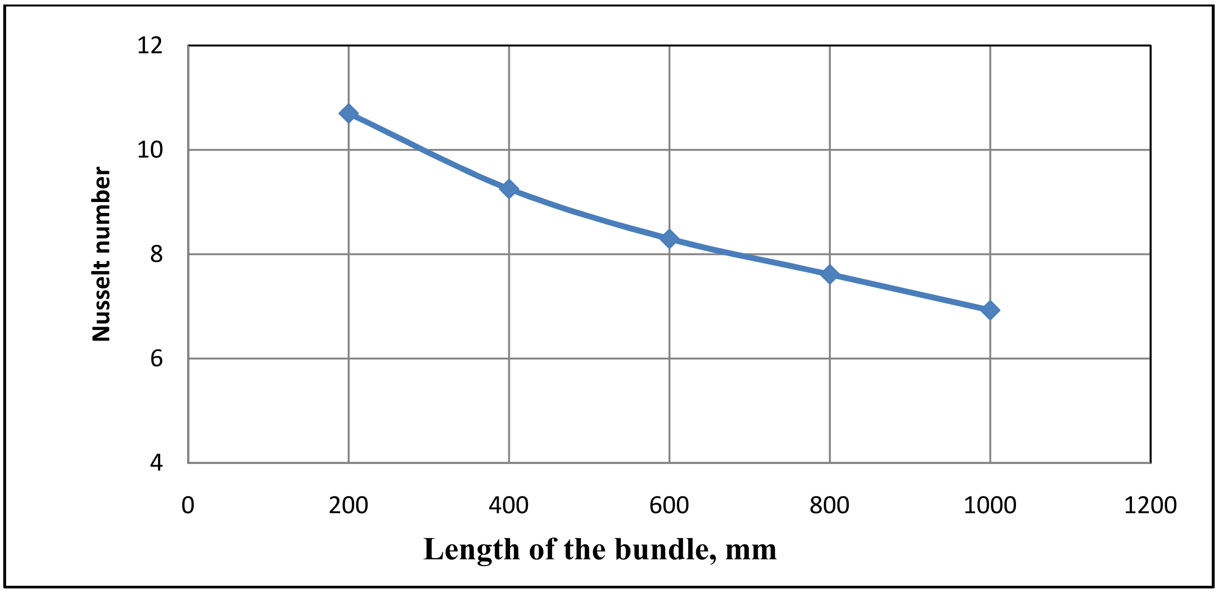

Fig. 9.1 (c) Variation of Nusselt number with length of the bundle

The variation of hot spot factor with the helical pitch length of the spacer wire obtained from CFD study is presented in Fig.9.1 (d). It is seen that the hot spot factor remains nearly constant (2.0 to 1.5) when the helical pitch increases from 100 mm to 600 mm. This mild increase in hotspot factor (increase in maximum clad temperature and decrease in average clad temperature) at short helical pitches is due to strong wake behind the helical wire when large scale cross flow is induced in the pin bundle with short helical pitches. Except for this local non-uniformity, the overall heat transfer coefficient increases as the helical pitch shortens.

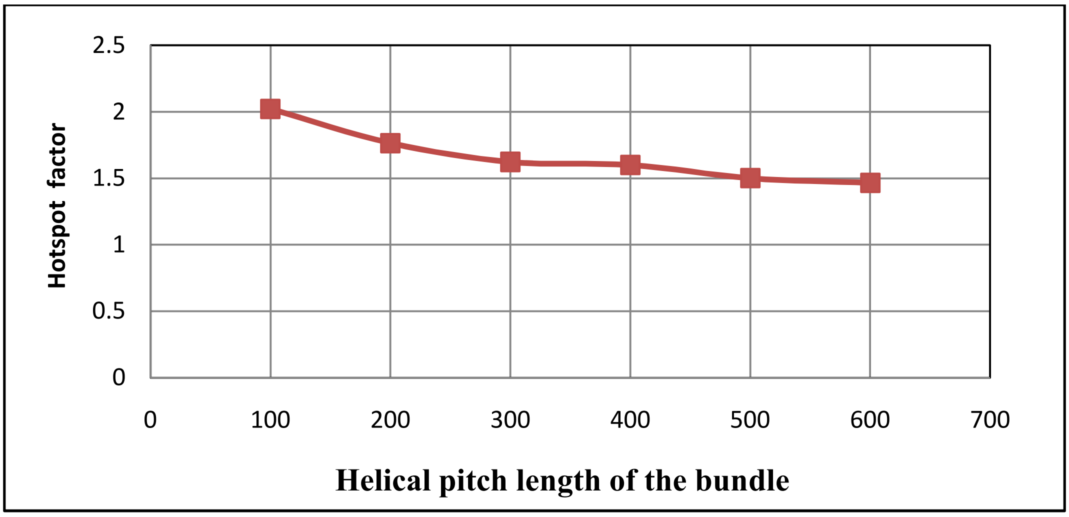

Fig. 9.1 (d) Variation of hotspot factor with helical pitch of the wire

The hot spot factor used in the traditional safety analysis of core is 1.7 (Walter and Reynolds, 1981) which is very close to the value predicted by CFD for pin bundle with 200 mm helical pitch (viz. 1.7). This confirms the adequacy of the core design.

9.2 HOT CHANNEL FACTOR

The hot channel factor β is defined as follows

$$\beta = \frac{T_{max-Na} - T_{inlet}}{T_{av-Na} - T_{inlet}} \tag{9.3}$$

Where T_{max-Na} is the maximum sodium temperature in the bundle, T_{av-Na} is the average sodium temperature at the outlet of the bundle and T_{inlet} is the inlet sodium temperature through the bundle.

Once the value of β is found from CFD study, the peak clad temperature is determined from mean clad temperature evaluated by one dimensional analysis, as follows,

$$T_{max-Na} = \beta * (T_{av-Na} - T_{inlet}) + T_{inlet} \qquad (9.4)$$

The variation of hot channel factor with number of pins forming the bundle obtained from CFD study is presented in Fig.9.2 (a) It is seen that the hot channel factor decreases from1.64 (7 pin bundle) to 1.26 (217 pin bundle). Normally, the hot channel occurs in the central region of the bundle and channels of low sodium temperature occur in the periphery. Also, as the number of pins in the bundle increases the ratio of number of central sub-channels to number of peripheral sub-channels increases. As a consequence of these, the value of T_{max-Na} approaches to the value of T_{av-Na} as the number of pins increases. Thus, the hot channel factor reduces with increase in number of pins approaching unity.

The variation of hot channel factor with the length of the 217 bundle with 5 axial pitches (total length of the bundle is 1000 mm) obtained from CFD study is presented in Fig. 9.2 (b). It is seen that the hot channel factor monotonically decreases from 1.25 to 1.16 due to flow distribution effects.

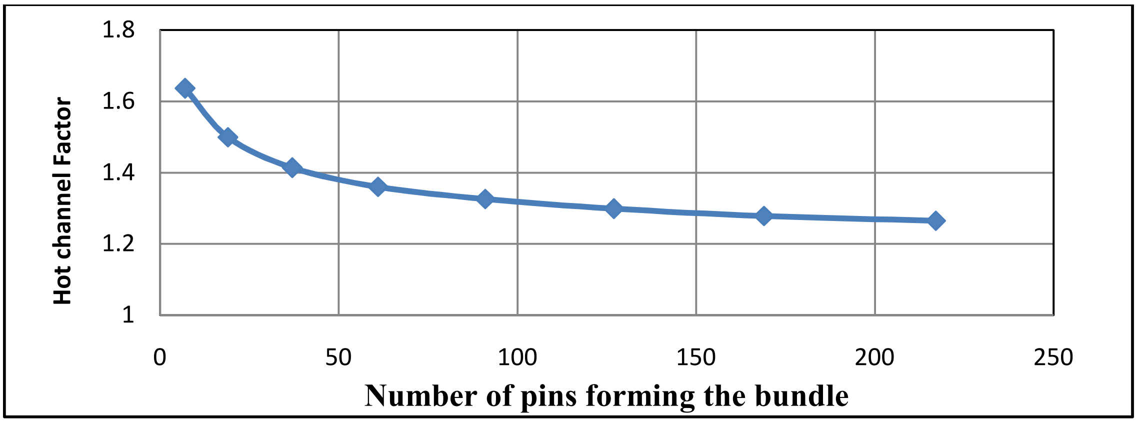

Fig. 9.2 (a) Variation of hotchannel factor with number of pins

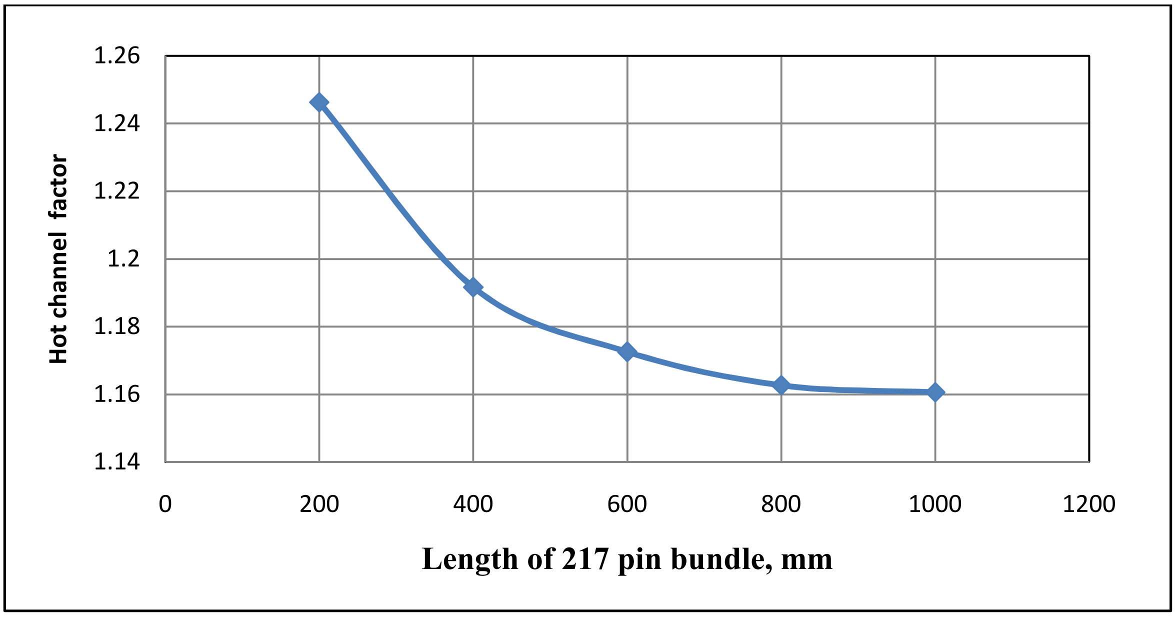

Fig. 9.2 (b) Variation of hotchannel factor with length of the bundle

The variation of hot channel factor with the helical pitch length of the spacer wire obtained from CFD study is presented in Fig. 9.2 (c) It is seen that the hot channel factor decreases from 1.4 for 100 mm pitch to 1.2 for 200 mm pitch and beyond this, it is insensitive to the pitch value. The decrease in hot channel factor with helical pitch is due to the fact that higher the helical pitch, lesser is the heat exchange from the clad to sodium. Hence, sodium temperature is lesser in the case of longer helical pitch.

The hot channel factor used in the traditional safety analysis is 1.2, which is more than the CFD prediction value of 1.16), confirming the adequacy of the core design.

9.3 CLOSURE

The hot spot factor and hot channel factor were estimated from the CFD studies. Their dependence on the number of pins, wire dimensions and helical pitch are studied. Their variation along the flow direction has also been investigated. It is seen that these factors are lower than that used in conventional safety analysis indicating conservatism in the core design.

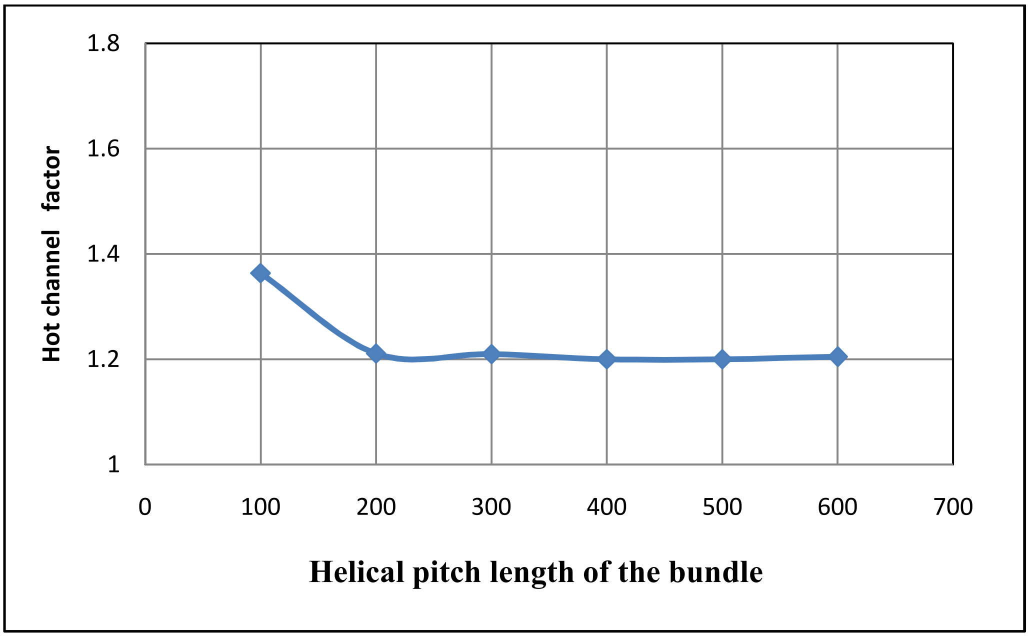

Fig. 9.2 (c) Variation of hotchannel factor with helical pitch of the wire

CHAPTER - 10

EXTENDIBILITY OF PIN BUNDLE RESULTS WITH FEWER PINS TO 217 PIN BUNDLE

10.0 INTRODUCTION

As the CFD study demands a huge computer resource in terms of CPU time and memory, it is not possible always to adopt 3-D simulation study for the pin bundle with large number of pins. Hence, to predict the results for pin bundles with large number of pins by hand calculation based on the results of pin bundle with small number of pins, a simple procedure is arrived at. This procedure is validated against the results of a 3-D CFD study for large size pin bundle. For this purpose the results of fuel pin bundle with various number of pins presented in previous chapters are relooked here.

10.1 VARIATION OF MEAN SODIUM VELOCITY WITH NUMBER OF PINS

Thermal hydraulic results of pin bundle with various number of pins indicate that the axial and transverse velocity distributions are independent of the length of the bundle as the flow development beyond entrance region. Also, the distributions at the outlet of the pin bundle are almost independent of the number of pins. There are two hydraulic regions at the exit of the bundle. These are regions formed by the central and the peripheral sub channels. The mean velocities in these regions exhibit a predictable pattern with increasing number of pins. The mean velocities of the central and peripheral sub channels regions are presented in the Fig. 10.1

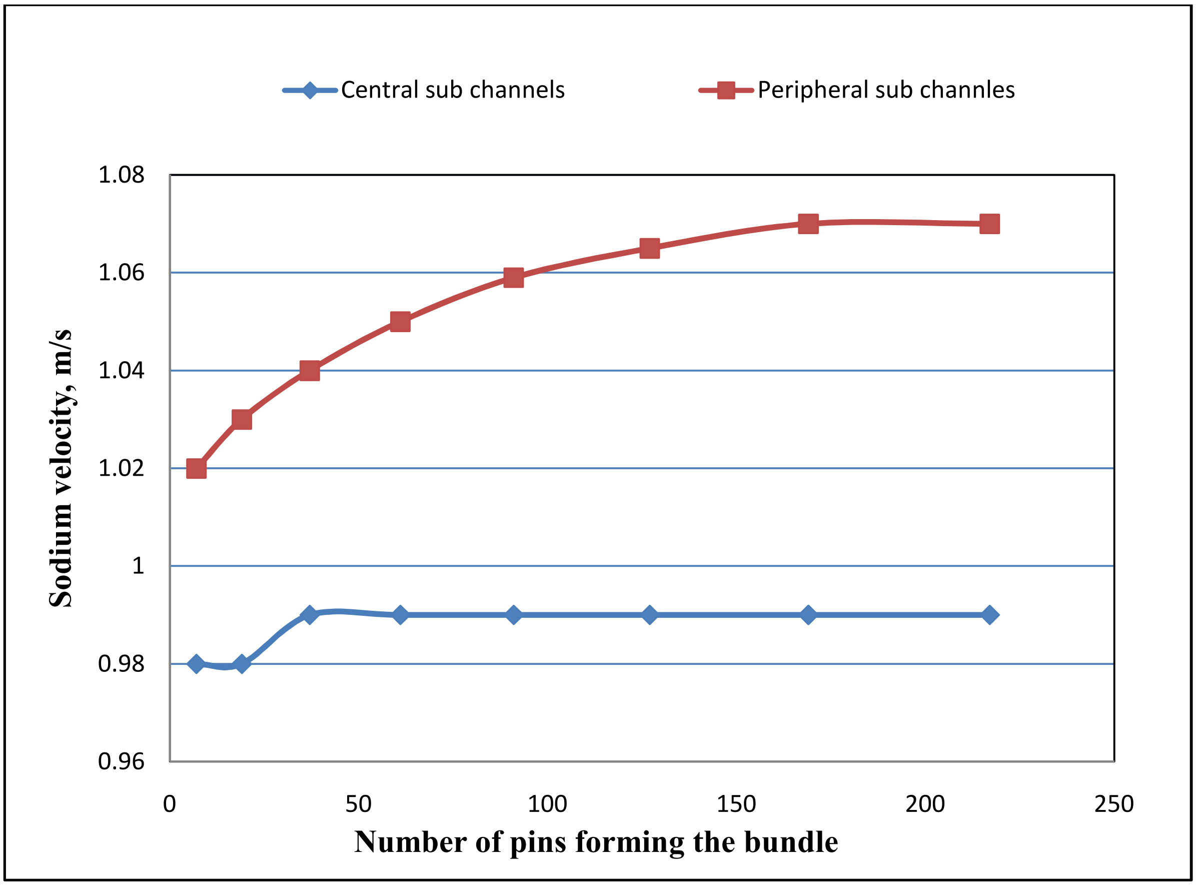

Fig 10.1 Variation of mean sodium velocity in central and peripheral sub-channels at the outlet of the bundle with number of pins

It can be seen that the mean velocity of central sub-channels remains almost independent of number of pins beyond 37 pin bundle. This is due to the fact that the flow within the central sub channels is constrained by the different rows of the pin bundle. On the other hand, mean velocity of peripheral sub-channels continue to increase with number of pins right from 7 pin bundle to 217 pin bundle. This is due to the fact that the transverse velocity induced by the helical wire diverts the flow in and out of the central sub-channels into the peripheral sub-channels. When the number of pins increases, the diversion of flow becomes more as the number of wires causing this increases with number of pins. Hence, from these mean velocity patterns, it is possible to predict the mean velocity of any pin bundle at least up to 217 pin bundle.

10.2 EXTENDIBILITY OF MEAN SODIUM VELOCITIES

It is seen from Table 10.1 that the average velocity of all peripheral sub channels is 1.03 for 19 pin bundle while it is 1.04 for 37 pin bundle. It is evident that the mean peripheral sub channel velocity increases mildly with the number of rows. Considering the fact that the number of rows for the 19, 37 and 217 pin bundle are 2, 3 and 8, the mean velocity for the peripheral sub channels for 217 pin bundle ($\overline{V_w}$) would be extrapolated as 1.07. Imposing the condition that the mass conservation has to be satisfied, the mean velocity in the central sub channels for 217 pin bundle $\overline{V_c}$ would be determined from the following mass conservation equation,

$$\frac{A_{w-T}\,\overline{V_w} + A_{c-T}\,\overline{V_c}}{A_T\,V_{in}} = 1 \qquad (10.1)$$

Where A_{w-T} – Total flow area of wall sub-channels, A_{c-T} – Total area of central sub-channels, $\overline{V_w}$ – Mean velocity of sodium in the peripheral sub-channels, $\overline{V_c}$ - Mean velocity of sodium in the central sub-channels, A_T – Total area of all sub-channels, V_{in} – Inlet velocity of sodium through the bundle.

As the area of central zone is 80 % of the total flow area in the case of 217 pin bundle, the value of $\overline{V_c}$ is estimated to be 0.99. This matches closely with the computed values of 0.98 for 19 pin bundle and 0.99 corresponding to 37 pin bundle (Table. 10.1).

10.3 EXTENDIBILITY OF MEAN SODIUM TEMPERATURE

The CFD results of mean sodium temperatures of central and peripheral sub channels for different number of pins is presented in Fig. 10.2. The bulk sodium temperature is kept constant in the analysis for different number of pins. The mean sodium temperature of central and peripheral sub channels decreases from 7 to 217 pin bundles. But, the mean sodium temperatures of central and peripheral sub channels can be predicted from the difference between them.

Table 10.1 Variation of axial velocity in the central and peripheral sub channels with number of pins

No. of pins	CFD result of $\overline{V_c}$	CFD result of $\overline{V_w}$
7	0.98	1.02
19	0.98	1.03
37	0.99	1.04
61	0.99	1.04
91	0.99	1.05
127	0.99	1.06
167	0.99	1.07
217	0.99	1.07

It is seen that for 19 and 37 pin bundles the mean temperature difference between the central sub channels ($\overline{T}_c$) and the peripheral sub channel ($\overline{T}_w$) is close to 19 K. The variation of this temperature difference with number of pins is presented in the Fig. 10.3. It is seen that this difference decreases with the number of pins in the bundle. This is due to the increase in Nusselt number with the increase in number of pins in the pin bundle leading to more uniform sodium outlet temperature. Since this temperature difference is nearly constant for all pin bundles with different number of pins, for a 217 pin bundle we have,

$$\overline{T}_c - \overline{T}_w = 18 \qquad (10.2)$$

Where $\overline{T_c}$ is the mean sodium temperature in the central sub-channels and $\overline{T_w}$ is the mean sodium temperature in the peripheral sub-channels.

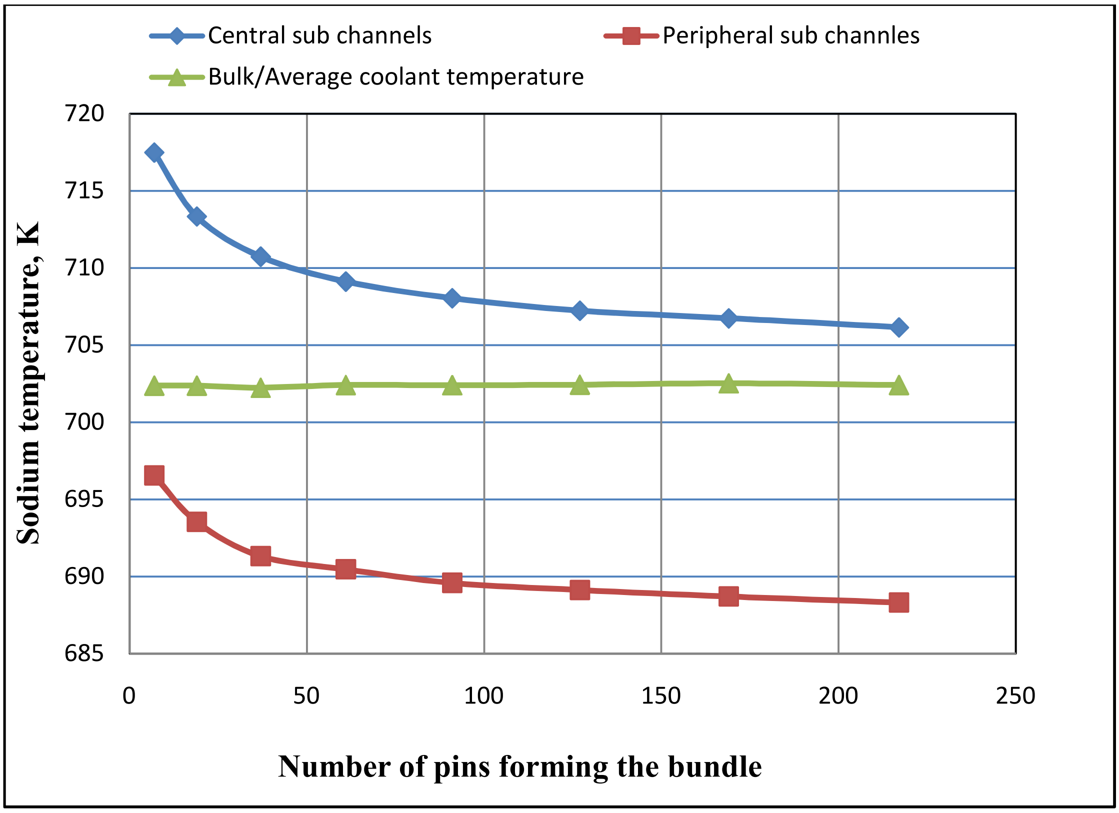

Fig. 10.2 Variation of sodium temperature in central and peripheral sub-channels at the outlet of the bundle with number of pins.

Hence, the bulk temperature of sodium at the outlet (T_{bulk}) can be calculated from heat balance equation. From the values of $\overline{V_w}$, $\overline{V_c}$ and T_{bulk}, the mean temperatures of peripheral sub channels ($\overline{T}_w$) and the central sub channels ($\overline{T}_c$) can be estimated from Eqs. (10.2) - (10.3).

$$\frac{(\overline{T_c}-T_{in})\overline{V_c}\ A_{c-T}+(\overline{T_w}-T_{in})\overline{V_w}\ A_{w-T}}{A_T V_{in}(T_{bulk}-T_{in})} = 1 \quad \text{(10.3)}$$

Where T_{in} is the inlet temperature sodium through the bundle and T_{bulk} is the Bulk sodium temperature at the outlet of the bundle.

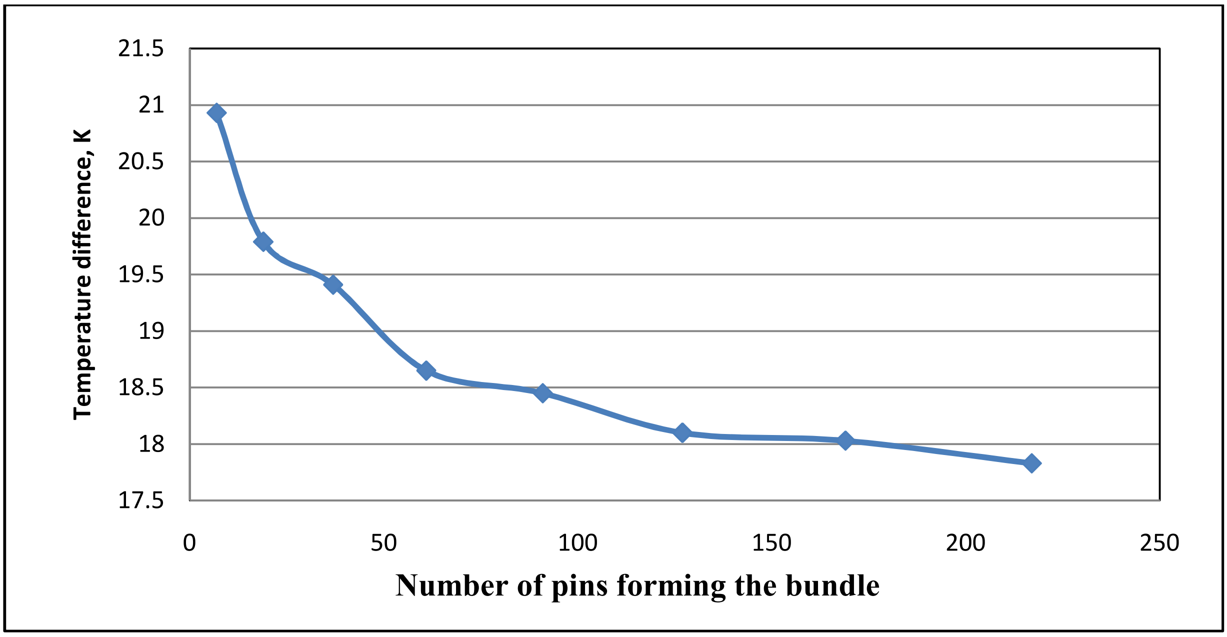

Fig. 10.3 Variation of temperature difference between central and peripheral sub-channels at the outlet of the bundle with number of pins

The predicted values of mean temperatures of central and peripheral sub channels from extendibility procedure are compared with the actual CFD results in Fig.10.4. It is seen that extendibility procedure prediction agrees well with the CFD prediction.

The estimated values of $\overline{T}_w$ and $\overline{T}_c$ for the 217 pin bundle are 688.32 and 706.15 K respectively. As the results of pin bundle are for only one axial pitch distance of the bundle, the effect of 5 axial pitch of the 217 pin bundle is studied for the purpose of developing extendibility to more number of axial pitches also.

10.4 EXTENDIBILITY TO 5 AXIAL PITCH 217 PIN BUNDLE

The results of 217 pin bundle with 5 axial pitches are presented in the Chapter 7.0. From these results, the temperature difference between the mean temperatures of the central and peripheral sub channels is plotted and presented in the Fig.10.5 It is seen that this difference increases with the axial pitch length. This is due to the decrease in Nusselt number with the axial length of the pin bundle.

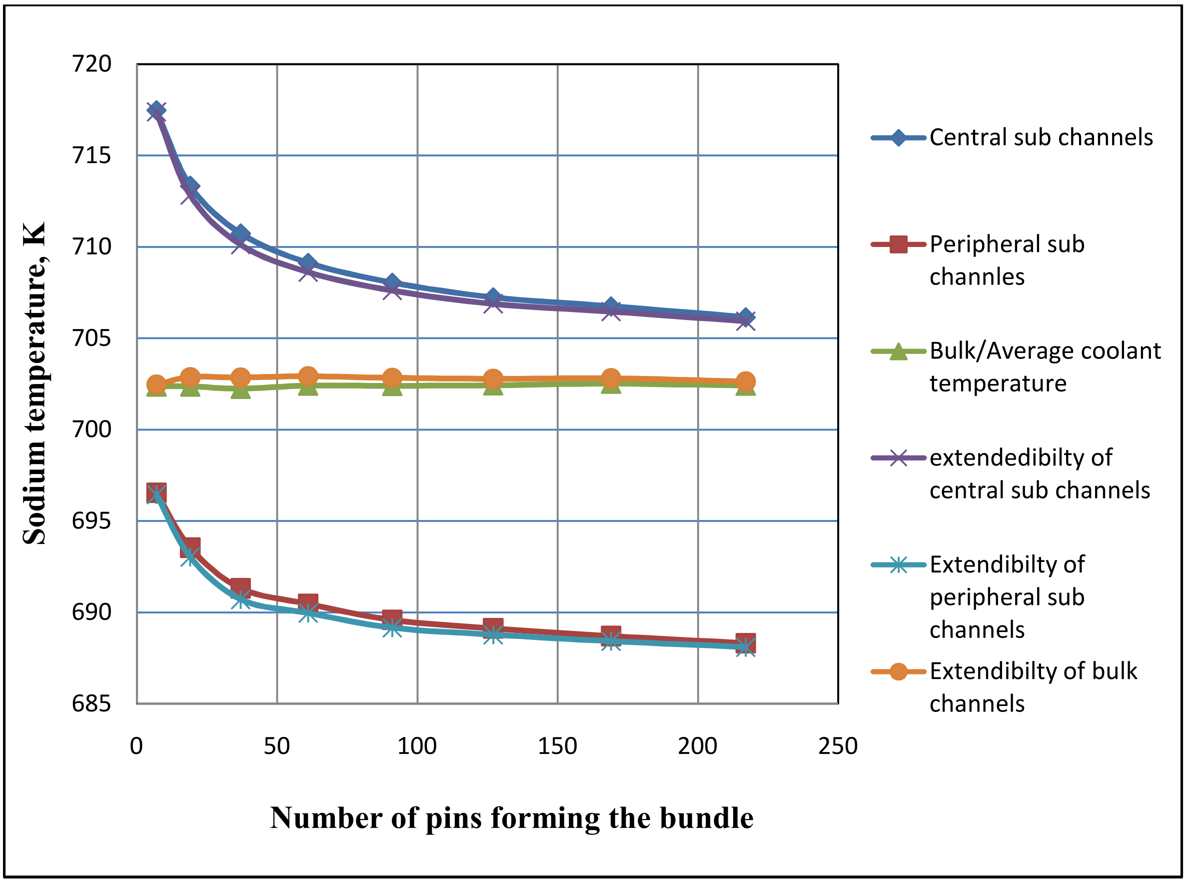

Fig. 10.4 Comparison of CFD predicted sodium temperatures in central and peripheral sub-channels with that of the calculated using extendibility procedure.

Hence, this difference of 18 K grows with axial pitch and the sodium difference between central and peripheral sub channels is 65 K for 5 axial pitches. From this, the values of peripheral sub channels (T_w) and the central sub channels (T_c) will be 781 K and 846 K respectively. Since the peak difference between clad temperature and sodium temperature is 24 K, the peak clad temperature is estimated to be 870 K. This is less than the acceptable temperature of 973 K from safety design considerations.

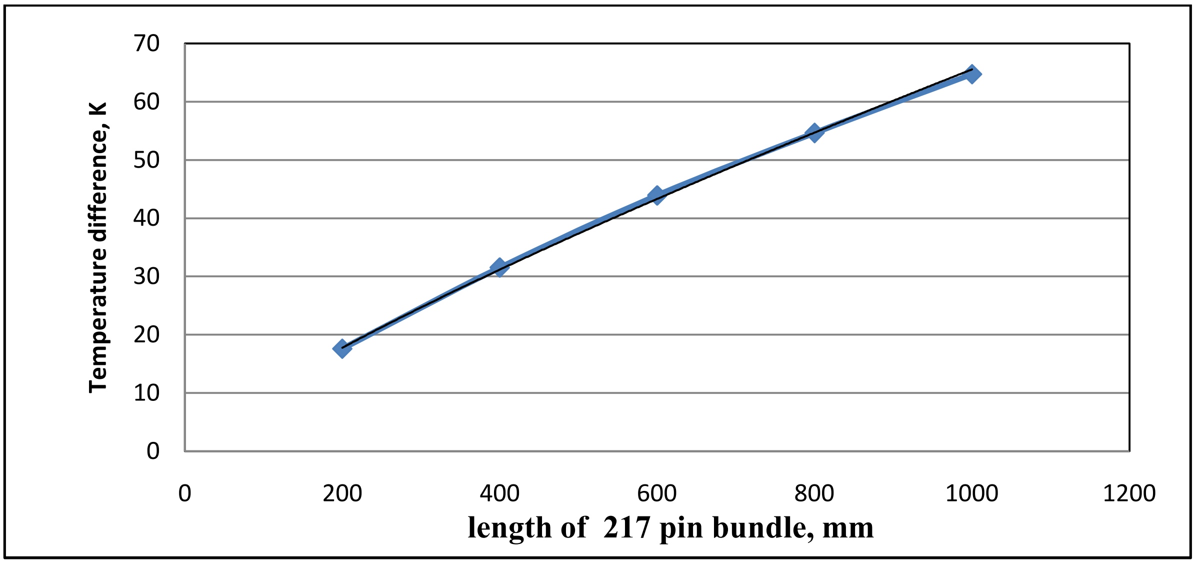

Fig. 10. 5 Variation of temperature difference between the mean temperatures of central and peripheral sub-channels of the bundle of 1000 mm.

10.5 CLOSURE

From the results of CFD study with different number of pins in the bundle, it is seen that the transverse velocity induced by the helical wire is able to reduce the temperature difference between the central and peripheral sub channels significantly and makes the sodium outlet temperature more uniform. A simple relationship has been developed to predict the mean sodium velocities and temperatures of central and peripheral sub channels from the results of CFD study. From this relationship, it is possible to extend the results of pin bundle with small number of pins to pin bundle with large number of pins. The validity of this relationship has been verified by comparing the predictions against detailed CFD study.

CHAPTER - 11

SUMMARY AND CONCLUSIONS

11.0 INTRODUCTION

Detailed flow and temperature distribution of sodium in helical wire wrapped fuel pin bundles have been investigated. The 3-dimensional conservation equations of mass, momentum and energy have been solved by finite volume based CFD codes. Both laminar and turbulent flow regimes have been studied. The focus of the investigations has been cross flow induced mixing, axial and circumferential variations temperatures, sub-channel sodium temperatures, clad hotspot factors, hot channel factors, friction factor and Nusselt number. The number of pins in the bundles, pitch of the helical spacer wire, diameter of the spacer wire and Reynolds number have been varied systematically to understand their influence on critical parameters of interest in the thermal design of FBR fuel subassembly. Satisfactory validation of the computational model has been established by comparing the predicted results against published data. The major conclusions of the investigations are highlighted below under various headings.

11.1 FLOW CHARACTERISTICS

- The helical wire induces transverse velocity in the bundle and increases the friction factor and Nusselt number in the pin bundle.
- The intensity of transverse velocity is found to be inversely proportional to the helical pitch. The ratio of transverse velocity to axial velocity is higher for higher wire diameter.
- The ratio of axial velocity to transverse velocity is nearly equal to the tangent of the rolling up angle of the helical wire.

- It is seen that the normalized velocities of the peripheral and central zones vary from 1.1 to 0.9 for all the bundles. This is in good agreement with reported experimental measurements of 1.1 and 0.85 for a 91 pin bundle.
- The axial velocity is maximum in the peripheral zone where spacer wires are located between the pins and hexagonal sheath. The velocity is minimum in the zone which is diametrically opposite to the respective zone of maximum velocity.
- The ratio of axial velocity to transverse velocity increases with number of pins and reaches a constant value for higher number of pins.

11.2 TEMPERATURE CHARACTERISTICS

- It is observed that the helical wire induced secondary swirl in the pin bundle promotes cross stream mixing of the coolant to make its temperature more uniform.
- The sodium temperature is higher in the zones where the flow area and hence the mass flow rate are less due to the presence of the spacer wires though the axial velocity is higher.
- It is seen that the sodium outlet temperature distribution in all the central sub-channels are uniform except in the row which is adjacent to the peripheral row. The peripheral sub-channels sodium temperature is much lower and non-uniform than that of the central sub-channels.
- It is seen that the sodium temperature difference between the central sub-channels in the eight rows of pin bundle and the peripheral sub-channels at the same hexagonal face is lower for shorter helical pitch which is attributed to the enhanced mixing due to higher cross flow in the shorter helical pitch case.
- The maximum sodium temperature occurs at the location beneath the wire wrap as well as in the minimum gap between the wire wrap and the neighboring fuel pin.
- It is seen from the sodium temperature distribution at the outlet of the bundle (i.e.) at 1000 mm from the sodium entry, there exist three temperature regions, viz. hottest,

coldest and intermediate becomes more distinct with the increase in the length of the bundle and becomes more uniform.

- ❖ It is seen that the location of the pin having maximum clad temperature moves towards the center with the increase in the length of the bundle.

11.3 FRICTION FACTOR

- ❖ The helical wire induces transverse velocity in the bundle increases the friction factor in the pin bundle.
- ❖ The friction factor of the pin bundle with and without spacer wire obtained from the present study is seen to agree well with the experimental values.
- ❖ The value of friction factor is larger for shorter helical pitch for all values of Reynolds number. It is seen that the values of friction factor are smaller for smaller values of helical wire diameter.
- ❖ The friction factor values in the turbulent regime obtained by CFD analysis matches with that of the experimental values within 2 %. The friction factor values in the laminar regime obtained by CFD analysis are higher (15 %) than that of the experimental values.
- ❖ The friction factor marginally increases with number of pins in the pin bundle.

11.4 NUSSELT NUMBER

- ❖ The helical wire induces transverse velocity in the bundle increases the Nusselt number in the pin bundle.
- ❖ The value of Nusselt number is larger for shorter helical pitch for all values of Reynolds number. The Nusselt number increases with increase in wire diameter.
- ❖ The Nusselt number values in the turbulent regime obtained by CFD analysis are higher than that of the experimental values within 20 %. The Nusselt number values

in the laminar regime obtained by CFD analysis matches with that of the experimental values.

- ❖ Based on the detailed parametric study, correlations for Nusselt number are proposed for 217 pin bundle with different helical pitches and helical wire diameter and for a range of Reynolds number.
- ❖ The Nusselt number marginally increases with number of pins in the pin bundle.
- ❖ The Nusselt number decreases with the length of the pin bundle.

11.5 CLAD TEMPERATURE

- ❖ The clad temperature decreases with decrease in helical pitch for central pin as the transverse flow increases the heat transfer coefficient in the central sub-channels.
- ❖ The clad temperature variation exhibits intensity distribution with alternate crests and troughs. These crests and troughs are strongly influenced by (i) the radial gap between the pin under consideration and the neighboring pin and (ii) cross flow velocity induced by the spacer wire.
- ❖ While a smaller radial gap increases the clad temperature, larger cross stream velocity reduces the clad temperature.
- ❖ In the peripheral pins, the clad temperature decreases with decrease in helical pitch and increase in wire diameter as the transverse flow increases the heat transfer coefficient in this row of pins.
- ❖ The clad temperature for 100 mm helical pitch is higher from 0-180 which is facing the central pins and the same is lower from 180-360 which is facing the hexagonal sheath.
- ❖ The clad temperatures for 200 and 300 mm helical pitch are more or less uniform due to reduced transverse velocities.

11.6 HOTSPOT AND HOTCHANNEL FACTORS

- ❖ The hot spot factor increases from a value of 1.87 (for 19 pin bundle) to 2.05 (for 217 pin bundle). Further, the hot spot factor increases from 2.05 to 2.6 for total length of the fuel bundle viz. 1000 mm.
- ❖ The increase in hot spot factor with length is due to the decrease in Nusselt number along the length of the bundle.
- ❖ It is seen that the hot channel factor decreases from 1.64 in a 7 pin bundle to 1.26 in a 217 pin bundle.
- ❖ The hot channel factor decreases from 1.26 for single pitch to 1.16 for total length of the fuel bundle (1000 mm).
- ❖ The hot spot factor and hot channel factor used in the safety analysis are more than that predicted by CFD simulation. This confirms the conservation in the core design.

11.7 EXTENDIBILITY

- ❖ A simple relationship has been developed to predict the mean sodium velocities and temperatures of central and peripheral sub channels from the results of CFD study.
- ❖ From this relationship, it is possible to either extend the results of pin bundle with less number of pins to pin bundle with more number of pins or predict the results of 217 pin bundle by hand calculation.
- ❖ The extendibility relationship prediction agrees well with the CFD prediction.

11.8 SUGGESTION FOR FUTURE STUDY

- ❖ In the present investigations, only standard High Reynolds number k-ε model has been adopted. The predictive capabilities of advanced turbulence models such as Low

Reynolds number k-ε model and Reynolds Stress Turbulence Model (RSTM) can be explored.

- ❖ The influence of buoyancy on fuel pin bundle thermal hydraulics characteristics, especially in Low Reynolds number regime may be assessed.
- ❖ In the present investigations, an axially invariant uniform heat flux has been considered. However, in the fuel pin, the heat flux exhibits a cosine profile. Influence of the profile on thermal hydraulics including hotspot factor can be assessed.
- ❖ The effect of blockage inside the fuel subassembly and flow mal-distributions can be studied.

APPENDIX - A

EQUATIONS FOR HYDRAULIC DIAMETER CALCULATION

Equations for hydraulic diameter for bare and helical wire wrapped pin bundle developed by Chen et al (2014) and used in this thesis work for the calculation of hydraulic diameter are presented here.

Bare pin flow area and wetted perimeter

$$A'_{Cen} = \left(\frac{\sqrt{3}}{4}\right) P^2 - \pi D^2/8$$

$$A'_{Wa} = P(W - D/2) - \pi D^2/8$$

$$A'_{Cor} = \left((W - D/2)^2/\sqrt{3}\right) - \pi\, D^2/24$$

$$A'_b = N_{Cen} A'_{Cen} + N_{Wa} A'_{Wa} + N_{Cor} A'_{Cor}$$

$$P'_{Cen} = \pi D/2$$

$$P'_{wa} = P + \pi D/2$$

$$P'_{cor} = \pi D/6 + 2(w - d/2)/\sqrt{3}$$

$$P'_b = N_{Cen} P'_{Cen} + N_{Wa} P'_{Wa} + N_{Cor} P'_{Cor}$$

Wire-wrapped pin flow area and wetted perimeter

$$A_{cen} = A'_{cen} - \pi D_w^2/(8\cos(\theta))$$

$$A_{Wa} = A'_{Wa} - \pi D_w^2/(8\cos(\theta))$$

$$A_{Cor} = A'_{Cor} - \pi D_w^2/(24\cos(\theta))$$

$$A_b = N_{Cen} A_{Cen} + N_{Wa} A_{Wa} + N_{Cor} A_{cor}$$

$$P_{cen} = P'_{cen} + \pi D_w/(2\cos(\theta))$$

$$P_{Wa} = P'_{Wa} + \pi D_w/(2\cos(\theta))$$

$$P_{Cor} = P'_{Cor} + \pi D_w/(6\cos(\theta))$$

$$P_b = N_{Cen}P_{Cen} + N_{Wa}P_{Wa} + N_{Cor}P_{cor}$$

$$\cos(\theta) = \frac{H}{\sqrt{H^2 + (D + D_w)^2}}$$

$$D_e' = 4A_b'/P_b'$$

$$D_e = 4A_b/P_b$$

Where

D	Pin Diameter
D_w	Wire diameter
P	Triangular pitch distance between the pins
W	Ligament gap between the pin and the wrapper
A'_{Cen}	Area of central sub channel for bare pin bundle
A'_{Wa}	Area of Wall sub channel for bare pin bundle
A'_{Cor}	Area of corner sub channel for bare pin bundle
A'_b	Total area of bare pin bundle
N_{Cen}	Number of central sub channels
N_{Wa}	Number of wall sub channels
N_{Cor}	Number of corner sub channels
P'_{Cen}	Perimeter of central sub channel for bare pin bundle
P'_{wa}	Perimeter of wall sub channel for bare pin bundle
P'_{cor}	Perimeter of corner sub channel for bare pin bundle
P'_b	Total perimeter of bare pin bundle
A_{cen}	Area of central sub channel for wire wrapped pin bundle
A_{Wa}	Area of wall sub channel for wire wrapped pin bundle

A_{Cor} Area of corner sub channel for wire wrapped pin bundle

P_{cen} Perimeter of central sub channel for wire wrapped pin bundle

P_{Wa} Perimeter of wall sub channel for wire wrapped pin bundle

P_{Cor} Perimeter of corner sub channel for wire wrapped pin bundle

D'_e Equivalent diameter of bare pin bundle

D_e Equivalent diameter of wire wrapped pin bundle

θ Rolling up angle of the helical wire

FRICTION FACTOR FOR SMOOTH PIPES

Correlations for friction factor for smooth pipes (used for straight wire-wrap pin bundle) for turbulent flow developed by Blasius (1913) and used in this thesis work for the calculation of friction factor is presented here.

$$\text{Friction factor} = 4 * 0.08 * \text{Re}^{-0.025}$$

FRICTION FACTOR FOR HELICAL WIRE-WRAP BUNDLES

Correlations for friction factor for helical wire wrapped pin bundle for different flow regimes developed by Chen et al. (2014) and used in this thesis work for the calculation of friction factor are presented here.

$$\text{Log}\left(\frac{R_e L}{300}\right) = 1.7\left(\left(\frac{P}{D}\right) - 1.0\right)$$

$$\text{Log}\left(\frac{R_e T}{10000}\right) = 0.7\left(\left(\frac{P}{D}\right) - 1.0\right)$$

$$f_{btr} = f_{bL}\left(1 - \gamma_p\right)^{1/3}\left(1 - \gamma_p^{1/3}\right) + f_{bT}\gamma_p^{1/3}$$

$$\gamma_p = \log\left(R_{eb}/ReL\right)/\log\left(R_e T/R_e\, L\right)$$

For laminar regime, $R_e < R_{eL}$

$$f_{bL} = C_{fL}/R_e$$

For Turbulent regime, $R_e > R_{eT}$

$$f_{bT} = C_{fT}/{R_e}^{0.18}$$

For Transition regime, $R_{eL} \le R_e \le R_{eT}$

$$f_{btr} = f_{bL}\left(1-\gamma_p\right)^{1/3}\left(1-\gamma_p^{1/3}\right) + f_{bT}\gamma_p^{1/3}$$

$$C_{fL} = (-974.6 + 1612.0\left(\frac{P}{D}\right) - 598.5(P/D)^2\ (H/D)^{0.06-0.085(P/D)}$$

$$C_{fT} = (0.8063 - 0.9022(\log(H/D)) + 0.03526(\log(H/D))^2\ (P/D)^{9.7}\ (H/D)^{1.78-2.0(P/D)}$$

Where

R_eL	Laminar Reynolds number
R_eT	Turbulent Reynolds number
$\frac{P}{D}$	Triangular Pitch to pin diameter ratio
C_{fL}	Coefficient of friction for laminar flow
C_{fT}	Coefficient of friction for turbulent flow
γ_p	Intermittency factor
f_{bL}	Laminar friction factor
f_{bT}	Turbulent friction factor
f_{btr}	Transition friction factor

NUSSELT NUMBER FOR HELICAL WIRE-WRAP BUNDLES

Correlations for Nusselt number for helical wire wrapped pin bundle for different flow regimes developed by Kazimi and Carelli (1980) and used in this thesis work for the calculation of Nusselt number is presented here.

$$Nu = 4.0 + 0.33(P/D)^{3.8}\,(P_e/100)^{0.86} + 0.16(P/D)^{5.0}$$

For $1.1 \leq (P/D) \leq 1.4$ and $10 \leq P_e \leq 5000$

Where $P_e = R_e * Pr$; P/D – Ratio of pitch distance between pins to pin diameter.

APPENDIX - B

DEDUCION OF CONSTANTS IN THE NUSSELT NUMBER CORRELATIONS

The average Nusselt number values at the exit of 217 pin bundle as a function of Peclet number is obtained for various values of helical wire pitch and wire diameters. The Nusselt number for each helical pitch as function of Peclet number is fitted with an empirical correlation using a power law.

$$(Nu)_d = a * (Pe)^b$$

The equation for one of the helical pitch is selected and its exponent portion $(Pe)^b$ is kept as a constant. The value of the constant portion is retained as the constant for this helical pitch. Then, the ratio of Nusselt number for second helical pitch to the value of $(Pe)^b$ for the selected helical pitch is calculated for various Peclet number. From these values of the ratios calculated for various Peclet number, a suitable median value is selected and is kept as a new constant corresponding to the second helical pitch. Similarly, the new constant for the third helical pitch is obtained. From these three constants corresponding to these three helical pitches, a representative empirical correlation is fitted using a power law such as

$$c * (H/D)^e$$

Finally, the representative proposed correlation for Nusselt number for various helical wire pitches and Peclet number is arrived at by multiplying the newly fitted equation by the exponent portion $(Pe)^b$ of the selected helical pitch.

$$Nu = c * (H/D)^e * (Pe)^b$$

The same procedure is adopted for arriving at the representative proposed correlation for Nusselt number for various helical wire diameters and Peclet number.

$$Nu = m * (d/D)^f * (Pe)^g$$

Where a - g and m are constants.

DATA SCATTER ANALYSIS FOR THE NUSSEL NUMBER CORRELATIONS

The Nusselt number values obtained from the proposed correlations for various helical wire pitches and wire diameters is plotted against the actual Nusselt number values obtained from the study to analyze the data scatter and maximum possible error.

Figures B1- B3 present the data scatter of the actual values of Nusselt number obtained from the CFD study in comparison with the values obtained from the proposed correlations for various helical wire pitches. Figures B4- B6 present the data scatter of the actual values of Nusselt number values obtained from the CFD study in comparison with the values obtained from the proposed correlations for various helical wire diameters. It is seen that the proposed correlations are best fitted against the actual values. The maximum error in all these cases is 10%.

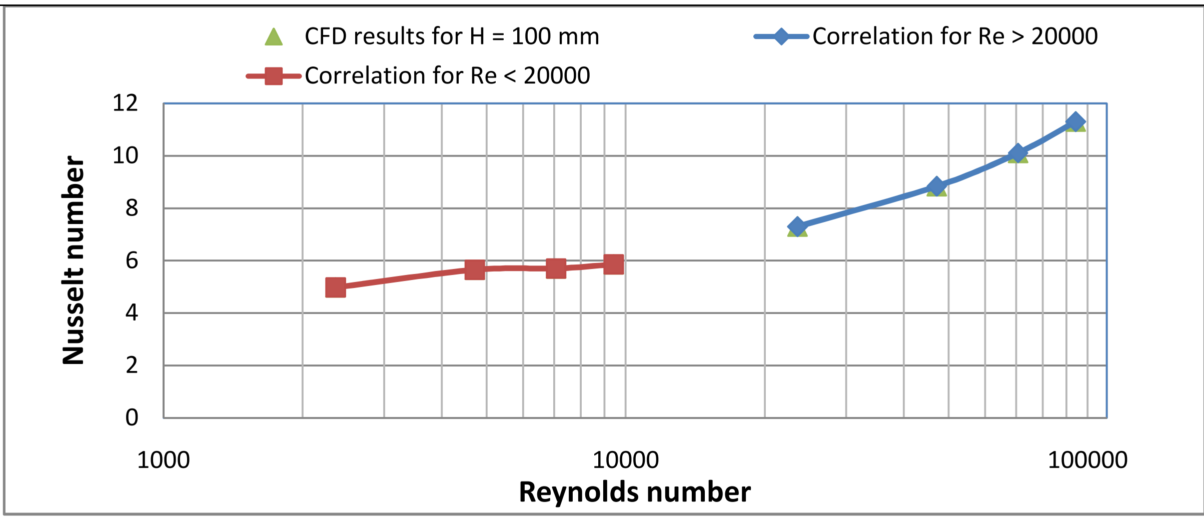

Fig. B1 Comparison of CFD results of Nusselt number for H= 100 mm with that of the Proposed correlations

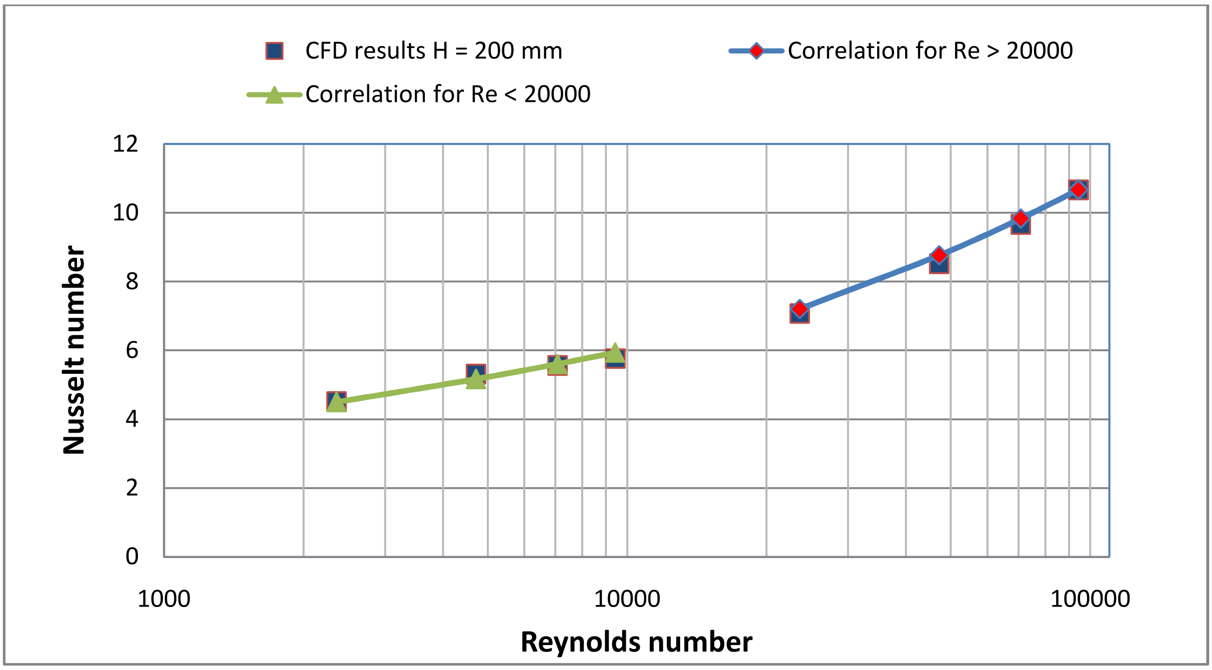

Fig. B2 Comparison of CFD results of Nusselt number for H= 200 mm with that of the Proposed correlations

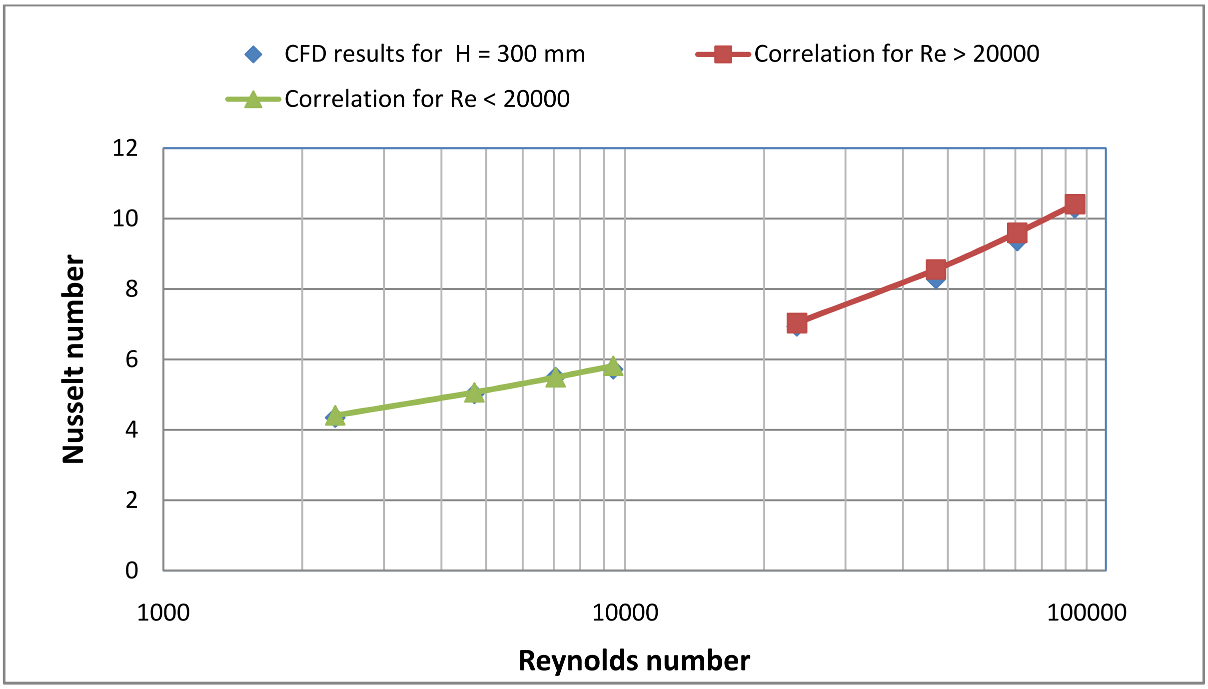

Fig. B3 Comparison of CFD results of Nusselt number for H= 300 mm with that of the Proposed correlations

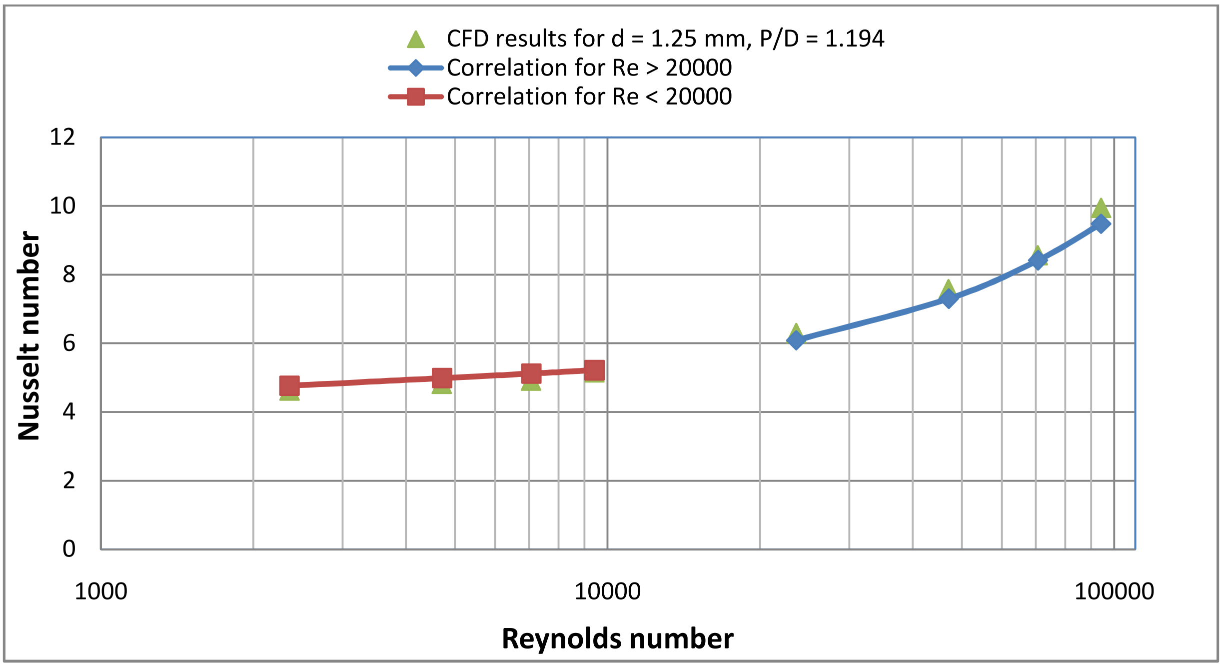

Fig. B4 Comparison of CFD results of Nusselt number for d= 1.25 mm with that of the Proposed correlations

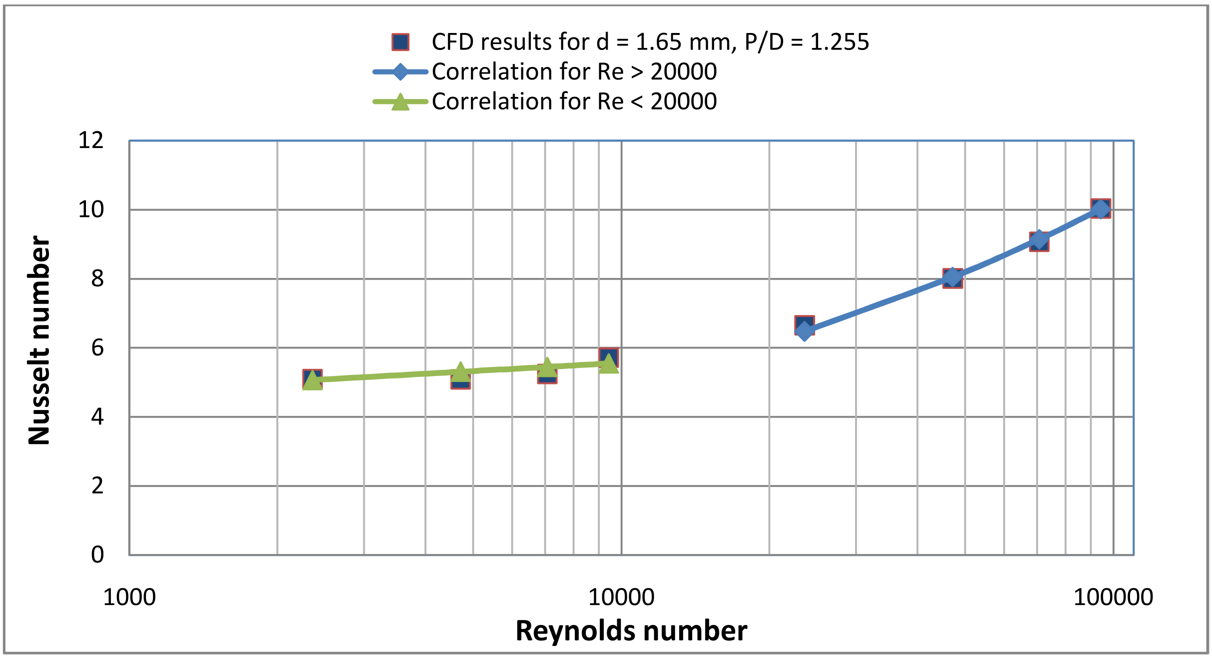

Fig. B5 Comparison of CFD results of Nusselt number for d= 1.65 mm with that of the Proposed correlations

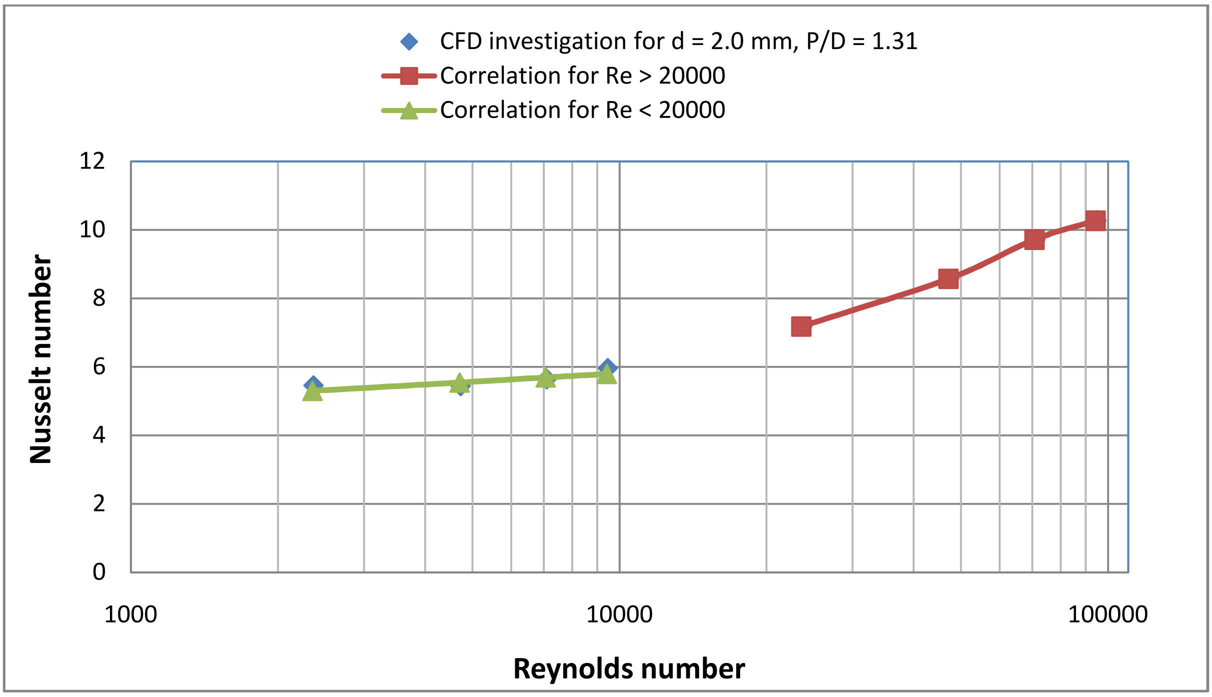

Fig. B6 Comparison of CFD results of Nusselt number for d= 2.0 mm with that of the Proposed correlations

REFERENCES

Acharya N, Sen M, Chang H.C, 1993, Thermal entrance length and Nusselt numbers in coiled tubes, *International Journal of Heat and Mass Transfer,* 37, 336-340.

Ahmad A, Kim K.Y 2005, Three dimensional analysis of flow and heat transfer in a wire-wrapped fuel assembly. *In: proceedings of ICAPP 05*, Seoul, Korea.

Arwikar K and Henri Fenech, 1979, Heat transfer, momentum losses and flow mixing in a 61 tube bundle with wire wrap, *Nuclear. Engineering and Design*, 55, 403-417.

Asty M, 1993, Fast reactor development programme in France during 1992, *Proc. 26th Meeting of Int. Working Group on Fast Reactors*, Vienna, IAEA-TECDOC-741.

Baxi, Dalle-Donne, 1981, Heat Transfer and Fluid Flow in *Nuclear Systems. In: Pergamon Press*, ISBN 0-08-027181-2.

Bauman W, V. Casal, H. Hoffmann, R. Moeller and K. Rust, 1968, Fuel elements with spiral spacers for fast breeder reactors, Kernforschungszentrum, Karlsruhe, EURFNR-571.

Bejan, A., 2004, *Convection Heat Transfer, 3rd edition, Wiley-India*, Delhi.

Bieder, U., Barthel, V., Ducros, F., Quéméré, P., Vandroux, S., 2008, CFD calculations of wire-wrapped fuel bundles: modeling and validation strategies, CEA-Grenoble, DEN/ DER/ SSTH/LDAL, 15 rue des Martyrs, F-38054 Grenoble

Blasius, H 1913, Forschungsarbeiten auf dem Gebiete des Ingenieusersens, 131, referred in Convection heat transfer by Adrian Bejan, Wiley student edition, Chapter -8, Turbulent duct flow, 387.

Borishanskii V. M, M. A Gotovskii and E. V. Firsova, 1969, Heat transfer to liquid metal flowing longitudinally in wetted bundles of rods, Soviet Atomic. Energy, 27.

Bubelis E, Schikorr M, 2008, Review and proposal for best fit of wire-wrapped fuel bundle friction factor and pressure drop predictions using various existing correlations, *Nuclear Engineering and Design*, 238, 3299-3320.

Cengel Y.A, 2007, Heat and Mass Transfer, third edition, *Tata McGraw-Hill Education Private limited*, New Delhi, 457.

CFDEXPERT, 2008 *Zeus Numerix Pvt. Ltd.,* Pune, India.

Chandra L, Roelofs F, Houkema M, Jonker B, 2009, A stepwise development and validation of a RANS based CFD modeling approach for the hydraulic and thermal-hydraulic analysis of liquid metal flow in a fuel assembly, *Nuclear Engineering and Design* 239(10), 1988 - 2003.

Chandra L, Roelofs F, 2011, CFD analyses of liquid metal flow in sub-channels for gen IV reactors, *Nuclear Engineering and Design*, 241, 4391-4403.

Chauhan A.K, Prasad B.V.S.S.S, Patnaik B.S.V, 2013, Thermal hydraulics of rod bundles: The effect of eccentricity, *Nuclear Engineering and Design*, 263, 218-240.

Chen S.K and Todreas N.E, 1986a, Prediction of coolant temperature field in a breeder reactor including inter assembly heat transfer, COO-2245-20 TR, Rev. 1.

Chen S.K and Todreas N.E, 1986b, Hydraulic models and correlations for bare and Wire wrapped hexagonal rod bundles – bundle friction factors, sub-channel friction factors and mixing parameters, *Nuclear Engineering and Design*, 92, 1-10.

Chen S.K, Todreas N. E, Nguyen N.T 2014 Evaluation of existing correlations for the prediction of pressure drop in wire-wrapped hexagonal array pin bundles. *Nuclear Engineering and Design,* 267, 109-131.

Chen S.K, Petroski R, Todreas N. E 2013 Numerical implementation of the Cheng and Todreas correlation for wire-wrapped bundle friction factors-desirable improvements in the transition flow region, *Nuclear Engineering and design*, 263, 406-410

Chetal, S.C, Balasubramaniun, V, Chellapandi, P, mohanakrishnan, P, Pudhiyavinayagam, P, Pillai, C.P, Raghupathi, S, Shanmugham, T.K, Sivathanu Pillai, C, 2006, The Design of the Prototype Fast Breeder Reactor, *Nuclear Engineering and Design,* 236, 852-860.

Chun, M.H., Seo, K.W., 2001, An Experimental study and assessment of existing friction factor correlations for wire-wrapped fuel assemblies, *Annals of Nuclear Energy,* 28, 1683 - 1695.

Collingham, R.E., Yatabe, J.M., Hill, V. R., 1970, Development and results of an electrically heated seven-pin bundle assembly for thermal hydraulic testing in liquid metals, *Liquid Metal Heat Transfer and Fluid Dynamics, ASME Winter Annual Meeting,* CONF-701110-2, New York,.

Dwyer, O.E., Tu, P.S., 1960, Analytical study of heat transfer rates for parallel flow of liquid metals through tube bundles, Part 1. *Chemical Engineering Progress Symposium Series,* 56 (30), 183 –193.

Ergun, S., 1952, Fluid Flow through Packed Columns, *Journal of Chemical Engineering Progress,* 48(2), 89 - 94.

Engel, F.C., Markley, R.A., Bishop, A.A., 1979, Laminar, transition and turbulent parallel flow pressure drop across wire-wrap-spaced rod bundles, *Nuclear Science and Engineering,* 69, 290–296.

Fanning T.H, Pointer W.D, Thomas J.W 2009 Multi resolution modeling of sub-assembly pin bundles for advanced fast reactor simulations In: Int. Conf. on Mathematics, *Computational Methods & Reactor Physics* (M&C 2009).

Fei Chen, Xiulan Huai, Jun Cai, Xunfeng Li and Ruixue Meng (2013), Investigation on the applicability of turbulent-prandtl number models for liquid-bismuth eutectic. *Nuclear Engineering and Design,* 257, 128-133.

Fenech H, 1985, Local heat transfer and hotspot factors in wire-wrap tube bundle, *Nuclear Engineering and Design,* 88, 357-365.

Feldman E.E, Hornbeck R.W, Osterle J.F, 1982, A numerical solution of laminar developing flow in eccentric annular ducts, *International Journal of Heat and Mass Transfer*, 25, 231-241.

Fischer P, Lottes J, Siegal A, Palmiotti G, 2007, Large eddy simulation of wire wrapped fuel pins I: hydrodynamics in periodic array. *In: Joint International Topical Meeting on Mathematics & Computation and Supercomputing in Nuclear applications* (M&C +SNA 2007).

Friedland, A.J., Bonilla, C.F., 1961, Analytical study of heat transfer rates for parallel flow of liquid metals through tube bundles, *American Institute of Chemical Engineers Journal,* 7 (1), 107 – 112.

Fricano, J.W and Baglietto. E, 2014, A quantitative CFD bench mark for sodium fast reactor fuel assembly modeling, *Annals of Nuclear Energy,* 64, 32-42.

Gajapathy, R. Velusamy, K., Selvaraj, P, Chellapandi, P and Chetal, S.C, 2007, CFD study of helical wire-wrapped 7- fuel pin bundle and the challenges in modeling full scale 217 fuel pin bundle, *Nuclear Engineering and Design,* 237, 2332-2342.

Gajapathy, R. Velusamy, K, Selvaraj, P, Chellapandi, P. and Chetal, S.C, 2009, A comparative CFD investigation of helical wire-wrapped 7,19 and 37- fuel pin bundles and its extendibility to 217 fuel pin bundle, *Nuclear Engineering and Design,* 239, 2279-2292.

Govindarasu Velusamy, K, T. Sundararajan, Chellapandi, P, 2014, Simultaneous development of flow and temperature fields in wire wrapped fuel pin bundles of sodium cooled fast reactors, *Nuclear Engineering and Design,* 267, 44-60.

Hazi G, 2005, On turbulence models for rod bundle flow computations, *Annals of Nuclear Energy,* 32, 755-761.

Hughes W.F, Gaylord E.W 1964, Basic equations of engineering science, *Schaum's outline series, McGraw-Hill,* New York.

Incropera F.P., Dewitt, D.P., 2009, *Fundamentals of Heat and Mass Transfer*, 5th edition, John Wiley & Sons (Asia), pp. 485 – 487.

Kamide H, K. Hayashi, S. Toda, 1998, An experimental study of inter sub assembly heat transfer during natural convection heat removal in Fast breeder reactors, *Nuclear Engineering and design,* 183, 97-106.

Kawamura, H., Ohsaka, K., Abe, H., Yamamoto, K., 1998, DNS of turbulent heat transfer in channel flow with low to medium-high Prandtl number fluid, *International Journal of Heat and Fluid Flow,* 19, 482-491.

Kazimi M.S and Carelli M.D 1980 Heat transfer correlations for analysis of CRBRP assemblies', *Atomic Energy Review*, 18(2), 329-552.

Kazimi and Todreas, 2012, Nuclear Systems volume 1, *Thermal Hydraulic Fundamentals, 2nd edition, published by CRC Press Taylor & Francis, Levittown,* pp 588-589.

Khan, E. U., Rohsenow, W.M., Sonin, A.A., Todreas, N.E., 1975, A porous body model for predicting temperature distribution in wire wrapped fuel rod assemblies, *Nuclear Engineering and Design,* 35, 1-12.

Knudsen J.G, Katz, D.L 1958 *Fluid Dynamics and Heat Transfer*, *McGraw-Hill*, New York.

Lorenz, J, J, Ginsberg T, Morris R. A 1974, Experimental mixing studies and velocity measurements with a simulated 91 – element LMFBR fuel assembly. *ANL – CT- 74-09.*

Lorenz, J.J. and Ginsberg, T., 1977, Coolant mixing and sub channel velocities in an LMFBR fuel subassembly', *Nuclear Engineering and Design,* 40, 315-326.

Launder, B. E and Spalding, D.B., 1974, The numerical computation of turbulent flows, *Computer Methods in Applied Mechanics and Engineering,* 3, 269-289.

Laurent Bricteux, Matthieu Duponcheel and Yann Bartosiewicz, (2010) Direct and Large Eddy simulation of turbulent heat transfer at very low Prandtl number: Application to Lead-bismuth flows, *International conference on Nuclear Energy for New Europe* Slovenia.

Mikityuk K, 2009, Heat transfer to liquid metal: Review of data and correlations for tube bundles, *Nuclear Engineering and design,* 239, 680-687.

Manglik, R. M., Bergles, A.E., 1988, Laminar flow heat transfer in a semi-circular tube with uniform wall temperature, *International Journal of Heat and Mass Transfer*, 31, 625-636.

Manglik, R.M., Bergles, A.E., 1996, Thermally developing laminar flows in circular-segment ducts with uniform wall temperature, *Proc. 9th International Symposium on Transport Phenomena in Thermal-Fluids Engineering*, 2, 831-836.

Mareska, M.V, Dwyer, O.E., 1964, Heat transfer in a mercury flow along bundles of cylindrical rods, ASME *Journal of Heat Transfer,* 86, 180 - 186.

Massoud, M., 2005, Engineering Thermo fluids: *Thermodynamics, Fluid Mechanics, and Heat Transfer, Springer*, Berlin Heidelberg, New York.

Merzari E, Pointer W.D, Smith J. G, Tentner A, Fischer P, 2012, Numerical simulation of the flow in wire-wrapped pin bundles: Effect of pin-wire contact modeling, *Nuclear Engineering and Design,* 253, 374-386.

Mikic, B E. U. Khan, and N.E. Todreas, 1977, An approximate method for predicting temperature distributions in wire wrapped fuel subassemblies of a LMFBR Massachusetts Institute of Technology, Cambridge, *COO-2245-37TR.*

Natesan K, Soundararajan T, Arunn Narasimhan, Velusamy K, 2010, Turbulent flow simulation in a wire-wrap rod bundle of an LMFBR, *Nuclear Engineering and Design,* 240, 1063-1072.

Nishimura M, H. Kamide, K. Hayashi, K. Momoi, 2000, Transient experiments on fast reactor core thermal hydraulics and its numerical analysis Inter-sub assembly heat transfer and inter wrapper flow under natural circulation conditions *Nuclear Engineering and design,* 200, 157-175.

Novendstern E. H., 1972, Turbulent flow pressure drop model for fuel assemblies utilizing a helical wire wrap system', *Nuclear Engineering and Design,* 22, 19-27.

Patankar S. V 1980 *Numerical Heat transfer and fluid flow, Mc Graw-Hill, New York.*

Peniquel, C., Rupp, I., Juhel, J.P, 2009, Three dimensional conjugate heat transfer analysis in sodium fast reactor wire wrapped fuel assembly. *In: Proceeding of the International Congress on Advanced Power Plants, (ICAPP"09),* Paper No. 9311, Tokyo, Japan.

Pointer, W.D., Fischer, P.F., Siegal, A Smith, J., 2008, RANS based CDF simulations of wire wrapped fast reactor fuel assemblies *In: Proceedings of ICAPP 08,* Anaheim, CA.

Raza W and Kim K.Y 2008, Comparative Analysis of Flow and Convective Heat Transfer between 7-Pin and 19-Pin Wire-Wrapped Fuel assemblies, *Journal of Nuclear Science and Technology,* 45(7), 653 - 661.

Rehme 1973, Pressure drop correlations for fuel element spacers, *Nuclear Technology,* 17, 15-22.

Rehme, 1987, Convective heat transfer over rod bundles, *Handbook on single-phase convection heat transfer. A Wiley Inter science Publication.*

Rensen, Q., 1981, Experimental investigation of turbulent heat transfer to liquid sodium in the thermal entrance region of an annulus, *Nuclear Engineering and Design*, 68, 397 – 404

Rolfoa, S., Péniguelb, C., Guillaudc, M., Laurencea, D., 2012, Thermal-hydraulic study of a wire spacer fuel assembly, *Nuclear Engineering Design,* 243, 251-262.

Roychowdhury D, S. Govindarajan, R.D. Kale, 1998, Thermal hydraulic design of PFBR core IAEA specialists meeting on LMFR core thermo hydraulics – Status and prospects, Obninsk, Russia, *IAEA-TECDOC-1157.*

Rowe D. S., 1973, COBRA-IIIC: A digital computer program for steady state and transient thermal hydraulic analysis of nuclear fuel elements', Battle Pacific Northwest Laboratories, *BNWL-1695.*

Sangster W. A. 1968, 'Calculation of rod bundle pressure loss', *Paper 68-WA/HT-35, ASME.*

Shang, Z., 2009, CFD investigation of vertical rod bundles of supercritical water-cooled nuclear reactor, *Nuclear Engineering and Design*, 239, 2562 - 2572.

Smith, J.G., Babin, B.R., pointer, W.D., Fischer, P.F., 2008, Effects of mesh density and flow conditioning in simulating 7 pin wire wrapped fuel pins, *In: Proceedings of ICONE 16,* Orlando, FL.

Smith, J.G, Tokuhiro, A., Pointer, W.D, Fischer, P.F, 2009, Predictions in CFD simulation of wire-wrapped SFR fuel assemblies, *In: Proceedings of the International Congress on Advanced Power Plants (ICAPP'09),* paper no. 9096, Tokyo, Japan.

Spalding D.B and Launder B. E, 1974, The numerical computation of turbulent flows, *Computer Methods in Applied Mechanics and Engineering,* 3, 269-289.

Shah R.K, London A.L 1978, Laminar flow forced convection in ducts, *Advances in Heat Transfer Academic Press,* New York.

Sreenivasulu, T, Prasad, B.V.S.S.S., 2009, Prasad, Flow and heat transfer characteristics in an annulus wrapped with a helical wire, *International Journal of Thermal Sciences,* 48, 1377 - 1391.

Sreenivasulu, T., Prasad, B.V.S.S.S., 2011, Flow and heat transfer characteristics in a seven tube-bundle wrapped with helical wires, *International Journal of Advancements in Technology,* 2(3), 350-381.

Sreenivasulu T., K. Thean Mani Rajan and B. V. S. S. S. Prasad 2008 'Convective heat transfer characteristics in an annulus wrapped with a helical wire', *Proc. 8 th ISHMT-ASME Heat and Mass Transfer Conference,* JNTU, Hyderabad, India, HTE-4.

Srinivasan, G, Suresh Kumar, K.V, Rajendran, B, Ramalingam, P.V, 2006, The Fast Breeder Test Reactor-Design and operating experiences, *Nuclear Engineering and Design,* 236, 796-811.

Steiner, H., Konys, J., 2006, Heat and mass transfer calculations in heavy liquid metal loops under forced convection conditions, *Nuclear Engineering and Design,* 348, 18-25.

Subbotin, V.I., Ushakov, P.A., Kirillov, P.L., Ibragimov, M.H., Ivanovski, M.N., Nomofilov, E.M., Ovechkin, D.M., Sorokin, L.N., Sorokin, V.P., 1965, Heat transfer in elements of reactors with a liquid metal coolant. In: *Proceedings of 3rd International Conference on Peaceful uses of Nuclear Energy*, 8, New York, pp. 192–200.

STAR CD version 3.15, 2001, *Computational dynamics limited.*

Tenchine, D., 2010, Some thermal hydraulic challenges in sodium cooled fast reactors, *Nuclear Engineering and Design*, 240, 1195–1217.

Ushakov, P.A., Zhukov, A.V., Matyukhin, M.M., 1977, Heat transfer to liquid metals in regular arrays of fuel elements, *High Temp*erature, 15, 868 - 873.

Velusamy, K., Chellapandi, P., Chetal, S.C., Raj, B., 2010, Overview of pool hydraulic design of Indian prototype fast breeder reactor, *Sadhana*, 35(2), 97–128.

Valentin, B., 2000, The thermal hydraulics of a pin bundle with a helical wire wrap spacer. Modeling and qualification for a new sub-assembly concept. *LMFBR core thermal hydraulics, IAEA-TECDOC-1157, Status and prospects.*

Walter A. E and Reynolds A. B, 1981 Fast Breeder Reactors, Pergamon Press, NY.

Wantland J. L, 1974 ORRIBLE – A computer program for flow and temperature distribution in 19 rod LMFBR fuel subassemblies', *Nuclear Technology.* 24, pp. 168-175.

Wasim Raza, Kwang-yong Kim, 2008, Effects of wire-spacer shape in LMR on thermal-hydraulic performance, *Nuclear Engineering and Design,* 238, 2678-2683.

Weber D. P 2005, The numerical nuclear reactor for high fidelity integrated simulation of neutronic, thermal-hydraulic and thermo-mechanical phenomena, *STAR American conference, Detroit, Michigan.*

NOMENCLATURE

C_p Specific heat, J/kg-K

d Helical wire diameter, mm

d_{eq} Equivalent diameter of the pin bundle, mm

D Diameter of fuel pin, mm

f Friction factor

$F_{h,j}$ Diffusional energy flux in direction x_j

g_m Gravitational field components

$h^{'}$ The turbulent diffusional flux of energy

h Heat transfer coefficient, W/ m- K

H – Helical wire pitch length, mm

k Turbulent kinetic energy

K Von Karman constant

Kf_{cond} Thermal conductivity of Sodium, W/m-K

l Length of the bundle, m

MWe MegaWatt (Electrical)

Nu Nusselt number

p Pizeometric pressure = $p_s - \rho_0 g_m x_m$

p_s Static pressure, Pascal

P Triangular pitch distance between pins, mm

q''	Heat flux from the fuel pin surface, W/m^2
s_{ij}	The rate of strain tensor
T	Temperature, K
T_0	Reference temperature, K
T_c	Clad temperature, K
T_f	Average sodium outlet temperature, K
u_i	Velocity component in different directions
u'	Fluctuations about the ensemble average velocity
v	Inlet axial velocity in the pin bundle, m/s
x_i	Cartesian coordinates
x_m	Coordinates from datum
δ_{ij}	The "Kronecker delta", is unity when i=j and zero otherwise
ε	Turbulent dissipation rate
μ	Molecular dynamic fluid viscosity, Ns/m^2
ν	Kinematic viscosity, m^2/s
ρ_0	Reference density, kg/m^3
ρ	density, kg/m^3
ΔP	Pressure drop in pin bundle, Pascal
τ_{ij}	Viscous stress tensor components.
τ_w	Wall shear stress, N/m^2

LIST OF PUBLICATIONS BASED ON THE THESIS

INTERNATIONAL JOURNAL PAPERS

1. **Gajapathy, R**., Velusamy, K., Selvaraj, P., Chellapandi, P. and Chetal, S.C., 2007. CFD study of helical wire-wrapped 7- fuel pin bundle and the challenges in modeling full scale 217 fuel pin bundle, Nuclear Engineering and Design, 237, 2332-2342.

2. **Gajapathy, R**., Velusamy, K., Selvaraj, P., Chellapandi, P. and Chetal, S.C., 2009. A comparative CFD investigation of helical wire-wrapped 7,19 and 37- fuel pin bundles and its extendibility to 217 fuel pin bundle, Nuclear Engineering and Design, 239, 2279-2292.

3. **Gajapathy, R**., Velusamy, K., Selvaraj, P., and Chellapandi, P., 2015. "CFD investigation of effect of helical wire parameters on the thermal hydraulic performance of 217- fuel pin bundle", Annals of Nuclear Energy, 77, 498-513.

4. **Gajapathy, R**., Velusamy, K., Selvaraj, P., and Chellapandi, P., "CFD investigation of helical wire-wrapped 217- fuel pin bundle with variable heat flux", (Under preparation).

CONFERENCE PROCEEDINGS

1. **Gajapathy, R**., Velusamy, K., Selvaraj, P., Chellapandi, P. and Chetal, S.C, Studies on Core temperature monitoring for the startup conditions of PFBR, ANUP-2010, India.

2. **Gajapathy, R,** Velusamy, K, CFD investigations of full heat generating length of 217 fuel pin bundle Proceedings of the 23rd National Heat and Mass Transfer Conference and 1st International ISHMT-ASTFE Heat and Mass Transfer Conference, IHMTC2015, 17-20 December, 2015, Thiruvananthapuram, India. (Accepted)